Simulations of air quality in West Africa: An evaluation of the emissions, sources, seasonality and impacts of pollutants

Eleanor Rose Morris
PhD
University of York
Chemistry

September 2019

Abstract

Poor air quality and its impacts on human and ecosystem health are a major global environmental concern. Anthropogenic emissions in West Africa are forecast to rise significantly as a result of rapid population growth and economic development; yet unlike regions such as Europe, North America, China and India, air quality in West Africa remains considerably understudied.

In this thesis, a new regional configuration of the GEOS-Chem model has been used to evaluate global and regional anthropogenic emissions for West Africa against airborne measurements from the Dynamics-Aerosol-Chemistry-Cloud Interactions in West Africa (DACCIWA) campaign. Serious failings have been identified in these inventories. Anthropogenic emissions of nitric oxide and sulfur dioxide are significantly under represented, with significant differences also found in both the anthropogenic and biomass burning emissions of carbon monoxide, organic carbon and black carbon. Simple optimisation of the emissions produces an improved simulation and results in a two-fold enhancement of fine particulate matter concentrations.

The emission and meteorological factors driving seasonal changes in pollutant concentrations have also been investigated. Surface concentrations in West Africa have been found to be influenced by anthropogenic activities throughout the year and also by biomass burning and dust during the dry season (October to March). Whilst gaseous pollutants rarely exceed World Health Organisation guidelines, particulate matter is frequently in exceedance of the limits and poses a major health risk in West Africa. These exceedances are predominantly caused by dust and anthropogenic emissions, with biomass burning also playing a role in elevating concentrations, mainly as a result of local burning events during the dry season.

Modelling studies of West African air quality remain limited by the paucity of observations. Increased collection and open dissemination of pollutant measurements is required to fully optimise inventories, improve models, assess the impacts of pollution and hence develop effective control strategies in the region.

Contents

List of Figures

List of Tables

Acknowledgements

I would firstly like to acknowledge the invaluable support and guidance of my supervisor, Mat Evans, throughout this PhD. His knowledge, expertise and enthusiasm have been inspirational to work alongside.

Thanks also go to the Natural Environment Research Council SPHERES Doctoral Training Partnership and the Dynamics-Aerosol-Chemistry-Cloud Interactions in West Africa (DACCIWA) programme for funding this studentship.

Thanks to the DACCIWA family for making the field campaign and project meetings so enjoyable. It has been a pleasure working alongside so many people from different fields with a common interest in researching the atmosphere over West Africa.

I am particularly grateful for the assistance given by Christoph Keller to incorporate injection altitudes into the GFAS biomass burning inventory within the GEOS-Chem HEMCO module.

In addition I would also like to thank colleagues, family and friends for their continued support and encouragement over the past four years.

And finally to my husband, Oliver, for his expert handling of the Twin Otter aircraft during the DACCIWA campaign and for his unwavering optimism and support throughout the development of this thesis.

Author's Declaration

I declare that this thesis is a presentation of original work and I am the sole author. This work has not previously been presented for an award at this, or any other University. All sources are acknowledged as References.

Chapter 1

Air quality challenges facing West Africa

Ambient outdoor air pollution is a leading cause of premature deaths globally [149, 174]. An estimated 4.9 million premature deaths worldwide were attributed to air pollution in 2017 [174]. 2.9 million of these deaths were attributed to ambient fine particulate matter ($PM_{2.5}$) and 0.47 million were attributed to ambient ozone (O_3) [174]. Statistics for both pollutants show an approximately 20% increase over the ten year period from 2007 to 2017, emphasising the growing risk of air pollution to human health [174]. Poor air quality affects the entire global population in both developed and developing countries, urban and rural areas and across all socio-economic groups. Air pollution is therefore considered a major environmental risk to health.

Air pollution and its links with poor health have been hypothesised for hundreds of years [159]. However, key events such as the great smog in London in December 1952 [25], as well as photochemical smog events in Los Angeles [240], prompted governments and policymakers to introduce regulations for the protection of health [190,191,249]. Pollutant concentrations are now regulated to varying extents across the world.

Sources of pollutants are extremely varied and, as such, air quality issues vary dramatically between countries. In Europe and North America, the predominant source of pollutants is from anthropogenic activities [140, 176]. In South America, Asia and Africa there is also a strong influence from biomass burning, which elevates pollutant concentrations further [126, 176]. Close to deserts (such as the Sahara and Arabian deserts) there is also a significant influence from dust [211]. There are also many other emission sources that can impact air quality such as volcanoes, ocean emissions and biogenic sources [42, 98, 176]. In addition to this, pollutant concentrations are heavily influenced by meteorological conditions and transport patterns [22, 220, 245, 271, 281].

Air quality is therefore a complex issue which varies greatly depending on geographical location, meteorological conditions and emission sources. The wide array of factors which determine pollutant concentrations in any given area means that policies for controlling

and reducing these concentrations must also vary. Whilst developed countries, such as the UK, have well established monitoring networks and policies in place for managing air pollution [57, 191], developing countries often lack the observational and monitoring infrastructure and a paucity of research in these regions leads to poor understanding of the processes controlling air quality [196]. The factors controlling pollution concentrations in these countries must be better understood before effective policies can be designed and implemented for mitigating the impacts of pollution on human health and the environment.

1.1 Sources and impacts of air pollution

There are many different air pollutants that, when present at high enough concentrations, can have significant impacts on the health of both humans and the environment [7, 73, 80, 148, 149, 174, 234]. These pollutants are emitted from a wide range of both natural and anthropogenic sources but, in many parts of the world, anthropogenic combustion processes are the dominant source of emissions [77, 107, 109, 134, 140, 176, 218, 229, 277]. These combustion sources include energy generation, industrial processes and domestic burning such as wood fired stoves as well as road, rail, shipping and air transport. Depending on location and season, some parts of the world also experience a large impact from sources such as desert dust and biomass burning [126, 211].

Once released from the emission sources, pollutants are dispersed by meteorological processes including large scale transport, convection and turbulent mixing [220, 245, 271, 281]. Pollutants from the different sources therefore not only cause impacts in the immediate vicinity of the emissions, but also over large areas due to transport [22]. The distance a pollutant species is transported depends on its atmospheric lifetime [71]. For some species such as carbon monoxide, this lifetime is long ($\sim$months) which allows the pollutant to be transported over distances of thousands of kilometres. Shorter lived species such as nitrogen oxides (lifetime of hours to days) are not able to travel over such large distances in their originally emitted form but may be transported over larger areas in other chemical forms such as peroxy acetyl nitrate which is the major tropospheric reservoir for nitrogen oxides [84]. In addition to this, pollutants can chemically react in the atmosphere forming new "secondary" compounds, such as ozone and particulate matter, which also contribute to poor air quality [72, 82, 171, 268]. The impact that any given pollutant has on the population and environment is therefore dependent on the magnitude of the emissions, the location of the sources, reactions in the atmosphere, transport patterns and atmospheric lifetimes.

Poor air quality affects the entire population; however, in general, young children, the elderly and those already suffering from existing health conditions are the most vulnerable [216]. Air pollution plays a key role in exacerbating existing respiratory and cardiovascular diseases as well as causing irritation of the eyes and airways, inflammation of the lungs

and some forms of cancer [52, 64, 127, 149, 153, 172, 174, 188, 198, 202, 221, 224, 241, 261, 280]. Reducing air pollution concentrations can reduce the burden of disease and improve both the short- and long- term health of the population; however, most sources of outdoor air pollution are beyond the control of individuals and require action from policymakers at local and national scales, and in some cases at continental and global scales [190, 191, 249, 274].

Key air pollutants (which are known to be harmful to health and as such are subject to standards in the UK as well as other countries [236]) are carbon monoxide (CO), nitrogen oxides (NO_x), sulfur dioxide (SO_2), non-methane volatile organic compounds (NMVOCs), ozone (O_3) and particulate matter (PM). The sources and impacts of these pollutants are now discussed in Sections 1.1.1 to 1.1.6.

1.1.1 Carbon Monoxide (CO)

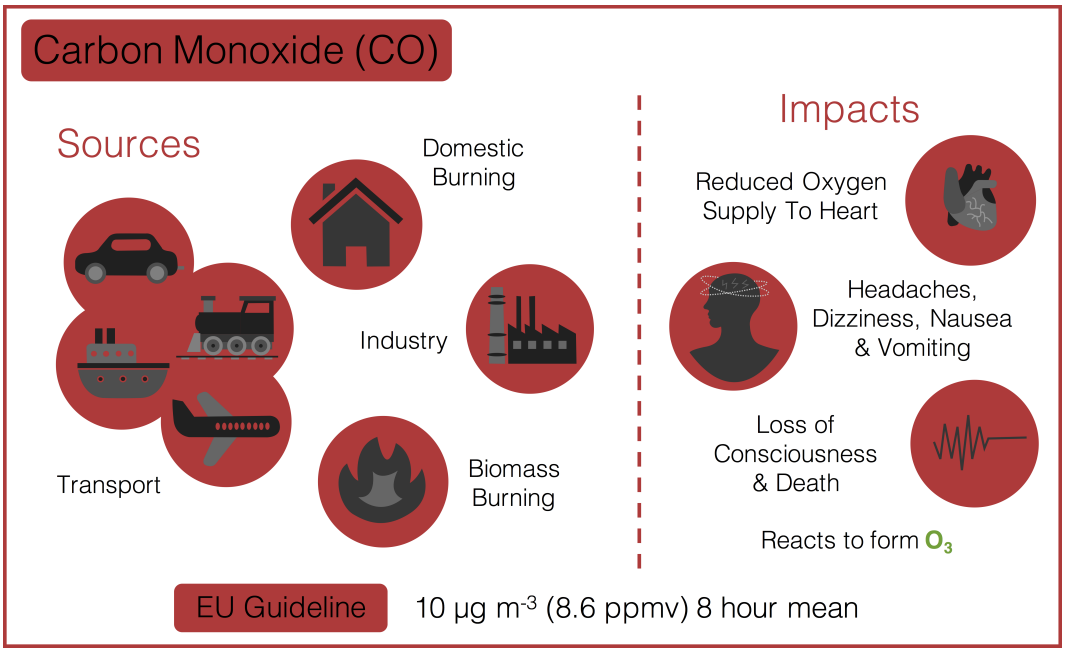

Figure 1.1: Graphic illustrating the sources and impacts of carbon monoxide (CO).

Carbon monoxide (CO) is released from the incomplete combustion of fuels which contain carbon [109, 218]. CO is emitted from many different sources but primarily from road transport, industry and domestic burning, as well as from biomass burning activities in some parts of the world [70, 125, 126, 182].

Background concentrations of CO are typically higher in the northern hemisphere, due to more anthropogenic combustion sources; however, it has a long lifetime in the troposphere (months) [71] which means transport and mixing across vast areas occurs [218]. The long lifetime of CO also makes it an excellent tracer for identifying combustion sources and studying transport patterns [218].

Exposure to high concentrations of CO can have negative impacts on human health. CO binds to haemoglobin in the blood, preventing the uptake of oxygen [153,241,250]. The reduced supply of oxygen to the heart can cause headaches, dizziness, nausea and vomiting and at very high concentrations can lead to a loss of consciousness and death [153,241,250]. As with most pollutants, the effects are greatest in those already suffering from heart disease, as well as young children and the elderly [241]. The European Union (EU) air quality standard for CO is 10 mg m^{-3} (8.6 ppmv) maximum daily 8 hour mean [75]. Other than in confined spaces, CO is rarely at high enough concentrations to be a significant health concern. However, CO is also a precursor for ozone formation [72, 171] which has many other impacts on both human and ecosystem health (Section 1.1.5).

1.1.2 Nitrogen Oxides (NO_x)

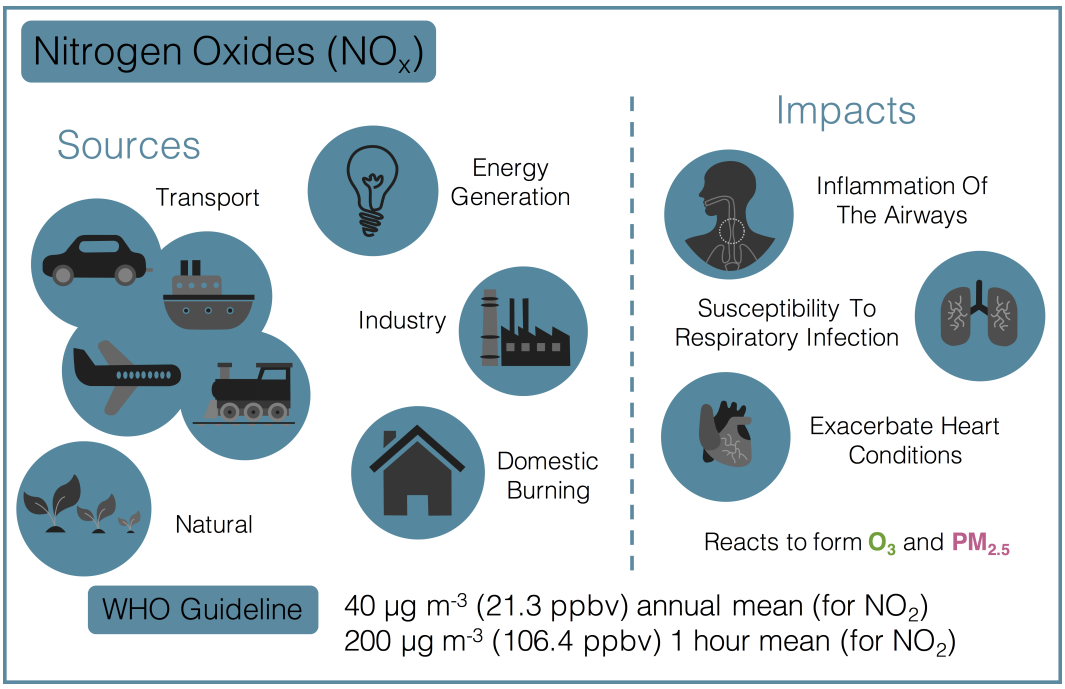

Figure 1.2: Graphic illustrating the sources and impacts of nitrogen oxides (NO_x).

Nitrogen oxides (NO_x) are predominantly emitted from high temperature combustion processes such as electricity generation and vehicle exhausts [146, 218]. NO_x is also emitted from low temperature combustion processes including biomass burning and domestic burning [126, 151, 218], as well as from natural sources such as lightning [175] and soils [116]. During combustion, the majority of NO_x is emitted in the form of nitric oxide (NO) which reacts rapidly with ozone in the atmosphere to form nitrogen dioxide (NO_2), therefore the two gases are considered together as NO_x ($[NO_x] = [NO] + [NO_2]$) [133].

NO_2 is harmful to human health as exposure to high levels can result in significant inflammation of the airways and increased susceptibility to respiratory infections [188,221, 261]. It can also exacerbate symptoms in people already suffering from heart conditions

or lung diseases and hence reduce their quality of life and life expectancy [261]. The tropospheric lifetime of NO_x is short (hours to days) [71]; therefore, the direct impacts of NO_x on human health are felt in the vicinity of the emission sources [106, 218]. The effects of high NO_x concentrations are often highest at roadside locations where vehicle exhausts are a major contributing source to surface concentrations [11, 43–45, 131]. The World Health Organisation (WHO) recommend an annual mean limit of 40 μg m^{-3} (21.3 ppbv) and a 1 hour mean limit of 200 μg m^{-3} (106.4 ppbv) for NO_2 for the protection of human health [274].

As well as the direct effects that NO_2 has on human health, it can also react with other pollutants in the atmosphere to form tropospheric ozone which itself has impacts on human and ecosystem health (Section 1.1.5) [72, 171]. NO_2 is also a source of nitrate aerosol (NO_3^-) which is a contributing fraction of $PM_{2.5}$ (Section 1.1.6) [121, 197].

1.1.3 Sulfur Dioxide (SO_2)

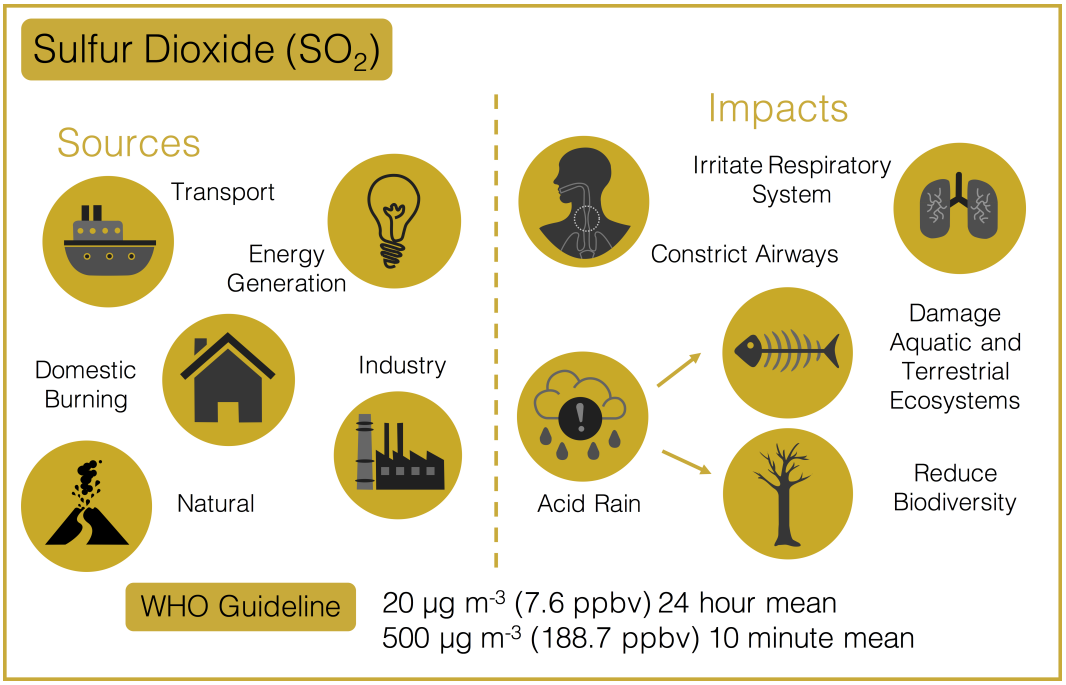

Figure 1.3: Graphic illustrating the sources and impacts of sulfur dioxide (SO_2).

Sulfur dioxide (SO_2) is an acidic gas which is primarily emitted from the combustion of solid and liquid fuels which contain sulfur [134, 229]. The major emission sources include energy generation, industrial processes, domestic burning and transport (in particular shipping) [77, 134, 229].

These anthropogenic sources are regulated to varying extents throughout the world. Across much of Europe and North America the sulfur content of liquid fuels is below 15 ppm [246]. Whereas across South America, Asia and Africa the sulfur content of these fuels is considerably higher, with a sulfur content of over 5000 ppm seen in the Middle

East and some African countries and a sulfur content of over 2000 ppm seen for many nations in West Africa [246]. There are also natural sources of SO_2 to the atmosphere, such as volcanic emissions and the degradation of sulfur source gases (such as dimethyl sulfide (DMS)), which cannot be easily regulated [42].

SO_2 can cause constriction of the airways and irritate the respiratory system [198,202]. People with asthma or existing respiratory conditions are particularly sensitive to high concentrations of SO_2 [202]. The WHO guideline values for SO_2 concentrations are 20 μg m^{-3} (7.6 ppbv) over a 24 hour mean period and 500 μg m^{-3} (188.7 ppbv) over a 10 minute mean period [274].

SO_2 can react in the atmosphere to form sulfuric acid, resulting in acid rain [148,213]. Acid rain can significantly harm both terrestrial and aquatic ecosystems and result in a reduction in biodiversity [148]. SO_2 is also a precursor for sulfate aerosol which is a contributing fraction of $PM_{2.5}$. Sulfate aerosol also acts as a cloud condensation nuclei and increases cloud reflectivity which leads to a cooling of the Earth's surface [31].

1.1.4 Non-Methane Volatile Organic Compounds (NMVOCs)

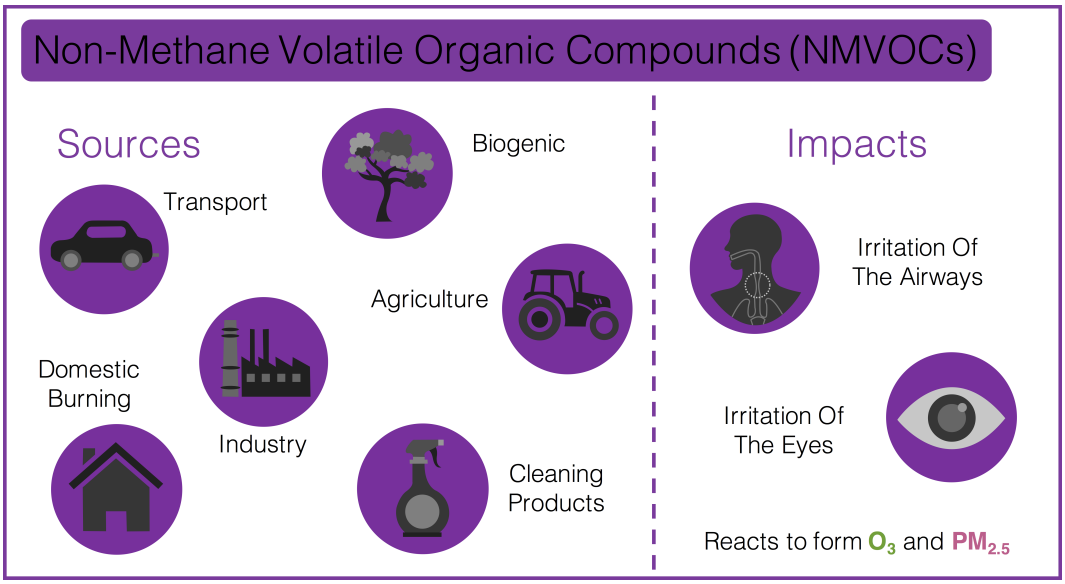

Figure 1.4: Graphic illustrating the sources and impacts of non-methane volatile organic compounds (NMVOCs).

Non-methane volatile organic compounds (NMVOCs) include a wide range of gaseous species from short chain alkanes to complex aromatic compounds [218]. These compounds are emitted from a vast array of anthropogenic sources including combustion processes such as transport, industrial and residential activities, household cleaning products, direct evaporation of fuels and agriculture [49, 107, 155, 277]. There is also a major source of VOC emissions from biogenic sources, as trees and vegetation can emit vast amounts of specific VOCs such as isoprene and monoterpenes [98,113]. The varied range of compounds

encompassed in the NMVOC category means that NMVOCs have very varied atmospheric lifetimes (in the range of minutes to months) and different reactivities [218].

Some NMVOCs have direct health impacts themselves, for example benzene and other mono- and poly- aromatics are widely known to be carcinogenic as well as to cause problems with the reproductive, immune, nervous, cardiovascular and respiratory systems [52, 127, 224]. NMVOCs can also react with other pollutants to form ozone and particulate matter [72, 171] (Sections 1.1.5 and 1.1.6).

1.1.5 Ozone (O_3)

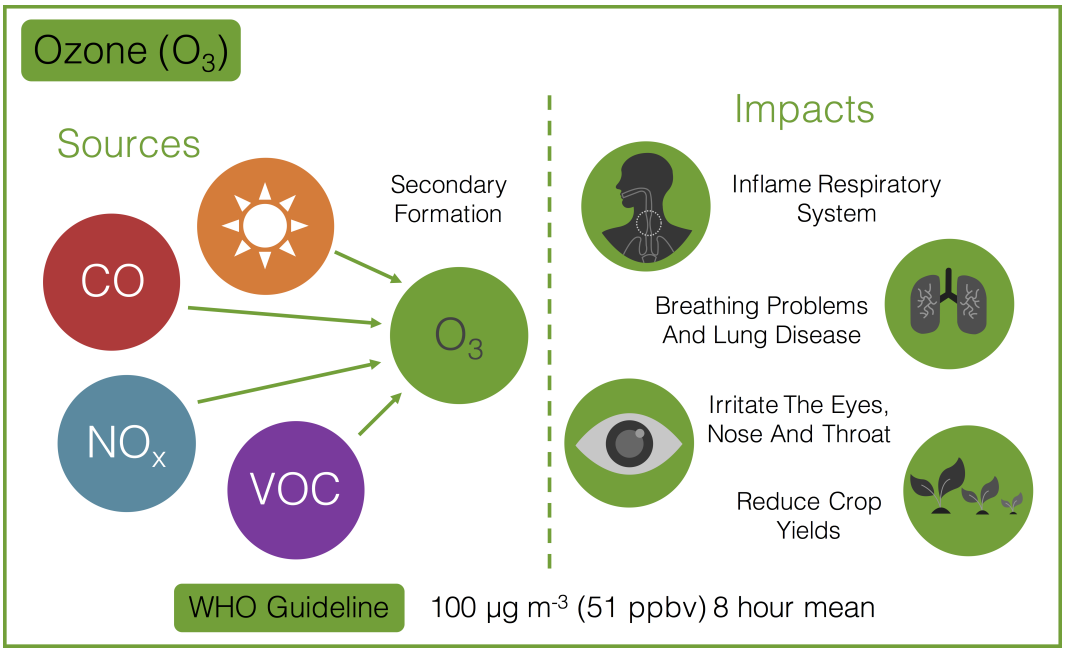

Figure 1.5: Graphic illustrating the sources and impacts of ozone (O_3).

Ozone (O_3) is a secondary pollutant so it is not directly emitted from pollution sources, but is instead formed in the atmosphere from the reactions of other pollutants [72, 171]. The major production pathway is from the reaction of NO_x, CO and VOCs in the presence of sunlight [72, 171]. This production mechanism is illustrated in Figure 1.6.

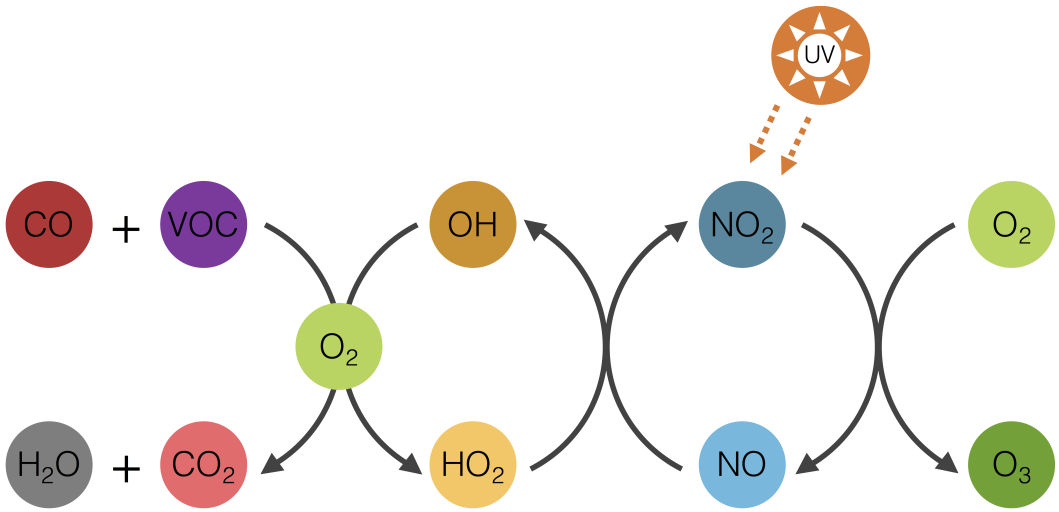

Figure 1.6: Photochemical production pathway of ozone in the troposphere from carbon monoxide, nitrogen oxides and volatile organic compounds.

Tropospheric ozone is formed from a series of radical reactions [72,171]. Firstly, carbon monoxide or volatile organic compounds are oxidised by the hydroxyl radical (OH) which produces a hydroperoxyl radical (HO_2). HO_2 then reacts with nitric oxide (NO) to form nitrogen dioxide (NO_2). Photolysis of NO_2 produces a ground state atomic oxygen atom which reacts with molecular oxygen (O_2) to form ozone.

Tropospheric ozone is predominantly lost through photolysis or by reactions with hydroxyl and hydroperoxyl radical [145]. Halogenated compounds can also acts as sinks for ozone [48, 222, 259]. Ozone can also be lost through deposition to surfaces [93, 273].

As O_3 is a secondary pollutant, it is essential to consider the concentrations of precursor compounds when developing strategies to reduce O_3 concentrations [209]. O_3 concentrations are generally considered to be "NO_x limited" in regions where VOC concentrations are high and the production of O_3 is limited by the availability of NO_x, and "VOC limited" in regions of high NO_x concentrations where production rates are limited by the concentrations of VOCs (which form the peroxy radicals which are needed to oxidise NO to NO_2) [200, 263]. Introducing policies aimed to reduce O_3 concentrations must therefore take this into account, as reducing the emissions of one precursor compound may not necessarily result in a decrease in O_3 concentration [209]. The sources of the key O_3 precursor compounds are discussed in Sections 1.1.1, 1.1.2 and 1.1.4.

Stratospheric O_3 (formed by the photolysis of oxygen (O_2) by high energy photons [157,233]) may also be transported into the troposphere [105,123,168,232,235], thus further increasing the concentrations of tropospheric O_3. Its long lifetime in the troposphere (several weeks) [71] means that O_3 can travel long distances, including across continents [282]. O_3 concentrations in any given area are therefore governed not only by the local emissions of precursor compounds but also by large scale transport processes [172].

In the stratosphere, O_3 plays a key role in filtering ultraviolet (UV) radiation from the

sun, protecting organisms from damage [203]. In the troposphere, however, O_3 acts as a greenhouse gas and contributes to global warming [7, 172]. It is also a key component of photochemical smog [225,240]. In addition to this, tropospheric O_3 is harmful to vegetation [7,80,234]. It can cause damage to the pigmentation in leaves and a reduction in chlorophyll which results in reduced photosynthesis and hence reduced plant growth [73, 80]. Damage from ozone can therefore significantly reduce crop yields [54, 73, 170, 276]. As well as the effects on crops and vegetation, O_3 is damaging to human health [149, 172, 174]. For the protection of human health, the WHO recommends that mean O_3 concentrations do not exceed 100 μg m^{-3} (51 ppbv) during an 8 hour period [274]. O_3 is a highly reactive oxidant that can inflame the respiratory tract, irritate the eyes, nose and throat, trigger asthma attacks and cause breathing problems and lung disease [149]. In 2017, over 470 000 deaths were attributed to ambient ozone pollution worldwide [174].

1.1.6 Particulate Matter (PM)

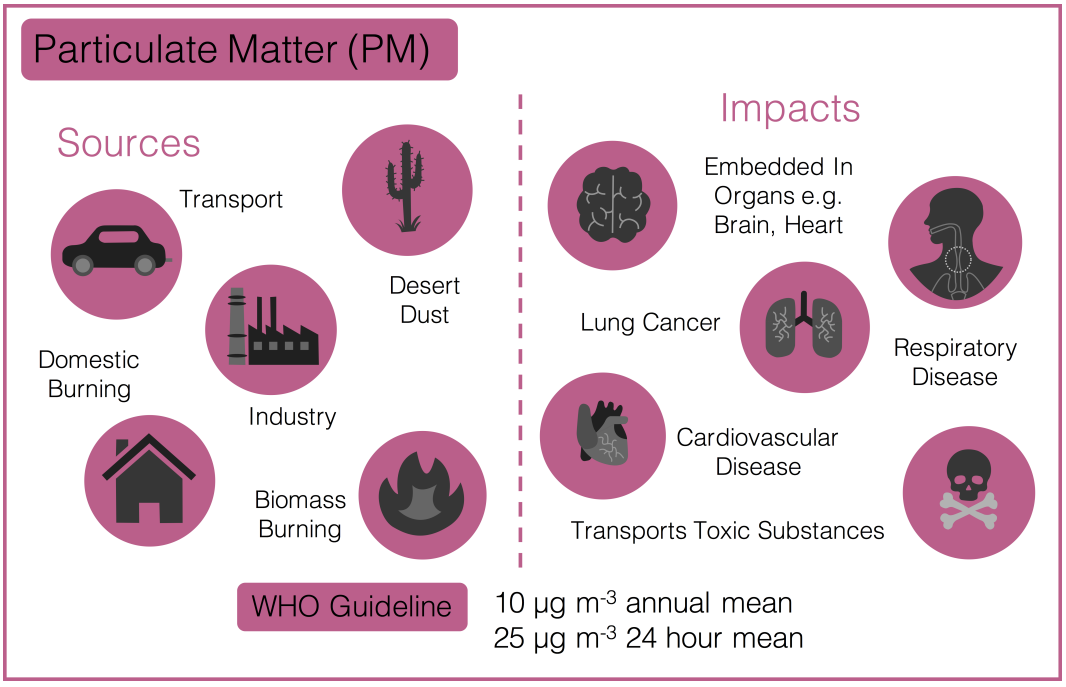

Figure 1.7: Graphic illustrating the sources and impacts of particulate matter (PM).

Particulate matter (PM) includes solid and liquid particles suspended in the atmosphere which come from a range of both natural and anthropogenic sources [2]. It is a complex mixture of components including carbon, inorganic ions, dust, sea salt and water [2, 16].

PM can be released directly from emission sources as well as being formed by secondary production pathways [82, 268]. The major sources of PM vary greatly around the world depending on geographical location and season [176]. In urban areas, the major anthropogenic sources of PM are from domestic burning of wood and coal, energy generation, road transport and industrial processes [62, 140, 176]. Close to deserts, such as the

Sahara, dust can dominate the concentrations of particulate matter [211]. In Africa, Asia and South America biomass burning can play a strong seasonal role in influencing PM concentrations [126, 152, 176]. Other natural sources such as sea salt and volcanic emissions can also contribute to the concentrations in some locations [140, 176]. Secondary PM includes inorganic aerosols such as sulfate ($SO_4{}^{2-}$), nitrate ($NO_3{}^{-}$) and ammonium ($NH_4{}^{+}$) and it is formed in the atmosphere from the reactions of precursor gases including sulfur dioxide, nitrogen oxides and ammonia which themselves are emitted from a wide range of sources [82, 268].

The lifetime of PM in the atmosphere can vary depending on the composition and size; however, the lifetimes are often long (hours to weeks) [71]. The wide array of primary emission sources combined with secondary production pathways and long lifetimes means that transport can play a key role in influencing PM concentrations over wide areas [22].

Particulate matter is commonly classified into different size categories. Fine particulate matter ($PM_{2.5}$) includes particles up to 2.5 microns in diameter whilst coarse particulate matter (PM_{10}) includes particles up to 10 microns in diameter [2, 16, 22]. $PM_{2.5}$ is more damaging to health, as the finer particles can penetrate deeper into the lungs and can enter the circulatory system [2, 33]. $PM_{2.5}$ can be transported around the body where it can become embedded in organs such as the heart and brain [23,63,280]. $PM_{2.5}$ can be harmful both by being toxic itself or by providing a surface for transporting toxic substances within the body [23, 63, 280]. The WHO recommend an annual mean guideline value of 10 μg m^{-3} and a 24 hour mean guideline value of 25 μg m^{-3} for $PM_{2.5}$ in order to minimise the harmful effects on human health [274]. Exposure to high concentrations of $PM_{2.5}$ can cause cardiovascular and respiratory diseases as well as lung cancer, ultimately resulting in a decreased lifespan [23, 63, 64, 280]. Elderly people, young children and pregnant women are most susceptible to the effects of $PM_{2.5}$, along with those who are already suffering from heart and lung conditions [216]. Over 2.9 million premature deaths worldwide were attributed to ambient particulate matter pollution in 2017 [174], making it a significant global concern.

In addition to the impacts on human health, particulate matter can also have a large impact on the climate system [39, 208]. Aerosols in the atmosphere can influence the climate system by scattering light which impacts the radiation balance and leads to a cooling effect [208]. Some components of particulate matter, primarily black carbon, can absorb solar radiation which leads to a warming effect [208]. The aerosols can also interact with cloud micro physical processes and influence cloud albedo and lifetime [208].

1.2 Air quality issues in West Africa and across the world

Whilst these pollutants can be found throughout the world, their concentrations and sources are not uniform. Pollutant concentrations vary greatly depending on geographical location, emission sources and meteorology as well as on the population, industrialisation, urbanisation and economic status of a country [160].

Historically, air quality research has focused on the industrialised regions of North America and Europe [25, 99, 190, 191, 240, 249]; however, over the last decade the emphasis has switched to rapidly developing regions in Asia (notably China and India) [20, 115, 156] with substantial advances in our understanding. Despite a large and rapidly growing population, Africa remains a significantly understudied region for air pollution [136].

Figure 1.8 shows how fine particulate matter ($PM_{2.5}$) observations in West African cities compare to selected cities in Europe and Asia.

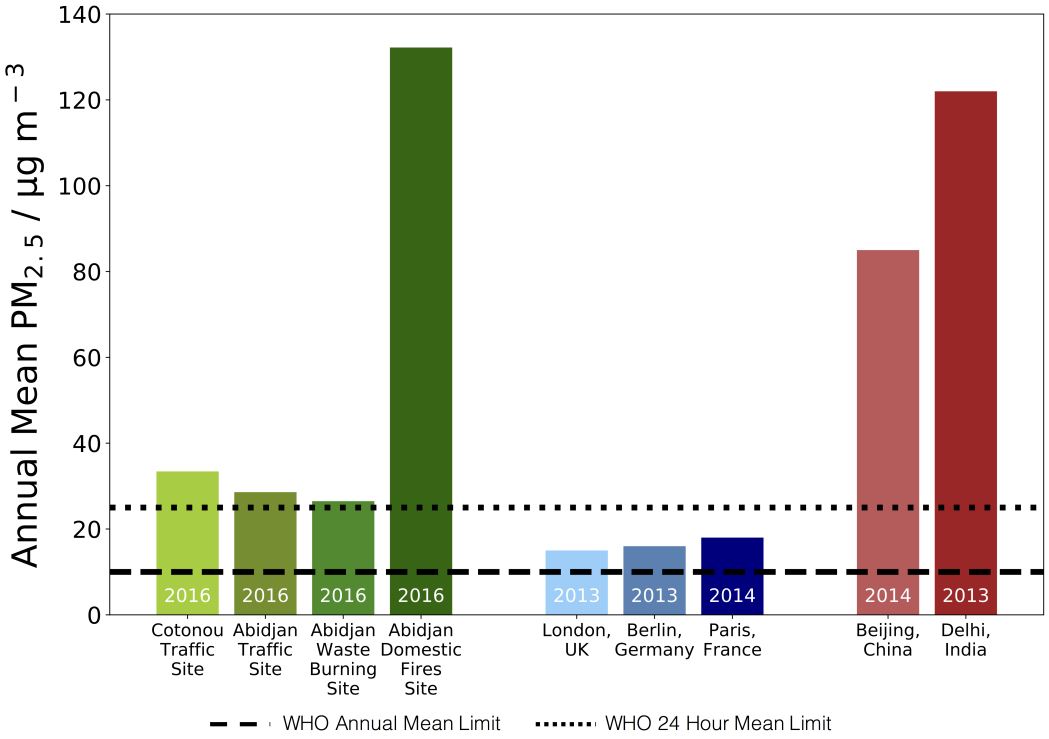

Figure 1.8: Annual mean $PM_{2.5}$ concentrations for four ground sites in West Africa and for major cities in Europe and Asia. Data for Europe and Asia is from the World Health Organisation (WHO) global ambient air quality database [278]. Data for the West African ground sites is from the Dynamics-Aerosol-Chemistry-Cloud Interactions in West Africa (DACCIWA) project [62]. Note that the Abidjan domestic fire site is a semi covered area used for cooking.

Whilst the particulate matter concentrations in the African cities are in general lower than seen for the large Asian cities of Beijing (China) and Delhi (India), they are significantly higher (factor 2) than seen for the European cities of London (UK), Berlin

(Germany) and Paris (France). The World Health Organisation (WHO) guideline values for $PM_{2.5}$ are also indicated in this figure [274]. This data shows that all sites are above the annual mean limit (10 μg m^{-3}), with the sites in West Africa and Asia also above the 24 hour mean limit (25 μg m^{-3}) [37, 132, 160, 176]. Concentrations in the European cities slightly exceed the annual mean guideline value, whereas concentrations at the West African and Asian sites exceed the limit by factors of between around 3 and 13. $PM_{2.5}$ is therefore a significant cause for concern from a human health perspective in these regions. It is important to note that the four measurement sites in West Africa were close to major sources of air pollution: semi covered domestic fires for cooking, waste burning at a landfill site and motor vehicles [62]. These concentrations may therefore be expected to be higher than the typical values experienced across the city and may not be representative of the concentrations experienced by the general population in these areas. More data for West Africa is needed to generate a more accurate representation of the concentrations.

There are many different sources which contribute to pollutant concentrations in West Africa and some examples of these are shown in Figure 1.9. These include anthropogenic sources such as road transport, industry and waste burning as well as natural biogenic emissions from vegetation.

Figure 1.9: Photographs illustrating some of the pollution sources in West Africa including road traffic, residential emissions, waste burning, agriculture, mining, biogenic, shipping and industry. Photographs taken during the Dynamics-Aerosol-Chemistry-Cloud Interactions in West Africa (DACCIWA) aircraft campaign in June-July 2016.

One of the key factors influencing the locations and sources of emissions in West Africa is the location of the population. Figure 1.10 shows the population density across West Africa for the year 2016, extrapolated linearly from gridded population data for 2015 and 2020 from the NASA Socioeconomic Data and Applications Center (SEDAC) [47].

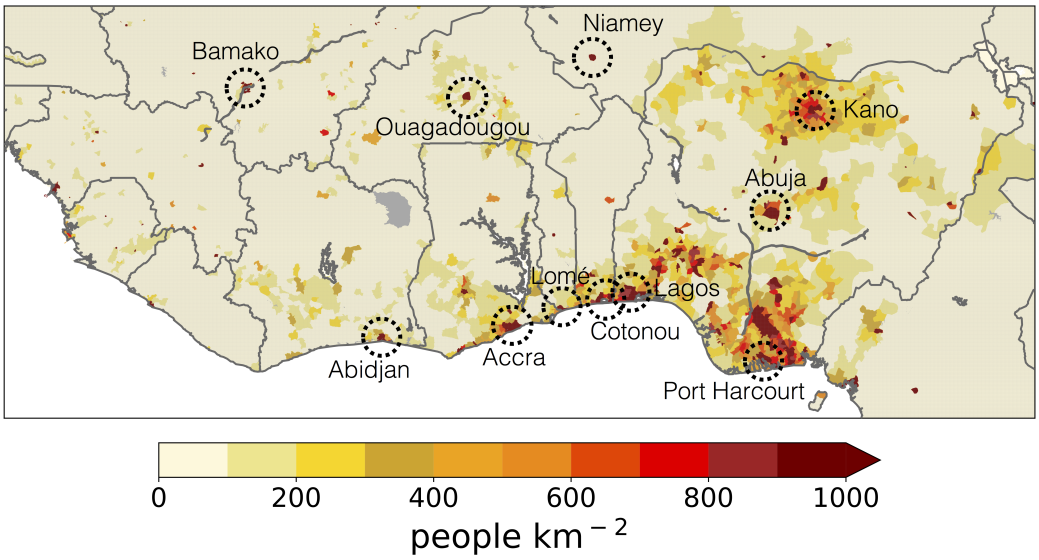

Figure 1.10: Population density map for 2016. Population data from NASA Socioeconomic Data and Applications Center (SEDAC) gridded population of the world (version 4) [47]. Population data for 2015 and 2020 has been linearly interpolated to obtain a population estimate for 2016. Major cities in the region are identified.

The population density in West Africa is highest along the coastline. The major coastal cities contain large port infrastructures therefore emissions from shipping are a key source of pollution along the coastline, particularly along the major shipping lanes and at offshore oil and gas sites [77, 262]. Within the cities themselves, emissions from industries and power stations contribute to pollution as well as emissions from road transport and domestic emissions including wood fired stoves for cooking and burning of waste [62, 151]. Inland from the coast, the population density is generally much lower (except for the Nigerian cities of Abuja and Kano), with large areas of forests and crop land which leads to agricultural emissions as well as natural biogenic emissions from soils and vegetation [98, 113, 116]. To the far north of the region lies the Sahara desert where population density is low.

Anthropogenic emissions are one of the key sources that impact human health as man-made emission sources such as road transport, domestic burning and industries tend to be located close to areas of high population density. Anthropogenic emissions can therefore generally be expected to scale as a function of population [151]. Figure 1.11 shows the projected continental population changes from 2015 to 2100, using data provided by the United Nations (UN) Department of Economic and Social Affairs Population Division [199].

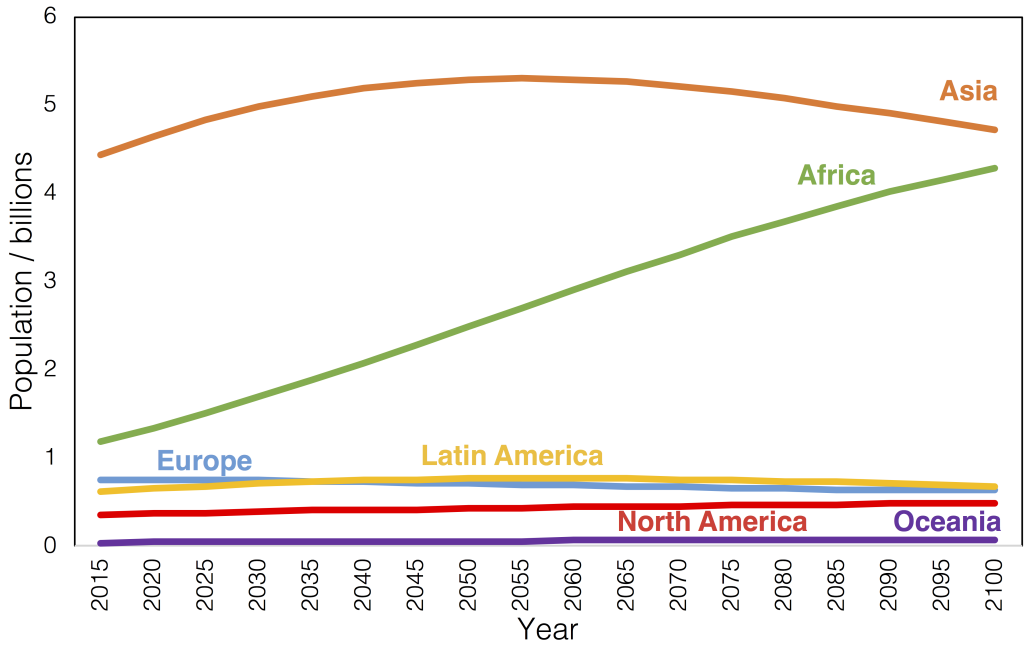

Figure 1.11: Projected continental population changes from 2015 to 2100. Population data from the United Nations Department of Economic and Social Affairs Population Division [199].

The populations of Europe, North America, Latin America and Oceania all remain below 1 billion with no significant changes projected to occur. The population of Asia remains the highest throughout the century but shows a peak in population around the year 2050 and then a fall in the population towards the end of the century. The population of Africa, however, shows a steady rate of increase with the population projected to reach over 4 billion by 2100. A lot of this population increase is expected to occur along the already densely populated coastal region of southern West Africa, in particular in Nigeria which accounts for just less than 50% of the total population growth in West Africa [199].

Although anthropogenic emissions are one of the major sources of pollution worldwide, much of the emphasis of research on African air pollution has focused on its natural sources from desert dust [74, 227], biomass burning [102, 152, 270] and biogenic sources [185], with anthropogenic pollution receiving less attention [23, 162]. Emissions of anthropogenic pollutants in Africa are forecast to rise significantly over the next century [141, 151] as a result of the extensive economic growth and rapid rates of urbanisation and industrial development, together with the increasing population [199]. Much of this development is expected to occur along the West African coastline [199]. Whilst the human health impacts of anthropogenic pollutants have been widely studied throughout the world [63, 149, 172, 174, 202, 261], quantification of the adverse effects on the West African population is difficult without observational data from the region.

An understanding of air quality in the present day is essential for quantifying the impacts on health as well assessing the effects of future changes in emissions and concen-

trations. This understanding is typically achieved through a combination of observational and modelling studies. The observational system over West Africa (as is the case for most of Africa) is limited [219] and, without verification, confidence in computer models is low [91, 158].

Figure 1.12 illustrates the current sparsity of observational data for Africa [184]. An extensive network of measurements can be seen across Europe and North America, as well as across China and India. Measurements for Africa, however, are extremely limited.

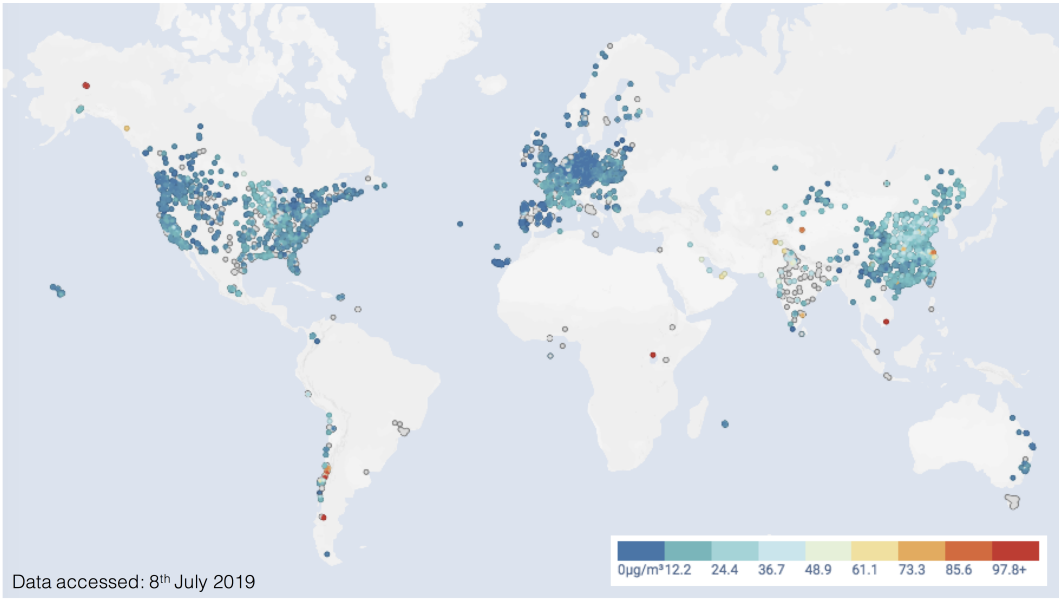

Figure 1.12: Map showing the locations of the most recently reported values of $PM_{2.5}$ concentrations worldwide. Data from OpenAQ [184] accessed on 8th July 2019.

1.3 The Dynamics-Aerosol-Chemistry-Cloud Interactions in West Africa (DACCIWA) project

It is evident that there is a significant lack of understanding and observational data relating to atmospheric composition and air pollution in West Africa. This knowledge gap has been somewhat addressed through the Dynamics-Aerosol-Chemistry-Cloud Interactions in West Africa (DACCIWA) project, funded by €8.75 million from the European Commission's Framework 7 programme [135].

The DACCIWA consortium consisted of partner organisations from both European and West African countries and included operational weather and climate services as well as universities and research institutes [135]. The locations of the DACCIWA partner organisations, along with collaborating institutes, are shown in Figure 1.13.

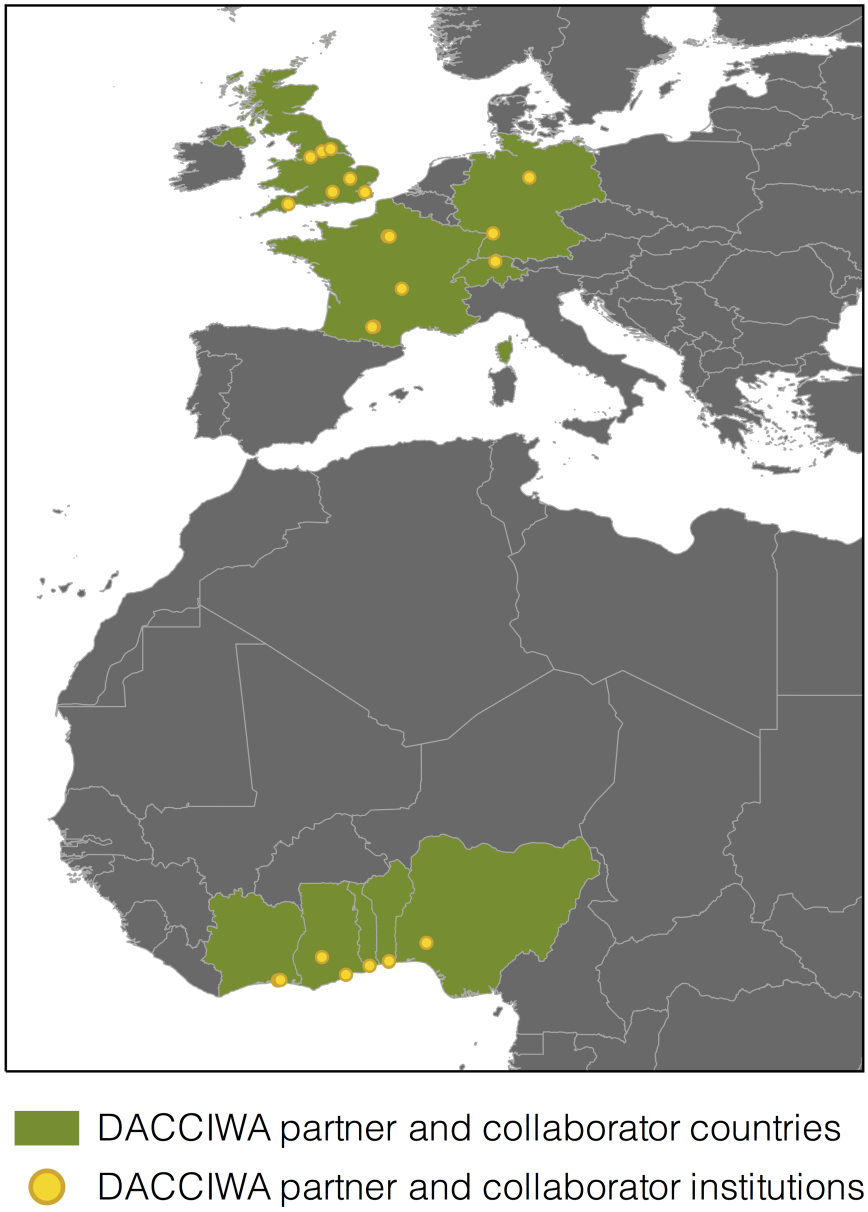

Figure 1.13: Locations of the DACCIWA partners and collaborators.

Whilst previous programmes have investigated atmospheric conditions in West Africa, such as the African Monsoon Multidisciplinary Analysis (AMMA) programme [205], the DACCIWA project has focused, for the first time, on the densely populated southern West African (SWA) coastal region [135,137]. The project aimed to improve scientific knowledge of the region and provide data for use by operational centres and policymakers [135]. In order to achieve this, the project covered seven key scientific areas (work packages):

1. Boundary Layer Dynamics
2. Air Pollution and Health
3. Atmospheric Chemistry

4. Cloud-Aerosol Interactions

5. Radiative Processes

6. Precipitation Processes

7. Monsoon Processes

A final work package covered data management, dissemination of research findings and knowledge transfer to non-academic partners. The different work packages of the DACCIWA project are illustrated in Figure 1.14.

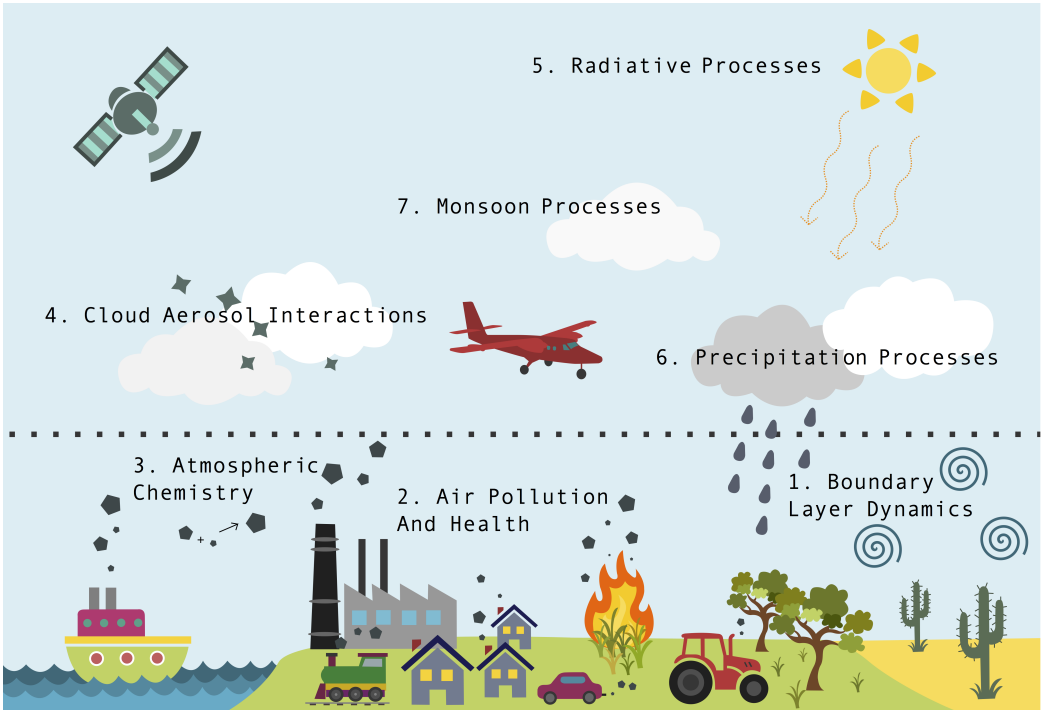

Figure 1.14: Schematic overview of the DACCIWA project, illustrating the different work packages of the programme.

Overall, the individual components of the project aimed to contribute to the following key research objectives [135]:

- Determine the impact of multiple emission sources (natural and anthropogenic), as well as mixing and transport processes, on atmospheric composition during the wet season in southern West Africa.
- Assess the impact of pollutants at the surface (in particular particulate matter and ozone) on human health, ecosystem health and agricultural productivity.
- Quantify two-way aerosol-cloud coupling with a focus on the characteristics and distribution of cloud condensation nuclei and the impact on cloud characteristics and aerosol removal by precipitation.

- Identify the controls on the formation, persistence and dissolution of low-level clouds.
- Identify the meteorological controls on precipitation.
- Quantify the impact of aerosols and clouds on energy and radiation budgets, focusing on the effects of aerosols on cloud properties.
- Evaluate meteorological, chemical and air quality models along with satellite retrievals of precipitation, radiation, clouds and aerosols.
- Analyse the effects of precipitation and cloud radiative forcing on the water budget and West African monsoon circulation.
- Assess the socio-economic impacts of future changes in emissions, climate and land use on human health, ecosystem health, agricultural productivity and water.
- Disseminate key findings to the general public, scientists, operational centres and policymakers.

All modelling studies and data analysis discussed in this thesis predominantly fall into the category of "Atmospheric Chemistry" (work package 3) with the main aims of evaluating and optimising air quality modelling of the West Africa region and assessing the impacts of air quality on human and ecosystem health and agricultural productivity.

As discussed in Section 1.2, one of the major factors limiting atmospheric research in West Africa is a lack of observational data [218]. In order to address this issue, the DACCIWA project conducted a major field campaign during the wet season (June-July) in 2016 [86]. As well as a network of surface based instrumentation [62], the campaign also involved coordinated flights from three research aircraft [86]: the British Antarctic Survey (BAS) DHC-6 Twin Otter, the Deutsches Zentrum für Luft- und Raumfahrt (DLR) Falcon 20 and the Service des Avions Français Instrumentés pour la Recherche en Environnement (SAFIRE) ATR-42. Figure 1.15 gives an overview of the locations of the research flights.

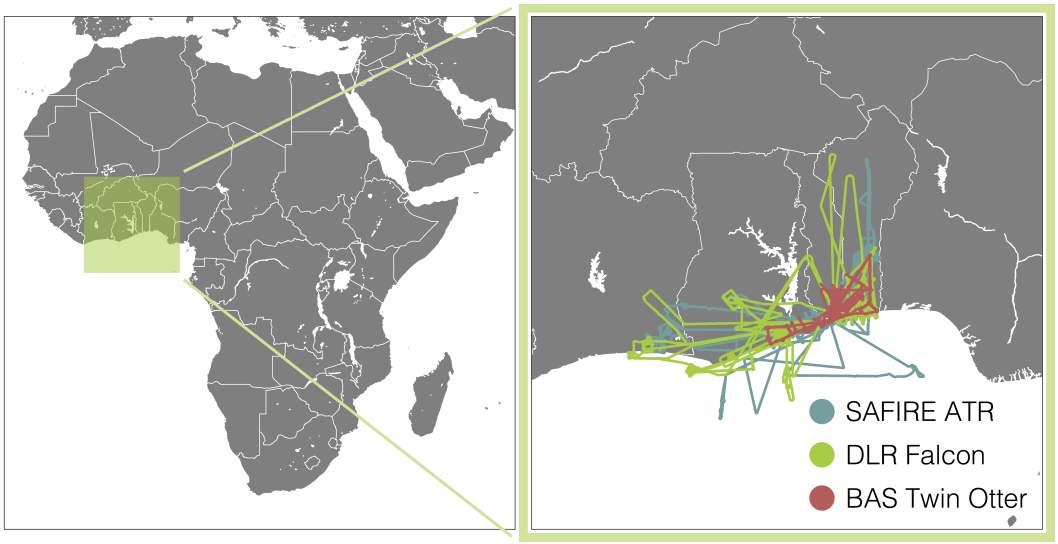

Figure 1.15: Location of the DACCIWA campaign region, showing the flight tracks taken by the three DACCIWA aircraft during the campaign in June-July 2016.

The three aircraft performed 50 research flights during the three week campaign period (29th June to 16th July 2016) and covered areas of Côte d'Ivoire, Ghana, Togo and Benin. Further details of the flight tracks and data collected are given in Chapter 2.

One of the objectives of the research flights was to obtain measurements of air pollution in and around some of the major cities [86,137]. The DACCIWA flight tracks targeted the cities of Abidjan (Côte d'Ivoire), Accra and Kumasi (Ghana), Lomé (Togo) and Cotonou and Savè (Benin). The locations of these cities, along with other key cities in West Africa are shown in Figure 1.16.

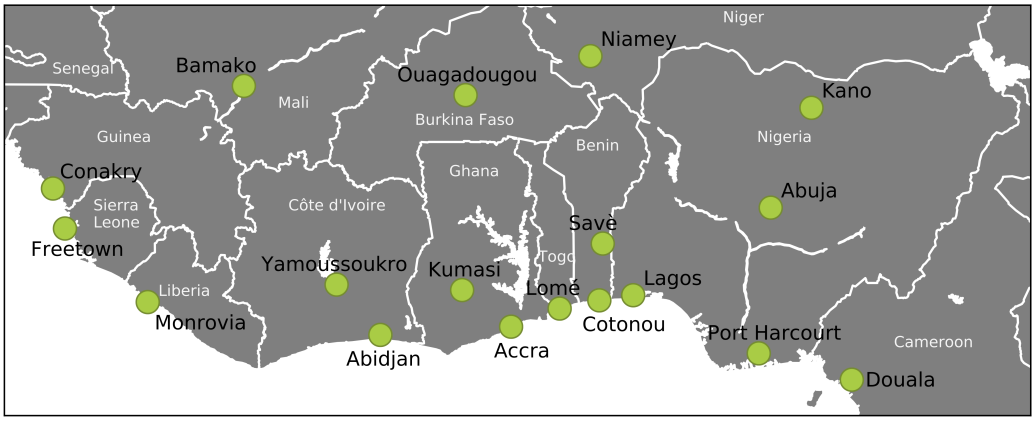

Figure 1.16: Locations of some of the major cities in West Africa.

Each aircraft was equipped with a similar payload of instrumentation for measuring meteorological conditions, chemical concentrations as well as aerosol and cloud properties [86, 137]. Many of the measurements were taken in-situ on board the aircraft; however, some offline analysis of samples collected in flight was also performed.

Figure 1.17 shows the three DACCIWA aircraft (a, b, f and g) as well as the instrumentation on board the Twin Otter aircraft (c and d) and the set up for offline analysis of volatile organic compound (VOC) samples collected in flight (e).

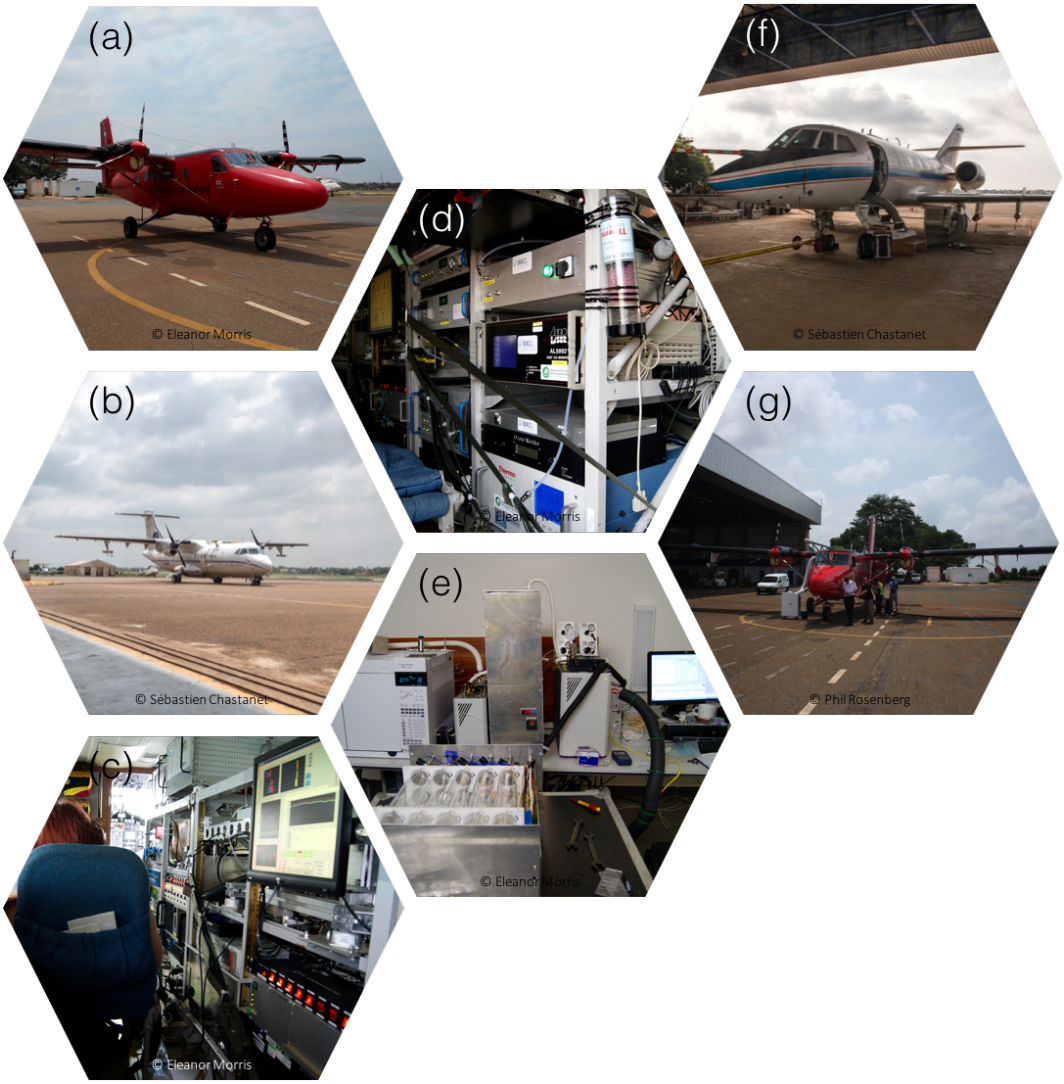

Figure 1.17: Photographs taken during the DACCIWA aircraft campaign: (a) BAS Twin Otter aircraft; (b) SAFIRE ATR aircraft; (c) and (d) instrumentation on board the BAS Twin Otter aircraft; (e) offline analysis of volatile organic compounds from the BAS Twin Otter; (f) DLR Falcon aircraft; (g) BAS Twin Otter aircraft.

The DACCIWA aircraft data set, along with data from the ground based network, provides a unique new set of observations for understanding the atmospheric processes in the region during the wet season [62, 86, 137]. The DACCIWA partners have used this data to address a wide range of research questions and the key findings of the project have been disseminated to governments, operational centres and stakeholders [76].

Despite a large focus of the project being on meteorological conditions, a number of significant conclusions relating to air quality and impacts on human health were found [62,76]. From the measurements that were made during the project, concentrations of fine particu-

late matter ($PM_{2.5}$) pollution were shown to be in exceedance of recommended limits and these concentrations pose substantial risks to public health [62]. Significant uncertainties have also been found in the available emission inventories for the region, resulting in modelling studies being unable to accurately quantify the impacts of air pollution [128]. Whilst the DACCIWA project has greatly expanded the current knowledge and understanding of atmospheric conditions in West Africa, there are still many more research questions to be answered and these largely depend upon the availability of more extensive long term measurements in the region.

1.4 Computer simulations of air quality in West Africa

Despite the ground based and airborne campaign activities of the DACCIWA project, a lack of observational data remains one of the major factors limiting air quality research in West Africa [62, 86, 219]. The observational data sets from the DACCIWA project cover only a small time period and spatial range [86] and therefore little information about long term trends or transport patterns can be inferred from this data. Modelling studies are therefore essential in helping to develop a better understanding of the processes occurring and the concentrations of pollutants across the region. These modelling studies are able to investigate diurnal, seasonal and interannual trends in pollutant concentrations throughout the atmosphere for the entire region of interest. Modelling studies can also be used to test the sensitivity of the atmospheric composition to different sources of pollution and investigate the potential future trends in emissions and the impacts that the resulting concentrations have on the population and environment. The outcomes of modelling studies can be tested using existing observational data as well as new data from across the region as it becomes available. It is important to note that little confidence can be placed in conclusions drawn from modelling activities until simulation data has been evaluated against observations.

Modelling studies of the West Africa region are becoming more common, with researchers investigating both meteorological conditions [3, 38, 56, 68, 83, 101] and chemical composition [36, 55, 60, 104, 111, 169, 186] in the region using a range of different numerical models. These meteorological investigations include modelling rainfall during the West African Monsoon [68], the formation of low-level clouds [3, 101], the impact of aerosols on the cloud formation and atmospheric dynamics in the region [56] and evaluate operational meteorological forecasts [83]. Chemical studies have included evaluating the source, seasonality and spatial variability of aerosols over Africa for use in climate simulations [104, 111], improved modelling of emission sources specific to the region such as gas flaring [55] and assessments of the influence of biomass burning activities on surface level concentrations of pollutants in cities in the Gulf of Guinea [169]. Some of these studies form part of the DACCIWA project and others are the result of the African Monsoon Mul-

tidisciplinary Analysis (AMMA) research project [205]. For all studies of West African atmospheric composition discussed in this thesis, the GEOS-Chem Classic chemical transport model (version 11-01) is used [28, 94]. The model configuration and emissions are discussed in greater detail in Chapter 2; however, the basic model operation is described below.

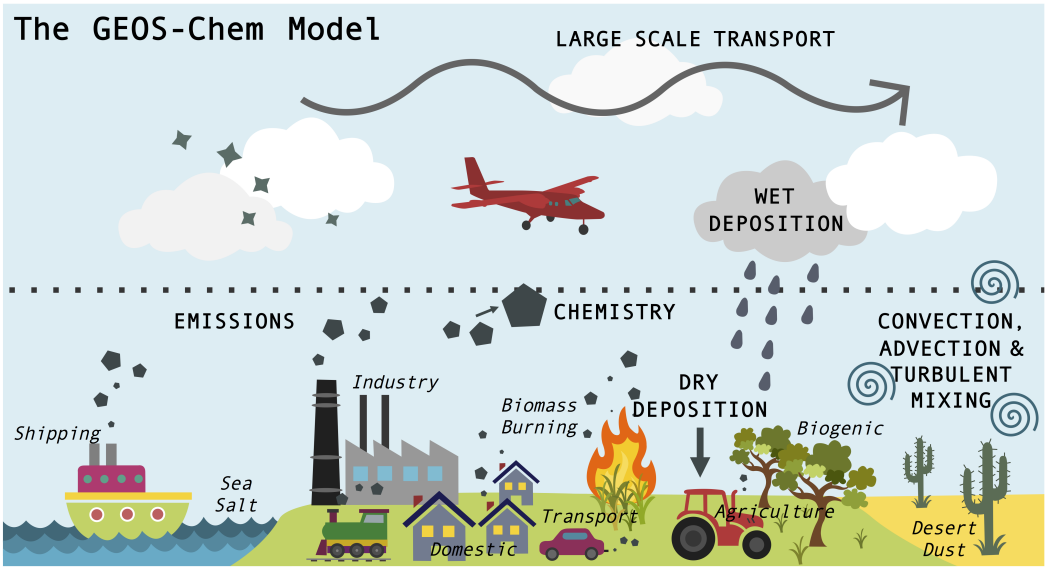

Figure 1.18: Diagram illustrating the key features of the GEOS-Chem atmospheric chemical transport model.

The GEOS-Chem model is a complex atmospheric chemical transport model but it can be considered simply as four key processes: emissions, deposition, transport and chemical reactions. These processes are illustrated in Figure 1.18.

Emissions within the GEOS-Chem model are configured at run time using the Harvard-NASA Emissions Component (HEMCO) module [129]. GEOS-Chem incorporates emissions of primary pollutants from a wide range of sources and this emission module enables many different inventories to be handled and also allows diurnal profiles, scale factors and masks to be easily applied to the inventories.

Standard anthropogenic inventories, such as the EDGAR inventory [70, 182], are available globally and these include sources such as road transport, residential emissions, industrial processes and energy generation. These inventories are superseded in the model by regional inventories containing improved emission data and location specific sources where this data is available. The National Emissions Inventory (NEI) is used over the United States [243], the Criteria Air Contaminants (CAC) inventory is used over Canada [255], the Big Bend Regional Aerosol and Visibility Observational study (BRAVO) inventory is used over Mexico [139], European Monitoring and Evaluation Programme (EMEP) emissions are used over Europe [255] and MIX is used over East Asia [147]. For all other parts of the world the EDGAR inventory is used for anthropogenic emissions [70, 182].

As well as anthropogenic emissions, biomass burning emissions are also included from

the Global Fire Emissions Database (GFED) inventory [9,18,97,204,253]. The Global Fire Assimilation System (GFAS) inventory has also been added to the model and is discussed in detail in Chapter 4 [126]. The model also incorporates emissions of dust [283, 284], sea salt [10, 120], emissions from aircraft [231] and shipping [262], along with biogenic emissions [98,113], soil emissions [116], marine emissions [35,142], volcanic activities [61,85] and lightning [175].

The model includes a detailed O_x-HO_x-NO_x-BrO_x-VOC-aerosol tropospheric chemistry scheme and uses the Kinetic PreProcessor (KPP) chemical solver [51]. This version of the model contains 68 advected chemical tracers and over 500 chemical reactions. Aerosol and gas phase compounds interact through heterogeneous chemistry [119], the effect of aerosol extinction on photolysis rates [166] and gas-aerosol partitioning of semi-volatile compounds. Sulfate (SO_4^{2-}), nitrate (NO_3^-) and ammonium (NH_4^+) aerosols [189], carbonaceous aerosols (BC and OC) [265], dust [78] and sea salt [120] are all included. Although primary organic aerosol is considered in these simulations, secondary organic aerosol is not. Aerosol optical depths are also calculated in the model at user-specified wavelengths [166, 211].

As well as chemical reactions, concentrations of species within the model are influenced by transport and deposition processes. Advection [150], convective transport [279] and boundary layer mixing distribute pollutant concentrations between vertical levels and across horizontal grid boxes. Wet deposition of gases [13] and water soluble aerosols [154] is included, along with scavenging of aerosols by snow [264]. Dry deposition is based on the scheme of Wesely [266, 273]. The dry deposition module includes aerosol deposition [85, 120, 285] as well as gravitational settling of dust [78] and of sea salt [10].

The model computes the changes in atmospheric composition as a result of the emissions, chemistry, transport and deposition for each position in the horizontal and vertical grid for each specified time step. This develops a comprehensive picture of the concentrations of pollutants throughout the atmosphere on a global scale.

The GEOS-Chem model also offers the capability to run higher resolution regional simulations in a nested configuration [267]. This enables the West Africa region to be simulated at higher spatial resolution as well as at higher temporal resolution, thus providing more resolved fine detail on the distribution of pollutants. This in turn enables better quantification of the impacts on specific populations or ecosystems within the region. The newly developed West Africa regional model is described in full in Chapter 2.

1.5 Key research questions for improving current understanding of air quality in West Africa

The purpose of the research presented here is to address the following key questions relating to air quality and atmospheric composition in West Africa:

1. How representative are the default global anthropogenic emission inventories for use in simulations of West African air quality? Are new regional-specific inventories better able to simulate the atmospheric composition? Where are the remaining uncertainties in the inventories?

2. How do the concentrations of policy relevant pollutants change throughout the year? Are the concentrations of these pollutants within the guidelines recommended by the World Health Organisation? What is the impact on the population and ecosystems from concentrations in exceedance of these guidelines?

3. How is air quality in West Africa influenced by emissions from biomass burning? What are the seasonal variations in location and magnitude of the biomass burning emission sources as well as transport patterns? What is the interannual variability in biomass burning events?

These questions are all addressed through the framework of the regional GEOS-Chem model for West Africa in subsequent chapters.

Chapter 2

Evaluation and optimisation of the emission inventories for simulations of atmospheric composition in West Africa using the regional GEOS-Chem model

Emission inventories are databases which contain information on the quantities and sources of air pollutants emitted into the atmosphere over a given time period. They are an essential component of atmospheric models and the accuracy with which atmospheric composition can be simulated is highly dependent upon the emission inventories used. In order to accurately simulate the system, the inventories must be representative of both the magnitude and location of a range of emission sources for each species.

Simulations of the atmosphere over West Africa have historically been dependent on emission inventories developed from a global perspective; however, continent-specific regional inventories are now also becoming available [128,151,163]. The GEOS-Chem model is used here in a regional configuration to evaluate the emission estimates from both global and regional anthropogenic inventories. Using aircraft observations from the DACCIWA campaign, the anthropogenic and biomass burning emission estimates are also optimised to produce enhanced agreement for the West Africa region.

It is important to note that this assessment of the emission inventories uses only aircraft data collected during a 3 week period in a single year (2016). The recommended adjustments to the anthropogenic and biomass burning inventories discussed here are therefore likely only valid for this time of year and for the area covered by the research flights. A long term observational data set is required in order to fully assess the uncertainties in the inventories and determine whether the scale factors calculated here hold true outside the DACCIWA operational period.

2.1 Development of a regional GEOS-Chem model for West Africa

GEOS-Chem is a global, three dimensional chemical transport model [94], driven by assimilated meteorological data from the Goddard Earth Observation System (GEOS) of the NASA Global Modeling and Assimilation Office (GMAO) [28]. All simulations performed in this work use GEOS-Chem Classic version 11-01. The model contains an O_x-HO_x-NO_x-BrO_x-VOC chemistry scheme and a mass based aerosol module which advects sulfate (SO_4^{2-}), nitrate (NO_3^-), ammonium (NH_4^+), sea salt, dust, organic carbon (OC) and black carbon (BC) aerosols [119, 166, 189]. The model version used here includes primary organic carbon aerosol with no secondary organic aerosol (SOA) generation. The model also includes advection and convective transport [150, 279] as well as wet and dry deposition [13, 154, 266, 285].

Global model simulations are run at a horizontal resolution of 2° × 2.5° and 47 vertical levels from the ground up to 0.01 hPa. For the West African region, the model grid boxes at this resolution are equivalent to approximately 200 km × 250 km. These coarse global model simulations are therefore unable to provide any fine detail of the atmospheric composition in the region; however, the computational cost of increasing the resolution globally is great.

In addition to the standard global simulations, the GEOS-Chem model can also be run in a nested configuration [267]. The nested version of the model allows higher resolution, regional simulations to be performed using boundary conditions from coarser global simulations. Several nested grid regions are currently integrated into the standard GEOS-Chem model, covering North America, Europe, China and South East Asia. For this work, an additional nested grid for the West Africa region has been added to the model. The West Africa nested grid covers a domain from 6 °S to 16 °N and 18.123 °W to 26.875 °E at a horizontal resolution of 0.25° × 0.3125° (Figure 2.1(b)), which equates to approximately 25 km × 30 km resolution in this region. All nested simulations in this work use 1-way nesting; boundary conditions for West Africa are generated from global model simulations at a horizontal resolution of 2° × 2.5°, with no influence from the nested domain back onto the global domain. Global simulations use meteorological input from the Modern-Era Retrospective analysis for Research and Applications Version 2 (MERRA-2), whilst regional simulations use GEOS Forward Processing (GEOS-FP) meteorology. MERRA-2 is a reanalysis data set, produced at a native resolution of 0.5° × 0.625° (regridded to the 2° × 2.5° resolution for global simulations) which is produced from 1979 to present day. GEOS-FP is a "forward processing" operational meteorological product, produced at a higher native resolution of 0.25° × 0.3125° from 2012 to present day. Both data sets use the GEOS Data Assimilation System; however, GEOS-FP is an operational data stream with inconsistencies in the data assimilation system version throughout the data

set whereas the MERRA-2 reanalysis uses a consistent data assimilation system, incorporating more than 30 years of assimilated data. A limitation of the MERRA-2 data set is that the native resolution of 0.5° × 0.625° means it is unsuitable for use in the higher resolution resolution simulations at 0.25° × 0.3125°.

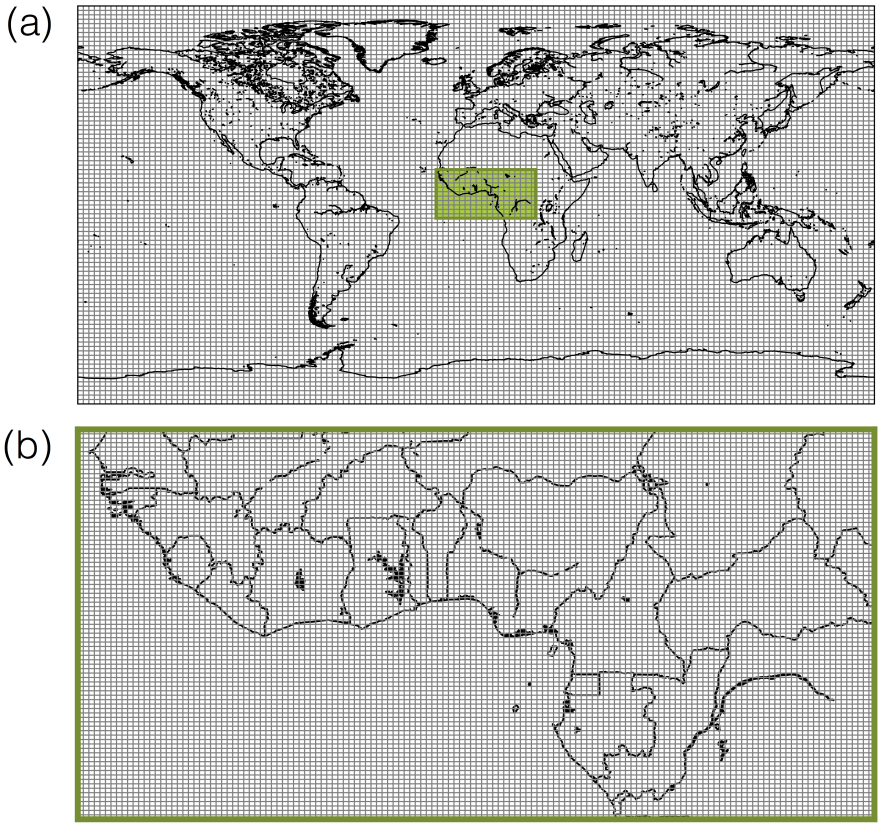

Figure 2.1: Domains and resolutions used by the model: (a) global model domain illustrating the horizontal model resolution of 2° × 2.5° and the location of the West Africa regional model domain (green); (b) West Africa regional model domain illustrating the horizontal model resolution of 0.25° × 0.3125°.

Whilst model data is available for the entire West Africa domain (Figure 2.1(b)), two key areas are considered in this work (Figure 2.2). Firstly, the "DACCIWA region", which is considered as the area covering Côte d'Ivoire, Ghana, Togo and Benin from 4.5 °N to 11.0 °N and 8.5 °W to 3.0 °E. The research flights performed by the three DACCIWA aircraft lie within this domain and hence this is the region for which there are aircraft observations for evaluating and constraining the model. Secondly, the "Guinea region", which is considered as the area from Senegal in the west to Cameroon in the east and from just south of the West African coastline to the southern edge of the Sahara. This region covers a domain from 3.0 °N to 15.0 °N and 15.0 °W to 15.0 °E and is used for an assessment of the whole coastal region, rather than the more local DACCIWA operational area.

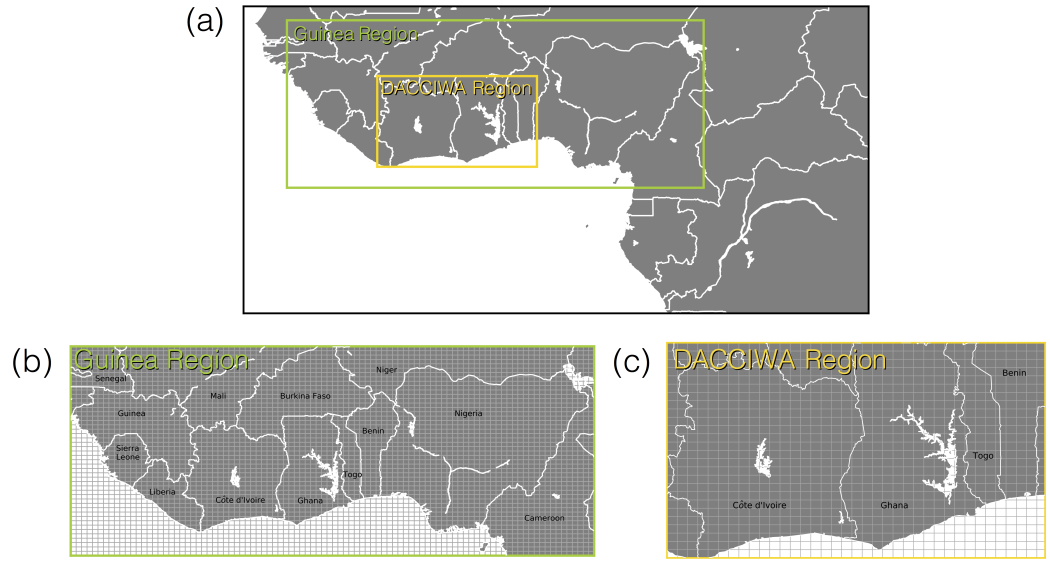

Figure 2.2: Location of the Guinea and DACCIWA regions of interest: (a) map of West Africa highlighting the locations of these two regions of interest; (b) Guinea region (3 °N - 15 °N; 15 °W - 15 °E) with regional horizontal model resolution of 0.25° × 0.3125° overlaid; (c) DACCIWA region (4.5 °N - 11 °N; 8.5 °W - 3 °E) with regional horizontal model resolution of 0.25° × 0.3125° overlaid.

The terms "DACCIWA region" and "Guinea region" are used throughout this work to refer to the areas defined above.

2.2 Anthropogenic emission inventories for West Africa

Representative emission inventories are essential for producing accurate simulations of atmospheric composition. The emission inventories need to be representative of both the location and magnitude of the emission sources for each of the individual emitted species. Both the default global anthropogenic inventories, and an Africa-specific anthropogenic inventory are evaluated here and these emissions are further optimised for the DACCIWA region using airborne measurements from the DACCIWA campaign.

2.2.1 Global anthropogenic emission inventories

The default anthropogenic emissions for West Africa in GEOS-Chem are from global emission inventories. Emissions of carbon monoxide (CO), nitric oxide (NO) and sulfur dioxide (SO_2) are from the Emissions Database for Global Atmospheric Research (EDGAR) version 4.2 [70, 182], emissions of black carbon (BC) and organic carbon (OC) are from the BOND inventory [29, 141] and emissions of non-methane volatile organic compounds (NMVOCs) are from the RETRO inventory [112]. The EDGAR inventory provides annual emission data from 1970 to 2008 at a horizontal resolution of 0.1° × 0.1°, whilst the BOND and RETRO inventories both provide monthly emission data for the year 2000

with BOND at a horizontal resolution of 1° × 1° and RETRO at a horizontal resolution of 0.5° × 0.5°. All three of these inventories are therefore significantly outdated for simulations of the DACCIWA campaign year (2016) and the coarser spatial resolutions of the BOND and RETRO inventories makes them unsuitable for the high resolution regional simulations of West Africa. In addition to this, these global emission inventories lack emission sources specific to the West Africa region such as biofuel cooking in homes, domestic waste burning, oil extraction and flaring [55, 62, 151]. Emission factors are used to relate activities to the quantity of pollutant released into the atmosphere; however, the lack of observational data relating to emission factors in West Africa could also lead to inaccurate emission estimates.

2.2.2 Africa-specific regional anthropogenic emission inventories

The Africa-specific DACCIWA anthropogenic emission inventory [125, 135], developed as part of the DACCIWA project, provides emissions of CO, NO, SO_2, BC, OC and NMVOCs from 1990 to 2015 at a horizontal resolution of 0.125° × 0.125°. This inventory has been constructed using emission data specific to the continent and incorporates sources not included in the EDGAR inventory such as flaring, domestic waste burning and wood burning cook stoves in homes. The mean annual emissions from the DACCIWA inventory for 2015 are displayed in Figure 2.3.

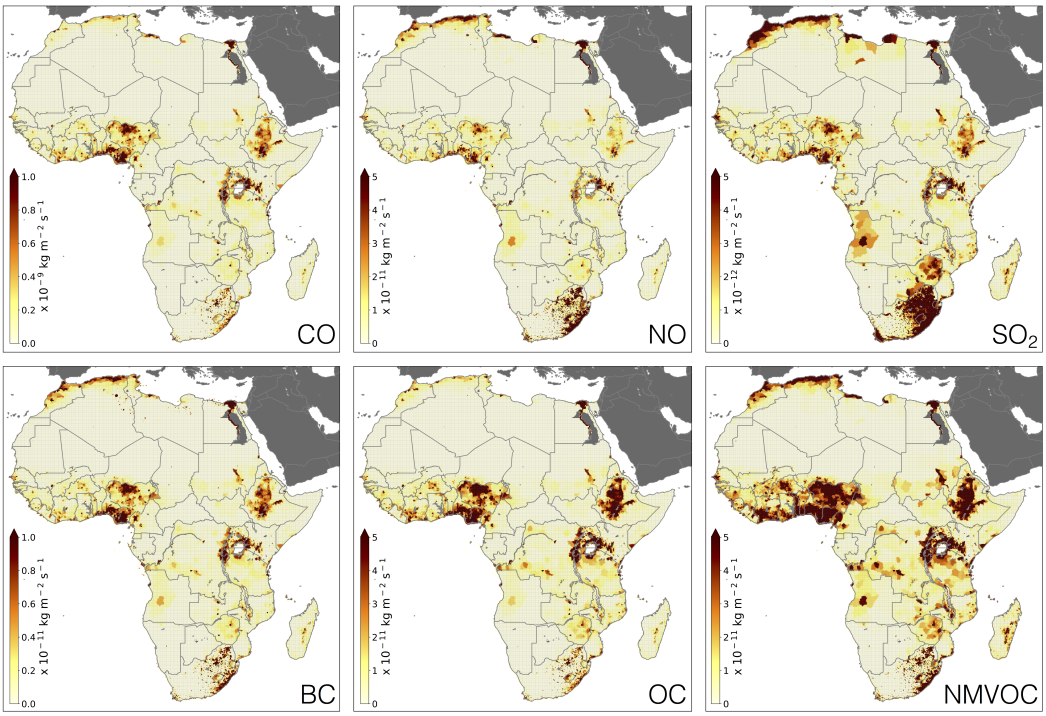

Figure 2.3: Mean annual African anthropogenic emissions for the year 2015 from the DACCIWA emission inventory at a horizontal resolution of 0.125° × 0.125°.

The distribution of emissions across the continent is similar for all species (following

population), with the highest emissions generally seen along the northern coastline of Morocco and Algeria, the countries surrounding Lake Victoria, South Africa and the West African coastline (but most prominently Nigeria). These maps clearly highlight West Africa as a region of significant anthropogenic activity. In order to quantify the regional contribution to anthropogenic emissions in Africa, the continent can be divided into five zones: north Africa (15 °N - 39 °N; 19 °W - 55 °E), west Africa (0 °N - 15 °N; 19 °W - 15 °E), east Africa (0 °N - 15 °N; 15 °E - 55 °E), central Africa (15 °S - 0 °N; 19 °W - 55 °E) and south Africa (37 °S - 15 °S; 19 °W - 55 °E). The mean annual emissions for 2015 for each of these regions are compared in Figure 2.4, along with the 2016 population data for each of the regions. Population data is from the NASA Socioeconomic Data and Applications Center (SEDAC) gridded population of the world data set (version 4) [47]. Population data for 2015 and 2020 has been linearly interpolated to obtain a population estimate for 2016.

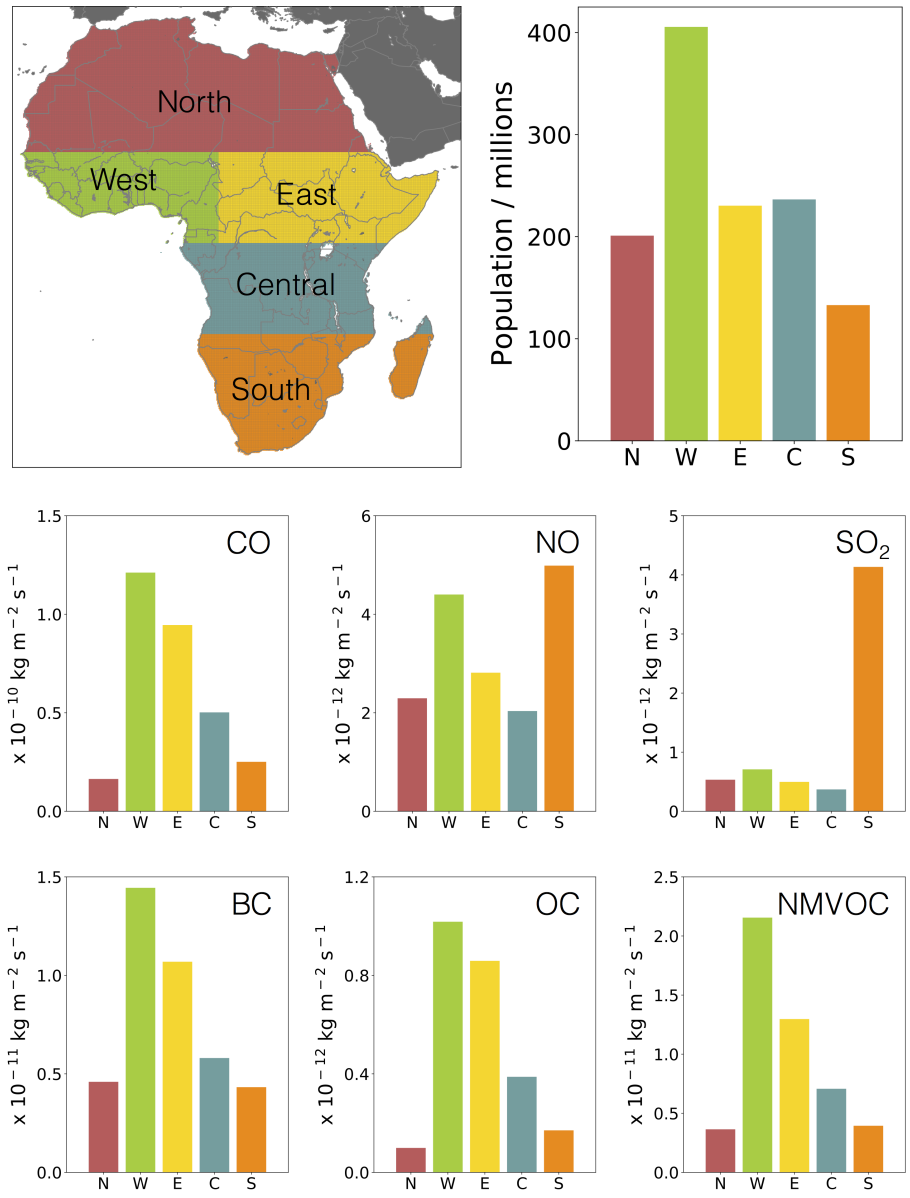

Figure 2.4: Regional populations and mean annual anthropogenic emissions from the DACCIWA emission inventory. The African continent is divided into five regions: north Africa (15 °N - 39 °N; 19 °W - 55 °E); west Africa (0 °N - 15 °N; 19 °W - 15 °E); east Africa (0 °N - 15 °N; 15 °E - 55 °E); central Africa (15 °S - 0 °N; 19 °W - 55 °E); south Africa (37 °S - 15 °S; 19 °W - 55 °E). DACCIWA emission data is for the year 2015, population data is for the year 2016.

With the exception of NO and SO_2, emissions from the western African region are found to be the highest (reflecting population), highlighting West Africa as an area of large anthropogenic activity. Emissions of NO and SO_2 in southern Africa are higher as a result of significant energy generation from coal fired power stations [40, 50, 58, 59]. Figure 2.4 therefore further emphasises the importance of developing a better knowledge and understanding of the atmospheric composition in this region, and the impact that pollutant concentrations have on the population.

As well as providing the total emissions of a given species, the DACCIWA inventory

also contains a breakdown of the emissions from residential, traffic, industry, waste, energy, flaring and other anthropogenic sources. The source composition of each emission species for the Guinea region is shown in Figure 2.5.

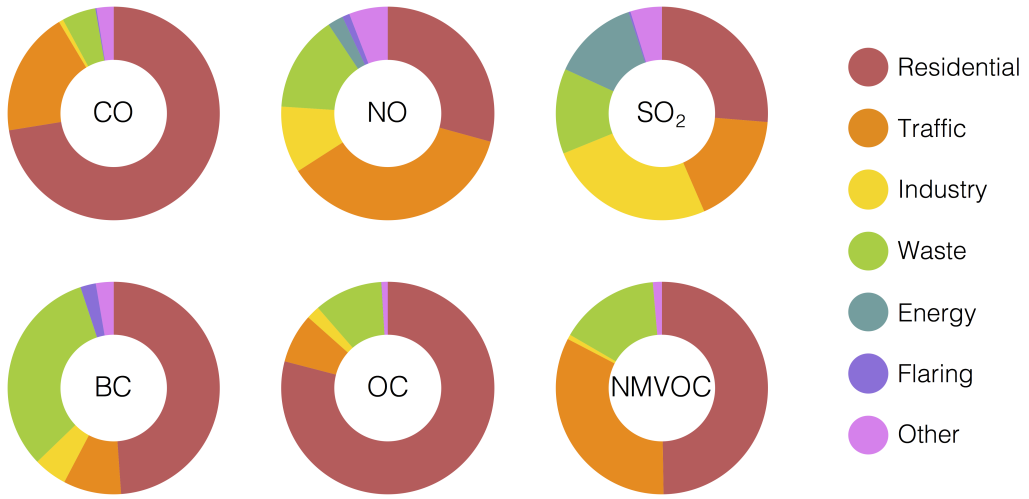

Figure 2.5: Fractional contribution of different sources to the total emissions of CO, NO, SO_2, BC, OC and NMVOCs for the Guinea region (3 °N - 15 °N; 15 °W - 15 °E). Emission data is from the DACCIWA anthropogenic inventory for the year 2015.

For CO, OC and NMVOCs, the largest emission source in the region from the inventory is residential activities, followed by traffic and waste, with much smaller contributions from other sources. Residential and traffic emissions are also the largest sources of NO; however, there are substantial contributions from industry, waste and other sources as well as small contributions from energy and flaring activities. BC emissions are dominated by residential and waste sources with smaller fractions from traffic, industry, flaring and other sources. For SO_2, the largest emission sources are residential and industry, with traffic, waste and energy also making up large fractions of the total emission along with smaller contributions from flaring and other sources.

It is evident from the species source breakdowns that policy options for regulating emissions and reducing pollutant concentrations in the region will vary depending upon the species being considered. Although, residential, traffic and waste appear to be key emission sources for all species.

The DACCIWA inventory contains anthropogenic NMVOC emissions which can be used to replace the global RETRO emissions over Africa. These emissions need to be speciated to incorporate them into the model. The EDGAR v4.3.2 inventory contains emissions of 25 individual NMVOC species [114]. For the year 2012 (the most recent year of EDGAR v4.3.2 emission data), the mean fractional contribution of each individual species to the total NMVOC emission in the EDGAR inventory has been calculated for the African continent and these speciation fractions have been applied to the DACCIWA inventory in

order to separate the lumped NMVOCs into GEOS-Chem species. The speciation factors applied to the DACCIWA inventory are detailed in Table 2.1.

Table 2.1: Speciation factors applied to the DACCIWA anthropogenic lumped NMVOC emissions in order to assign the emissions to species within the GEOS-Chem model.

EDGAR Species	Molecular Formula	GEOS-Chem Species	NMVOC Speciation Scale Factor
Ethane	C_2H_6	C2H6	0.030
Propane	C_3H_8	C3H8	0.042
Butanes	C_4H_{10}	ALK4	0.059
Pentanes	C_5H_{12}	ALK4	0.031
Hexanes and higher alkanes	C_nH_{2n+2} (n $\geq$ 6)	ALK4	0.097
Propene	C_3H_6	PRPE	0.013
Isoprenes	C_5H_8	ISOP	0.00043
Methanal (formaldehyde)	CH_2O	CH2O	0.056
Other alkanals (aldehydes)	R-CHO	ALD2	0.12
Alkanones (ketones)	R-C(=O)-R'	ACET	0.069
Benzene (benzol)	C_6H_6	BENZ	0.023
Methylbenzene (toluene)	C_7H_8	TOLU	0.023
Dimethylbenzenes (xylenes)	$C_6H_4(CH_3)_2$	XYLE	0.018
Trimethylbenzenes	$C_6H_3(CH_3)_3$	XYLE	0.0039
Other aromatics	C_nH_{2n-6}	XYLE	0.042
Monoterpenes	$C_{10}H_{16}$	MONX	0.0013
Other	-	-	0.37

"Other" refers to speciated EDGAR VOCs such as alcohols, acids and esters which are not currently considered as emissions by the GEOS-Chem model.

2.2.3 Additional emission inventories

In addition to the anthropogenic emission inventories for West Africa, global simulations use regional inventories for other parts of the world where this data is available. Over the United States the National Emissions Inventory (NEI) is used [243], the Criteria Air Contaminants (CAC) inventory is used over Canada [255], the Big Bend Regional Aerosol and Visibility Observational study (BRAVO) inventory is used over Mexico [139], European Monitoring and Evaluation Programme (EMEP) emissions are used over Europe [255] and MIX is used over East Asia [147]. For all other parts of the world the EDGAR inventory is used for anthropogenic emissions [70, 182].

Biogenic emissions of VOCs use the Model of Emissions of Gases and Aerosols from Nature (MEGAN) inventory [98, 113], biogenic soil emissions of NO are from Hudman et al. [116] and NO from lightning is described by Murray et al. [175]. Aircraft emissions are from the Aviation Emissions Inventory Code (AEIC) [231], and shipping emissions of

SO_2, CO and NO are also included [262]. The model also incorporates marine emissions of dimethyl sulfide (DMS) [35, 142] as well as volcanic emissions of SO_2 from the Aerosol Comparisons between Observations and Models inventory (AEROCOM) [61, 85]. Dust follows the work of Zender et al. [283, 284], sea-salt of Alexander et al. and Jaeglé et al. [10,120], natural emissions of ammonia (NH_3) are from the Global Emissions InitiAtive (GEIA) and global biofuel emissions of OC and BC are from the BOND inventory [29,144].

Biomass burning emissions use the Global Fire Assimilation System (GFAS) emissions from the European Centre for Medium-Range Weather Forecasts (ECMWF) [126] and these emissions are discussed in greater detail in Chapter 4.

The impact of these emissions on the concentrations of pollutants over Africa is now explored.

2.3 Spatial distribution of pollutant concentrations during the DACCIWA campaign

The spatial distribution of primary pollutants across the continent is largely dependent upon the location of the polluting activities, transport patterns and species lifetimes.

As pollutant concentrations are strongly influenced by the meteorology, a basic understanding of the meteorological conditions in the region is required. During the campaign period (29th June to 16th July 2016), the prevailing winds were from the south / south east to the north west, bringing air masses from the Gulf of Guinea across the West Africa region (Figure 2.6). This follows the monsoonal annual cycle discussed in Section 3.1.1 of Chapter 3. There was also a band of rainfall over the land along the West African coastline [12, 68, 194].

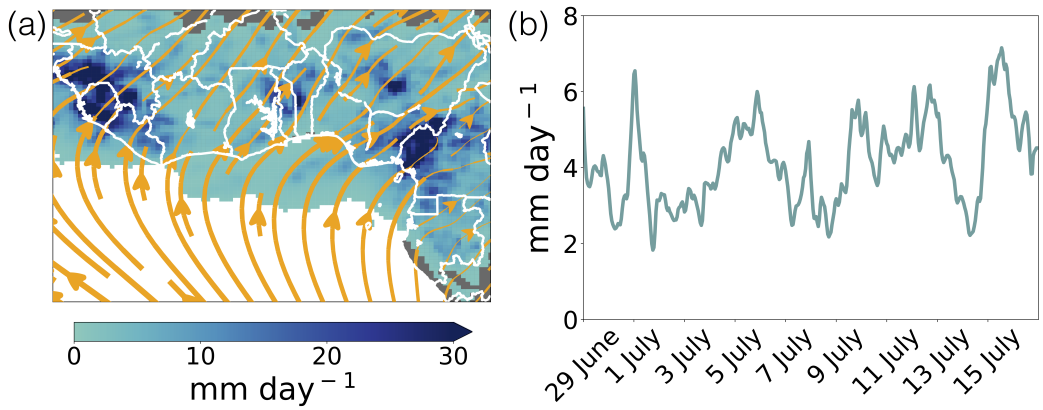

Figure 2.6: (a) mean precipitation rates and surface wind stream functions in West Africa during the DACCIWA aircraft campaign. GEOS-FP meteorological data averaged for 29th June to 16th July 2016. Precipitation rates below 1 mm day^{-1} are masked (b) timeseries of mean precipitation in the region during the DACCIWA campaign from the GEOS-FP meteorological data displayed in (a).

In addition to evaluating the model performance for pollutant concentrations, a simple evaluation of simulated meteorology can be done using some of the meteorological measurements collected on board the aircraft. Figure 2.7 shows the comparison between aircraft measurements and model data for temperature and wind speed from the DACCIWA campaign.

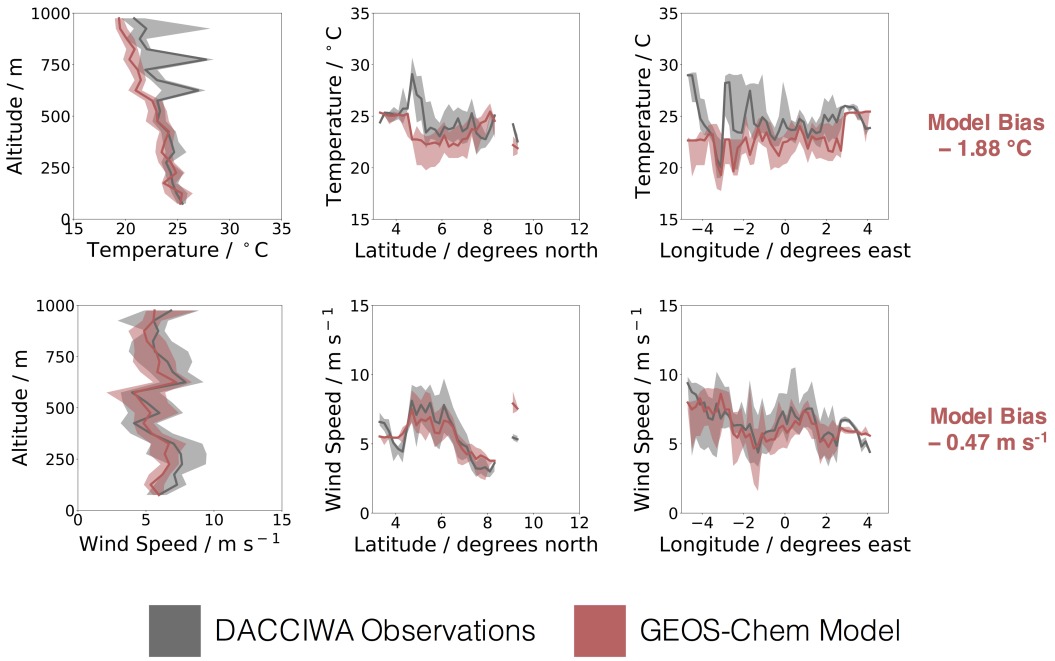

Figure 2.7: Vertical, latitudinal and longitudinal profiles of aircraft meteorological observational data (grey) and simulated meteorological data (red). Solid lines represent the median, shaded areas represent the 25th to 75th percentile range. All data is from altitudes below 1 km.

There is strong agreement between the model and observations for both temperature and wind speed with model biases of -1.88 ^{o}C and -0.47 m s^{-1} respectively. Whilst this provides some confidence in the representation of the meteorological conditions in the model, a more detailed analysis would be required to fully evaluate the simulated meteorology for West Africa in the GEOS-Chem model.

Figure 2.8 shows the mean surface concentrations of key pollutants during the campaign period (29th June to 16th July 2016) for the African continent (2° × 2.5° horizontal resolution) and for West Africa (0.25° × 0.3125° horizontal resolution) calculated using the GEOS-Chem model. These simulations use the default global EDGAR / BOND / RETRO inventories for anthropogenic emissions.

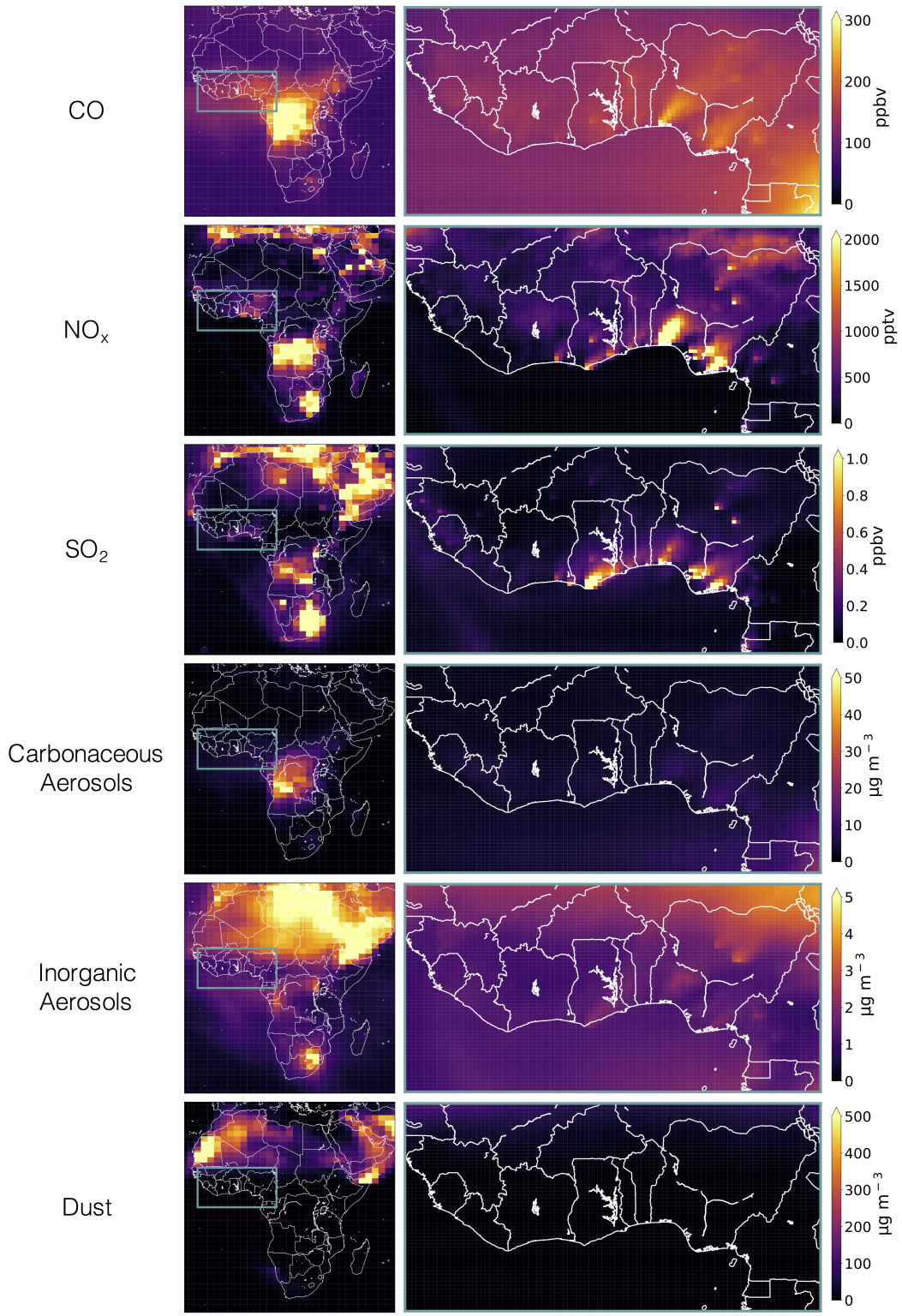

Figure 2.8: Mean surface concentrations of CO, NO_x, SO_2, carbonaceous aerosols (OC + BC), inorganic aerosols ($SO_4^{2-} + NH_4^+ + NO_3^-$) and dust averaged over the DACCIWA campaign period (29th June 2016 to 16th July 2016). Left-hand panel shows the African continent at 2° × 2.5° horizontal resolution, right-hand panel shows the West Africa region at 0.25° × 0.3125° horizontal resolution. This simulation uses anthropogenic emissions from the EDGAR, BOND and RETRO inventories.

Anthropogenic sources of pollutants are evident for species such as CO, NO_x and SO_2.

High concentrations are visible over the industrialised regions of South Africa, along the coastal cities of southern West Africa, around the Mediterranean and over the Arabian peninsula. For SO_2, elevated concentrations as a result of shipping can also be seen over the ocean. Inorganic aerosols are visible from the industrialised regions of South Africa and over the Sahara and Arabian deserts where their lifetimes are extended due to a lack of rainfall.

In June-July, the largest biomass burning activities on the continent occur in central Africa, whilst burning activities in West Africa are limited due to rainfall [21, 96, 212]. Biomass burning acts as a significant source of CO, NO_x, SO_2 and carbonaceous aerosols [126,152]. NO_x and SO_2 have relatively short lifetimes in the atmosphere [71] and therefore the elevated concentrations of these species are seen only in the vicinity of the burning activities. CO and carbonaceous aerosols are longer lived [71] and therefore the prevailing winds transport these species from central Africa across the Gulf of Guinea where they contribute to the surface concentrations along the West African coastline [102, 137].

High dust concentrations are located over the Sahara and Arabian deserts. During the DACCIWA campaign period, there are low concentrations along the West African coastline, largely due to the prevailing south westerly winds preventing southwards transport of the dust into the region (Figure 2.6).

Some of these continental scale features are visible on the regional scale; however, the dominant feature over southern West Africa at this time of year are the anthropogenic sources. Plumes of CO, NO_x and carbonaceous aerosols are visible moving from the coastal cities north eastwards inland, reflecting the prevailing wind direction [137]. Despite limited biomass burning in the domain, transport of CO and carbonaceous aerosols from biomass burning in central Africa gives an elevated background.

It is evident from this initial model analysis that there are many factors contributing to the concentrations of pollutant species in West Africa and one of the most significant factors is the location and magnitude of the emission sources. It is therefore critical for accurate modelling studies to ensure that the emission inventories are providing representative estimates.

2.4 Evaluation of the emission inventories for West Africa

Airborne measurements, taken during the DACCIWA aircraft campaign in June-July 2016, are used to evaluate the emission inventories for West Africa. Three research aircraft were involved in the DACCIWA aircraft campaign, based out of Lomé (Togo), with science flights taking place from 29th June 2016 to 16th July 2016 inclusively [86, 135, 137]. The British Antarctic Survey (BAS) DHC-6 Twin Otter, the Deutsches Zentrum für Luft- und Raumfahrt (DLR) Falcon 20 and the Service des Avions Français Instrumentés pour

la Recherche en Environnement (SAFIRE) ATR-42 performed a combined total of 50 research flights and collected data covering an area from 3.3 °N to 11.0 °N and 4.7 °W to 4.0 °E, flying at altitudes of up to 13 km [86]. The flight profiles of the three aircraft are shown in Figure 2.9.

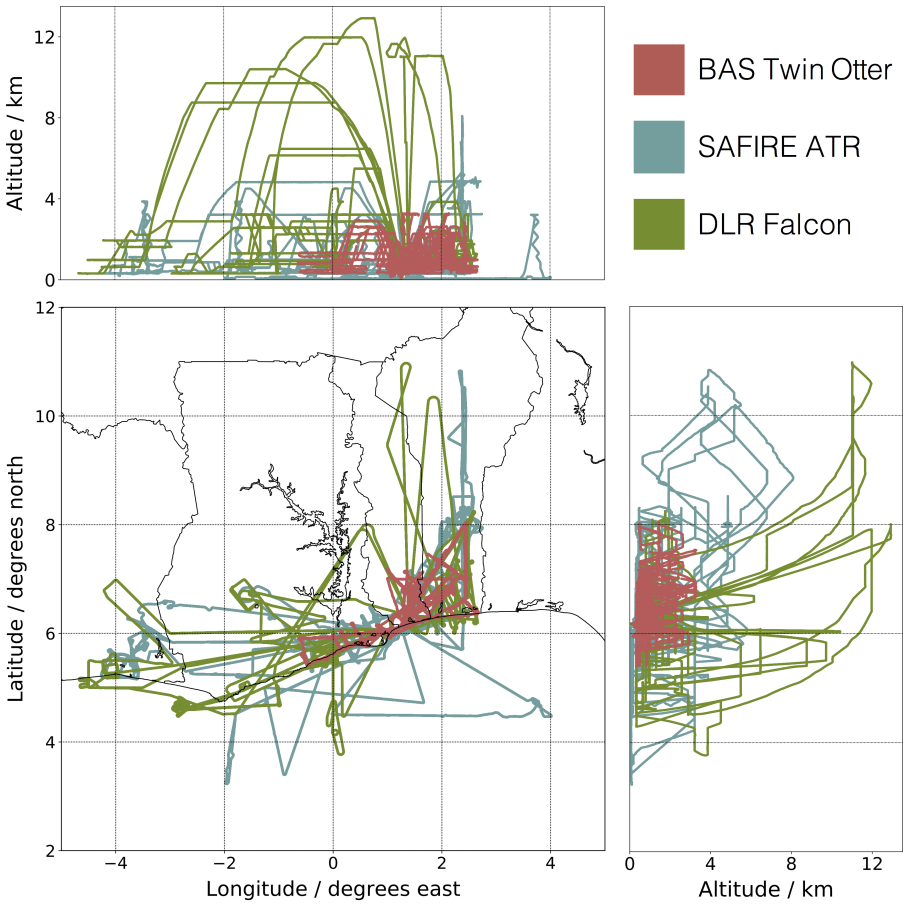

Figure 2.9: Map showing the flight tracks taken by the BAS Twin Otter, DLR Falcon and SAFIRE ATR aircraft during the DACCIWA aircraft campaign from 29th June 2016 to 16th July 2016.

Measurements of gaseous and aerosol species were made from each aircraft producing a unique data set for the coastal region of southern West Africa. The aircraft data sets provide observations of carbon monoxide (CO), nitrogen oxides (NO_x), sulfur dioxide (SO_2) and ozone (O_3) as well as sulfate (SO_4^{2-}), nitrate (NO_3^-), ammonium (NH_4^+), black carbon (BC) and organic carbon (OC) aerosols and a range of volatile organic compounds (VOCs). A summary of the aircraft observational data and instrumentation used is given in Table 2.2.

Table 2.2: Summary of the observational data and instrumentation on board the BAS Twin Otter, DLR Falcon and SAFIRE ATR aircraft during the DACCIWA campaign. Data is averaged on a 60 second time step. Final column indicates the number of 60 second data points collected.

Species	BAS Twin Otter	DLR Falcon	SAFIRE ATR	Data Set Size
Carbon Monoxide (CO)	Aerolaser AL5002 [95]	SPIRIT Instrument [46]	Picarro G2401m [195]	8289
Nitrogen Oxides (NO_x)	Air Quality Design Fast NO_x Instrument [8]	-	Thermo Fisher Scientific TEI 42 CTL [238]	5895
Ozone (O_3)	2B Technologies 205 Instrument [1]	Thermo Fisher Scientific TE 49i [238]	Thermo Fisher Scientific TE 49i [238]	8914
Black Carbon (BC)	Droplet Measurement Technologies Single Particle Soot Photometer (DMT SP2) [230]	-	Droplet Measurement Technologies Single Particle Soot Photometer (DMT SP2) [230]	4543
Organic Carbon (OC) Sulfate ($SO_4{}^{2-}$) Nitrate ($NO_3{}^-$) Ammonium ($NH_4{}^+$)	Aerodyne Compact Time-of-Flight Aerosol Mass Spectrometer (C-Tof-AMS) [67]	-	Aerodyne Compact Time-of-Flight Aerosol Mass Spectrometer (C-Tof-AMS) [67]	4581 4570 4424 4516
Formaldehyde (CH_2O)	-	-	Aerolaser AL4021 [6]	2456
Isoprene (C_5H_8)	Offline Gas Chromatography Flame Ionization Detector (GC-FID) [110]	Offline Thermal Desorption Gas Chromatography Mass Spectrometry (TD-GC-MS)	-	120
Ethane (C_2H_6) Propane (C_3H_8) Alkanes $\geq C_4$ Alkenes $\geq C_3$	Offline Gas Chromatography Flame Ionization Detector (GC-FID) [110]	-	-	105 105 75 16

The approach of this work has been to use observational data collected from all three research aircraft. This introduces some additional uncertainty into the analyses as the instruments used to measure each species varied between aircraft. In addition to this, different instruments may have different limit of detection levels and not every species was measured by all three aircraft which reduces the dataset size for some species. Measurements of air pollutants from an aircraft platform are made challenging by the pitch, roll and yaw of the aircraft as well as the changes in pressure, temperature and humidity which could affect the performance of the instruments. Futhermore, in some cases, samples were taken in flight to enable offline analysis; however, this introduces the risk of the sample degrading over time and hence an inaccurate measurement of the pollutant concentration at the time of sample collection.

Not all of the observational data collected by the three aircraft has been used in this work. Measurements of sulfur dioxide (SO_2) were made on board the BAS Twin Otter and DLR Falcon; however, both data sets were below the instrumental limit of detection for the majority of the flights. When they were observed it was often in narrow plumes which made interpretation with a chemical transport model difficult. VOC measurements were also made on board all three aircraft but the data set is limited to only a small number of observations for each species which are insufficient to accurately assess the concentrations and emissions of these species in the GEOS-Chem model. In addition to this, the VOC observational data set from the French and German aircraft includes mainly heavier weight VOCs which are not considered by the GEOS-Chem model. Finally, there are significant differences between the Single Particle Soot Photometer (SP2) instruments on board the BAS Twin Otter and the SAFIRE ATR, with the Twin Otter observations being approximately 1 μg m^{-3} higher. There is no ready explanation for this difference and it is not obvious which of these observations is closer to reality. These data sets are combined in the analysis but it must be acknowledged that there is a large uncertainty in these observations which places significant doubt upon the subsequent analysis of black carbon in the region.

The ensemble of observational data from the three aircraft has been used to evaluate the two different sets of emission inventories for the DACCIWA region:

1. the global EDGAR / BOND / RETRO inventories

2. the regional DACCIWA inventory

A comparison of the mean emissions from the DACCIWA region is shown in Figure 2.10 for these two emission scenarios. EDGAR emission data is for the year 2008, BOND and RETRO data is for the year 2000 and DACCIWA emissions are for the year 2015.

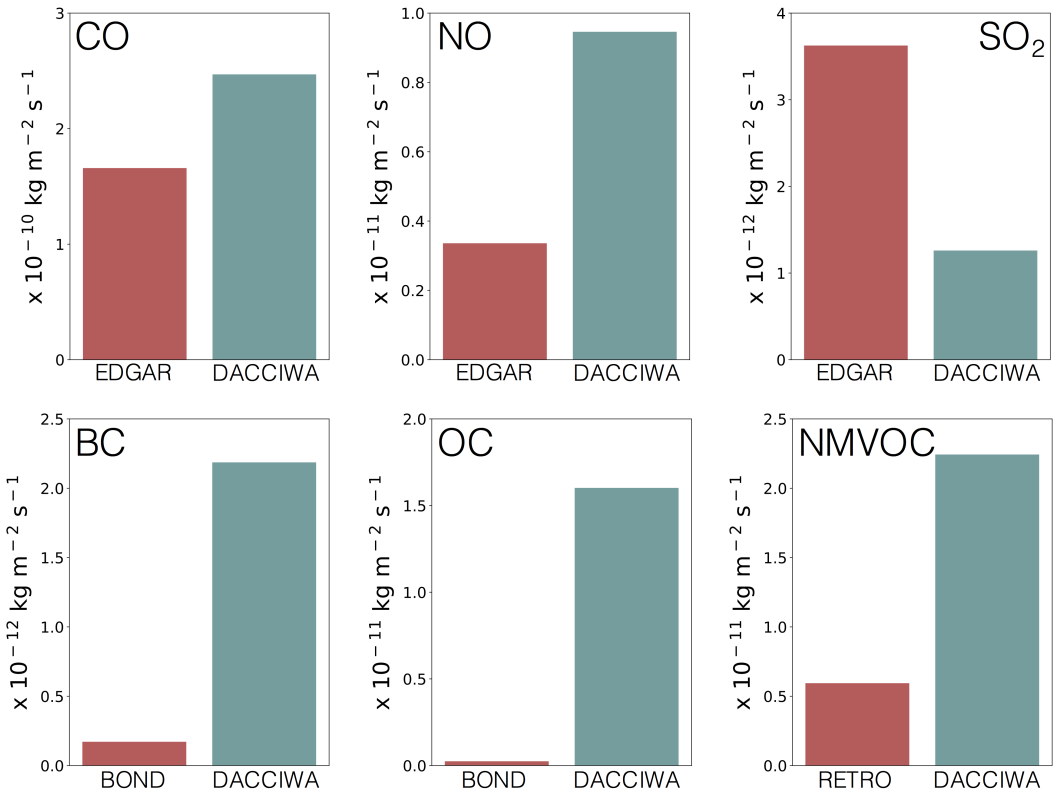

Figure 2.10: Mean annual anthropogenic emission rates of CO, NO, SO_2, BC, OC and NMVOC for the DACCIWA region for the two emission scenarios: EDGAR / BOND / RETRO global inventories and DACCIWA regional inventory. EDGAR emissions are for the year 2008, BOND and RETRO emissions are for the year 2000 and DACCIWA emissions are for the year 2015. NMVOC emissions include ethane, propane, alkanes $\geq$ C_4, alkenes $\geq$ C_3, isoprene, formaldehyde, acetaldehyde and acetone.

Uncertainties exist in both the activity data and emission ratios used to construct emission inventories [91,158,193]. These uncertainties are reflected in the significant differences between the regional (DACCIWA) and global (EDGAR / BOND / RETRO) emission estimates. The DACCIWA inventory shows increased emissions of CO and NO relative to the EDGAR inventory and decreased emissions of SO_2. Emissions of OC and BC from the DACCIWA inventory are an order of magnitude higher than the BOND inventory and anthropogenic NMVOC emissions in the DACCIWA inventory are approximately four times higher than seen in RETRO.

In order to assess how well these inventories are able to replicate the atmospheric conditions in the region, the West Africa GEOS-Chem model has been run for the period of the aircraft campaign and simulated species concentrations have been output along the flight tracks of each aircraft at 60 second time intervals. This enables direct comparisons to be made between the model data and aircraft observations.

The ensemble of data from all three aircraft has been considered. No major differences in conclusions were found by considering the aircraft individually, other than for black carbon (due to instrument differences discussed previously).

Data is filtered to select altitudes up to 1 km above sea level as the composition near the surface is most heavily influenced by local emissions, thereby enabling the best assessment of the inventories in this region. The relationship between the model and observations are investigated for the vertical, latitudinal and longitudinal profiles in the region for the two emission scenarios: EDGAR / BOND / RETRO (red) and DACCIWA (blue) (Figure 2.11). Both simulations use the GFAS emission inventory for biomass burning emissions.

Boundary conditions for all regional simulations of the DACCIWA campaign period are generated from global model simulations ($2^\circ \times 2.5^\circ$ horizontal resolution) which are spun up for one year (2016 used as the spin up year) before being run for the full year of 2016, outputting boundary conditions for the West Africa nested grid. The regional simulations are spun up for one week (22nd June 2016 to 29th June 2016) before simulations of the campaign period are run from 29th June to 16th July 2016.

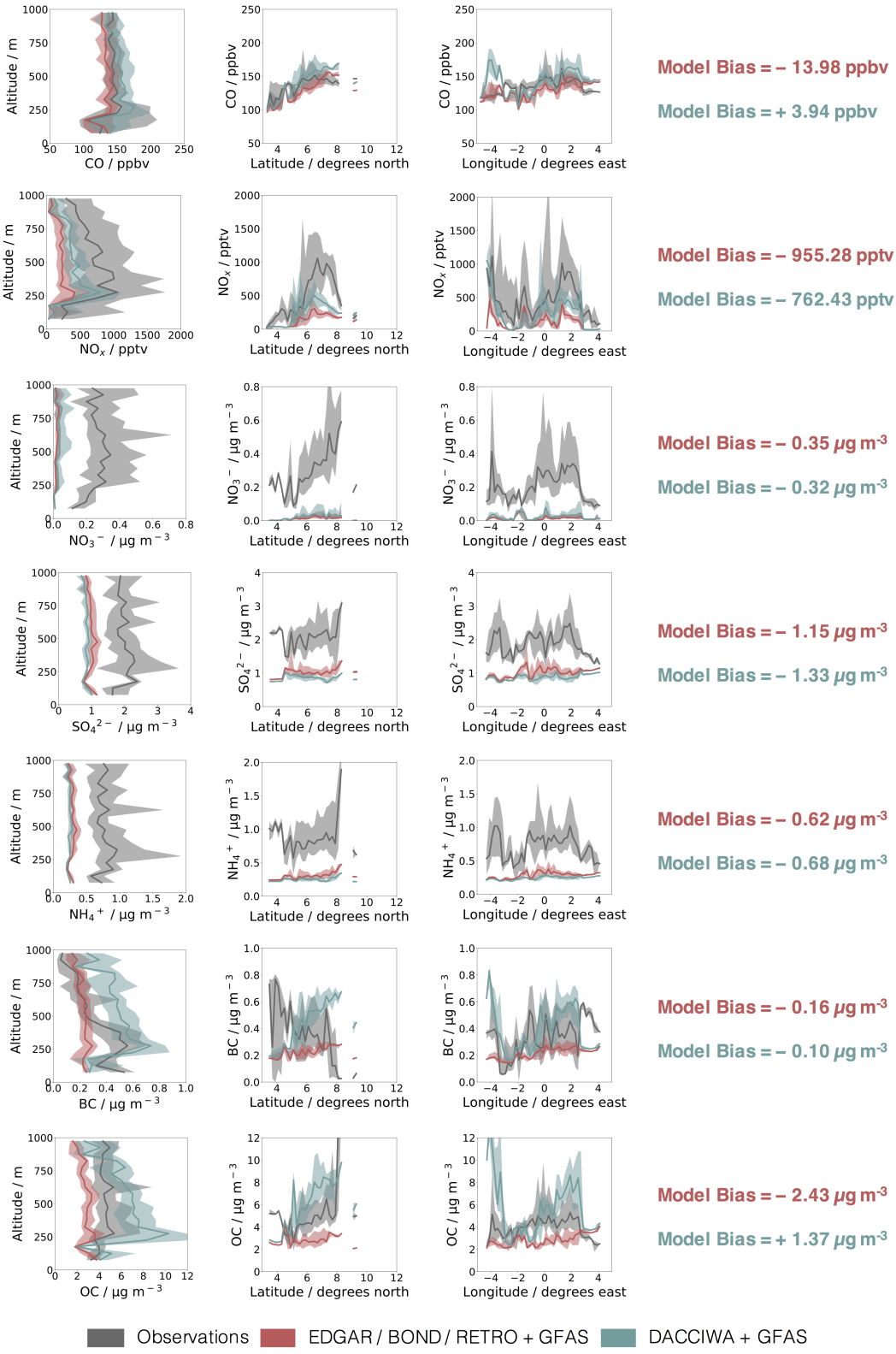

Figure 2.11: Vertical, latitudinal and longitudinal profiles of aircraft observational data (grey) and simulated concentrations using the EDGAR / BOND / RETRO and GFAS inventories (red) and the DACCIWA and GFAS inventories (blue). Solid lines represent the median, shaded areas represent the 25th to 75th percentile range. All data is from altitudes below 1 km.

For CO, the vertical profile is relatively flat and good agreement is seen for both in-

ventories (model biases of -13.98 ppbv and +3.94 ppbv for the EDGAR and DACCIWA simulations respectively). Consistent with emissions from the coastal cities and the prevailing wind (Figure 2.6), the concentration of CO increases from south to north across the region and the highest concentrations are seen at longitudes which correspond to the locations of the major cities of Abidjan (4.0 °W), Accra (0.2 °W), Lomé (1.2 °E) and Cotonou (2.4 °E). NO_x concentrations are low at altitudes up to 250 m, with concentrations peaking just above this height and then decreasing. This reflects the operations of the aircraft, where extended periods below 250 m were only made over the ocean where concentrations are low due to the prevailing wind and the low emissions [86]. The concentrations show a peak at 6 °N - 7 °N in the latitudinal profile and peaks in the longitudinal profile corresponding with the locations of the four largest coastal cities in the area. Both inventories show under predictions in NO_x concentrations, with the DACCIWA emissions showing slightly better performance (model bias of -762.43 pptv compared with -955.28 for the EDGAR simulation). The model substantially under estimates the inorganic aerosol components (NO_3^-, SO_4^{2-}, NH_4^+) under all conditions, with little difference in the under estimate by either of the emission data sets. Black carbon concentrations are highest in the region of 250 m - 500 m over the southern part of the domain. The different emission scenarios show mixed ability to simulate this compound. This may reflect the differences seen in the SP2 observations between the two aircraft (BAS Twin Otter and SAFIRE ATR). Organic carbon shows a relatively flat vertical profile and increased concentrations heading inland. The DACCIWA emission inventory over estimates the organic carbon concentrations (model bias of +1.37 μg m^{-3}) but simulates many of the features in the profiles.

VOC observations from the DACCIWA aircraft are limited in number (Table 2.2). Observing the regional structure from this limited data set is difficult. Instead, the entire data set of observed concentrations at all altitudes is simply compared to the simulated concentrations from the two emission scenarios (Figure 2.12).

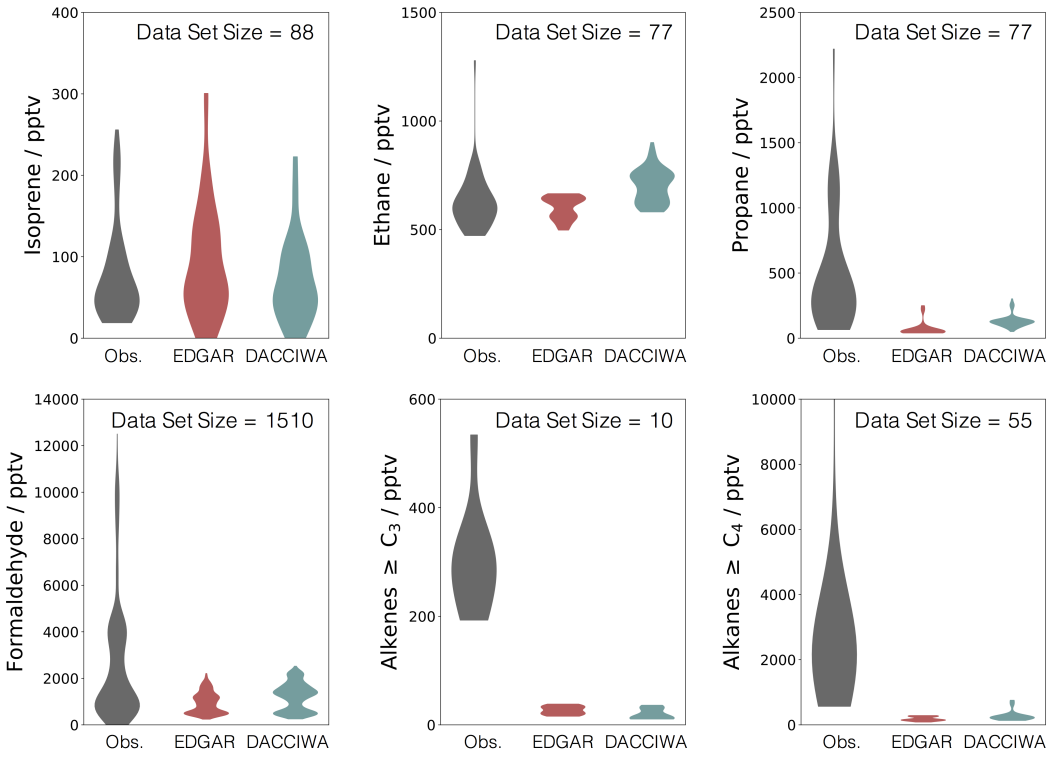

Figure 2.12: "Violin" plot (frequency distribution) showing VOC concentrations from aircraft observational data (grey), and simulated concentrations using the EDGAR / BOND / RETRO and GFAS inventories (red) and the DACCIWA and GFAS inventories (blue). All data is from altitudes below 1 km. The data set size is given for each species.

The RETRO inventory contains anthropogenic emissions of ethane, propane, formaldehyde, alkanes and alkenes but does not include anthropogenic emissions of isoprene. The DACCIWA inventory includes emission data for the same VOCs as the RETRO inventory but in addition contains anthropogenic emissions of isoprene. However, anthropogenic isoprene emissions are insignificant compared to the biogenic sources.

Isoprene concentrations are in relatively good agreement with both simulations, reflecting the MEGAN biogenic inventory used by both simulations. The differences between the two simulations may reflect the small difference in emissions as the DACCIWA simulation includes anthropogenic emissions whereas the EDGAR / BOND / RETRO simulation does not. Ethane concentrations are also relatively well simulated by both emission data sets. The comparison with the other primary VOCs is poor. Very high concentrations of alkanes and alkenes were observed which the models completely fail to represent. These large disagreements are consistent with the study of Keita et al. [128] which suggests VOC emissions in West Africa are under estimated by a factor of 50 in the EDGAR inventory [70, 182]. Most of the formaldehyde concentrations are reasonably reproduced by the model, likely due to the ability of the model to predict isoprene. However, there is a population at the top end of the distribution which is not simulated by the model, this is likely due to the inability of the model to simulate the other short lived VOCs.

Due to the lack of VOC observational data available from the DACCIWA aircraft,

it is not possible to quantify the uncertainties in the VOC emissions here. A more extensive observational data set would be required to adequately explain the discrepancies seen between the model and observations, but it is evident that anthropogenic VOCs are significantly under estimated.

2.5 Optimisation of the emission inventories for West Africa

Although the comparisons between the model and the measurements show some level of agreement there are some obvious failings: significant under estimates in NO_x, NO_3^-, SO_4^{2-} and NH_4^+, and over estimates in OC and BC are evident. Whilst simulations using the DACCIWA inventory in general show improved agreement with the aircraft observations over simulations with the EDGAR / BOND / RETRO inventories, there are still many discrepancies between the model and observations that remain.

The differences between the model and measurements are interpreted as being due to errors in the emission inventories. The discrepancies could also be due to differences in the chemical lifetimes of the compounds or errors in the transport, including boundary layer height or strength of convective mixing and horizontal flow. Given the paucity of observational meteorological data that can be included in data assimilation schemes in this region [136] it is likely that the quality of the meteorology used in this region is poor compared to other regions. However, it is also likely that the quality of the emission data sets is even poorer [91, 158, 193]. The emphasis here is therefore on uncertainties in the emission inventories.

Two of the major sources of emissions in the DACCIWA region are from anthropogenic and biomass burning activities. Independently switching off these two sources of emissions in the model enables the contribution of each activity to the total species concentrations to be determined. This approach assumes that the concentrations vary linearly as a result of switching different emission sources off and does not consider the changes in chemistry as a result of altering the composition of the atmosphere. Figure 2.13 shows the results of the sensitivity simulations in which the percentage contributions from anthropogenic and biomass burning activities to the surface concentrations of CO, NO_x, SO_2, BC and OC in the DACCIWA region are determined.

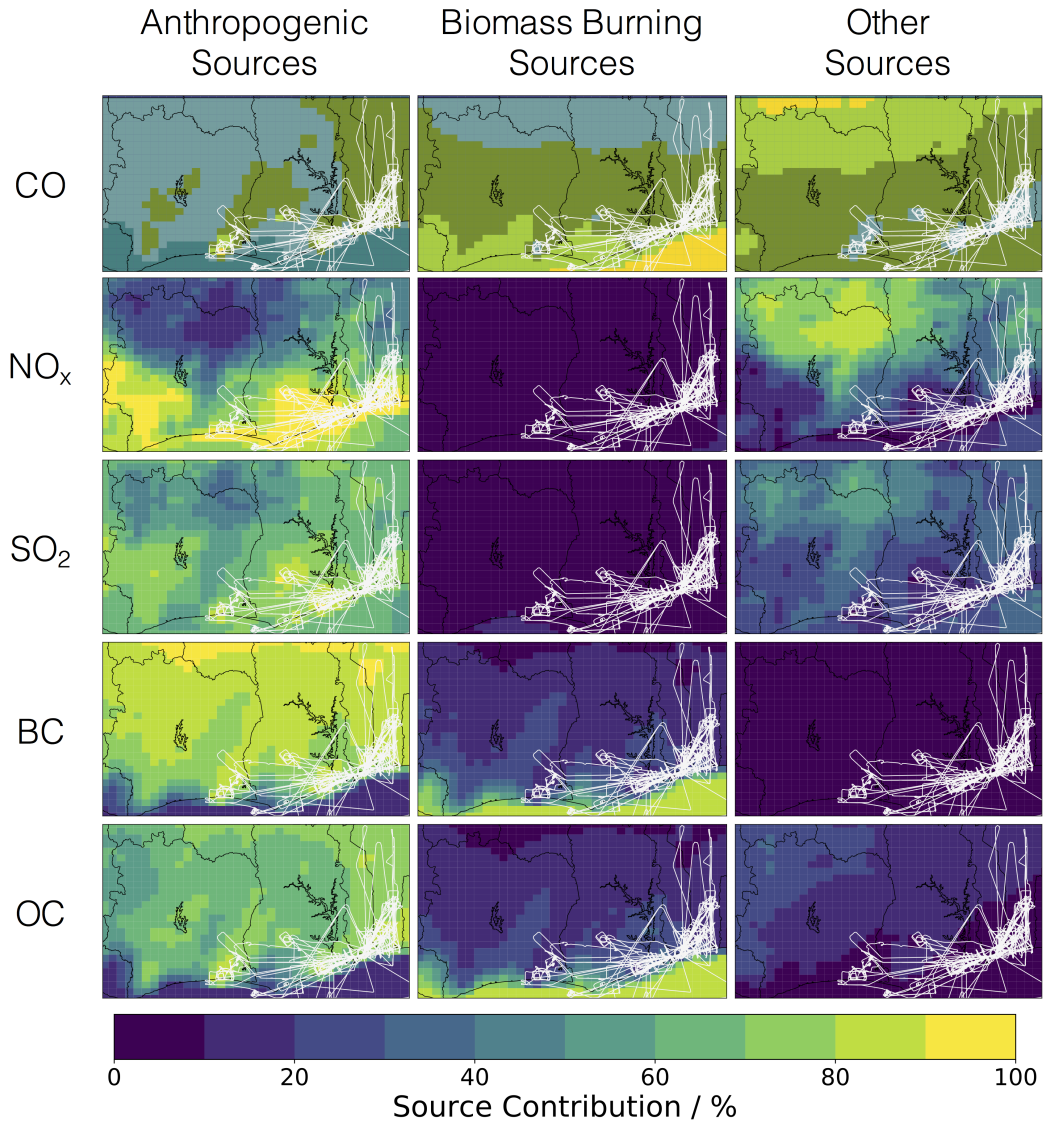

Figure 2.13: Percentage contribution of anthropogenic, biomass burning and other sources to the surface concentrations of CO, NO_x, SO_2, BC and OC in the DACCIWA region. Data is averaged for the period of the DACCIWA aircraft campaign (29th June 2016 to 16th July 2016). DACCIWA aircraft flight tracks are shown in white.

For all species, there is a clear contribution from anthropogenic sources to the surface concentrations in the region. This is particularly evident for the large cities along the coastline, where greater than 80% of the concentrations of NO_x, SO_2, BC and OC at this time of year in Abidjan (Côte d'Ivoire), Accra (Ghana), Lomé (Togo) and Cotonou (Benin) are attributable to anthropogenic sources. The long lifetime of CO means that anthropogenic contributions are limited to city plumes.

During the period of the aircraft campaign, the major biomass burning activities were located in central Africa (Figure 2.8) [21, 96, 212], away from the DACCIWA region of interest. The pollutants emitted from these fires have little influence on the concentrations of NO_x and SO_2 in West Africa due to the short lifetimes of these species. However, the concentrations of CO, BC and OC, especially over the ocean, are strongly influenced by this

biomass burning due to the transport of these compounds from central Africa across the Gulf of Guinea. 30% - 50% of the CO concentration along the coastline can be attributed to biomass burning sources.

As well as the anthropogenic and biomass burning sources, there is also a large contribution from soil emissions to NO_x concentrations, particularly to the north of the region [186]. There are also biogenic contributions to the concentrations of CO and OC, and some influence on concentrations from air masses transported from outside the domain.

Based upon this assessment, it is evident that for CO, BC and OC there is a clear influence from both anthropogenic and biomass burning sources on the concentrations in the DACCIWA region during the campaign period; therefore, uncertainties in both of these emissions have been considered. However, for NO_x and SO_2 there is little influence from biomass burning, hence for these species, only uncertainties in the anthropogenic emissions have been considered.

In order to provide a simple optimisation of the emissions, the ensemble of 60 second observational data from all three aircraft is considered. The data set is filtered to select data at altitudes up to 1 km. This is the zone where the species concentrations are most heavily influenced by local surface emissions. For any given modelled data point along a flight track, the concentrations of a species attributable to anthropogenic, biomass burning and other sources are determined from simulations in which these emission sources are switched off for the region. The system is assumed to follow a linear relationship between emissions and concentrations.

A cost function is calculated which is the root mean square difference between the modelled concentration and the measured. A multiplier can be applied to the anthropogenic and biomass burning contributions, and by minimising the cost function with respect to these multipliers, an optimal multiplier is found.

NO_x data is used to determine the uncertainties in NO emissions, and $SO_4{}^{2-}$ is used as a proxy for scaling SO_2 emissions given the paucity of useful SO_2 observations (Section 2.4). For NO_x and SO_2, where no biomass burning influences are found, the biomass burning multiplier is not allowed to vary.

The error range associated with each of the optimum scale factors is determined by considering a 5% deviation in the value of the cost function. The normalised cost functions are shown in Figure 2.14. In each case, the orange dot indicates the optimum scale factors determined.

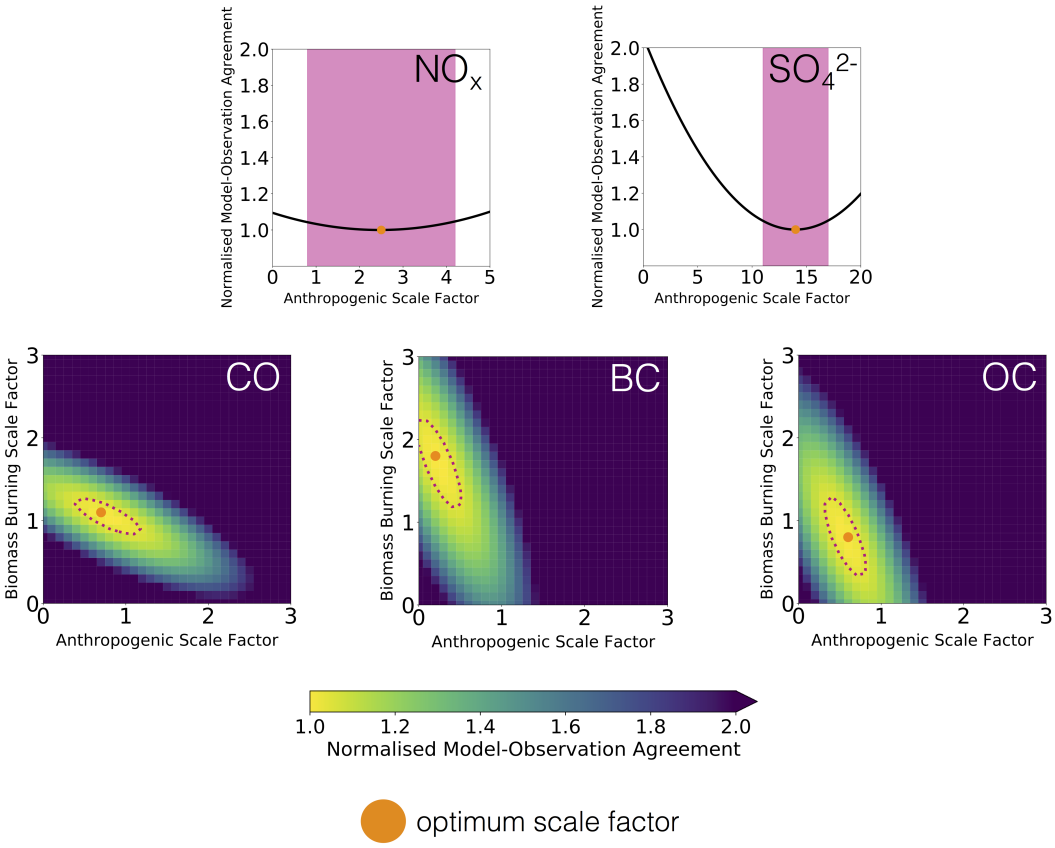

Figure 2.14: Impact of scaling anthropogenic (DACCIWA) and biomass burning (GFAS) emissions on the normalised cost function for NO_x, $SO_4{}^{2-}$, CO, BC and OC. The optimum scale factors for each species are represented by the position of the orange dot. The range of scale factors representing a 5% deviation from the optimum scale factor is represented by the pink shaded region (NO_x and $SO_4{}^{2-}$) and by the pink dotted line (CO, BC and OC).

The optimum calculated scale factors are summarised in Table 2.3.

Table 2.3: Optimum scale factors calculated for anthropogenic (DACCIWA) and biomass burning (GFAS) emissions for the DACCIWA region based on evaluation against DACCIWA aircraft observations.

Emission Species	DACCIWA Scale Factor	GFAS Scale Factor
CO	0.7 ± 0.2	1.1 ± 0.1
NO	2.5 ± 1.7	-
SO_2	14.0 ± 3.0	-
BC	0.2 ± 0.1	1.8 ± 0.3
OC	0.6 ± 0.1	0.8 ± 0.3

The most significant change in the DACCIWA emissions is for the emissions of SO_2 (recommending a 14 fold increase on the DACCIWA emissions). A likely explanation for the discrepancies is an under estimation in the sulfur content of liquid fuels. Most

developed countries use fuels with a sulfur content of 50 ppm or below; however, the majority of African countries use higher sulfur content liquid fuels, with the West African coastal countries typically using fuel containing 2000 - 5000 ppm of sulfur [246]. These countries are active in reducing the sulfur in fuels [247], but uncertainties over the current sulfur content of fuels used in these countries may explain the large increase in emissions needed to reconcile the model with the observations.

Similarly, the required increase in NO emissions (factor of 2.5) may reflect uncertainties in emission factors in the transport sector. Emission estimates for road transport are calculated based upon fuel consumption statistics and emission factors from specific vehicle types [19, 125, 151]. This data is commonly taken from large international databases [118, 248]. These statistics are often unable to account for poor fuel quality and the increase in illegal smuggling of fuel, particularly from Nigeria to surrounding countries including Togo and Benin [32, 79]. Neither does the data account for poorly maintained vehicles and the consequent changes in vehicle emission factors [100]. Therefore there are many uncertainties in the emission estimates from road transport which could account for the under predicted emissions of NO.

Over predictions of varying extents are seen for CO, BC and OC when the standard DACCIWA + GFAS simulation output is compared to the aircraft observations (Figure 2.11). Concentrations of CO, BC and OC in the region at this time of year are influenced heavily by both anthropogenic and biomass burning sources. Uncertainties in the DACCIWA and GFAS inventories were therefore tested simultaneously. The optimum calculated scale factors recommend lowering anthropogenic DACCIWA emissions for all three species by factors of 0.7, 0.2 and 0.6 for CO, BC and OC respectively. Increases in biomass burning emissions from the GFAS inventory by factors of 1.1 and 1.8 are recommended for CO and BC respectively, whilst it is recommended that the OC GFAS emissions are lowered by a factor of 0.8. Based upon comparisons to satellite data, it has been suggested that biomass burning emissions of aerosols in the GFAS inventory are under predicted by a factor of between 2 and 4 [126]; however, much smaller disagreements have been seen here in the comparison to DACCIWA observations. It is important to note that the optimum scale factors for the BC emissions are subject to considerable uncertainty due to the large discrepancies seen in the observations from the BAS Twin Otter and SAFIRE ATR aircraft.

A comparison of the optimised anthropogenic (DACCIWA) emissions to the default global and regional emissions is shown in Figure 2.15.

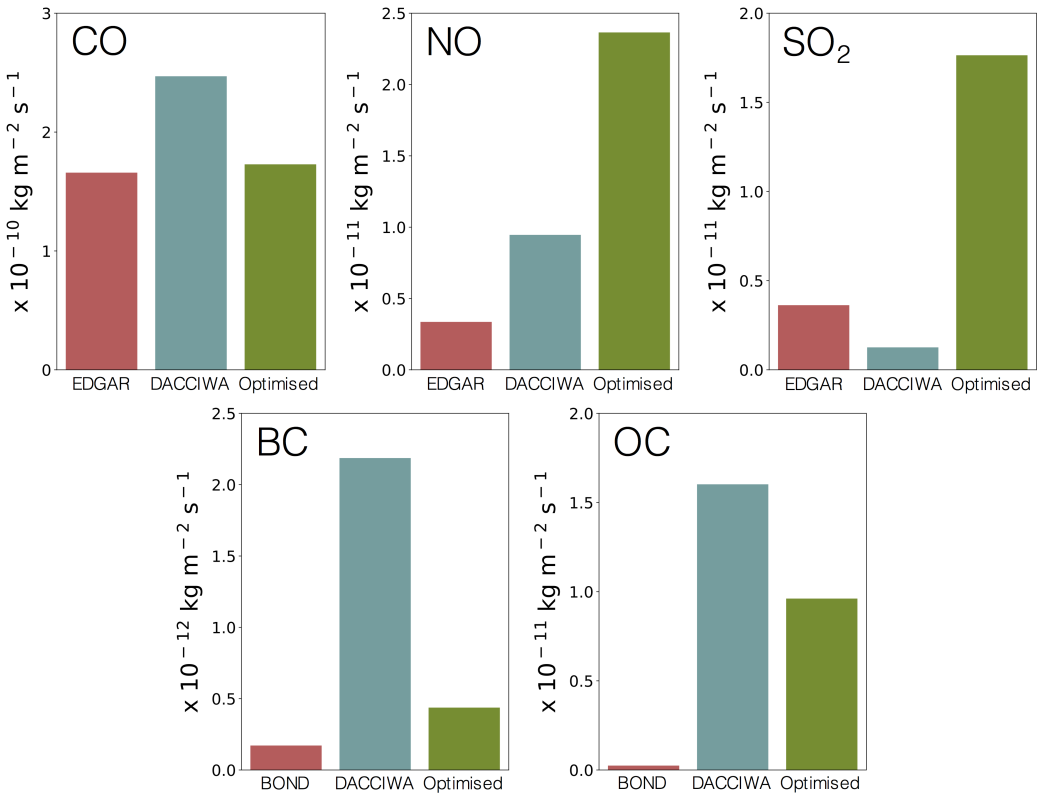

Figure 2.15: Mean annual anthropogenic emissions of CO, NO, SO_2, BC and OC for the DACCIWA region from three emission scenarios: EDGAR / BOND global inventories (red); DACCIWA regional inventory (blue); optimised DACCIWA regional inventory (green). EDGAR emissions are for the year 2008, BOND emissions are for the year 2000 and DACCIWA emissions are for the year 2015.

The optimised anthropogenic scale factors recommend reducing the DACCIWA CO emissions to a level similar to the EDGAR emissions. The optimised emissions of NO and SO_2 are significantly higher than both the global and regional standard inventories. Whilst anthropogenic BC and OC emissions are reduced relative to the DACCIWA emissions, the optimised emissions remain significantly higher than the global BOND emissions.

These optimum scale factors are calculated solely based upon the DACCIWA aircraft observations. This data set is limited to only a short time period during the West African wet season and whilst it gives some information on the vertical profile of concentrations, there is little information on the surface concentrations. Surface level measurements are ideal for optimising the emission inventories as concentrations at the surface experience the largest influence from the emission sources and are therefore most suited for evaluating and optimising the inventories. A long term ground based observational network of measurements in the region is required to formally optimise the inventories for the whole region over an extended time period [103, 122, 138, 187].

2.6 Impacts of scaling the emission inventories on pollutant concentrations in the DACCIWA region

The calculated scale factors have been applied to the DACCIWA and GFAS emission inventories within GEOS-Chem, allowing the impact of the optimised emissions to be assessed. The agreement between the optimised inventories and aircraft observations is assessed (Section 2.6.1) along with the wider impact on surface concentrations of primary pollutants in the region (Section 2.6.2) and the impact on policy relevant concentrations of fine particulate matter ($PM_{2.5}$) and ozone (O_3) (Section 2.6.3).

2.6.1 Evaluation of the agreement with DACCIWA aircraft observations

The comparison of the optimised simulation output to the aircraft observations is shown in Figure 2.16.

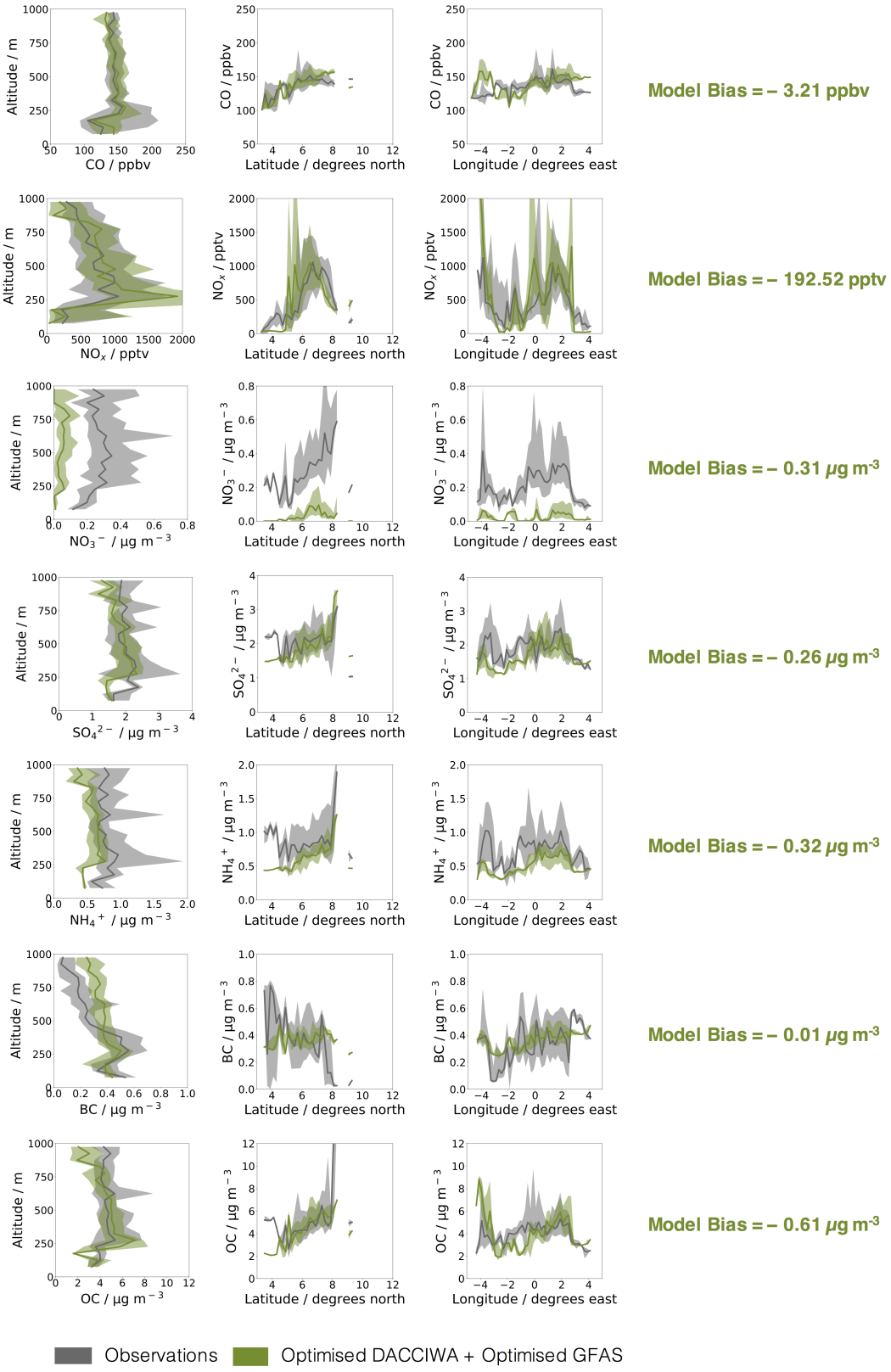

Figure 2.16: Vertical, latitudinal and longitudinal profiles of aircraft observational data (grey) and simulated concentrations using the optimised DACCIWA and optimised GFAS inventories (green). Solid lines represent the median, shaded areas represent the 25th to 75th percentile range. All data is from altitude below 1 km.

The adjusted inventories produce much better agreement with CO (optimised model

bias of -3.21 ppbv) and NO_x (optimised model bias of -192.53 pptv) observations, matching both the profiles and concentrations well. The model still under predicts NO_x in the south east of the flight area which is over the ocean to the south of Nigeria. The shipping emissions of NO have been investigated; however, these are not found to be the cause of the disagreement. A possible cause may be an under representation of flaring emissions from the oil industry which are extensive in this region [55, 66]. Agreement for $SO_4{}^{2-}$ is also significantly improved by the 14 fold increase in the emissions (from a model bias of -1.33 μg m^{-3} to -0.26 μg m^{-3}), with the distribution and concentrations well matched throughout the region. The agreement for $NH_4{}^+$ is also improved (from a model bias of -0.68 μg m^{-3} to -0.32 μg m^{-3}), although some under predictions remain, and $NO_3{}^-$ remains significantly under predicted (optimised model bias of -0.31 μg m^{-3}). An increase in the ammonia (NH_3) emissions would help remediate both the remaining under estimate in the $NH_4{}^+$ and significantly improve the $NO_3{}^-$ simulation. However, it is unclear whether this uncertainty in NH_3 emission is present in the anthropogenic, biomass burning or natural emissions (or a combination of these). Southern West Africa has been shown to be a hot spot for ammonia from satellite studies [251, 269]. Previous studies [27] have shown modelled ammonia concentrations to be under represented in other parts of the world; however, there is little information on NH_3 concentrations in Africa. Agreement between modelled and observed BC and OC concentrations is also greatly improved with model biases reduced in the optimised simulation, although some over prediction of BC remains above 500 m altitude. This may represent the different representation of data from the BAS Twin Otter and SAFIRE ATR aircraft in the 0 m to 500 m and 500 m to 1 km region. Although some differences remain between the measurements and the model, the increased emissions have significantly improved the simulation.

2.6.2 Impact of emission scaling on the surface level concentrations across the DACCIWA region

Whilst the aircraft observations enable model simulations to be evaluated, the observations along the flight tracks give little information on the wider pollutant concentrations at the surface. Changes in the emission inventories influence the atmospheric composition within the model across West Africa, and hence impact the estimates of pollutant concentrations that the population is exposed to. The distribution of pollutants across the DACCIWA region, calculated by the model during the campaign period, are shown in Figure 2.17 for the global, regional and enhanced regional emission scenarios, along with the percentage change between the default global inventory and enhanced regional inventory simulations.

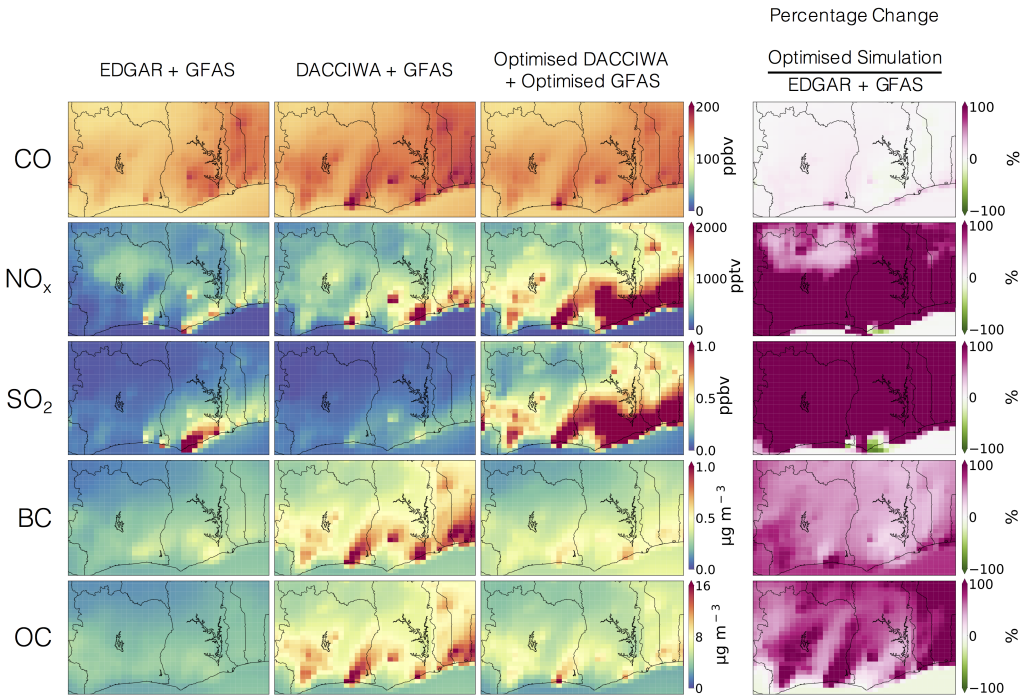

Figure 2.17: Surface concentrations of CO, NO_x, SO_2, BC and OC during the DACCIWA aircraft campaign period from simulations using the EDGAR + GFAS inventories, DACCIWA + GFAS inventories and optimised DACCIWA + GFAS inventories. The percentage change between the EDGAR + GFAS and optimised DACCIWA + GFAS simulations is shown in the final panel.

CO concentrations are increased between the EDGAR and DACCIWA simulations; however, the optimised scale factors reduce the DACCIWA emissions to a level which is similar to the EDGAR inventory. Overall, there is only a small change between the default global inventories and the optimised regional inventories.

For NO and SO_2, anthropogenic emissions are significantly increased between the EDGAR simulation and the enhanced simulation, leading to increased surface concentrations of NO_x and SO_2 across the region. The biggest increases are seen around the large coastal cities where the majority of the emissions occur. The percentage change in surface concentrations for both species is in exceedance of 100% for many locations.

For both BC and OC, the anthropogenic emissions are increased between the EDGAR and DACCIWA simulations and subsequently decreased by the optimisation. Overall, there is an increase in anthropogenic emissions between the EDGAR and optimised simulations, leading to increased concentrations of BC and OC over the land. The concentrations over the ocean are influenced largely by transported biomass burning from central Africa at this time of year. For BC, there is an increase in concentrations over the ocean as a result of increasing the biomass burning emissions. Whereas for OC, there is a slight decrease in concentrations over the ocean as a result of decreasing the biomass burning emissions.

2.6.3 Impact of scaling the emission inventories on the concentrations of policy relevant species

In addition to the direct effects that scaling the inventories have on the emitted species themselves, the combined changes in emissions have effects on secondary pollutants such as ozone (O_3) and fine particulate matter ($PM_{2.5}$). The adverse health effects of these compounds are well known (see Chapter 1) [23, 63, 64, 149, 172, 280], and as such they are subject to regulation by law in many countries [274]. Figure 2.18 shows the comparison between the modelled and measured O_3 and $PM_{2.5}$ from the DACCIWA aircraft.

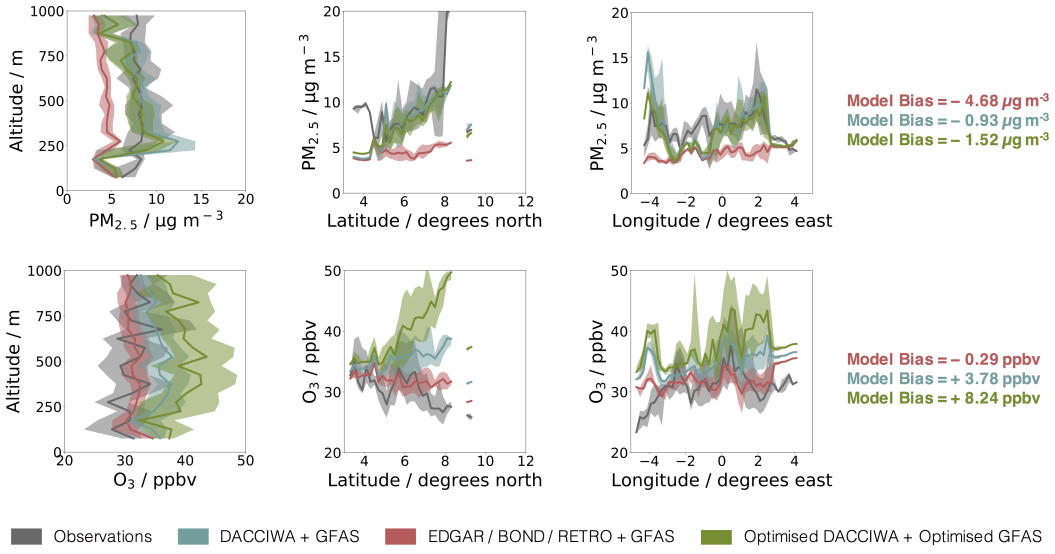

Figure 2.18: Vertical, latitudinal and longitudinal profiles of aircraft observational data (grey) and simulated concentrations using the EDGAR / BOND / RETRO and GFAS inventories (red), the standard DACCIWA and GFAS inventories (blue) and the optimised DACCIWA and optimised GFAS inventories (green) for O_3 and $PM_{2.5}$. Solid lines represent the median, shaded areas represent the 25th to 75th percentile range. All data is from altitudes below 1 km. $PM_{2.5}$ concentrations shown here do not account for the mass of dust or sea salt, or the uptake of water to the aerosols.

It should be noted that the calculated $PM_{2.5}$ concentrations in Figure 2.18 account for the mass of BC, OC, SO_4^{2-}, NO_3^- and NH_4^+; however, they do not include dust or sea salt as no measurements of these were taken on board the aircraft. Neither do the concentrations account for additional mass due to uptake of water to the aerosols.

For $PM_{2.5}$, the simulated concentrations using the EDGAR / BOND / RETRO and GFAS inventories show large under estimates (model bias of -4.68 μg m^{-3}), whereas simulated concentrations from the standard and enhanced DACCIWA and GFAS inventories match observational profiles well and show good agreement with the concentrations (model biases of -0.93 μg m^{-3} and -1.52 μg m^{-3} respectively). Concentrations simulated using the DACCIWA inventory are increased by a factor of approximately 2 compared to the EDGAR simulation.

The O_3 concentrations simulated by the EDGAR / BOND / RETRO and GFAS inventories are found to be in relatively good agreement with the observations (model bias of -0.29 ppbv), yet both the standard and enhanced DACCIWA and GFAS simulations over predict O_3 concentrations (model biases of +3.78 ppbv and 8.24 ppbv respectively), particularly at the higher latitudes. This is likely to be due to the increase in NO emissions in the DACCIWA inventory relative to EDGAR, and further increase in emissions (factor 2.5) as a result of the optimisation. Whilst the observations show decreasing O_3 concentrations moving northwards, the model has a tendency to give increasing O_3. Despite improved representation of NO_x and CO concentrations, together with evidence of VOC concentrations being consistent with or smaller than those observed (Figure 2.12), this is surprising.

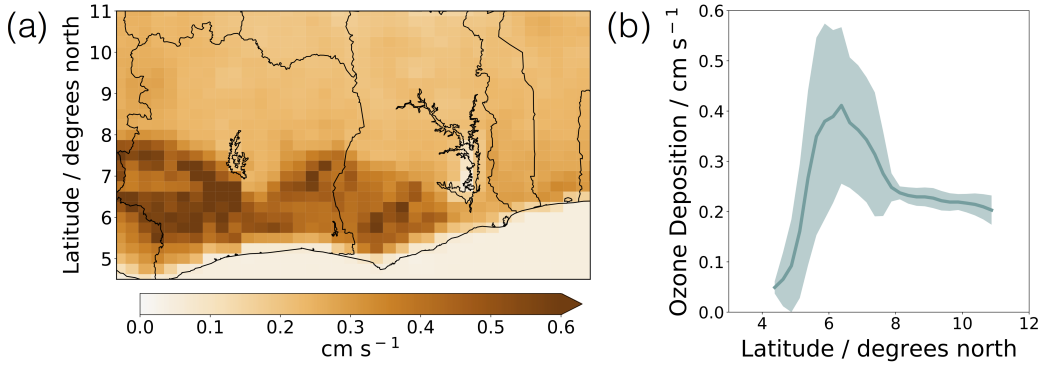

Figure 2.19: Simulated ozone deposition rates (a) spatial distribution for the West Africa region and (b) latitudinal profile for the West Africa region. Ozone deposition rates averaged during the period of the DACCIWA aircraft campaign (29th June 2016 to 16th July 2016).

One potential explanation for the over estimate involves the deposition of O_3 to vegetation. The latitudinal profile of ozone deposition in the DACCIWA region during the period of the aircraft campaign (Figure 2.19(b)) shows a sharp decrease in deposition rate from approximately 0.4 cm s^{-1} at 6 °N to 0.25 cm s^{-1} at 8 °N. This corresponds with the latitudinal range where the model data shows an increase in O_3 concentration which deviates from the observational data. Compared to the available observational data ozone deposition is generally considered well constrained in the GEOS-Chem model [226]; however, there is little understanding or evaluation of these rates for African vegetation due to a lack of observational data [218]. The work of Silva and Heald [226] suggests that ozone concentrations over the land in West Africa during the summer months may be under predicted as a result of bias in the ozone deposition rates. Travis and Jacob [242] though found over predictions in modelled ozone concentrations within GEOS-Chem and attribute some of the cause of this to the ozone deposition velocities being too low, especially on wet surfaces (such as may be present during the monsoonal wet season). Under predictions in modelled O_3 deposition could therefore be a cause of this model-observation

disagreement for O_3 and this requires further investigation.

The mean surface concentrations of O_3 and $PM_{2.5}$ within the DACCIWA region during the aircraft campaign period are shown in Figure 2.20, along with the percentage change in concentrations between the default EDGAR and GFAS simulation and optimised DACCIWA and GFAS simulation. Note that the $PM_{2.5}$ concentrations in Figure 2.20 include dust, sea salt and water uptake to the aerosols.

For both species, the concentrations show an increase between the EDGAR simulation and the optimised simulation. For O_3, the concentrations are increased by approximately 50% across the region, whilst for $PM_{2.5}$, increases of over 100% are seen around the large urban areas.

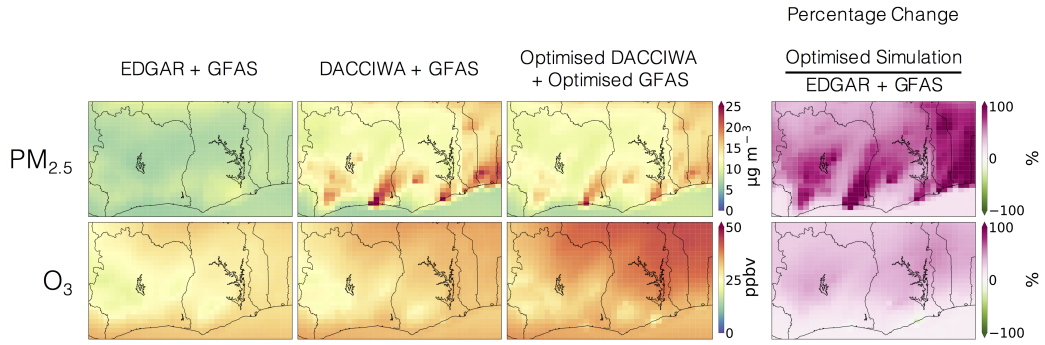

Figure 2.20: Surface concentrations of O_3 and $PM_{2.5}$ during the DACCIWA aircraft campaign period from simulations using the EDGAR + GFAS inventories, DACCIWA + GFAS inventories and optimised DACCIWA + GFAS inventories. The percentage change between the EDGAR + GFAS and optimised DACCIWA + GFAS simulations is shown in the final panel.

Despite the disagreements seen between the observed and simulated O_3 concentrations using the optimised emission inventories (Figure 2.18), the average surface O_3 concentrations in the DACCIWA region (using the optimised emissions) during the campaign period are below 45 ppbv. Even with some over predictions present in the model, the simulated concentrations indicate that there were few exceedances of the World Health Organisation (WHO) 8 hour mean limit of 100 μg m^{-3} (51 ppbv) [274] during this time. Although this suggests O_3 concentrations are not a significant concern for the region during this season, understanding the reasons for the over estimate in O_3 concentrations in this region should be subject to future research.

The concentrations of $PM_{2.5}$ in the enhanced simulation are, however, significantly above the WHO annual mean limit of 10 μg m^{-3} [274] for much of the region, with higher concentrations observed in areas surrounding the major coastal cities. During the DACCIWA campaign, modelled $PM_{2.5}$ concentrations frequently exceeded the WHO 24 hour limit of 25 μg m^{-3} [274] around these urban locations, indicating that $PM_{2.5}$ is an important health consideration for the southern coastal region of West Africa. The exceedances of air quality standards are discussed in more detail in Section 3.6 of Chapter

2.7 Concluding remarks on the emission inventories for simulating West African air quality

Accurate modelling studies of air quality in West Africa are dependent upon many factors but one of the key components is the emission inventories. These emission inventories must be accurate representations of the sources, locations and magnitudes of emissions throughout the region. Rapid population change and economic development in West Africa means that the sources and quantities of pollutants emitted into the atmosphere are constantly changing [141, 151, 199]. Emission inventories must therefore also be up to date.

Simulations of the West African atmosphere have been historically dependent upon global emission inventories which often lack emission sources specific to the region [70,182]. Recently, however, more research into African emission factors has led to the development of Africa-specific inventories [128, 151, 163]. Both the global and regional anthropogenic emission inventories have been evaluated for West Africa using airborne observations from the DACCIWA aircraft campaign [86]. This analysis has found the regional inventory to generally show improved agreement over the global inventory yet many discrepancies still remain, particularly in the simulation of NO_x and secondary aerosols (notably sulfate).

Two of the main sources of emissions in West Africa, and hence major sources of uncertainty, are biomass burning and anthropogenic activities. The anthropogenic emissions from the DACCIWA inventory, along with the biomass burning emissions from the GFAS inventory, have been optimised for the DACCIWA region using the aircraft observations.

Modelled CO concentrations are reasonably consistent with the observations, with the optimisation suggesting adjusting the anthropogenic and biomass burning emissions by factors of 0.7 and 1.1 respectively. Biomass burning does not significantly impact the concentrations of NO and SO_2 during the campaign period; however, the anthropogenic emissions were found to be considerably under represented by factors of 2.5 and 14.0 respectively. Carbonaceous aerosols are over estimated in the model and the results of the optimisation recommend anthropogenic scale factors of 0.2 and 0.6 and biomass burning scale factors of 1.8 and 0.8 for BC and OC aerosol emissions respectively. There are, however, large uncertainties associated with the BC scale factors due to discrepancies between the data from the Twin Otter and ATR aircraft. A lack of observational data prevented VOC emissions being formally optimised; however, comparisons of available data to the model suggest significantly under represented VOC emissions in the inventories. The emission evaluation also indicated that NH_3 emissions may be under predicted; however, there is no observational data to constrain these emissions.

This evaluation indicates that the global inventories are unsuitable for use in West

African air quality simulations, and that whilst the new regional inventory shows improved agreement, there are still some prominent failings. These conclusions are, however, based exclusively on the DACCIWA aircraft observations and the results from a single chemical transport model. This data set is limited to only a small time period and spatial range therefore more extensive long term observations are required to fully investigate the emission estimates for the region. A sparse network of long term, ground based measurements are available for West Africa and these are used in Chapter 3 to support assessments of the seasonal variability of pollutant concentrations in West Africa and the resulting impacts on health.

Chapter 3

Seasonal variability in regional atmospheric composition over West Africa

The DACCIWA aircraft campaign collected a unique observational data set of pollutant concentrations for the West Africa coastal region. These observations have been used in Chapter 2 to evaluate the anthropogenic and biomass burning emission inventories for the region within the framework of the high resolution regional GEOS-Chem model for West Africa. Whilst these observations provide a detailed picture of the atmospheric composition during the aircraft campaign (the wet season), they give no insight into the pollutant concentrations in the region throughout the rest of the year, in particular during the dry season.

The observational network of atmospheric pollutants over West Africa is limited [184, 219], therefore modelling studies are essential for understanding the full annual cycle of pollutants and assessing the impact that these pollutants have on human and ecosystem health. The GEOS-Chem West Africa model has been used here to investigate the meteorological and emission drivers that control the composition of the atmosphere in the region and examine the seasonal changes in the sources and concentrations of pollutants throughout the year. As the emission inventories for West Africa have only been evaluated and optimised for the period of the aircraft campaign (Chapter 2), all simulations analysing the seasonal changes in pollution use the standard DACCIWA (anthropogenic) and GFAS (biomass burning) emission inventories with no optimisation applied. The potential implications of this are discussed later.

3.1 Factors influencing the seasonal composition of the atmosphere over West Africa

There are two key factors which influence the seasonal change in atmospheric composition over West Africa: meteorology and emissions. A summary of these are given here.

3.1.1 Meteorological conditions in West Africa

The meteorological conditions in West Africa play a large role in influencing the atmospheric composition. The speed and direction of the winds controls how pollutants are dispersed from emission sources, whilst precipitation rates affect the loss of pollutants through wet deposition. The pollutants themselves can also influence the formation and albedo of clouds which in turn can influence photolysis reactions as well as deposition processes [31, 208]. These physical processes are therefore fundamental in influencing pollutant concentrations; however, they show large seasonal variations. The West African coastline experiences a monsoon climate with a distinct wet season and dry season [12,68,164,167,194,206]. Figure 3.1 shows the monthly precipitation and wind patterns in West Africa, with monthly mean surface temperatures and precipitation rates for the region shown in Figure 3.2.

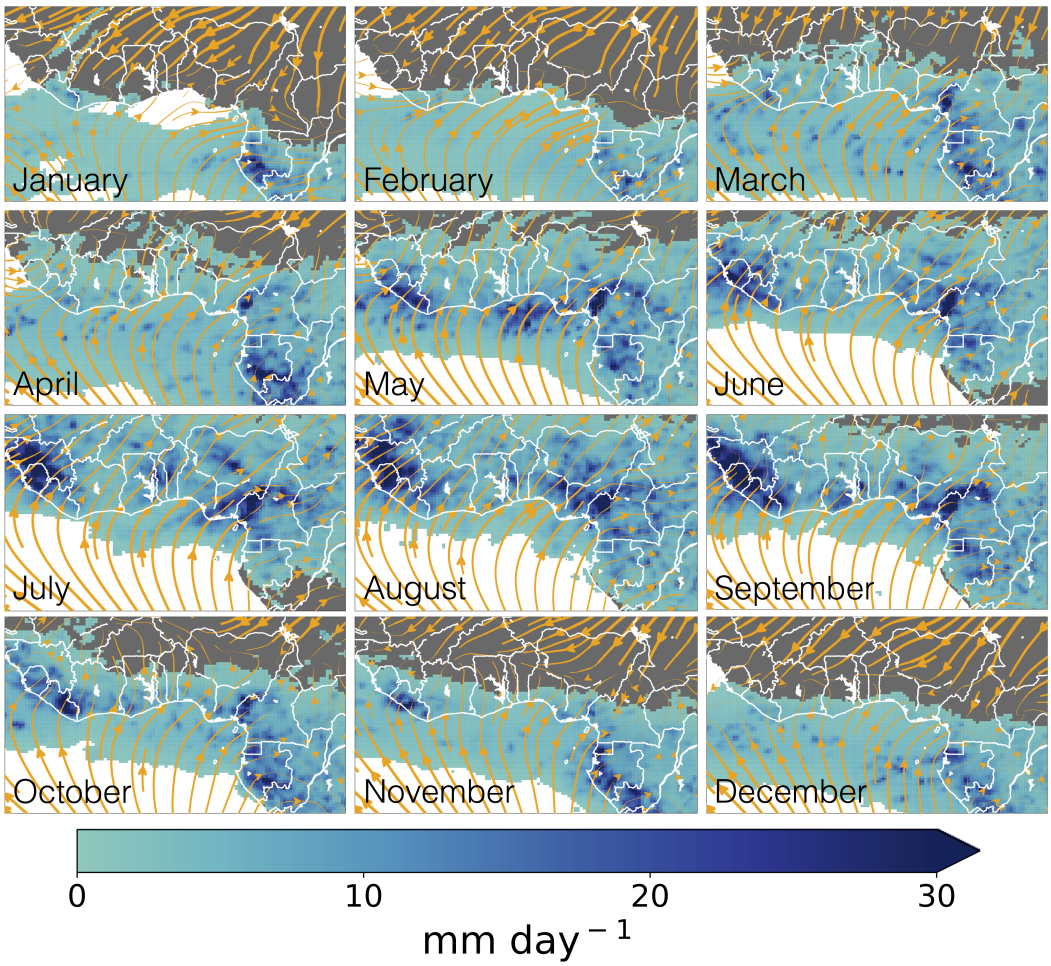

Figure 3.1: Annual pattern of surface wind stream functions and rainfall in West Africa. Monthly mean GEOS-FP meteorological data for the year 2016. Precipitation rates below 1 mm day^{-1} are masked.

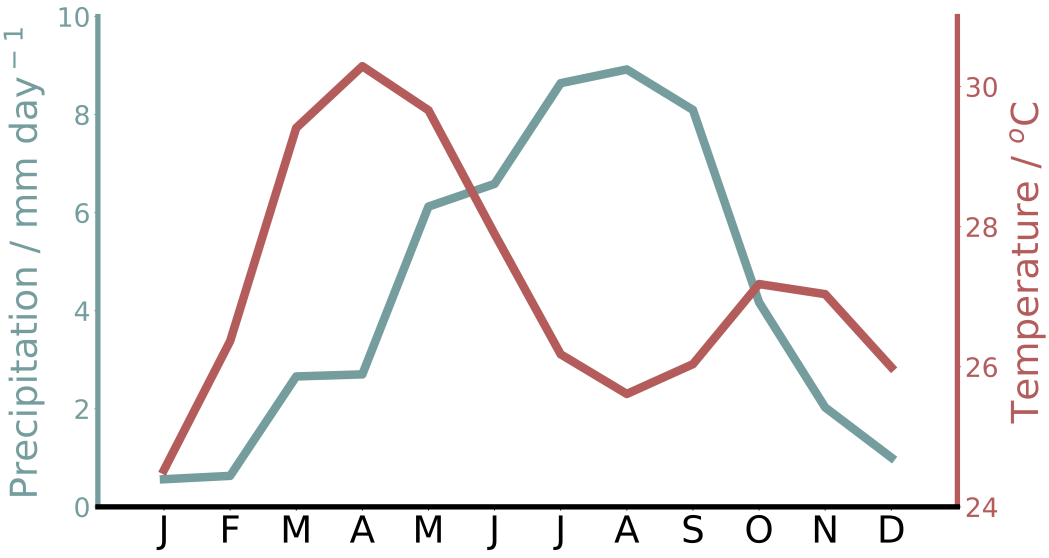

Figure 3.2: Monthly mean surface temperature and precipitation for the year 2016 for the Guinea region (3 °N - 15 °N; 15 °W - 15 °E) from GEOS-FP meteorological data.

The wet season typically covers the months of May to October, whilst the dry season covers the period from November to April [92]. As is typical of a tropical monsoon climate, the surface temperatures across the region remain relatively consistent throughout the year, with temperatures typically in the range of 25 °C to 30 °C [214]. Within this range, higher temperature occur during the dry season with lower temperatures during the wet season. The key features of the dry and wet seasons can be clearly seen for the months of January and July respectively (Figure 3.3).

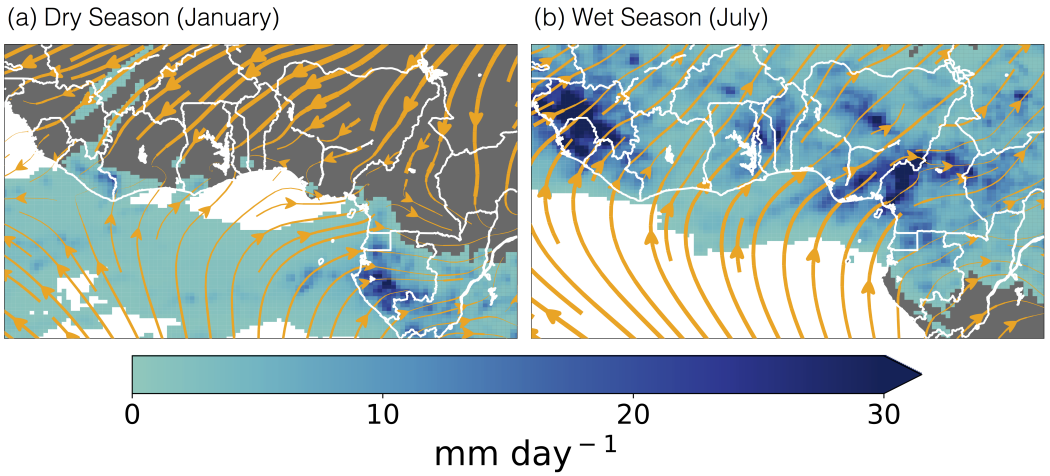

Figure 3.3: Monthly mean surface wind stream functions and rainfall in West Africa for January 2016 and July 2016, illustrating the key features seen during the dry and wet seasons respectively. Monthly mean GEOS-FP meteorological data for the year 2016. Precipitation rates below 1 mm day^{-1} are masked.

During the dry season there is little rainfall over the land, with a band of rainfall remaining to the south of the region over the ocean. This rainfall is associated with the Inter Tropical Convergence Zone (ITCZ) which is a region near the equator which circles the Earth and is where the Northern and Southern Hemispheres come together. Intense heating in this region, combined with the convergence of winds from the two hemispheres, results in rising air parcels which release the accumulated moisture as they cool and often result in intense thunderstorms. The predominant wind direction over the land during this season is from the north east, meeting a weaker flow from the south over the Gulf of Guinea. This results in a convergence zone of relatively weak flow along the coastal area with little rain.

During the wet season, the pattern of rainfall spreads across the West African countries and the flow of air is reversed. The predominant wind direction is from the south / south east to the north east, bringing air from the Gulf of Guinea across the region.

When used throughout this work, “dry season” and “wet season” refer specifically to the West African seasons discussed here.

3.1.2 Seasonal changes in regional emissions in West Africa

As well as the meteorological factors, the concentration of a given species in the region throughout the year is heavily dependent upon the magnitude of the emission sources and the seasonal variations in these emissions. The emission inventories used in the GEOS-Chem West Africa simulations are described in detail in Section 2.2. The seasonal variations in the emissions from different sources covering the Guinea region (Figure 2.2) are shown in Figure 3.4 for a range of species.

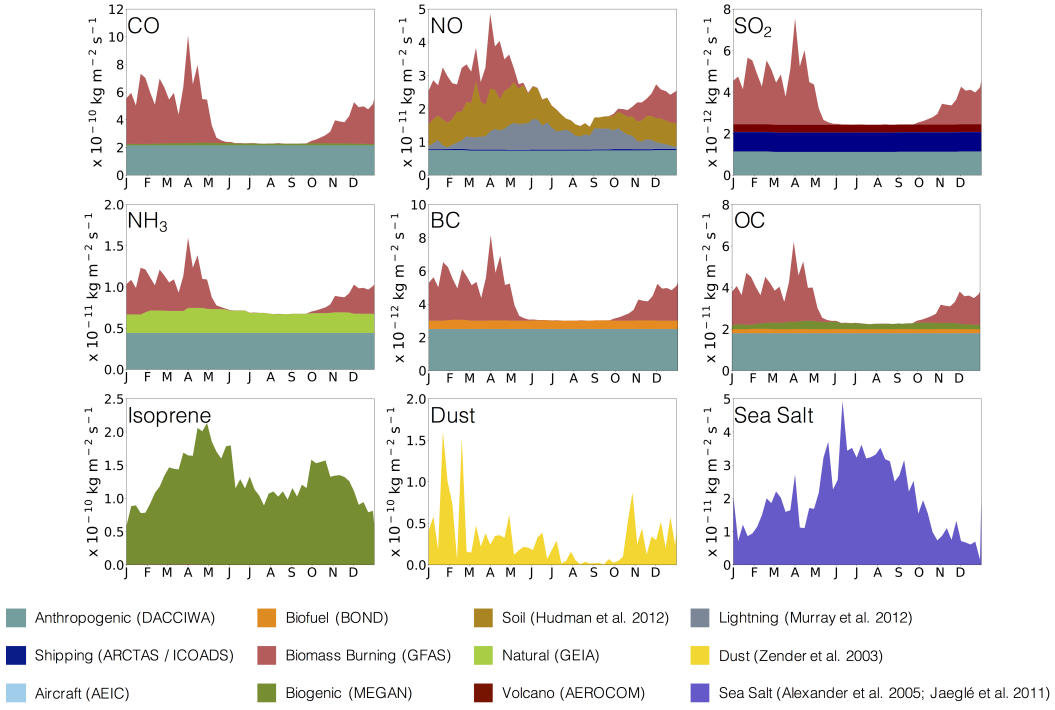

Figure 3.4: Annual cycle of model emissions in the Guinea region (3 °N - 15 °N; 15 °W - 15 °E). Emission data averaged weekly for the year 2016 from the surface to the tropopause.

As with all of the DACCIWA emissions, the anthropogenic CO emissions are constant throughout the year [125,135] as there is a diurnal scale factor but not seasonal scale factor applied to the emissions. There is, however, a strong seasonal pattern in biomass burning emissions (from the GFAS inventory [126]) with higher emissions during the dry season (November to April) and insignificant emissions during the wet season (May to October). NO also shows uniform emissions from terrestrial anthropogenic sources, shipping [262] and aircraft [231] activities. The signature from biomass burning sources is the same as seen for CO; however, there are also large seasonal emission sources from soils [116] and from lightning [175]. The soil emissions are highest during the dry season, whereas the lightning emissions (most of which are emitted outside the boundary layer [175]) show inter-season maxima with the highest emissions in May, June and October. The anthropogenic and biomass burning emissions of SO_2 follow the same patterns seen for CO and NO; however, SO_2 emissions throughout the year also show a large contribution

from shipping sources and volcanic activity [61, 85]. NH_3 shows uniform anthropogenic emission and strong seasonal patterns in biomass burning, with approximately a third of the total emissions being attributable to natural sources. OC and BC follow very similar profiles with contributions from biofuel [29,144] and biogenic sources (OC only) adding to the anthropogenic emissions and seasonal biomass burning emissions. Isoprene emissions are almost exclusively from biogenic sources (MEGAN inventory [98,113]) and show peaks in the emissions between the wet and dry seasons in April and October. Dust emissions are lowest during the wet season months and the highest peaks in emissions are present in January and February whilst the sea salt emissions are generally highest during the wet season months in July and August, reflecting wind speeds [10, 120, 283, 284].

Based upon evaluation against aircraft observations from the DACCIWA campaign, significant uncertainties were identified in the anthropogenic (DACCIWA) and biomass burning (GFAS) inventories for West Africa (Section 2.4). Anthropogenic NO and SO_2 were found to be under represented by factors of 2.5 and 14.0 respectively whilst anthropogenic emissions of CO, BC and OC were found to be over estimated and optimisation recommended lowering these emissions by factors of 0.7, 0.2 and 0.6 respectively. Although constraints on the central African biomass burning were much weaker, optimisation of the GFAS inventory recommended scaling the biomass burning emissions of CO, BC and OC by factors of 1.1, 1.8 and 0.8 respectively. Large under estimations of VOC emissions were found; however, the observational data was thought insufficient to constrain these emissions. It was also suggested that the NH_3 emissions in the model are under estimated, although it is unclear what the source of this under estimation is.

These uncertainties in the emission inventories have only been quantified for the period of the aircraft campaign (29th June to 16th July 2016). Figure 3.4 shows that the emissions of all species (except sea salt) are typically lowest during these months. The DACCIWA campaign period is therefore unrepresentative of the full annual cycle of emissions in the region and the optimised scale factors for the emissions, calculated based upon these aircraft observations, cannot be applied with confidence to simulations outside this period. Therefore, the standard DACCIWA and GFAS inventories are used for all model assessments of the seasonal composition of the atmosphere over West Africa.

3.2 Evaluation of modelled seasonal surface concentrations of pollutants using ground based measurement data

Observational data sets of pollutant concentrations in the region are sparse [219]. The DACCIWA aircraft campaign collected measurements of gases and aerosols during a three week operational period, yet it is unable to provide any detail on the seasonal variations

in composition and hence is unrepresentative for making assessments of the long term impacts of pollutant concentrations in the region.

Whilst long term measurements in the region are sparse, some observations of gaseous and aerosol species are available from a number of ground sites in the region. These measurement sites include those which are part of the Aerosol Robotic Network (AERONET) (Section 3.2.1), the International Network to study Deposition and Atmospheric composition in AFrica (INDAAF) programme (Section 3.2.2), as well as a number of DACCIWA ground sites which were operational from 2015 to 2017 as part of the programme (Section 3.2.3). The locations of these ground sites are shown in Figure 3.5.

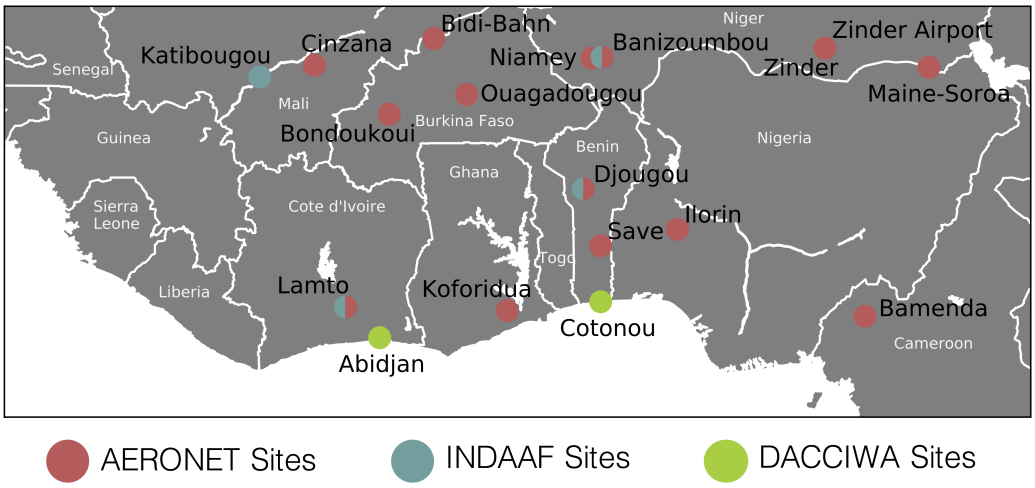

Figure 3.5: Locations of the AERONET, INDAAF and DACCIWA ground measurement sites in the Guinea region.

3.2.1 AERONET sites

Ground based total column aerosol optical depth (AOD) measurements are available from the Aerosol Robotic Network (AERONET) for fifteen sites within the Guinea region of interest. These sites are in varied locations including close to airports (Zinder Airport, Niamey), in agricultural land (Savé, Djougou, Banizoumbou, Cinzana) and in the grounds of research institutes in towns or cities (Ilorin, Bamenda, Ouagadougou). AOD gives an indication of the concentration of aerosol from the surface to the edge of the atmosphere. Level 2 (quality assured) data, recorded at 675 nm from these AERONET sites [177] is compared to simulated AOD values at this wavelength from the GEOS-Chem model. The AERONET data is averaged over a time period from 1995 to 2018 whilst the GEOS-Chem data is taken from a simulation of the year 2016.

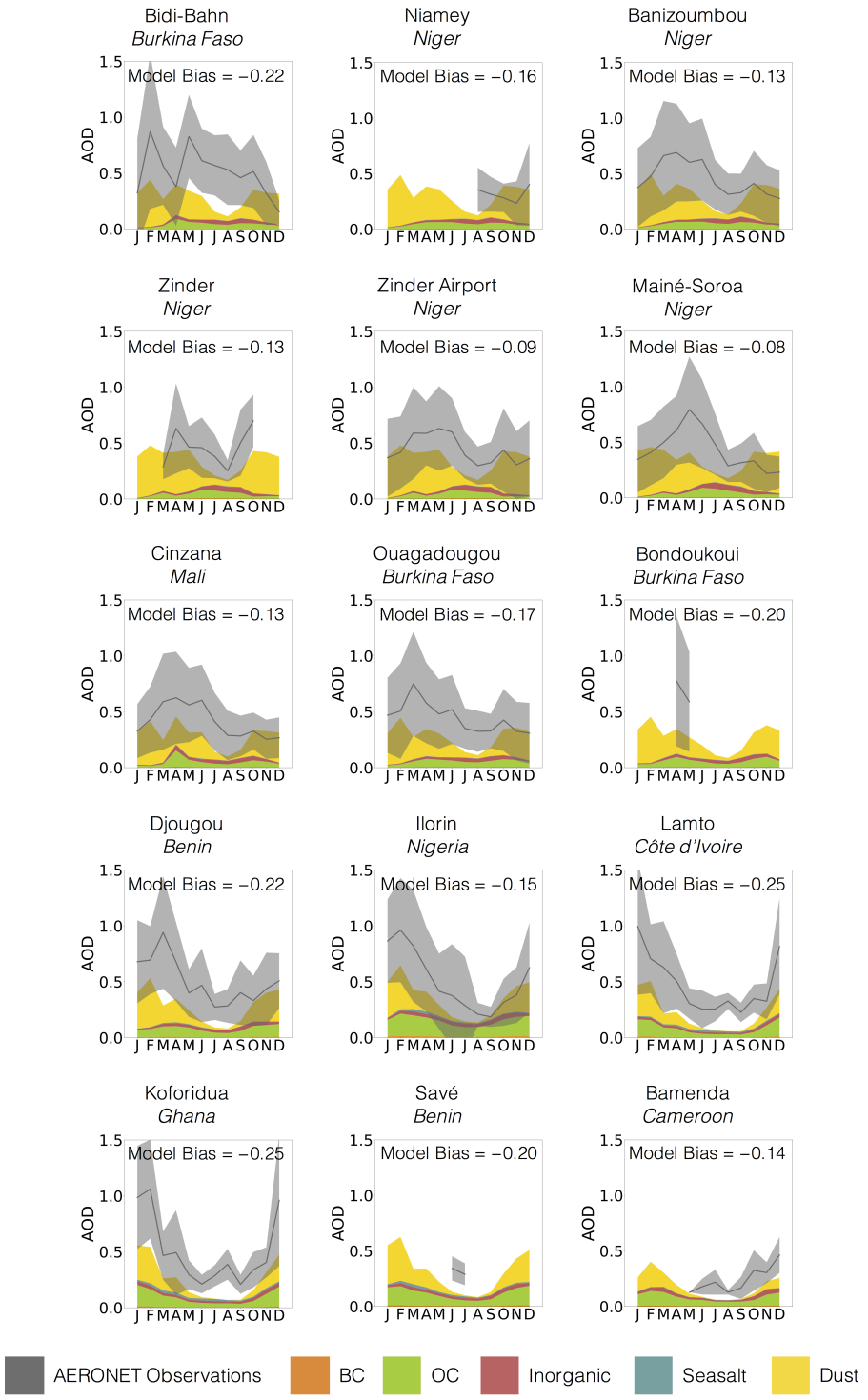

Figure 3.6: Comparisons between seasonal patterns in aerosol optical depth (AOD) from AERONET sites in the Guinea region and equivalent GEOS-Chem model data. AOD recorded at 675 nm. For the observational data (grey), solid lines represent the mean and shaded regions represent one standard deviation. Model data is coloured by species. Model data is for the year 2016, observational data is averaged over the period 1995 to 2018. Model bias calculated using monthly data is shown on the figures for each site.

The GEOS-Chem model has a tendency to under predict AOD at all locations with model biases ranging from -0.08 to -0.25, yet the seasonal patterns are well matched.

The under predictions in the AOD suggest that aerosol species in the model may be under represented. This is consistent with the findings in Chapter 2 (Figure 2.11) where inorganic aerosols (NO_3^-, SO_4^{2-} and NH_4^+) were shown to be under predicted in the DACCIWA anthropogenic inventory relative to DACCIWA aircraft observations. Dust makes up a large fraction of the modelled AOD. This is very difficult to accurately simulate given the uncertainties in emissions and sinks [211]. Some of the under predictions may also be accounted for by the lack of secondary organic aerosol (SOA) in the model version used.

The modelled AOD data is broken down into the individual components: BC, OC, inorganic aerosols, sea salt and dust. For all AERONET sites, the model data indicates that OC and dust are the two largest sources of aerosol in the region throughout the year. The dust also shows a strong seasonal pattern with higher concentrations during the dry season (November to April) and lower concentrations during the wet season (May - October). Due to the prevailing transport, this seasonality is strongest at the sites further south and less prominent at the sites in the north of the region due to the constant influence from dust from the Sahara desert. Inorganic aerosols, BC and sea salt show very small contributions to the AOD at all sites in the Guinea region.

3.2.2 INDAAF sites

The International Network to study Deposition and Atmospheric composition in AFrica (INDAAF) programme operates a long term monitoring network comprising of eight sites in west and central Africa [117]. The locations of these sites were chosen to be representative of the major ecosystems and the West African sites include both wet and dry savanna sites. Four of these sites fall within the Guinea study region: Banizoumbou, Niger (13.5 °N, 2.5 °E, dry savanna); Djougou, Benin (9.7 °N, 1.9 °E, wet savanna), Katibougou, Mali (12.9 °N, 7.5 °W, dry savanna); and Lamto, Côte d'Ivoire (6.2 °N, 5.0 °W, wet savanna). Passive sampling techniques using Teflon filters exposed for a period of one month are used to measure the atmospheric concentrations of gases at these sites. Automatic aerosol samplers are used to collect Teflon filters for mineral analysis and Quartz filters for carbon analysis which are analysed using ion chromatography at the Laboratoire d'Aerologie in Toulouse, France to determine chemical composition [4, 5, 41, 81]. Monthly measurements of gases (O_3, NO_2, SO_2, NH_3) and aerosols (NO_3^-, SO_4^{2-}, NH_4^+) are available at the West African sites for the periods of 1997 - 2013 and 1996 - 2005 respectively. No aerosol measurements are available for the site at Djougou in Benin.

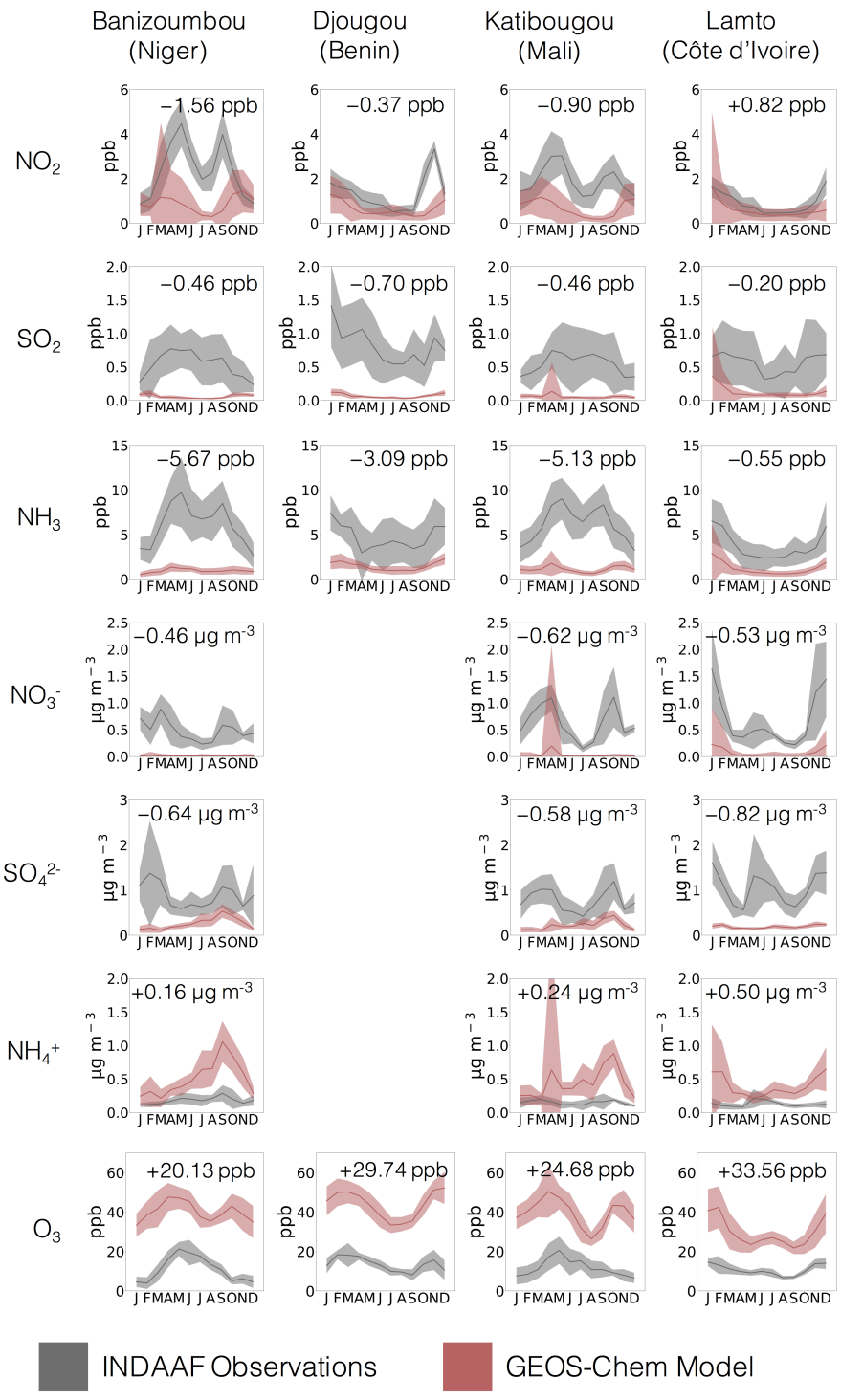

Figure 3.7: Comparisons between seasonal patterns in NO_2, SO_2, NH_3, NO_3^-, SO_4^{2-}, NH_4^+ and O_3 concentrations from four INDAAF ground sites in the Guinea region and equivalent GEOS-Chem model data. Solid lines represent the mean, shaded regions represent one standard deviation. Model data for the year 2016, observational data averaged over the period 1996 to 2013. Model bias calculated using monthly data is shown on the figures for each species and for each site.

The modelled NO_2 data replicates some of the seasonal variability, yet the concentrations are under predicted in general. In particular, the concentrations at the sites of

Katibougou and Banizoumbou (which are furthest north), between approximately April and September, are lower than the observations with model biases of -0.90 ppb and -1.56 ppb respectively. Anthropogenic NO emissions have been shown to be under estimated during the wet season months (Section 2.5) which may account for some of the disagreements, whilst another explanation may be under represented soil emissions in this typically more vegetated region [186].

SO_2 and NH_3 concentrations are under predicted at all four sites throughout the year by factors of approximately 2.3 and 8.8 respectively (from averaged data across all sites). This is also consistent with the findings in Section 2.5 where anthropogenic SO_2 emissions were found to be under predicted by a factor of 14. Under estimates in NH_3 emissions were suggested to be the cause of remaining under predictions of inorganic aerosol concentrations (Section 2.6.1). It is unclear whether the uncertainties in the ammonia emissions are present in the anthropogenic, biomass burning or natural sources, although the consistent under predictions throughout the year would suggest the seasonal biomass burning activities are not the major cause of uncertainty. Concentrations of NO_3^- and SO_4^{2-} are also under predicted at all sites which may be expected as a result of NO and SO_2 emissions being too low. In contrast to the under predictions seen in the NH_3 concentrations, NH_4^+ concentrations are over predicted at all sites with model biases of between +0.16 μg m^{-3} and +0.50 μg m^{-3}. This is surprising given the under estimate in sulfate and nitrate and requires further investigation to identify the cause of this behaviour.

For all sites, large discrepancies can be seen between the model and observations for O_3. O_3 observations are very low (0 to 20 ppb) whereas modelled O_3 is significantly higher (20 to 60 ppb). Whilst the model is able to replicate some of the seasonal patterns in O_3 concentrations, the modelled concentrations are significantly higher than those observed, with model biases of between +20.13 ppb and +33.56 present in all locations. Similar over predictions of approximately 15 ppbv were also seen in the comparisons to DACCIWA aircraft data (Section 2.6.3), and it is suggested that some of the discrepancies may be a result of uncertainty in dry deposition rates, particularly over the more vegetated inland regions. Further research is required in order to understand and resolve this model failing.

In general, the conclusions about the composition of the atmosphere gained from modelling the DACCIWA flights are consistent with those found from modelling the INDAAF data. With the suggestion being that under estimates in the emissions of SO_2 and NO, along with problems with the NH_3 emissions, then manifest in uncertainties in the SO_4^{2-} / NO_3^- / NH_4^+ aerosol system.

3.2.3 DACCIWA ground sites

As part of the DACCIWA project, fortnightly measurements of fine particulate matter ($PM_{2.5}$) were made at roadside locations in the cities of Abidjan (Côte d'Ivoire) and Cotonou (Benin) as well as at a waste burning site in Abidjan from 2015 to 2017 [62].

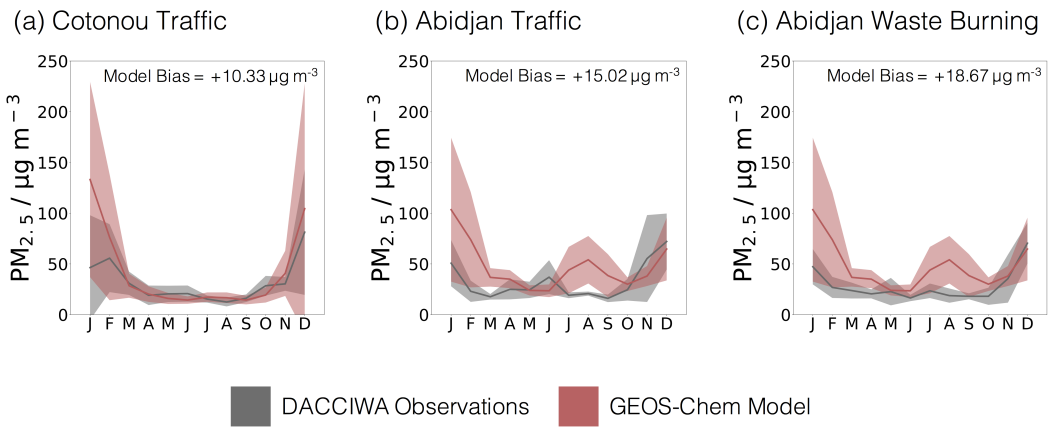

Figure 3.8: Comparisons between seasonal patterns in $PM_{2.5}$ concentrations from three DACCIWA ground sites in Abidjan (Côte d'Ivoire) and Cotonou (Benin) and equivalent GEOS-Chem model data. Solid lines represent the mean, shaded regions represent one standard deviation. Model data for the year 2016, observational data averaged over the period 2015 to 2017. Model bias calculated using monthly data is shown on the figures for each site.

Modelled data shows some agreement to the observations at all three sites with the mean annual model bias ranging from +10.33 μg m^{-3} to +18.67 μg m^{-3}. From November to February, the $PM_{2.5}$ concentrations are over predicted in all three locations, in contrast to the AERONET data. For the two sites in Abidjan, the model also predicts higher concentrations during July and August than observed. The cause of these discrepancies is hard to identify as the measurement sites are situated in the immediate vicinity of large emission sources whilst the corresponding model data is taken from a grid box of approximately 25 km $\times$ 30 km horizontal resolution which is inherently unable to identify these highly localised sources well. However, the over estimate in the dry season is likely to be due to uncertainties in the transport of dust as this is the major source of $PM_{2.5}$ during this season.

Comparisons to AERONET observations suggest modelled aerosol concentrations are under predicted, whilst comparison to DACCIWA ground sites suggests that the aerosol concentrations are over estimated. Despite this, comparisons for both AERONET and DACCIWA ground sites show close agreement within the variability range and therefore provide confidence in the model predictions of particulate matter. The comparison to INDAAF measurement sites suggests that there are some under predictions in NO, SO_2 and NH_3 emissions, this is in agreement with the evaluation in Chapter 2. The main issue highlighted by the comparison to the INDAAF sites is the very large over predictions of O_3 concentrations throughout the region (of $\sim$20-30 ppbv). It is therefore important to consider this when assessing the impacts of ozone in the region on human and ecosystem health.

Now that some assessment of the performance of the model against observations has

been made, the geographic and seasonal distribution of pollutants within the model can be investigated.

3.3 Seasonal patterns in surface level pollutant concentrations

As discussed in Section 3.1, the seasonal concentrations of pollutants are governed largely by emissions and meteorology. Figure 3.9 shows the mean surface level concentrations of CO, NO_x, SO_2, O_3 and $PM_{2.5}$ for the region for the dry season (January 2016) and the wet season (July 2016).

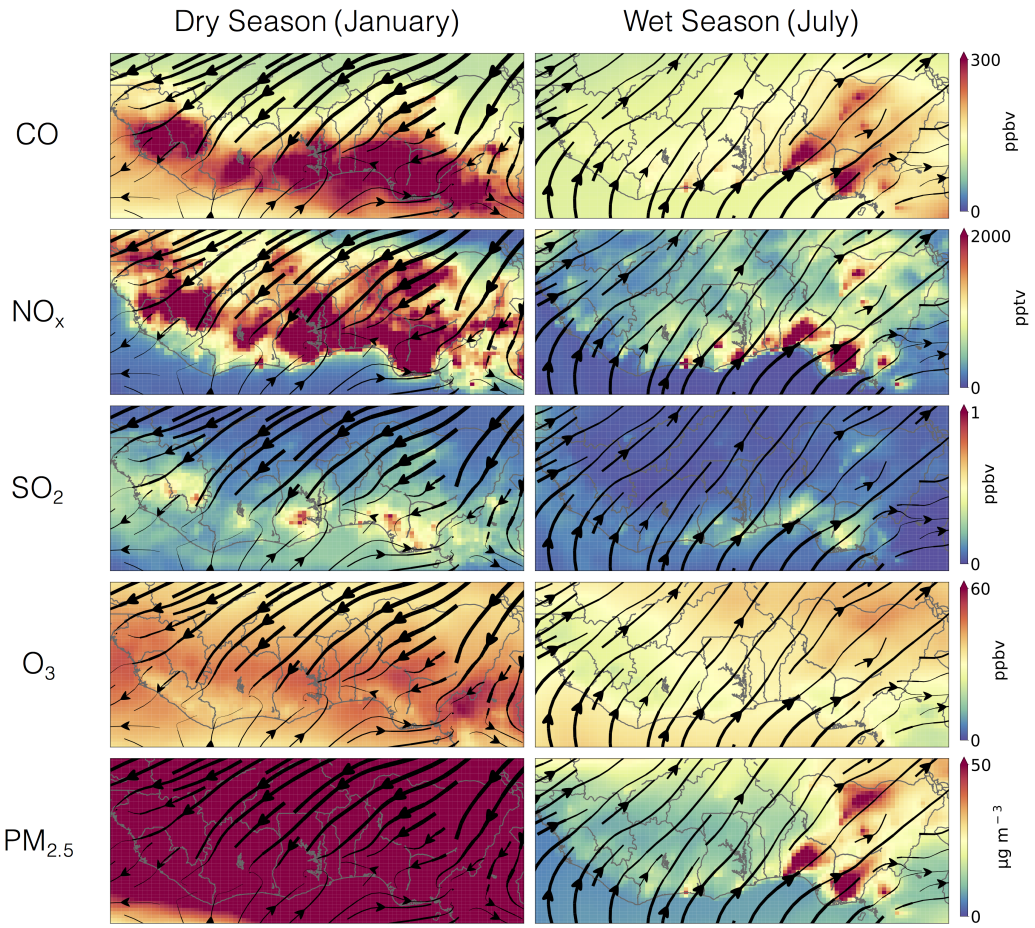

Figure 3.9: Seasonal surface level concentrations of CO, NO_x, SO_2, O_3 and $PM_{2.5}$. Left hand panel shows mean dry season (January 2016) concentration, right hand panel shows mean wet season (July 2016) concentration. Monthly mean surface wind stream functions from GEOS-FP meteorological data for the year 2016.

The surface level concentrations of all of these species are highest during the dry season. CO, NO_x and SO_2 show a distinct pattern of high concentrations along the coastline surrounding the major cities during the dry season and lower concentrations with more defined plumes towards the north east from these cities during the wet season. Figure 3.4

shows that the emissions of these species are highest during the dry season and lowest during the wet season. Furthermore, during the dry season, the convergence zone of weak flow along the coastline concentrates the pollutants further in this region. During the wet season, the flow of typically cleaner air from the Gulf of Guinea across the region to the north east disperses the pollutants and produces well defined plumes. During the dry season there is also an additional contribution to the concentrations of these species from biomass burning activities. Emissions of CO, NO and SO_2 from biomass burning during the dry season months are greater than the emissions from anthropogenic sources which significantly increases the concentrations of these pollutants. During the dry season, precipitation along the coastline suppresses the burning and hence pollutant concentrations are reduced. O_3 concentrations also follow the pattern of high dry season concentrations and lower wet season concentrations, as precursor concentrations are highest in this season.

Finally, fine particulate matter ($PM_{2.5}$) concentrations are higher in the dry season than the wet season. This is largely due to dust from the Sahara desert being brought down to the coastline by strong winds from the north east during the dry season. During the wet season, however, the flow of air from the south / south west disperses the particulate pollution from the cities and prevents dust from the Sahara moving southwards towards the coastline. Increased precipitation also increases the removal of soluble aerosol by wet deposition, overall resulting in lower concentrations across the region. Increased anthropogenic and biomass burning sources also contribute to the high concentrations of $PM_{2.5}$ during the dry season.

3.4 Annual cycle of surface composition in West Africa

It is evident that a range of different sources play a key role in determining surface concentrations of pollutants in the region. The contributions of these different sources to the concentrations of key pollutant species in the region is explored here. A series of model simulations have been performed in which the different emission sources are independently switched off, enabling the impact of the individual sources to be quantified. This approach assumes that the concentrations vary linearly as a result of switching different emission sources off and does not consider the changes in chemistry as a result of altering the composition of the atmosphere. The seasonal variations in the concentrations of gases (Section 3.4.1), aerosols (Section 3.4.2) and fine particulate matter (Section 3.4.3) are considered for two locations: (a) the average for the Guinea region (Figure 2.2); (b) the average for the coastal cities of Abidjan (Côte d'Ivoire), Accra (Ghana), Lomé (Togo), Cotonou (Benin) and Lagos (Nigeria).

3.4.1 Gaseous species

The annual concentrations of carbon monoxide (CO), nitrogen oxides (NO_x), sulfur dioxide (SO_2) and ozone (O_3) are considered here, all of which are subject to standards and regulations in many parts of the world due to the widely studied adverse effects on human health [149, 153, 172, 188, 198, 202, 221, 241, 250, 261].

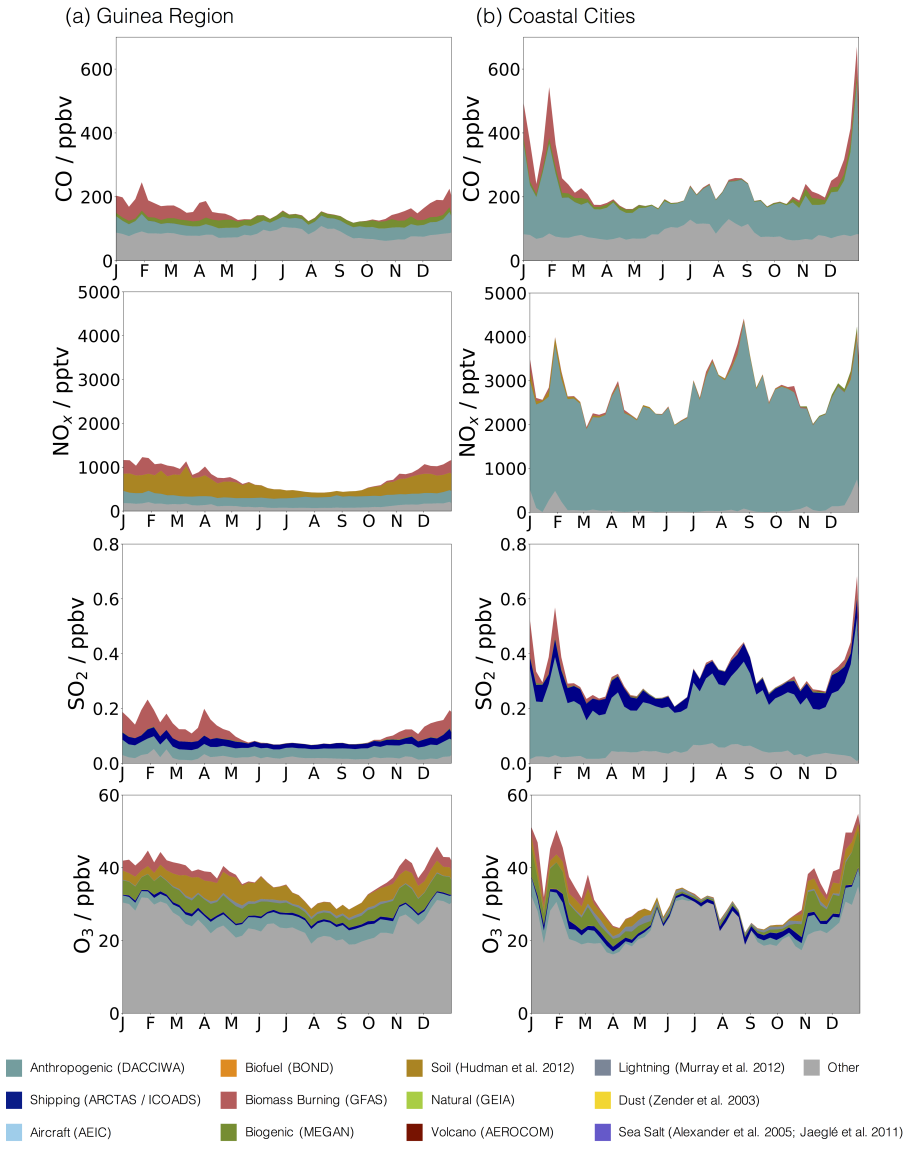

Figure 3.10: Seasonal variations in weekly mean surface level CO, NO_x, SO_2 and O_3 concentrations for the year 2016. Concentrations are divided into the contributions from different sources taken as a mean of the grid boxes. Model data averaged at surface level for: (a) the Guinea region; (b) the coastal cities of Abidjan (Côte d'Ivoire), Accra (Ghana), Lomé (Togo), Cotonou (Benin) and Lagos (Nigeria). "Other" refers to sources of concentrations which are not attributable to any of the other emission categories listed; this includes chemical production.

Throughout the Guinea region, the average CO concentrations are around 150 - 200 ppbv. There is a consistent contribution from anthropogenic and biogenic sources (both

direct emissions and as a result of oxidation of isoprene and other VOCs emitted from the MEGAN inventory) throughout the year as well as a seasonal contribution from biomass burning activities during the dry season (November to April). In the coastal cities, the anthropogenic source is significantly increased with CO concentrations reaching up to 600 ppbv during the dry season. Being closer to the sources results in higher concentrations and reduced dispersion of CO during the dry season enables concentrations to build up in the coastal cities.

The concentrations of NO_x in the coastal cities throughout the year are higher than the regional average by a factor of approximately 5, reflecting the anthropogenic sources and short lifetime. For the Guinea region, the anthropogenic contribution to the concentrations is consistent throughout the year, in agreement with the emissions seen in Figure 3.4. There is also a seasonal contribution from biomass burning activities during the dry season months and a large contribution from soil emission sources which is also largest during the dry season. For the city locations, the concentrations are dominated almost entirely by anthropogenic sources.

SO_2 concentrations are also significantly higher in the cities, with anthropogenic sources greatly increased relative to the regional average. Biomass burning activities show a greater contribution during the dry season to the regional concentrations. Concentrations from shipping are higher in the urban areas, due to the cities being coastal with large port infrastructure.

Whilst O_3 is a secondary pollutant, and is not emitted directly from these sources, switching off different emission sources in the simulations enables the ozone formation from these different sources to be quantified to some extent. Both the regional and urban concentrations are relatively similar, with both areas showing contributions from a range of different sources. The largest contributing sources to ozone formation are anthropogenic, biogenic and soil emissions of precursor compounds with seasonal contributions from biomass burning activities. During the wet season, the coastal cities show limited sensitivity to the local emissions, with the "Other" category making up most of the ozone concentration. This reflects the transport of air at this time of the year from the Gulf of Guinea. In the dry season, the local emissions make a larger contribution to the concentration as the flow of air from the north combined with low wind speeds along the coastline means that precursor emissions have time to react and create ozone.

3.4.2 Aerosol species

The contributions of the different emission sources to the concentrations of BC, OC, NO_3^-, SO_4^{2-} and NH_4^+ aerosols are displayed in Figure 3.11.

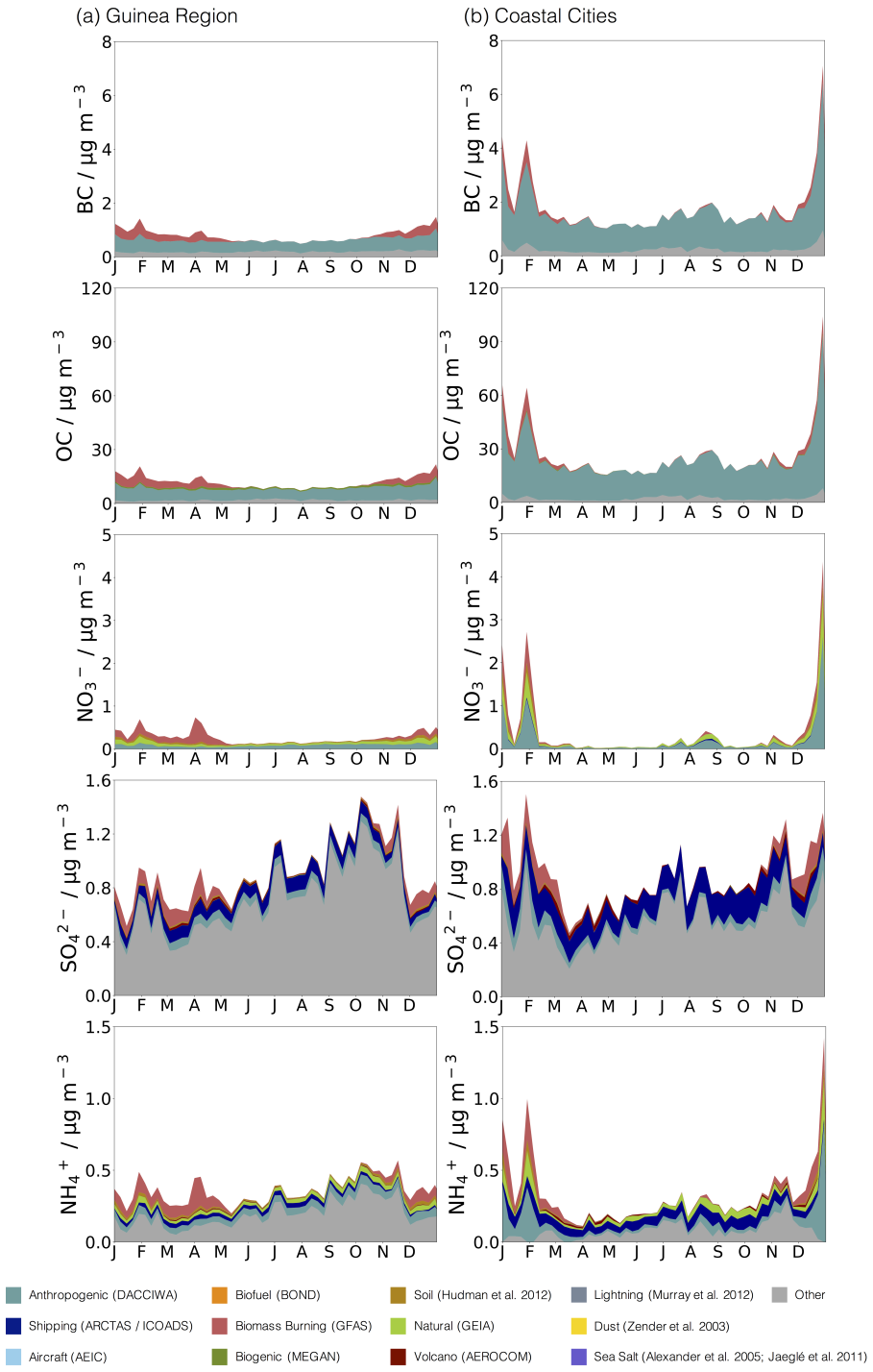

Figure 3.11: Seasonal variations in weekly mean surface level BC, OC, NO_3^-, SO_4^{2-} and NH_4^+ concentrations for the year 2016. Concentrations are divided into the contributions from different sources taken as a mean of the grid boxes. Model data averaged at surface level for: (a) the Guinea region of interest; (b) the coastal cities of Abidjan (Côte d'Ivoire), Accra (Ghana), Lomé (Togo), Cotonou (Benin) and Lagos (Nigeria). "Other" refers to sources of concentrations which are not attributable to any of the other emission categories listed; this includes chemical production.

For the Guinea region, anthropogenic sources provide a consistent contribution to the concentrations of BC and OC throughout the year. OC also shows a small contribu-

tion from biogenic sources and, for both species, biomass burning activities contribute to higher concentrations in the region during the dry season. For the coastal cities, the seasonal contribution from biomass burning sources is also seen, along with much higher concentrations attributed to anthropogenic sources.

For NO_3^-, the concentrations are made up of influences from anthropogenic, natural, soil and biomass burning sources. These sources are seen both for the regional average and for the coastal cities, with the urban locations showing much stronger peaks in concentrations (up to 4 μg m^{-3}) during the dry season.

SO_4^{2-} concentrations are influenced by anthropogenic, shipping and biomass burning sources, with some smaller impact from volcanic activities. For the Guinea region the concentrations are highest in October and November, whilst for the city locations the concentrations are highest from December to February.

Concentrations of NH_4^+ consist of contributions from anthropogenic, shipping, soil and natural sources and also show a strong seasonal signature from biomass burning. Concentrations are typically higher when considering the regional average, with the exception of some large peaks in the urban concentrations during December and January as a result of increased anthropogenic activity.

Whilst all aerosol concentrations show influences from anthropogenic activities and seasonal biomass burning, the largest differences between the regional and city data is seen for the carbonaceous aerosols. Anthropogenic concentrations of BC and OC aerosol are noticeably increased when considering the city weighted average, suggesting that anthropogenic sources of these aerosols are likely to be a major factor influencing the impacts on human health.

3.4.3 Fine particulate matter ($PM_{2.5}$)

Modelled fine particulate matter ($PM_{2.5}$) concentrations take into account the mass of all the aerosol tracers (sulfate, nitrate, ammonium, black carbon, organic carbon, dust and sea salt) and also include the additional mass due to uptake of water to these aerosols. The equation used to calculate $PM_{2.5}$ concentrations in the GEOS-Chem model is shown below [165].

$$\begin{aligned} PM25 = {} & 1.51(NH4 + NIT + SO4) + BCPI + BCPO \\ & + 2.1(OCPO + 1.24(OCPI)) + DST1 + 0.38DST2 + 2.42SALA \end{aligned}$$

Where NH4 is ammonium aerosol (NH_4^+), NIT is nitrate aerosol (NO_3^-), SO4 is sulfate aerosol (SO_4^{2-}), BCPI and OCPI refer to hydrophilic black and organic carbon aerosol respectively whilst BCPO and OCPO refer to hydrophobic BC and OC aerosol, DST1 and DST2 refers to dust aerosols with an effective radius of 0.7 and 1.4 microns respectively

and SALA is accumulation mode sea salt aerosol. The numbers included in this equation are factors which account for aerosol water, assuming a relative humidity of 50%.

The concentrations of $PM_{2.5}$ for both the Guinea region (Figure 3.12(a)) and the West African coastal cities (Figure 3.12(b)) show a clearly defined seasonal pattern with high concentrations during the dry season and much lower concentrations during the wet season.

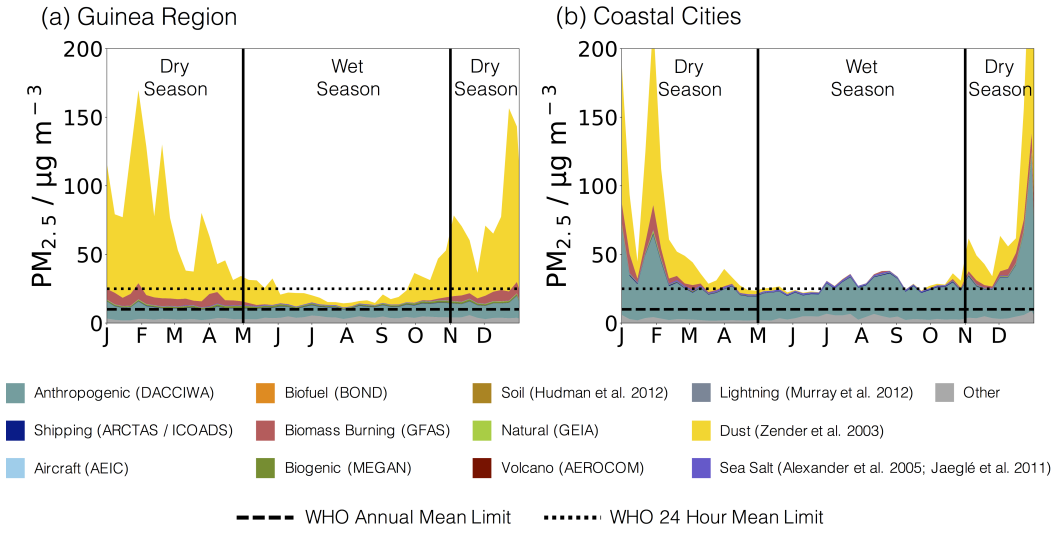

Figure 3.12: Seasonal variations in weekly mean surface level $PM_{2.5}$ concentrations for the year 2016. Total concentration is divided into the contributions from different sources. Model data averaged at surface level for: (a) the Guinea region of interest; (b) the coastal cities of Abidjan (Côte d'Ivoire), Accra (Ghana), Lomé (Togo), Cotonou (Benin) and Lagos (Nigeria). "Other" refers to sources of concentrations which are not attributable to any of the other emission categories listed; this includes chemical production. World Health Organisation (WHO) air quality annual mean guideline value indicated by dashed line and 24 hour mean guideline value indicated by dotted line.

For the Guinea region, the anthropogenic source of $PM_{2.5}$ remains largely consistent throughout the year (at around 10 μg m^{-3}) whilst the biomass burning contribution increases during the dry season due to local burning events. The largest source of $PM_{2.5}$ in the Guinea region in the model though is dust. During the wet season, the contribution from dust is small. During the dry season, there is a large influx of dust to the region from the Sahara to the north and this dominates the seasonal cycle.

For the coastal cities, the anthropogenic source of $PM_{2.5}$ is dominant, with consistent concentrations (of around 25 μg m^{-3}) throughout the wet season and higher concentrations (of up to 80 μg m^{-3}) during the dry season. The impact of biomass burning in the cities themselves is small; however, there is still a large contribution from dust during the dry season.

The World Health Organisation (WHO) air quality guidelines propose an annual mean limit of 10 μg m^{-3} and a 24 hour mean limit of 25 μg m^{-3} for $PM_{2.5}$ [274]. In Figure 3.12, the recommended annual mean limit (10 μg m^{-3}) is exceeded both for the Guinea region

and for the coastal cities. Whilst the daily mean limit (25 μg m^{-3}) is also exceeded for both locations for the majority of the year. Dust is a major source of $PM_{2.5}$ in this region and it would be challenging to control through policy changes. Anthropogenic sources may more easily be regulated on local scales [236] and the large contribution of these activities to $PM_{2.5}$ concentrations in urban regions (where population is typically highest) is evident in Figure 3.12(b).

3.5 Contributions of different emission sources to species concentrations in West Africa

Whilst the analysis in Section 3.4 gives an insight into the concentrations of pollutants in the Guinea region and coastal cities throughout the year, it is hard to identify the concentrations that a typical location or member of the population will be exposed to at the surface and what the most dominant sources influencing these concentrations are.

The area weighted (Guinea region) annual mean concentrations of both gaseous and aerosol species have been calculated along with the average contributions of different emission sources to these concentrations (Figure 3.13 - left hand bar labelled "Area"). The equivalent model data from a population weighted perspective is shown in the right hand bar labelled "Population". The population weighted mean is calculated by considering each model grid box in the region individually. The mean annual concentration in each grid box is multiplied by the population within the box [47]. These values are added together for all grid boxes within the region and then divided through by the total population to achieve the population weighted value.

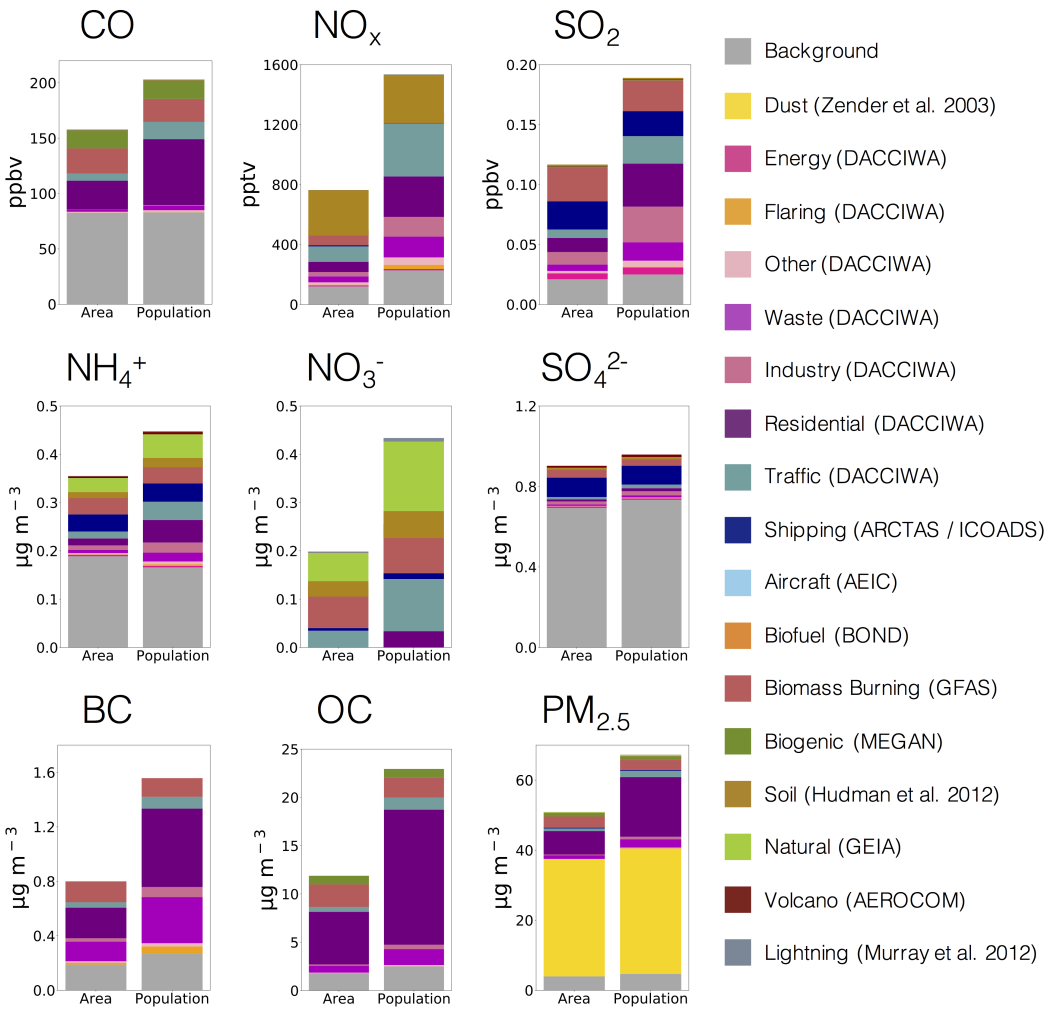

Figure 3.13: Contribution of different emission sources to the mean area weighted (left hand bar) and population weighted (right hand bar) surface concentration in the Guinea region. Note that the $PM_{2.5}$ concentrations include additional mass due to uptake of water whereas concentrations of other aerosol species do not.

The first difference to note is that the population weighted concentrations are higher than the area weighted concentrations. For example, the concentrations of NO_x, SO_2 and carbonaceous aerosols experienced by a typical member of the population are approximately double the area weighted average, whilst $PM_{2.5}$ concentrations are approximately 30% higher.

CO concentrations show a large influence from residential activities as well as from road traffic, biomass burning and biogenic sources in both the area and population weighted concentrations. The population weighted concentration shows a larger fractional contribution from residential and traffic sources and a smaller fractional contribution from biomass burning relative to the area weighted concentration.

The area weighted concentration of NO_x is dominated by the contribution from soil emission sources, accounting for approximately 40% of the concentration. The concentration is also influenced to a large extent by biomass burning and traffic emissions with

smaller contributions from residential activities, industry and waste. From a population weighted perspective, the fractional contribution of the anthropogenic sources (traffic, residential, industry and waste) are increased whilst the contributions from soils and biomass burning are reduced.

SO_2 concentrations exhibit contributions from a wide range of sources. For the area weighted average, the largest contributions are from biomass burning and shipping. Whereas, from a population weighted perspective, the fractional contribution from biomass burning, shipping, traffic, residential, industry and waste sources are more equal.

Inorganic aerosol (NH_4^+, NO_3^- and SO_4^{2-}) concentrations are influenced by a wide range of activities. For all three species, the composition of the different sources remains largely unchanged when considering the area weighted versus population weighted concentrations.

Natural, soil and biomass burning sources contribute to NH_4^+ concentrations along with anthropogenic contributions from shipping, traffic, residential, waste and industry. These anthropogenic contributions are larger when considering the population weighted concentration.

NO_3^- concentrations are influenced by a similar set of emission sources as NH_4^+ concentrations. From an area weighted perspective, natural, soil and biomass burning emissions are dominant, whilst from a population weighted perspective, the contribution from anthropogenic sources (predominantly residential and traffic) is increased.

SO_4^{2-} concentrations show both a similar magnitude and similar source composition for both scenarios. Shipping and biomass burning are the dominant sources, with smaller contributions from other sources.

BC and OC concentrations show a similar source composition. Considering the area weighted concentrations first, anthropogenic emission sources are dominant with large contributions from residential, waste and road traffic. Biomass burning also influences the concentrations of both species whilst approximately 7.5% of OC concentrations are attributable to biogenic sources. From a population weighted perspective, the composition remains largely the same although the residential contribution is increased and biomass burning contribution is decreased for both species.

The dominant contribution to $PM_{2.5}$ concentrations, whether on an area or population basis, is from dust (53% (population weighted) to 66% (area weighted)). This is followed by a key contribution from residential activities, which may be expected considering the large contribution this sector makes to concentrations of inorganic and carbonaceous aerosols. $PM_{2.5}$ concentrations are influenced to a smaller extent by waste, industry, road traffic and biomass burning activities.

It is evident that anthropogenic activities play a key role in influencing the concentrations of pollutants experienced by the population in the Guinea region. In particular, residential activities along with road traffic are leading factors influencing the pollutant

concentrations and may be suitable sectors to target when developing policies to reduce pollutant concentrations and mitigate the impacts of pollution on the West African population.

3.6 Estimate of the impact of air quality on human health

A variety of pollutants are either known or suspected to be harmful to human health as well as to the environment [7, 23, 80, 149, 215, 234] (see Section 1.1). These pollutants can come from a wide range of sources and have impacts both in the immediate vicinity of these sources as well as across vast areas due to transport of these species [2, 107, 109, 134, 218, 229, 277].

The exposure of the population to gaseous pollutants (CO, NO_2, SO_2 and O_3) (Section 3.6.1) and fine particulate matter (Section 3.6.2) above recommended limits can be assessed from the annual simulation data.

3.6.1 Human exposure to gaseous pollutants in West Africa

Four of the main gaseous pollutants that pose a threat to human health are carbon monoxide (CO), nitrogen dioxide (NO_2), sulfur dioxide (SO_2) and ozone (O_3) [149, 153, 172, 188, 198, 202, 221, 241, 250, 261]. All four of these play a role in exacerbating respiratory and cardiovascular diseases and the World Health Organisation (WHO) provides guideline values for each of these species (except CO) [75, 274]. The population weighted concentrations of these pollutants in the Guinea region are considered, along with the concentrations in five of the main coastal cities. For each location, the major sources contributing to the concentrations are also shown.

Whilst the WHO does not provide guideline values for CO, the European Union (EU) air quality standard for CO is 10 mg m^{-3} (8.6 ppmv) maximum daily 8 hour mean [75].

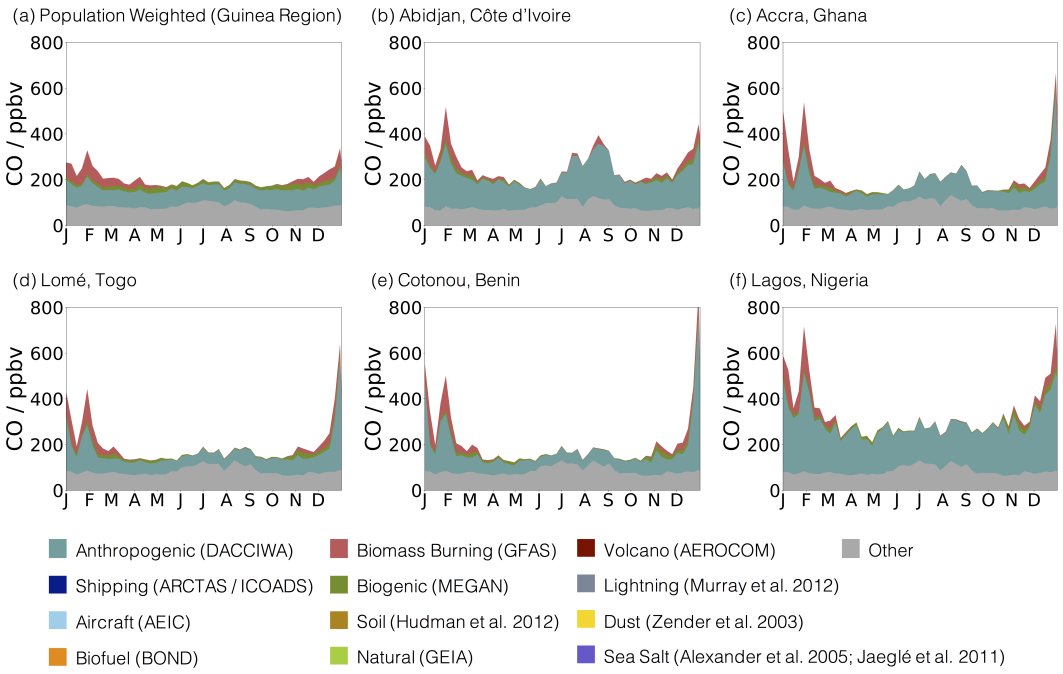

Figure 3.14: Annual cycle of surface level CO concentrations for 2016 (a) weighted by population for the Guinea region (b-f) for five of the main coastal cities. Total concentration is divided into the contributions from different sources. Data is averaged weekly.

It is clear that whilst CO concentrations are heavily influenced by anthropogenic emissions in all locations as well as biogenic and biomass burning sources, the concentrations are well below the 10 mg m^{-3} (8.6 ppmv) objective. The population weighted weekly concentrations in the region do not exceed 350 ppbv, whilst the concentrations in the cities rarely exceed 500 ppbv. Based on this, the outdoor concentrations of CO in West Africa do not appear to be a health concern at present. Of bigger concern is likely the indoor concentrations that the population is exposed to from sources such as wood burning for domestic cooking and heating.

The WHO guideline values for NO_2 are 40 μg m^{-3} (21.3 ppbv) annual mean and 200 μg m^{-3} (106.4 ppbv) 1 hour mean [274].

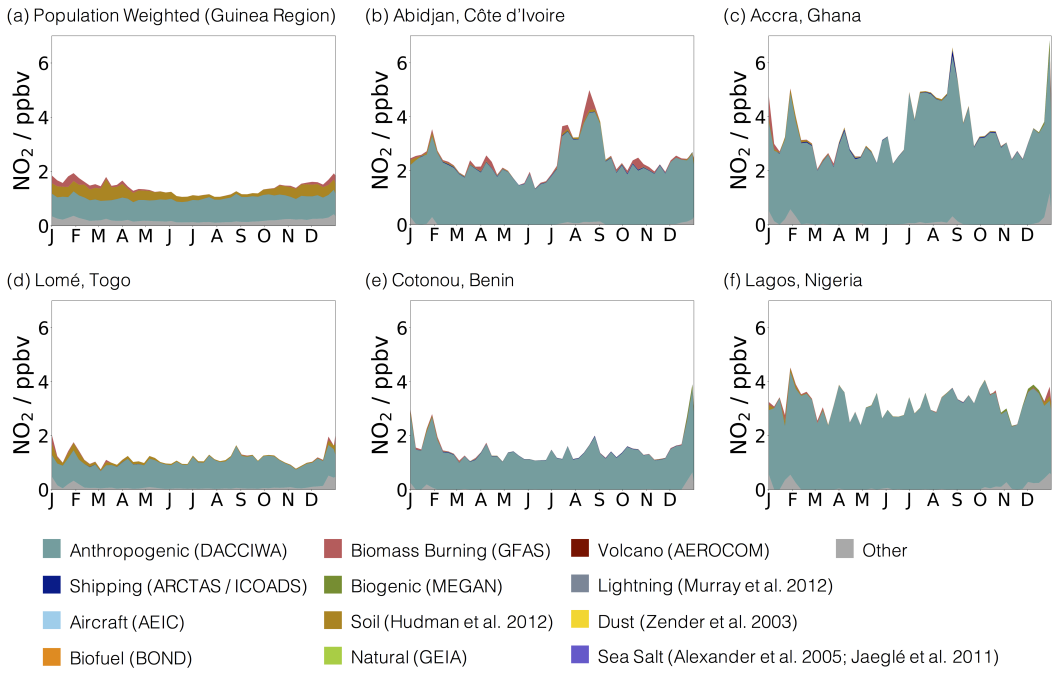

Figure 3.15: Annual cycle of surface level NO_2 concentrations for 2016 (a) weighted by population for the Guinea region (b-f) for five of the main coastal cities. Total concentration is divided into the contributions from different sources. Data is averaged weekly.

Considering the average concentrations that the population in the region is exposed to at the surface (Figure 3.15(a)), there are no exceedances of either of the WHO limits in the model data for 2016. The population weighted annual mean concentration of NO_2 in the Guinea region is 1.4 ppbv whilst the highest hourly mean concentration observed in the model data over the year is 4.3 ppbv. Taking into account the factor 2.5 under prediction in NO emissions calculated in Chapter 2, the NO_2 concentrations are still below the guideline values. The same is true when considering the concentrations in the five coastal cities. As the modelled outdoor NO_2 concentrations are below the WHO recommendations, NO_2 does not appear to currently be a health concern for the West African population. However, the regional GEOS-Chem model is still a coarse resolution ($\sim$25 km grid) so it is unable to simulate the steep concentration gradients often observed at street scale. Neither is it able to give any indication of the indoor concentrations.

For SO_2, the WHO guideline recommends that the 24 hour mean concentration does not exceed 20 μg m^{-3} (7.6 ppbv) [274].

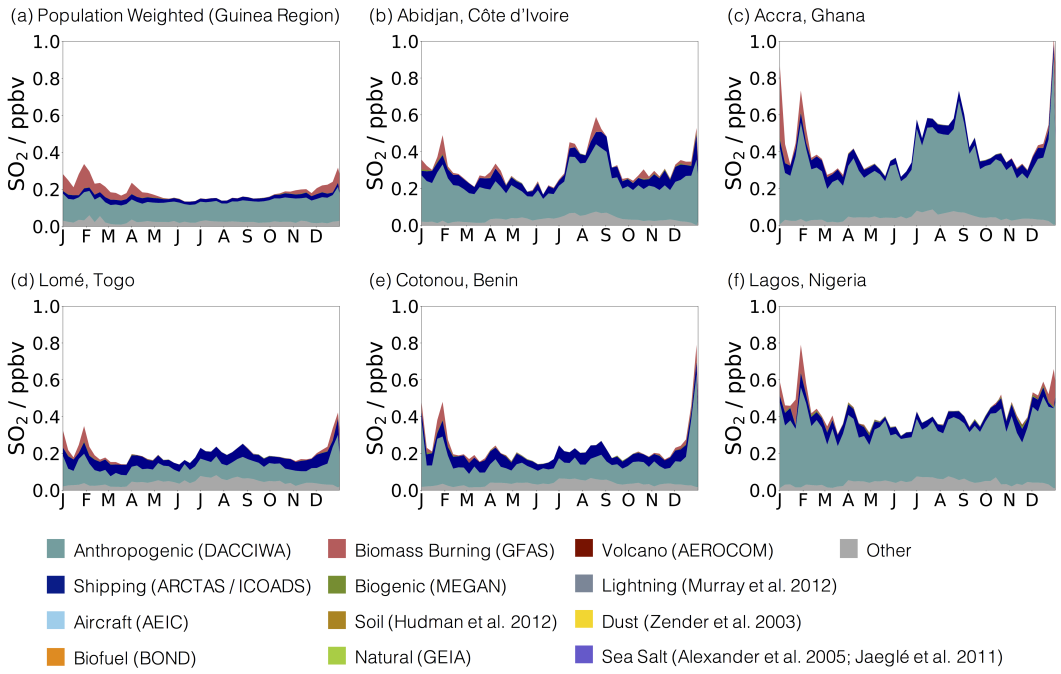

Figure 3.16: Annual cycle of surface level SO_2 concentrations for 2016 (a) weighted by population for the Guinea region (b-f) for five of the main coastal cities. Total concentration is divided into the contributions from different sources. Data is averaged weekly.

The maximum 24 hour mean SO_2 concentration seen in the population weighted regional average is 0.41 ppbv which is within the WHO guideline. Considering the factor 14 under prediction calculated in Chapter 2, SO_2 concentrations may actually be close to the 7.6 ppbv limit. The concentrations in the cities are, in general, higher than seen in the population weighted average. Monitoring of SO_2 concentrations in the region is recommended in order to better assess whether the concentrations are within the guideline values.

The 8 hour mean guideline value for O_3 from the WHO is 100 μg m^{-3} (51.0 ppbv) [274].

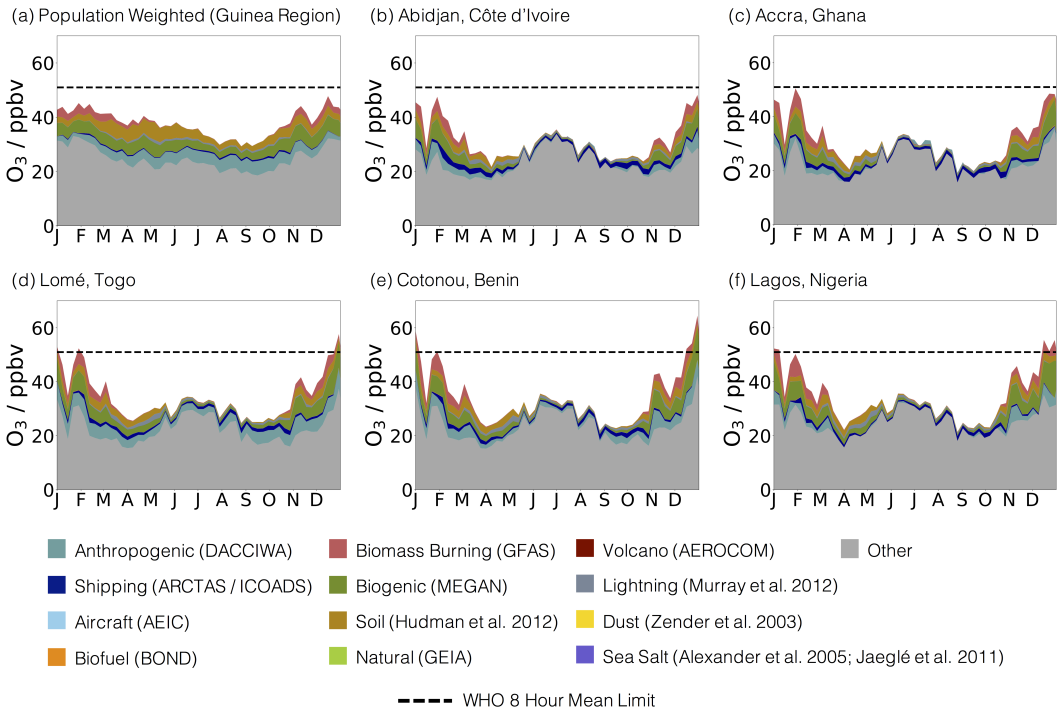

Figure 3.17: Annual cycle of surface level O_3 concentrations for 2016 (a) weighted by population for the Guinea region (b-f) for five of the main coastal cities. Total concentration is divided into the contributions from different sources. Data is averaged weekly.

Whilst the concentrations of CO, NO_2 and SO_2 are considerably lower than WHO guidelines, O_3 concentrations are much closer to the recommended limit when considering the regional weekly averaged concentrations (Figure 3.17(a)) and exceed the limit on occasions for some of the cities (Figure 3.17(b-f)). When 8 hour mean concentrations are calculated, the WHO limit is found to be exceeded on at least one occasion for all locations within the Guinea region. Most of the region experiences these high O_3 concentrations less than 10% of the time, with the areas most affected spending around 30% of the time above the recommended limit. The majority of these exceedances occur during the dry season (November to April) when the O_3 concentrations are at their highest. O_3 is therefore a health concern for the population in the Guinea region and is an important consideration when designing pollution reduction policies for the protection of human health. It must however be noted that comparisons of model data to aircraft observations from the DACCIWA campaign (Section 2.4) and ground based measurements from INDAAF sites (Section 3.2.2) found modelled ozone concentrations to be over predicted. It is therefore likely that the modelled ozone concentrations discussed here are higher than the true values. More work is necessary to understand this model problem. Improved monitoring of ozone concentrations in the region is also recommended in order to better assess whether concentrations are in exceedance of the guideline limits.

3.6.2 Human exposure to $PM_{2.5}$ in West Africa

Fine particulate matter, which includes particles up to 2.5 μm in diameter, is one of the key species when considering the impacts of air quality on human health due to its damaging effects on the respiratory system [2,23,33,63,64,280]. Exposure to high concentrations can exacerbate cardio-vascular and respiratory conditions with children and the elderly being most susceptible to these health impacts [216]. Unlike most other pollutants, $PM_{2.5}$ is made up of many different components (black carbon, organic carbon, inorganic aerosols, dust and sea salt) and therefore the concentrations are influenced by a wide range of sources. These sources can vary greatly depending on location and time of year. This makes $PM_{2.5}$ a challenging pollutant when developing policy options for best mitigating the impacts on human health.

The influence of seasonal emission sources on $PM_{2.5}$ concentrations in West Africa.

$PM_{2.5}$ concentrations across the Guinea region are not uniform and concentrations vary greatly depending upon location and upon season (Section 3.3). This is largely due to the wide range of species and sources which contribute to $PM_{2.5}$ concentrations, as well as seasonal changes in meteorological processes (Section 3.1.1). As shown in Figure 3.12, the annual $PM_{2.5}$ concentrations and sources can be classified into two key seasons: the wet season and the dry season. The mean surface level concentrations of $PM_{2.5}$ from the major sources are shown in Figure 3.18 for the dry season (January) and wet season (July).

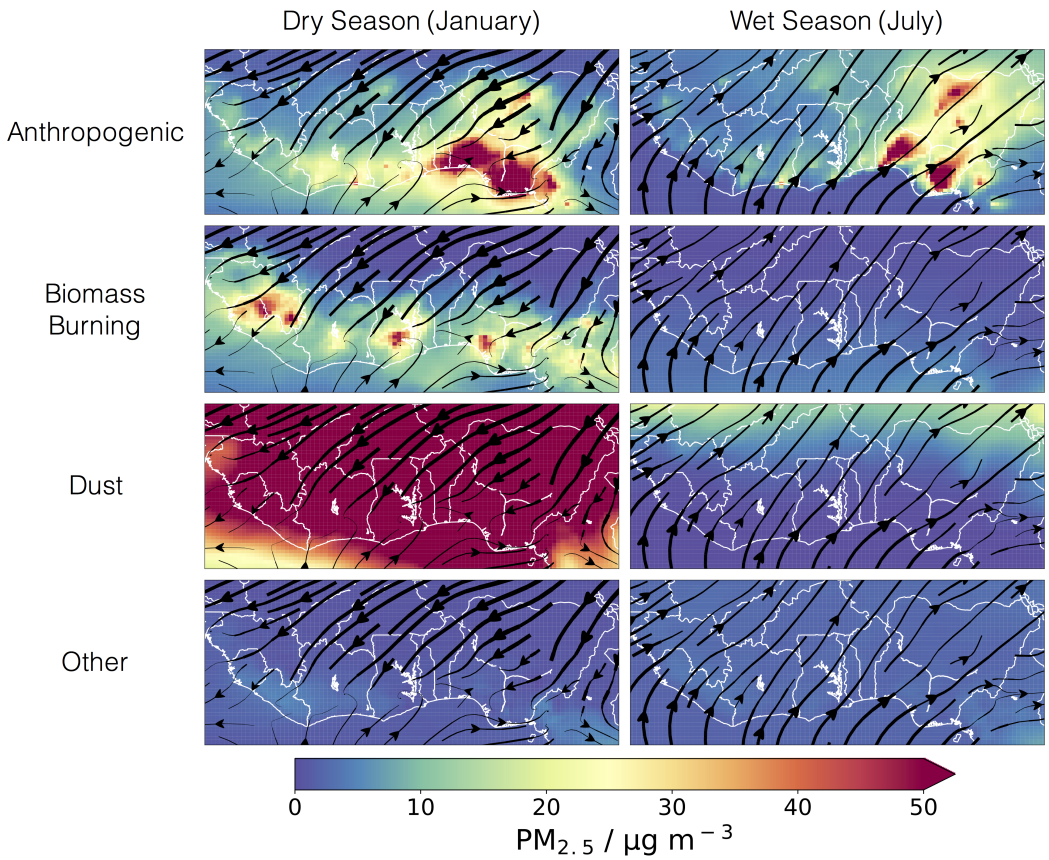

Figure 3.18: $PM_{2.5}$ surface level concentrations from anthropogenic, biomass burning, dust and other sources. Model data averaged for January 2016 (dry season) and July 2016 (wet season). Monthly mean surface wind stream functions from GEOS-FP meteorological data.

Higher concentrations of anthropogenic $PM_{2.5}$ are seen during the dry season when there is little rainfall in the region, resulting in less wet deposition, and the area of weak air flow along the coastline causes less dispersion of pollutants. During the wet season concentrations are lower as the flow of air from the Gulf of Guinea brings typically cleaner air masses to the region and disperses the $PM_{2.5}$ towards the north east producing well defined city plumes.

The concentrations from biomass burning are strongly influenced by the location of the burning activities [96, 212]. During the dry season burning activities take place in the West African coastal countries leading to high local emissions and increased $PM_{2.5}$ concentrations. During the wet season the biomass burning is located to the south east of the region in central Africa. As the predominant wind direction during this season is from the south to the north east, longer lived species are transported to the West African coastline and cause slightly elevated biomass burning $PM_{2.5}$ concentrations in the south of the region.

The dust contribution is influenced almost entirely by the wind. The prevailing wind from the north during the dry season brings high concentrations of dust down from the

Sahara to the West African coastline. During the wet season, the flow of air is reversed, so the dust remains in the north of the region and has little impact on $PM_{2.5}$ concentrations at the coast.

Anthropogenic, biomass burning and dust are the major sources of $PM_{2.5}$ in the Guinea region and the contribution from other sources is very small at all times of the year.

Exposure of the West African population to $PM_{2.5}$ concentrations above recommended limits

WHO air quality guidelines propose an annual mean limit of 10 μg m^{-3} and a 24 hour mean limit of 25 μg m^{-3} for $PM_{2.5}$ [274]. Modelled $PM_{2.5}$ concentrations in the Guinea region are related to these WHO guidelines by considering the proportion of time that the concentrations exceed the recommended 24 hour limit. A moving 24 hour mean is calculated throughout the year and the accumulated exceedances are used to determine the percentage of time over the limit.

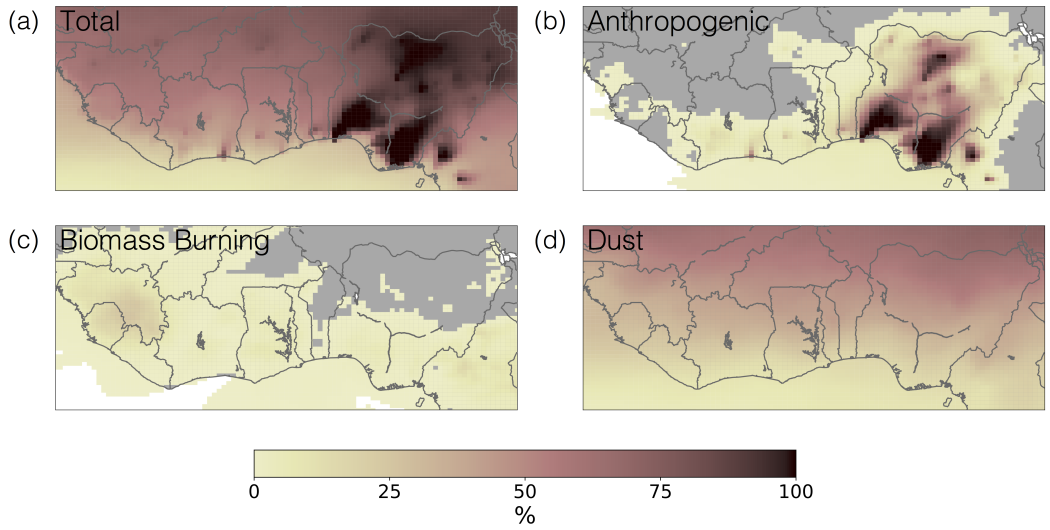

Figure 3.19: Percentage of 24 hour running mean $PM_{2.5}$ concentrations above the WHO 24 hour limit of 25 μg m^{-3} from modelled data for 2016. (a) total exceedances; (b) exceedances attributable to anthropogenic sources; (c) exceedances attributable to biomass burning sources; (d) exceedances attributable to dust sources.

For much of the region, the recommended limit is exceeded at least 50% of the time (Figure 3.19(a)). Considering each of the three key sources (anthropogenic, biomass burning and dust) individually enables the causes of these exceedances to be identified.

Anthropogenic sources alone (Figure 3.19(b)) cause the WHO limit to be exceeded along the coastal strip where many of the large cities are located and where population density is highest (Figure 1.10). This is particularly clear for the large Nigerian cities where anthropogenic sources cause the $PM_{2.5}$ limit to be exceeded up to 100% of the time. The influence from biomass burning (Figure 3.19(c)) is less distinctive but this source still

contributes to the exceedances across the Guinea region. Exceedances attributable to dust (Figure 3.19(d)) show a well defined north-south gradient with a high number of exceedances to the north of the region, closer to the Sahara desert, and fewer exceedances to the south.

The distribution and density of the population across the region must be considered when assessing potential impacts on human health. Figure 1.10 (Chapter 1) shows the population density across the Guinea region for the year 2016, extrapolated linearly from gridded population data for 2015 and 2020 from the NASA Socioeconomic Data and Applications Center (SEDAC) [47].

Across much of the region, the population density is below 100 people km^{-2}. The main exceptions to this are the the urban regions along the coastline. Population densities of 1000 people km^{-2} and above can be seen in the cities of Abidjan (Côte d'Ivoire), Accra (Ghana), Lomé (Togo) and Cotonou (Benin), as well as for substantial areas of Nigeria, predominantly around the large urban centres of Lagos and Port Harcourt on the coast and Abuja and Kano inland.

From a human health perspective it is important to consider the concentrations the population is exposed to. The simulation data presented in Figure 3.19 can therefore be considered from a population weighted perspective and Figure 3.20 displays an accumulated count of the population exposed to $PM_{2.5}$ concentrations above the daily guideline value.

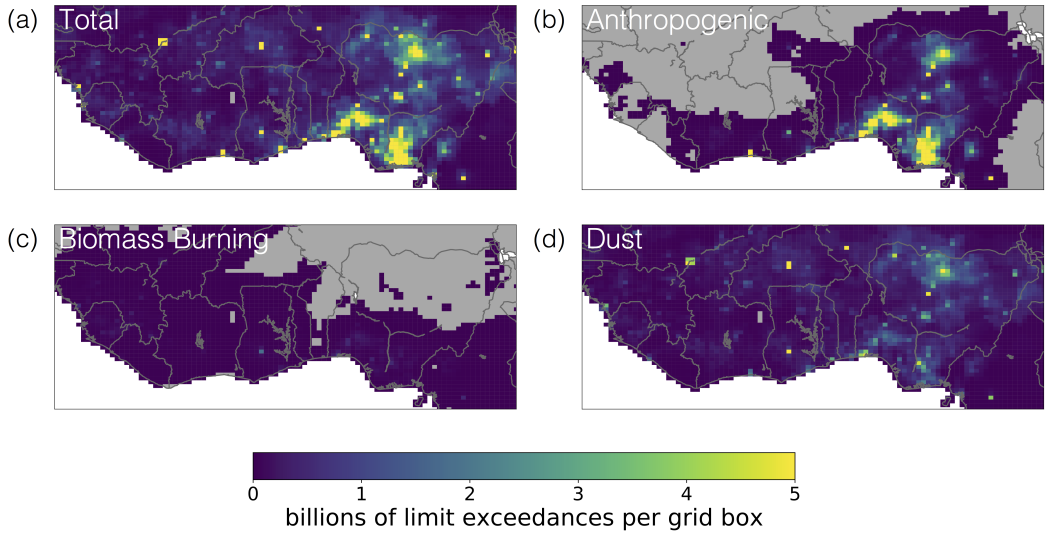

Figure 3.20: Accumulated population count of exposure to $PM_{2.5}$ concentrations above the WHO 24 hour limit of 25 μg m^{-3} for running mean 24 hour time periods for 2016. Statistics calculated by multiplying the population in each grid box by the accumulated number of 24 hour mean time periods over the WHO 24 hour limit. One person in continuous exceedance of the limit would produce a value of 8760.

Whilst Figure 3.19 suggests that dust has the largest influence on high $PM_{2.5}$ concentrations across the whole Guinea region, Figure 3.20 considers the concentration from a

population weighted perspective and highlights the large impact of anthropogenic sources on human exposure. The biggest effects of these anthropogenic sources are seen for the regions of high population density in Nigeria (mainly around the cities of Lagos, Port Harcourt, Abuja and Kano) as well as some of the large coastal cities in the region including Abidjan (Côte d'Ivoire). When population distribution is considered, it is clear that fewer people are affected by dust than by anthropogenic sources with the main impacts from dust being in the cities in the north of the region including Bamako (Mali), Ouagadougou (Burkina Faso), Niamey (Niger) and Kano (Nigeria). Biomass burning has a much smaller impact on the population than either dust or anthropogenic sources.

Sources contributing to high $PM_{2.5}$ concentrations in West Africa

It is evident from Figures 3.19 and 3.20 that dust and anthropogenic activities are the two largest sources contributing to the $PM_{2.5}$ concentrations in exceedance of WHO guideline values. However, these sources are not exclusively responsible for the limit exceedances and high $PM_{2.5}$ concentrations may be the result of a combination of two or more different sources. The different combinations of sources leading to high $PM_{2.5}$ concentrations in the Guinea region is further assessed here.

$PM_{2.5}$ concentrations can be divided into two key categories: concentrations which exceed the WHO limit and concentrations which are within the WHO limit. Of the concentrations that exceed the limit, these can be further categorised into the different combinations of sources that are attributable to these exceedances. These sources are considered for both the Guinea region (Figure 3.21(a)) and for the population within this region (Figure 3.21(b)).

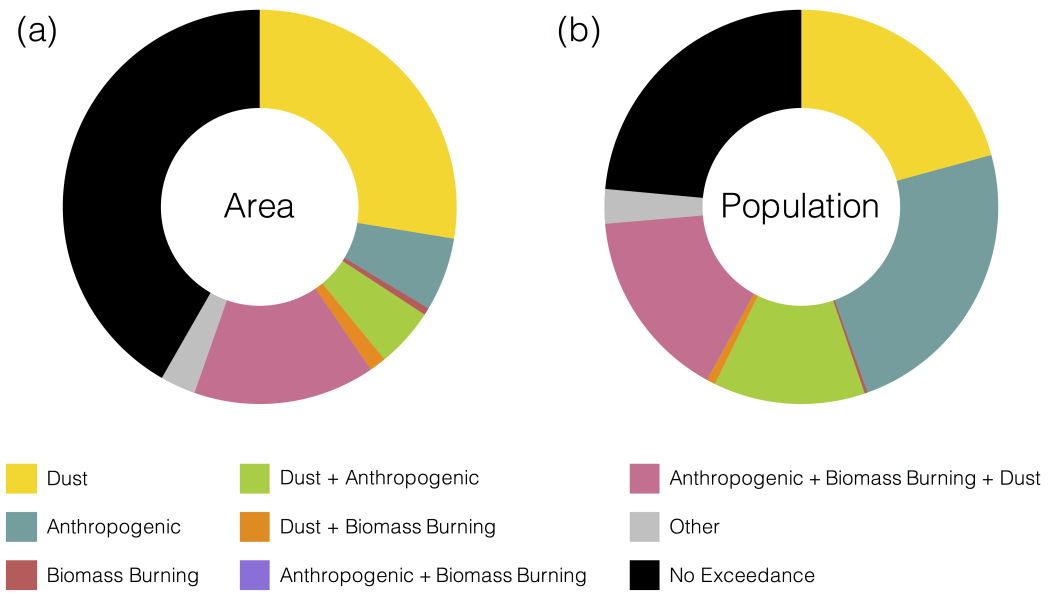

Figure 3.21: Pie charts showing the number of exceedances of the WHO $PM_{2.5}$ 24 hour limit of 25 μg m^{-3} in the year 2016 and associated causes of the exceedances. Causes of exceedances calculated as (a) area weighted for the Guinea region; (b) population weighted for the Guinea region.

For the area weighted Guinea region (Figure 3.21(a)), the $PM_{2.5}$ concentrations are in exceedance of the limit approximately 60% of the time. The largest single cause of these exceedances is from dust (approximately 47% of all exceedances). There is also a large impact from anthropogenic sources (approximately 10% of all exceedances) as well as the combination of anthropogenic and dust sources (around 8% of all exceedances). Biomass burning has a much smaller impact (1% of exceedances); however, the combination of all three of these key sources makes up a significant fraction (approximately 25%) of the total exceedances. Around 5% of the exceedances are attributed to "other" causes which is the combination of dust, anthropogenic and biomass burning sources along with other contributing sources such as sea salt.

Considering the same simulation from a population weighted perspective (Figure 3.21(b)), the impact from dust alone decreases (to around 27% of all exceedances) and anthropogenic activities become the largest source of the high $PM_{2.5}$ concentrations (31% of all exceedances). Exceedances attributed to the combination of anthropogenic and dust sources are increased (to over 16% of exceedances), and exceedances attributed to the combination of all three key sources remains a major contribution (around 20%). When the data is weighted by population rather than by area, the percentage of time that the $PM_{2.5}$ concentrations are within the WHO limit is decreased (from approximately 42% of the time to just 23% of the time). This emphasises the large impact that $PM_{2.5}$ concentrations have on the population.

With the projected increases in population [199] and increases in anthropogenic emis-

sions [141, 151] forecast for West Africa the issues surrounding high levels of $PM_{2.5}$, particularly in urban areas, are likely to become worse. It is therefore important that policies to reduce the concentrations of particulate matter and hence minimise the health impacts on the population are considered by the local governments. Dust has been found to be the largest source of $PM_{2.5}$ in the region; however, this is a complex challenge to regulate as it would require continental scale strategies involving methods such as irrigation and vegetation of the Sahara desert which has the potential to dramatically change the West African climate [34, 88]. Anthropogenic sources, in particular emissions from residential and road transport sectors, have also been shown to significantly contribute to the concentrations of $PM_{2.5}$. Emissions from these sectors may be regulated on a more local scale and therefore policies designed to reduce dependence on residential wood burning for cooking and heating as well as reduce emissions from vehicle exhausts could significantly reduce $PM_{2.5}$ concentrations, particularly in centres of high population density, and hence reduce the impact on human health [228, 236].

3.7 Estimates of the impact of air quality on ecosystem health

In addition to the impacts on human health, ecosystems are also affected by high concentrations of pollution. In particular, high concentrations of ozone can result in adverse effects on vegetation such as reduced root growth and crop yields, leaf damage and reduced drought tolerance [7, 54, 170, 234, 256, 276].

The Food and Agriculture Organisation (FAO) of the United Nations (UN) provides country level crop production data for 173 different crops [90]. Crops in West Africa are categorised into eight key groups and the annual production rates across the Guinea region are shown in Figure 3.22.

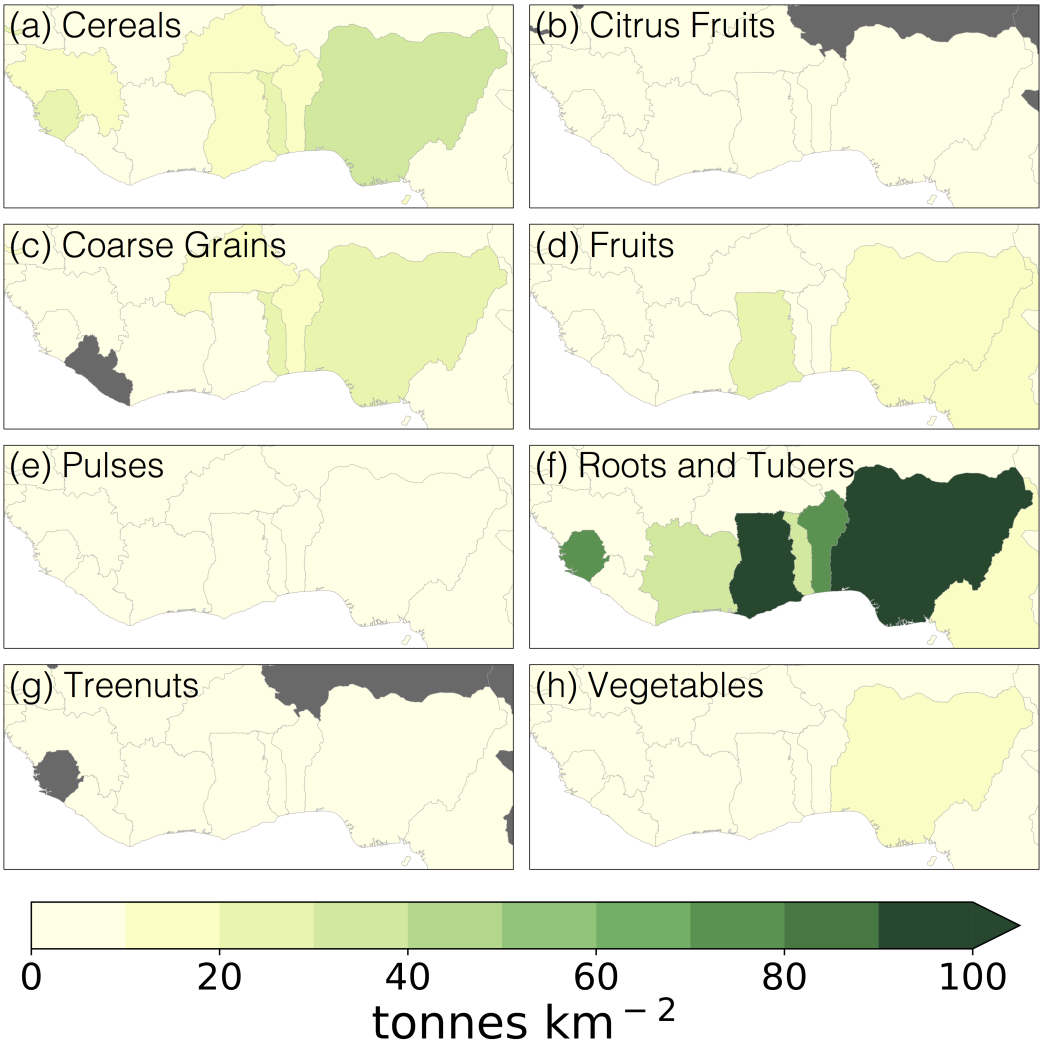

Figure 3.22: Crop production maps for the Guinea region for the year 2016. Data taken from the UN Food and Agriculture Organisation [90]. Grey regions indicate no available data.

Crop production totals in the region are dominated almost entirely by roots and tubers, with the highest production rates in Ghana and Nigeria [181]. The UN FAO Crop Calendar provides information on planting and harvesting schedules for more than 130 crops in specific agro-ecological zones [89]. The 2016 planting and harvesting schedules are presented in Figure 3.23 for three of the key roots and tubers in West Africa: cassava, sweet potato and yam.

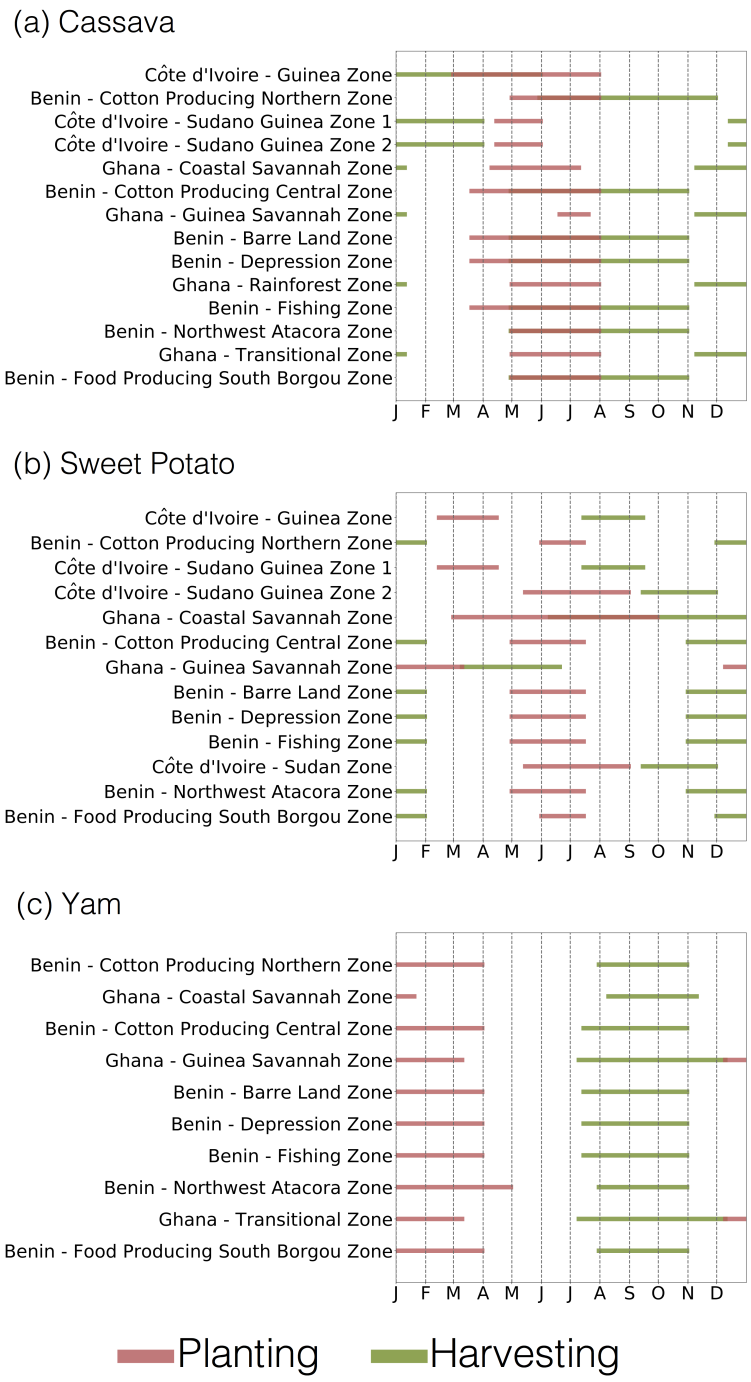

Figure 3.23: Crop planting and harvesting schedules for cassava, sweet potato and yam in 16 different agro-ecological zones in Côte d'Ivoire, Ghana and Benin for the year 2016 [89].

Within the Guinea region, planting and harvesting schedules are available for sixteen different agro-ecological zones in Ghana, Côte d'Ivoire and Benin [89]. For cassava, planting typically occurs between April and July with harvesting in Benin taking place from August to October and from November to February in Côte d'Ivoire and Ghana. The majority of sweet potato planting occurs between May and August with the harvesting season from September to January. Whereas planting of yam crops typically occurs from January to March with harvesting between July and October. The irrigation method in

West Africa is predominantly rain fed and therefore the planting and growing periods of most crops coincide with the wet season [260].

Ozone can impact on crop growth and productivity [7, 54, 170, 234, 256, 276] therefore the concentrations of O_3 must be considered for the growing seasons. Figure 3.24 shows the monthly mean O_3 concentrations during daylight hours (06:00 to 18:00) when photosynthesis occurs and O_3 concentrations have the largest impact on plant growth.

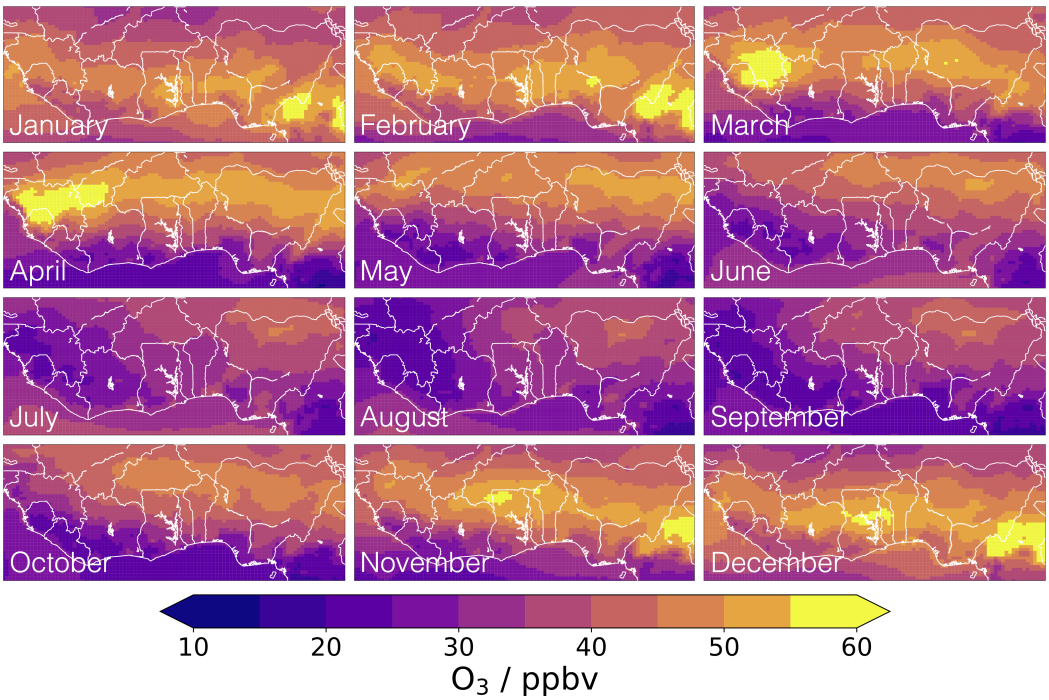

Figure 3.24: Monthly mean surface level O_3 concentrations for the year 2016. Data averaged between the hours of 06:00 and 18:00 (daylight hours).

The highest O_3 concentrations are seen during the dry season (November to April). During November and December high concentrations are seen over Ghana and Togo as well as to the east of the region over Cameroon. During January and February the high O_3 concentrations remain over Cameroon, whereas during March and April the highest concentrations are seen in the west of the region over Guinea and Sierra Leone. During the wet season, the O_3 concentrations are much lower with concentrations rarely exceeding 50 ppbv.

A number of metrics exist to assess the impact of ozone on plant health [143]. One of the simplest is the AOT40 index which is the accumulated exposure over a threshold of 40 ppb [244]. The accumulated monthly AOT40 values for the Guinea region are presented in Figure 3.25. These values are calculated using ozone concentrations during daylight hours (06:00 to 18:00).

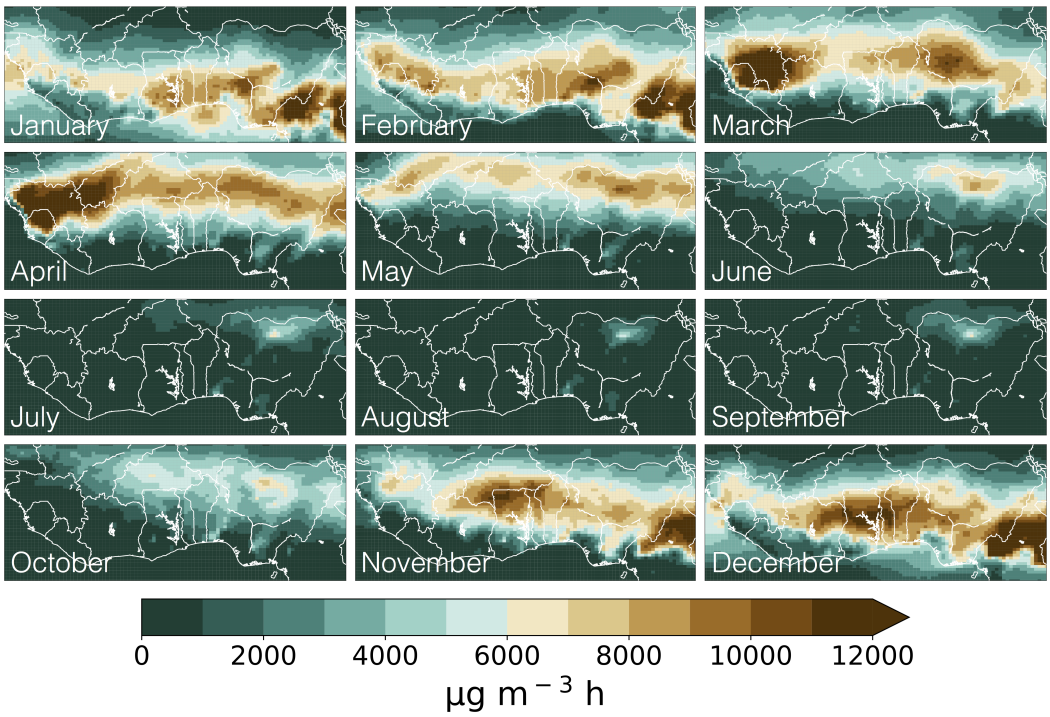

Figure 3.25: Monthly accumulated AOT40 for the year 2016. AOT40 calculated between the hours of 06:00 and 18:00 (daylight hours).

The European Union (EU) target for the protection of vegetation is 18000 μg m^{-3} h for May to July (the European growing season) [237]. Scaling this target to a monthly timescale suggests a monthly accumulated AOT40 target value of ~6000 μg m^{-3} h. In Figure 3.25, green areas represent AOT40 values below this target whilst brown represents AOT40 values above this target. It should be noted that little research has been performed to quantify safe exposure limits specific to the crop types grown in West Africa.

For the coastal countries in the Guinea region, the AOT40 values are below the EU target value during the wet season (May to October) which is the main growing season for root and tuber crops. Exceedances of the EU target AOT40 values are seen throughout the dry season along the coastline, with particularly high exceedances over Guinea and Sierra Leone during March and April and over Cameroon during November and December, corresponding to the regions of high O_3 concentration seen in Figure 3.25.

Evaluation of the model data against ground based observations suggested over predictions in ozone concentration (Sections 2.6.3 and 3.2.2). It is therefore likely that ozone concentrations are not high enough at present to cause concern for crop production rates in the region, particularly during the wet season. If artificial irrigation were to become more common in West Africa, enabling crops to be grown throughout the dry season, then ozone levels may be high enough to impact on agricultural productivity which could significantly impact the ability of this region to produce sufficient crops to feed the growing population. Previous studies have quantified the impacts of ozone on agricultural crop yields; however, many of these studies have focused on crops such as rice, wheat and

maize [7, 54, 170, 234, 276]. Little information is available on the impact on crops grown in the West African region such as yam and cassava [108, 254]. Future investigation into the ozone concentrations in the model is also needed before confidence can be placed in the conclusions made regarding the impact of O_3 on crop productivity in West Africa.

3.8 Concluding remarks on the seasonal changes in pollutant concentrations and sources in West Africa

The seasonal variability of pollutant concentrations in West Africa has been shown to be heavily dependent upon emissions and meteorology. During the West African dry season, strong winds from the north east bring large quantities of dust from the Sahara down into the region. Local biomass burning also takes place within the West African countries and a zone of low air flow along the coastline concentrates pollutants in this coastal area. The lack of precipitation reduces the loss of pollutants through wet deposition and overall these factors lead to higher pollutant concentrations. During the West African wet season, winds from central Africa to the north east prevent the southward transport of dust and transport biomass burning emissions from central Africa to the West African coastline. Precipitation across the region increases the loss of pollutants through wet deposition and the prevailing winds disperse pollution from the large cities. Concentrations of both gaseous and aerosol species are therefore typically lowest during the wet season.

Whilst the concentrations of gaseous pollutants are rarely found to exceed the air quality guidelines defined by the World Health Organisation, fine particulate matter concentrations in the region are often above these guideline values. $PM_{2.5}$ concentrations in the region are influenced by many different sources but three of the most significant influences in West Africa are anthropogenic, biomass burning and dust sources. Anthropogenic sources contribute to $PM_{2.5}$ concentrations in the region throughout the year and have a large impact on the population due to the close proximity of most of the population to these emission sources. Dust and biomass burning, however, show much stronger seasonal variations in their impact. Concentrations from both of these sources are highest during the dry season when local biomass burning activities take place across the region and dust from the Sahara is brought down to the coastal area by the prevailing winds. Whilst the impact from biomass burning is comparatively small, the contribution of dust to $PM_{2.5}$ causes the concentrations to be multiple times in exceedance of the WHO guidelines during the dry season. The different sources affecting the concentrations also vary depending on the metric used. When considering the area weighted concentrations, dust and biomass burning have a more profound impact, whereas when population weighted concentrations are considered the large impact of anthropogenic sources is evident. $PM_{2.5}$ is a major health concern for the region and the wide range of different sources must be considered when investigating the best strategies for reducing the concentrations.

Crop production in the region follows a seasonal pattern due to the fact that arable farming is largely dependent upon rainfall rather than artificial irrigation systems. Crops can be damaged by high ozone concentrations, resulting in a reduced yield, which may be a concern for regions such as West Africa which rely on these crops to feed a rapidly growing population. Ozone concentrations in West Africa are highest during the dry season when few crops are grown and lowest during the wet season when much of the agriculture occurs. Exposure to ozone concentrations during the main growing season is rarely above the European Union target value, suggesting that the ozone concentrations are not currently a large cause for concern. Evaluation against the available observations have however found ozone concentrations to be over predicted by the model. It is therefore likely that the simulated ozone vegetation metrics are over estimated which further supports the conclusion that ozone is not a large concern for agricultural productivity at present.

Chapter 4

The impact of biomass burning on atmospheric composition over West Africa

Biomass burning is a major source of aerosols and trace gases in the atmosphere [18]. It is the dominant source of carbonaceous aerosols globally [30], as well as contributing significantly to the emissions of carbon monoxide (CO) and nitrogen oxides (NO_x) [183, 275]. Although biomass burning occurs throughout the world, Africa is the largest continental source [17, 252, 272].

As well as covering vast areas and emitting large quantities of pollutants, the biomass burning activities in Africa also show strong seasonal variability [96, 212]. The location of the biomass burning events has been discussed briefly in Chapter 3 and has been shown to vary largely according to precipitation rates. During the West African dry season, biomass burning occurs throughout West Africa whereas during the wet season, biomass burning occurs in central Africa due to high precipitation rates along the West Africa coastline which inhibit the burning [12, 68, 164].

In this chapter, two different biomass burning emission inventories are compared: one which contains only surface level emissions (GFED) and one which incorporates injection altitudes (GFAS). The impact of changing the vertical emission profile on surface level concentrations in the region is also investigated. Biomass burning emissions have already been shown to vary throughout the year (Chapter 3) and this seasonal variability is investigated further here, along with changes in transport patterns, in order to explore the impact of the burning on atmospheric composition. Finally, the interannual variability in West African biomass burning is explored to determine whether the DACCIWA campaign year (2016) is representative of the typical burning events experienced in the region.

4.1 Emission inventories for biomass burning

The default emission inventory for simulating biomass burning activities in the GEOS-Chem model is the Global Fire Emissions Database (GFED) version 4 [9, 18, 97, 204, 253]. This inventory is constructed based upon vegetation productivity and burnt data from satellites and provides gridded monthly emissions of gaseous species, carbonaceous aerosols and volatile organic compounds at a horizontal resolution of $0.25^\circ \times 0.25^\circ$ for the years 1997 to 2016. The inventory does not include small fires which cannot be seen from the satellite data. The inventory also includes scaling factors which enable higher temporal resolution emissions to be calculated (daily), and these scale factors have been used in all simulations performed using the GFED inventory. An alternative inventory, based on similar methodology, for representing biomass burning activities is the Global Fire Assimilation System (GFAS) inventory from the European Centre for Medium-Range Weather Forecasts (ECMWF) (generated using Copernicus Atmospheric Monitoring Service (CAMS) information) [126]. As part of this project, the GFAS inventory has been incorporated into GEOS-Chem for use in both global and regional simulations. Details of its implementation in GEOS-Chem are now given.

4.1.1 The Global Fire Assimilation System (GFAS) biomass burning emission inventory

The GFAS inventory is constructed using observations of Fire Radiative Power (FRP) from the Moderate Resolution Imaging Spectroradiometer (MODIS) on board NASA's Terra and Aqua satellites [178–180], coupled to information about land types, emission factors and fire characteristics [126]. It provides emissions on a daily time step at a horizontal resolution of $0.1^\circ \times 0.1^\circ$ from 2003 to present day [126]. The inventory contains emission data for 40 compounds and groups of compounds; however, not all of these species are present in the GEOS-Chem model. GFAS emissions are assigned, where possible, to corresponding species within the model and these assignments are listed in Table 4.1.

Table 4.1: Assignment of emission species within the GFAS biomass burning inventory to species within the GEOS-Chem model.

GFAS Species Code	GFAS Description	GEOS-Chem Species
cofire	Wildfire flux of Carbon Monoxide	CO
noxfire	Wildfire flux of Nitrogen Oxides	NO
so2fire	Wildfire flux of Sulfur Dioxide	SO2
nh3fire	Wildfire flux of Ammonia	NH3
bcfire	Wildfire flux of Black Carbon	BCPI + BCPO
ocfire	Wildfire flux of Organic Carbon	OCPI + OCPO
c3h6ofire	Wildfire flux of Acetone	ACET
c2h4ofire	Wildfire flux of Acetaldehyde	ALD2
hialkanesfire	Wildfire flux of Higher Alkanes (C_nH_{2n+2}, C $\geq$ 4)	ALK4
hialkenesfire	Wildfire flux of Higher Alkenes (C_nH_{2n}, C $\geq$ 4)	PRPE
c3h6fire	Wildfire flux of Propene	PRPE
c2h6fire	Wildfire flux of Ethane	C2H6
c3h8fire	Wildfire flux of Propane	C3H8
ch2ofire	Wildfire flux of Formaldehyde	CH2O
c2h4fire	Wildfire flux of Ethene	C2H4
c5h8fire	Wildfire flux of Isoprene	ISOP
c2h6sfire	Wildfire flux of Dimethyl Sulfide	DMS
c7h8fire	Wildfire flux of Toluene	TOLU
c6h6fire	Wildfire flux of Benzene	BENZ
c8h10fire	Wildfire flux of Xylene	XYLE

GFAS emission species which are not incorporated into the GEOS-Chem model include alcohols such as methanol and ethanol.

The GFAS inventory is able to account for smaller fires than the GFED inventory as the detection of active fires (as used to construct GFAS) is more sensitive than the detection of burnt area (as used to construct GFED) [14]. The GFAS inventory is however unable to account for all fires as some smaller fires are not detectable from the satellite data. The inventory also makes assumptions to link the observed fire radiative power to emissions based upon land cover and vegetation type which is another source of uncertainty in the inventory.

One of the key species emitted from biomass burning is carbon monoxide (CO). The monthly mean emissions of CO for West Africa are shown in Figure 4.1 to illustrate the seasonal changes in the locations of the burning activities.

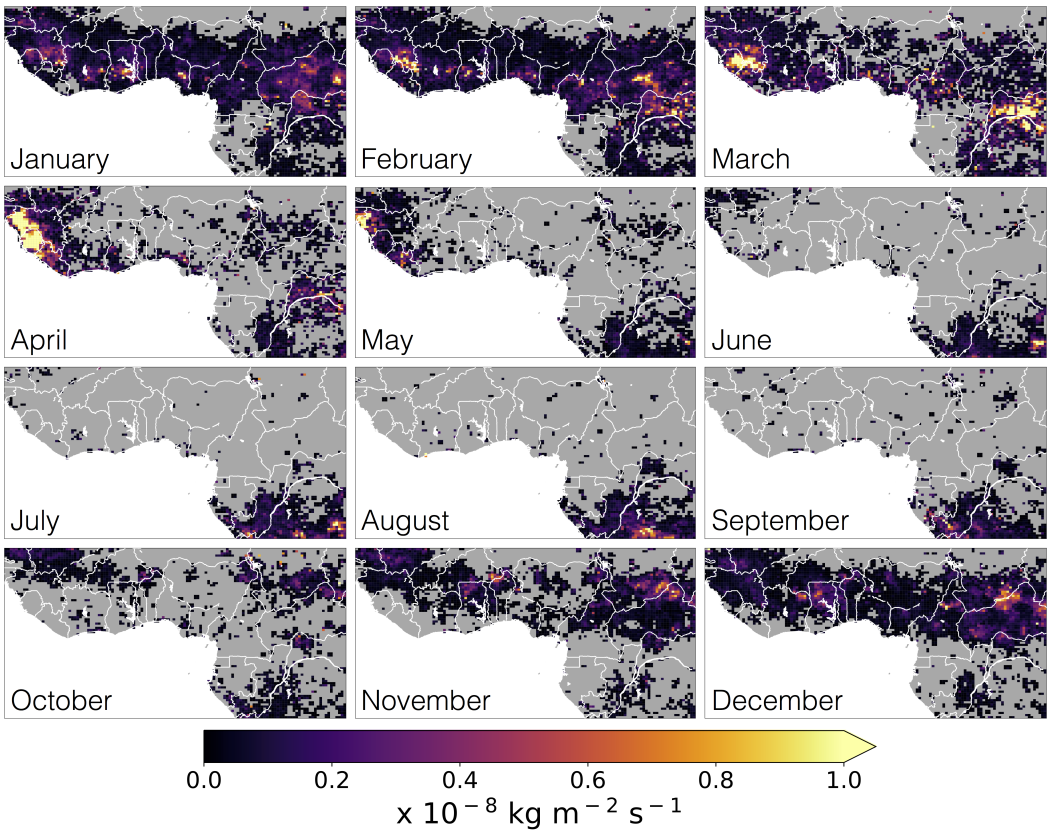

Figure 4.1: Monthly mean emissions of CO from the GFAS biomass burning emission inventory for the year 2016.

Biomass burning emissions along the Guinea coastline are highest from December to February, with a band of burning activities stretching across the region during these months [96, 152, 212]. Areas of particularly high emissions during these months can be seen in Guinea, the Central African Republic and the Democratic Republic of the Congo, as well as in central Ghana and Côte d'Ivoire (see Figure 1.16). During March, April and May, large burning events can still be seen in Guinea and Sierra Leone in the far west of the region, as well as in the south of the region in the Democratic Republic of the Congo. From June to September (the wet season along the Guinea coast), there is little burning in the Guinea region [96, 152, 212]. High rates of precipitation in the countries along the West African coastline limit the burning during this period (Figure 3.1) [12,68,164]. Large burning events during this time instead take place in central Africa [21, 152] (see Section 4.3). During October and November, biomass burning activities begin again inland from the Guinea coast.

The seasonality of the burning activities is further illustrated in Figure 4.2 which highlights the winter (December to February) maximum in the north of the domain and the summer (June to August) maximum in the south.

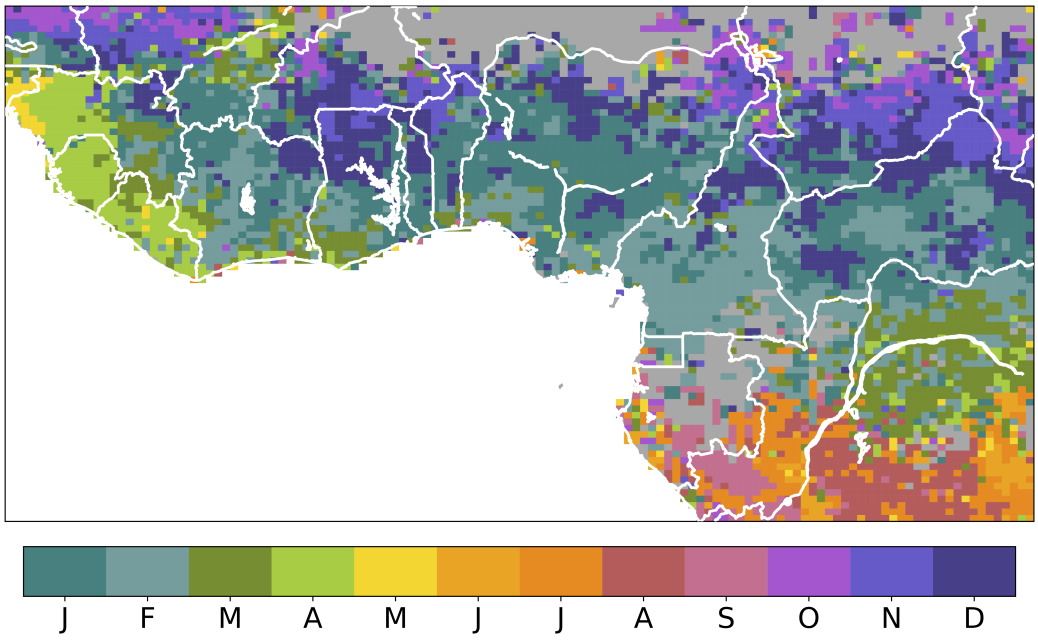

Figure 4.2: Month of peak CO emissions from biomass burning activities. Monthly mean emission data from the GFAS biomass burning emission inventory for the year 2016.

Biomass burning events in the north of the region, along the southern edge of the Sahara, are highest during October, November and December. These events then move southwards to the coastline during January and February, with the western edge of the region (Guinea, Sierra Leone and Liberia) experiencing large biomass burning events during March and April and into May. From June to September the burning activities are strongly focused in central Africa across Gabon, the Republic of Congo and the Democratic Republic of the Congo. Figure 3.3 (Chapter 3), shows monthly mean precipitation for 2016 and it can be seen that the locations of the burning activities correspond with areas of little or no rainfall. The location of the biomass burning events therefore appear to be largely dominated by the seasonal changes in precipitation. The DACCIWA campaign took place during June and July when the strongest burning events took place in central Africa, to the south east of the DACCIWA region.

4.1.2 Effect of emission altitude on the vertical distribution of pollutant concentrations

The GFAS emission inventory contains data on the altitudes of the emission plumes as well as on the quantity of each species emitted. Emission altitudes for the GFAS inventory are computed by a plume rise model [207]. These emission altitudes have been incorporated into the GEOS-Chem model, enabling the biomass burning emissions of each species to be evenly distributed between the surface and the mean altitude of maximum injection.

For each day, the emission data for each species is read into the model along with the mean altitude of maximum injection. The GEOS-Chem model level corresponding to

the maximum injection altitude is calculated, and the total emission for each species is divided evenly between the surface level and the calculated maximum level. This results in less emission released at the surface and some emitted into higher levels which in theory facilitates better representation of the behaviour of these large biomass burning plumes.

The monthly mean injection altitudes from the GFAS inventory for 2016 are shown in Figure 4.3.

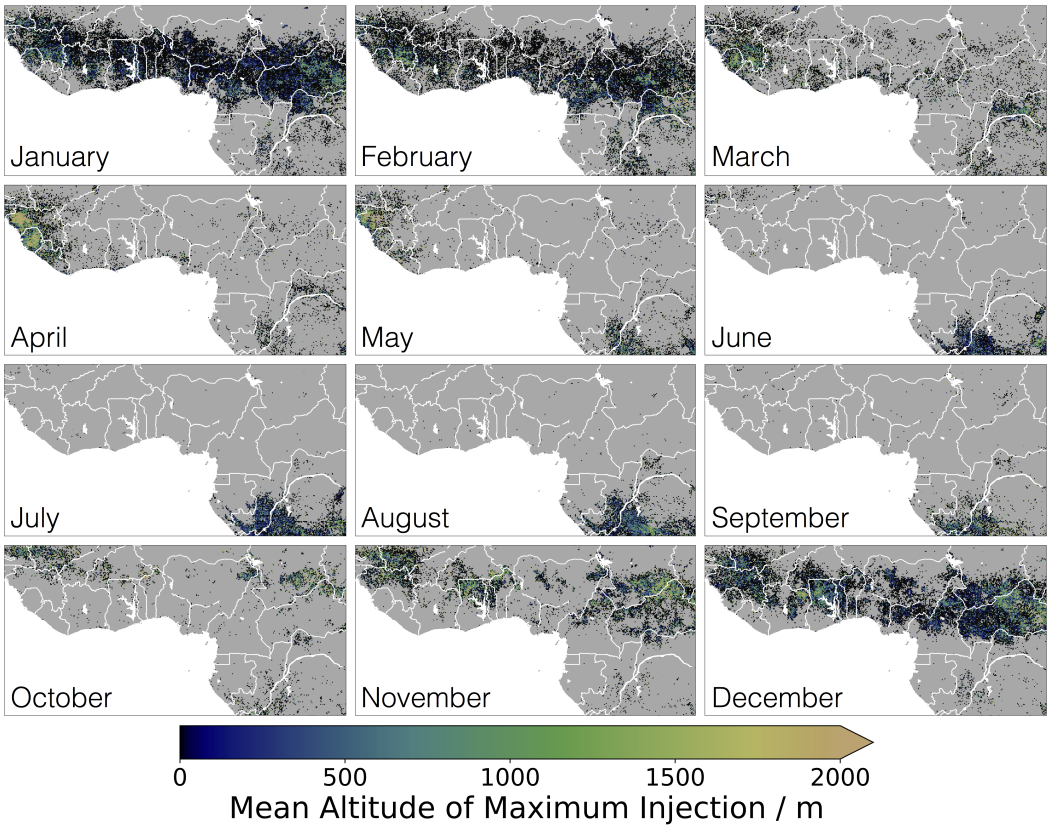

Figure 4.3: Monthly mean altitude of maximum injection for biomass burning emissions from the GFAS inventory for the year 2016.

The highest injection altitudes (of around 1500 m) are seen in Guinea and Sierra Leone during April and May as well as in Chad and the Central African Republic during November and December. These high injection altitudes correspond with the regions of most intense burning and also highest emissions (Figure 4.1). For the region, larger fires typically have higher emissions and taller plumes injecting further into the atmosphere, whereas smaller fires have lower emissions and the upwards transport of these plumes is reduced.

In order to assess the impact of incorporating emission injection altitudes on surface concentrations of pollutants two simulations have been performed:

1. simulation in which the GFAS emissions are released only at surface level

2. simulation in which the GFAS emissions are distributed evenly between the surface level and mean altitude of maximum injection

The percentage difference in the surface level concentrations of key pollutants between these two simulations is shown in Figure 4.4.

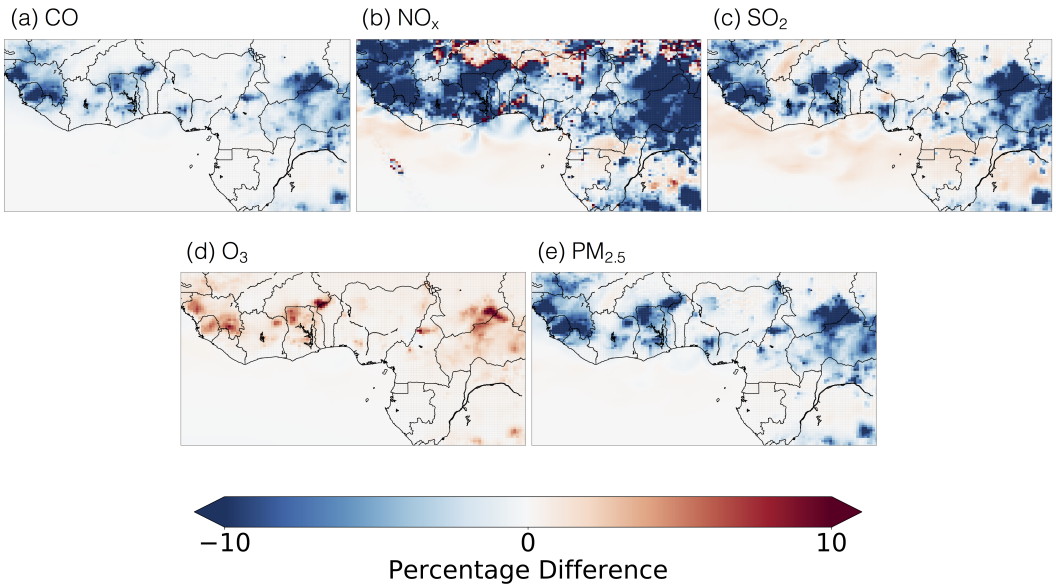

Figure 4.4: Annual mean percentage change in surface level concentrations between the simulation in which GFAS biomass burning emissions are emitted at the surface versus incorporation of emission altitudes. Difference calculated as [surface concentration when emissions are spread across emission altitudes] - [surface concentration when emissions are emitted only at surface level]. Annual mean data for 2016.

The surface level concentrations of CO, NO_x, SO_2 and $PM_{2.5}$ are decreased across most of the region, with the largest decreases in the locations corresponding to the highest biomass burning emissions (Figure 4.1). Incorporating the injection altitude into the emissions results in smaller emissions at the surface and larger emissions higher up the vertical column, thereby resulting in a decrease in surface level concentrations between the two simulations. Surface level O_3 concentrations are marginally increased as a result. One of the chemical mechanisms for ozone destruction in the lower troposphere is the reaction with NO [53, 172]. Reducing the concentrations of NO at the surface (Figure 4.4(b)) therefore results in a reduction in the chemical destruction rates and hence an increase in the ozone concentration. These increases are largest in the locations of the large burning events where the reduction in surface level NO is the greatest. For most of the region, the change in O_3 concentration is less than 10% and the area of change is much smaller than for NO_x.

During the large burning events, strong upward pyro-convection, combined with existing convective activity, results in rapid vertical mixing of pollutant concentrations. This pre-existing quick vertical mixing results in the surface concentrations being affected to only a small extent by the shape of the vertical emission profile. When considering the locations of the major cities in the region, there is very little difference between the two simulations. This indicates that the concentrations that the majority of the population

are exposed to changes little with a vertical change in the biomass burning emissions. This finding is in agreement with the work of Menut et al. [169].

The differences between the two simulations are emphasised further in Figure 4.5.

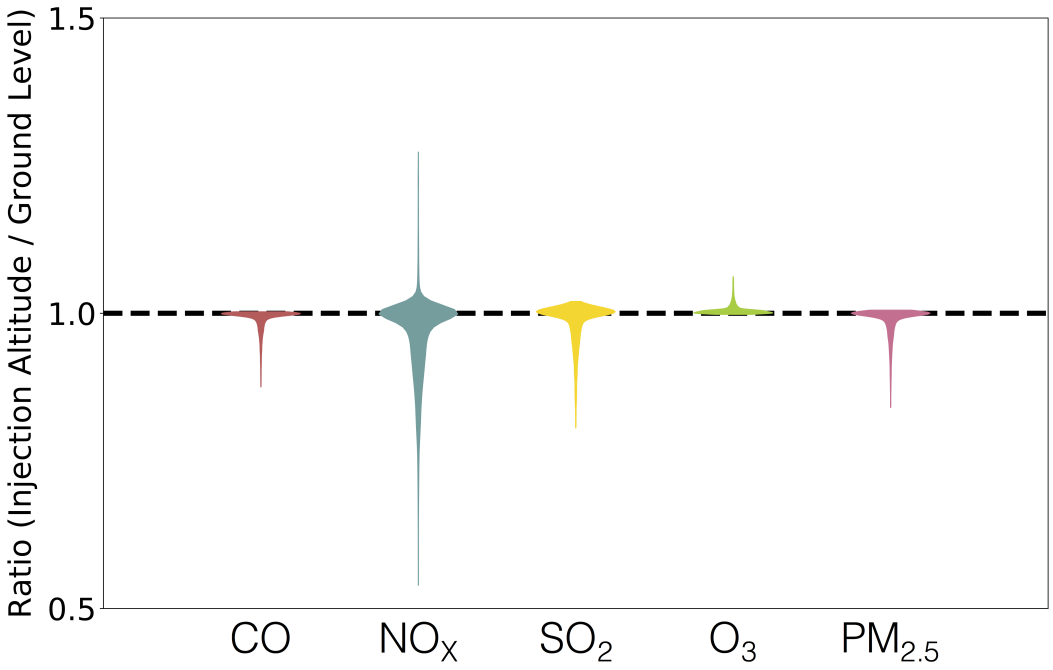

Figure 4.5: "Violin" plot (probability distribution) showing the ratio of surface concentrations between the simulation incorporating injection altitudes and the surface level emission simulation. Hourly data for 2016 accumulated from all grid boxes in the domain shown in Figure 4.4 (5 °S to 15 °N; 15 °W to 25 °E). Dashed line indicates a ratio of 1 showing no difference between the two simulations. Data for each species only includes the 1st to 99th percentile points.

This figure shows the ratios of the concentrations between the two simulations. A ratio of 1 indicates no change between the two emission configurations. Ratios of less than 1 indicate surface concentrations are lower as a result of incorporating injection altitudes, whereas ratios of greater than 1 indicate surface concentrations are higher.

For CO, NO_x, SO_2 and $PM_{2.5}$, the dominant pattern is a reduction in surface concentrations when injection altitudes are incorporated, whilst for O_3 the surface concentrations are increased. In general, the majority of data points are close to a value of 1, further supporting the conclusion that changing the vertical profile does not have a substantial impact on the surface concentrations.

Consistent with previous studies, incorporating the injection altitudes into the model emissions only has a small impact on surface concentrations. It does, however, provide a better representation of the behaviour of biomass burning plumes and therefore has been included in all simulations using the GFAS inventory.

4.1.3 Comparisons of the Global Fire Emissions Database (GFED) and Global Fire Assimilation System (GFAS) biomass burning emission inventories

Simulations of West Africa within GEOS-Chem can be performed using either the standard GFED inventory [9, 18, 97, 204, 253] or the newly incorporated GFAS inventory [126] (Section 4.1.1). GFED emissions are available on a monthly time resolution (with scale factors used to increase the resolution to daily emissions) and at a spatial resolution of 0.25° × 0.25° whilst the GFAS emissions are available at a higher spatial resolution of 0.1° × 0.1° and at a finer native time resolution of daily emissions. The annual mean emissions of some of the key species emitted from biomass burning events are compared for these two inventories in Figure 4.6.

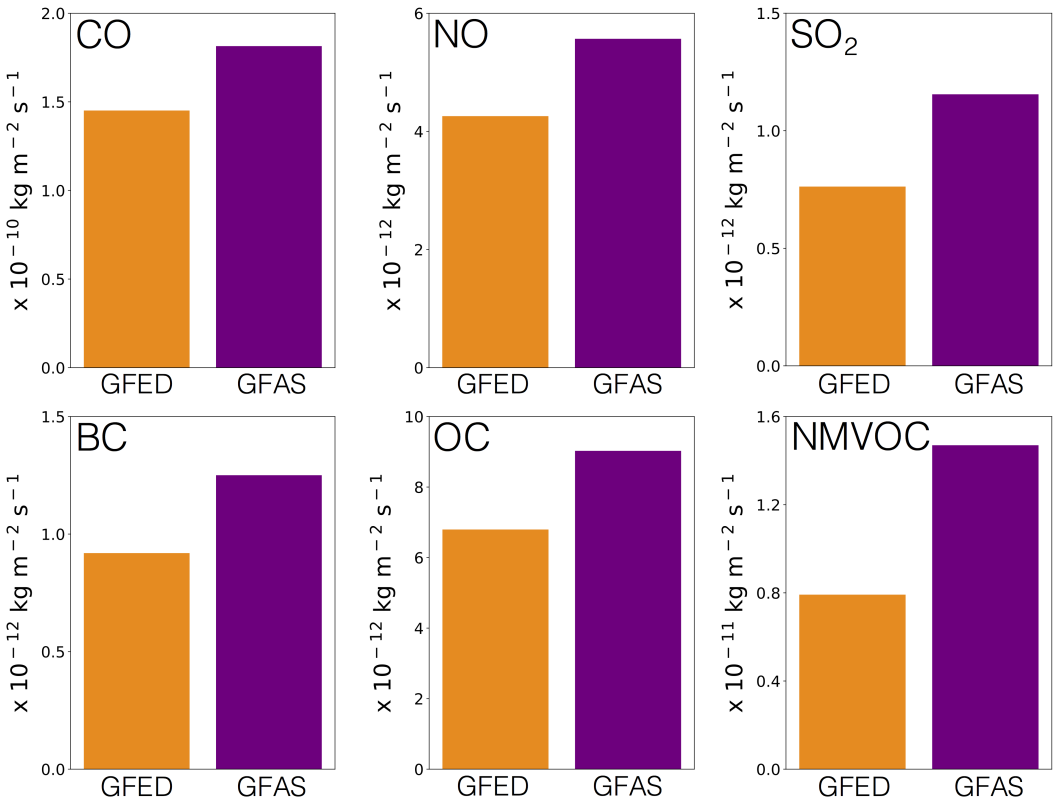

Figure 4.6: Mean annual biomass burning emissions of CO, NO, SO_2, BC, OC and NMVOC for the Guinea region from two emission inventories: GFED and GFAS. Data from both emission inventories is for the year 2016. NMVOC emissions include ethane, propane, alkanes ≥ C_4, alkenes ≥ C_3, formaldehyde, acetaldehyde and acetone.

For all of these species, the emissions from GFAS are higher than those from GFED for the Guinea region. The DACCIWA aircraft observations (Section 2.4) are used to evaluate the model performance using these two different inventories. The agreement between the two simulations and the observations from the DACCIWA aircraft is shown in Figure 4.7.

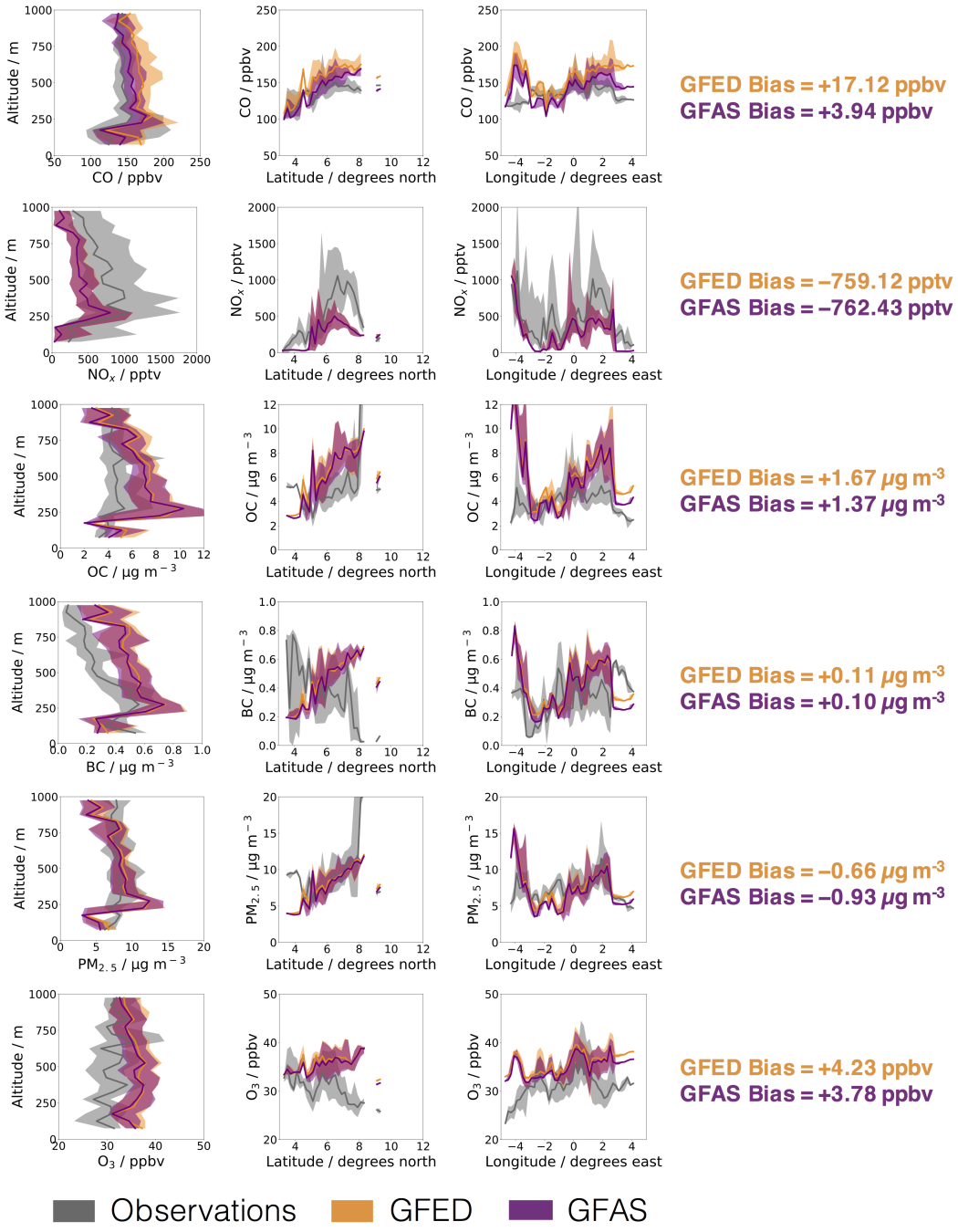

Figure 4.7: Vertical, latitudinal and longitudinal profiles of aircraft observational data (grey) and simulated concentrations using the GFED biomass burning inventory (orange) and the GFAS biomass burning inventory (purple). Both simulations use the DACCIWA anthropogenic emission inventory. Solid lines represent the median, shaded areas represent the 25th to 75th percentile range. All data is from altitudes below 1 km. $PM_{2.5}$ concentrations shown here do not account for the mass of dust or sea salt, or the uptake of water to the aerosols. The bias for each simulation is shown alongside the plots for each species.

As discussed in Section 2.5, during the period of the DACCIWA aircraft campaign the main biomass burning events were taking place in central Africa with few burning activities along the West African coastline [96, 152, 212]. This is largely due to the location of

the burning activities being governed by rainfall. As a result of this, the concentrations of pollutants observed by the aircraft experienced little recent influence from biomass burning activities. Thus, little difference is seen between the two different inventories when considering the concentrations of NO_x, BC and OC. CO has a longer lifetime in the atmosphere [71] and therefore transport of CO from the biomass burning events in central Africa, across the Gulf of Guinea to the West African coastline, resulted in CO concentrations in the DACCIWA region being influenced by these burning activities. Some differences can therefore be seen between the two inventories in the comparison for CO. Whilst both simulations follow very similar trends in the shapes of the profiles, the concentrations simulated using the GFAS inventory show closer agreement to the observations from the aircraft (bias in GFED simulation of 17.12 ppbv compared with a bias in the GFAS simulation of 3.94 ppbv). Both $PM_{2.5}$ and O_3 concentrations show little difference between the two inventories for the DACCIWA flight tracks.

As well as showing a slight improvement in the agreement with observations compared the the GFED inventory, the GFAS inventory is available at higher spatial resolution (0.1° compared with 0.25°) and higher native time resolution (native resolution of 1 day compared with 1 month) as well as being available up to present day at near real-time. The GFAS inventory also includes plume injection heights which offers the ability to include vertical distribution of the emissions in the model, enabling the plumes to be better represented. The GFAS inventory was therefore chosen to represent biomass burning emissions for all simulations of West Africa within both the global and regional GEOS-Chem model.

4.2 The impact of biomass burning activities on pollutant concentrations in West Africa

In Chapter 2, biomass burning events were found to have only a small impact on pollutant concentrations in the DACCIWA region during the dry season. However, the question remains about its influence in other seasons.

Simulations for the whole of 2016 have been performed with the GFAS biomass burning inventory switched both on and off. The difference between these two simulations enables the impact of biomass burning on pollutant concentrations to be quantified, assuming a linear relationship between emissions and concentrations. The percentage contribution that biomass burning events make to the mean concentrations of pollutants during the dry season (January) is shown in Figure 4.8 and during the wet season (July) is shown in Figure 4.9. For both seasons, the contribution is shown for three different altitudes to illustrate the changing patterns in the vertical column.

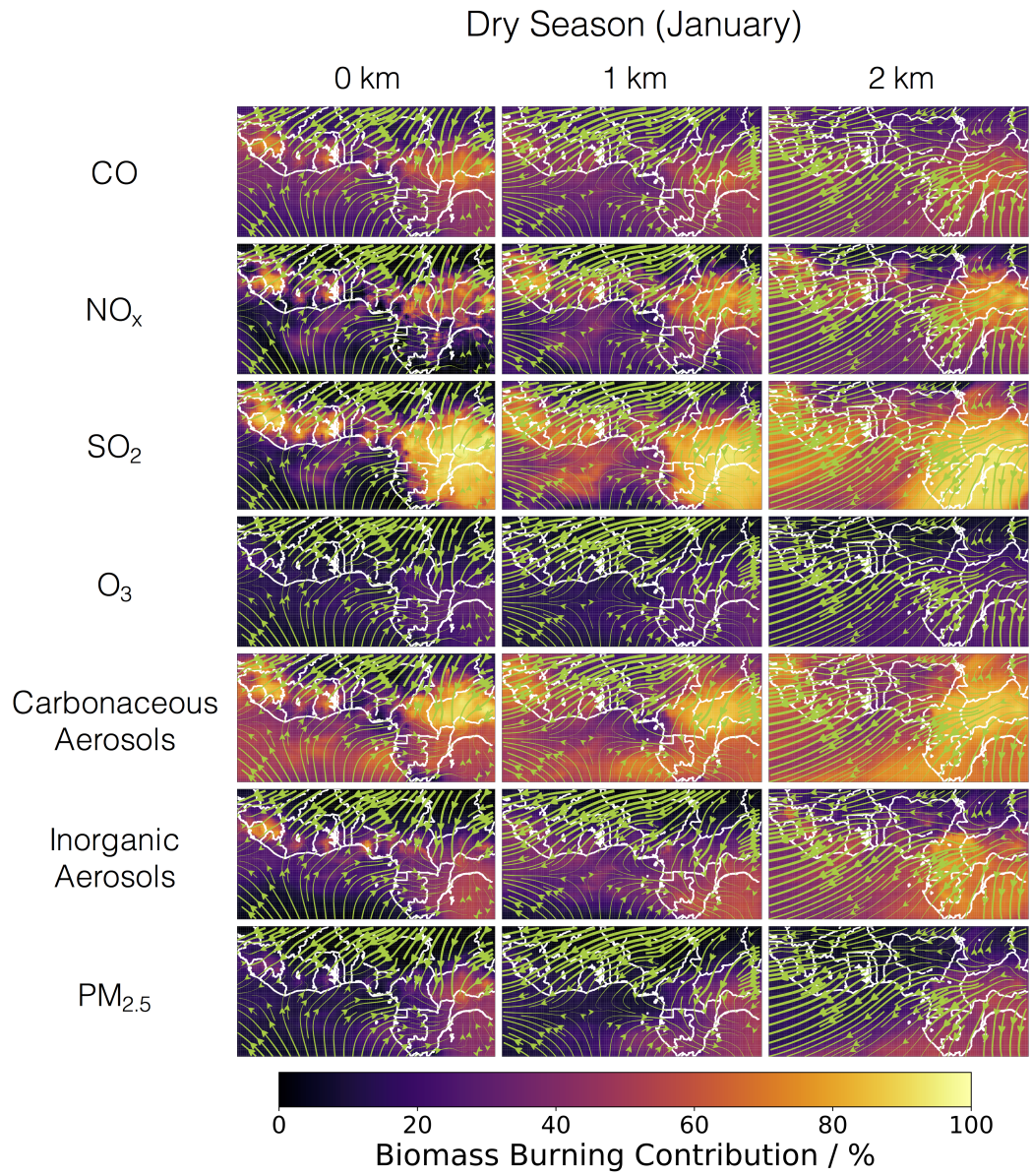

Figure 4.8: Percentage contribution of biomass burning activities to the concentrations of CO, NO_x, SO_2, O_3, carbonaceous aerosols (BC + OC), inorganic aerosols (NO_3^- + SO_4^{2-} + NH_4^+) and $PM_{2.5}$ in West Africa. Model data averaged for the dry season (January) at model levels corresponding to altitudes of 0 km, 1 km and 2 km. Monthly mean wind stream functions at each of the levels are from GEOS-FP meteorological data.

During the dry season (Figure 4.8), at the surface, strong winds from the north east meet weaker winds from the south resulting in an area of weak flow along the coastline (as discussed in Section 3.1.1). A similar pattern is also seen at 1 km. However, at this altitude, the flow from the north east over the land becomes stronger and the convergence zone moves further south over the ocean. At 2 km altitude, the flow of air is dominated by strong winds from the north east to the south west, moving from the continent across the Gulf of Guinea and Atlantic Ocean.

During the dry season, biomass burning takes place across West Africa; however, the

contribution of this burning to the pollutant concentrations varies greatly between species.

For CO, contributions of around 80% from biomass burning can be seen at the surface in the vicinity of the fires, particularly in Guinea to the west and the Central African Republic to the east. The high concentrations at the surface are concentrated along the coastal region due to the convergence of the winds. At higher altitudes, the flow of air transports some of the CO produced from biomass burning out over the ocean, with up to 50% of the concentration over the ocean being attributable to the burning.

Both NO_x and SO_2 concentrations follow a very similar pattern as CO, with the transport of the burning emissions at higher altitudes (particularly at 2 km) being clearly visible when considering the concentrations of SO_2.

Although O_3 is not directly emitted from biomass burning, its concentration is influenced by the concentrations of precursor species such as CO, NO_x and VOCs which are directly emitted from the burning. The contribution of biomass burning to O_3 concentrations can be seen to coincide with the locations of the burning events with O_3 concentrations being influenced by around 20% in these areas.

The concentrations of carbonaceous aerosols (BC + OC) are strongly influenced by biomass burning. During the dry season, around 90% of the carbonaceous aerosol in Guinea and the Central African Republic is from the biomass burning within the countries themselves. The contribution from biomass burning can be seen to be much lower around the large cities in the region where anthropogenic sources are the dominant contribution to the pollutant concentrations. Concentrations over the ocean are influenced by up to approximately 80% as a result of transported biomass burning emissions.

A similar pattern is also seen for the inorganic aerosols ($NO_3^- + SO_4^{2-} + NH_4^+$), although the contribution from biomass burning is much smaller than seen for the carbonaceous aerosols and there is little influence from biomass burning over the ocean.

The fine particulate matter ($PM_{2.5}$) concentrations are influenced by up to around 50% during the dry season around the locations of the large biomass burning events, with concentrations over the ocean also being influenced downwind of these burning sources. However, the large source of dust in the north overwhelms the biomass burning source which makes the impact of biomass burning relatively small.

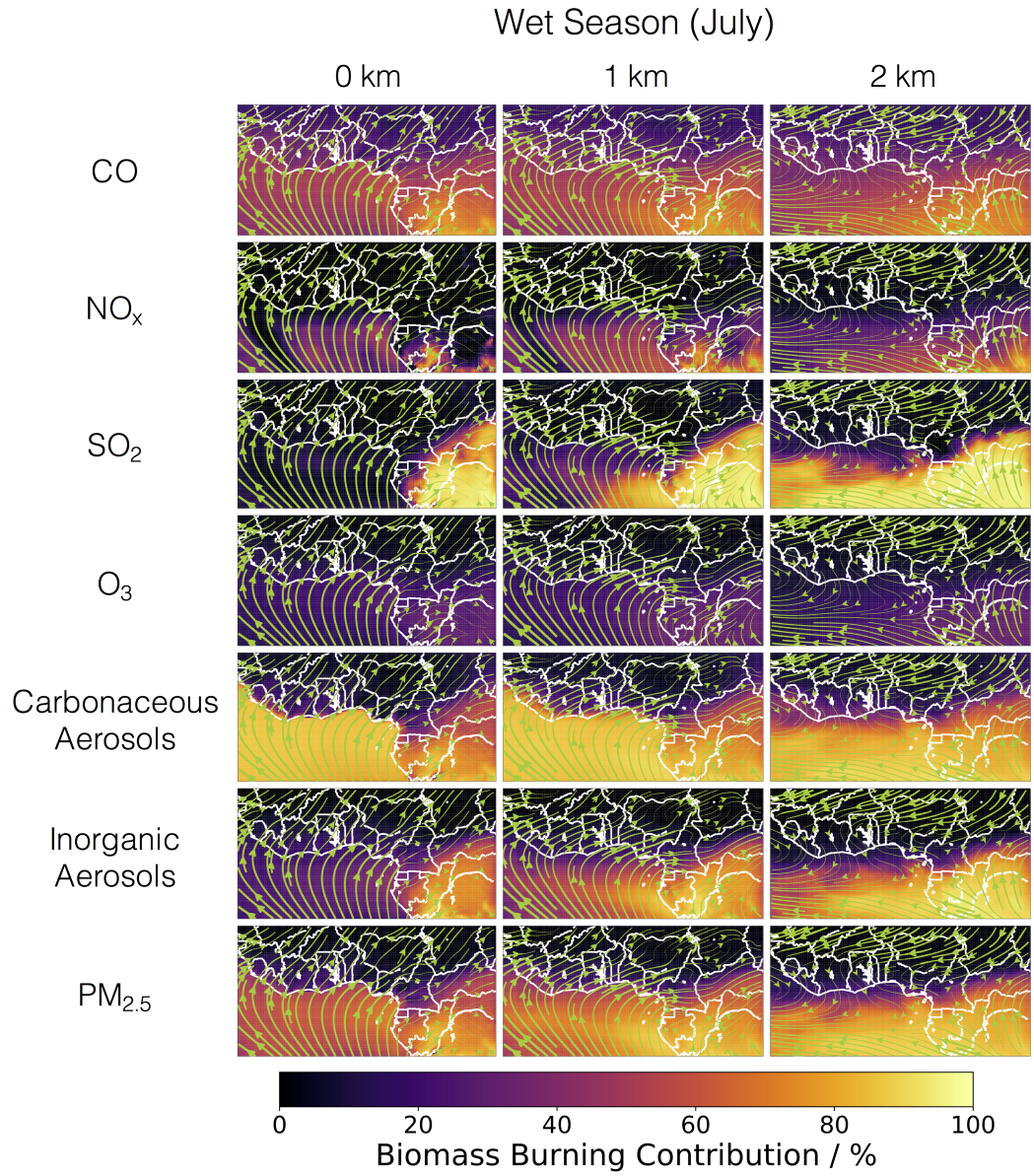

Figure 4.9: Percentage contribution of biomass burning activities to the concentrations of CO, NO_x, SO_2, O_3, carbonaceous aerosols (BC + OC), inorganic aerosols (NO_3^- + SO_4^{2-} + NH_4^+) and $PM_{2.5}$ in West Africa. Model data averaged for the wet season (July) at model levels corresponding to altitudes of 0 km, 1 km and 2 km. Monthly mean wind stream functions at each of the levels are from GEOS-FP meteorological data.

During the wet season (Figure 4.9), both at the surface and at 1 km, the prevailing winds are from the south over the ocean to the north east over the land resulting in a continuous flow of air from central Africa across the Gulf of Guinea and over West Africa towards the Sahara. At 2 km, the pattern of flow changes. The flow of air from central Africa is to the west, out over the Atlantic Ocean, whereas the movement of air over the land in West Africa shows strong winds following a predominantly east to west flow.

Rainfall throughout West Africa during the wet season (Figure 3.3) inhibits biomass burning along the coastline and the main burning during this season takes place in central

Africa [96, 152, 212].

Due to its long lifetime in the troposphere [71], the surface CO concentrations along the West African coastline are influenced by around 50% due to central African burning emissions being transported across the Gulf of Guinea. Similar influences can also be seen at the higher altitudes.

Both NO_x and SO_2 have short lifetimes ($\sim$ hours) [71]. During the wet season, the surface level concentrations are strongly influenced by biomass burning in the vicinity of the fires (south east of the domain), but there is little transport of these species to the West African coastline. At 2 km altitude, however, NO_x and SO_2 from the central African burning are transported to the west over the Atlantic Ocean, where they have a strong impact on the concentrations.

The impact of biomass burning on O_3 concentrations is largely unchanged and small between seasons. The contribution from biomass burning is highest in central Africa, close to the fires, yet the contribution remains below around 30%.

Around 90% of the carbonaceous aerosol at the surface in central Africa during the wet season is attributable to biomass burning. Transport from this region to the west results in close to 100% of the concentrations over the ocean being attributed to biomass burning for all three altitudes shown here, clearly defining the West African coastline. This transport also results in concentrations along the southern coast of West Africa experiencing a significant influence from biomass burning.

Inorganic aerosols follow a similar pattern to carbonaceous aerosols, although the impact on concentrations over the ocean is lower.

Finally, $PM_{2.5}$ concentrations at the surface in central Africa consist of up to 100% contribution from biomass burning and the concentrations over the ocean are also strongly influenced by the biomass burning emission sources. Around 20% of the $PM_{2.5}$ concentrations in the West African coastal countries are attributed to the biomass burning sources in central Africa as a result of transport across the Gulf of Guinea by the prevailing winds [102].

In general it can be seen that biomass burning activities have the largest impact on the Guinea region during the dry season when the burning events are occurring locally. For all species the impacts of the burning are greatest close to the emission sources with much lower impacts around the large cities in the region where other sources, likely anthropogenic, dominate the concentrations.

In Chapter 3, $PM_{2.5}$ was identified as one of the major concerns for human health in the Guinea region. The mean annual contributions of the major sources of $PM_{2.5}$ to the concentrations in five of the large cities along the West African coastline are considered in Figure 4.10. These contributions have been calculated by performing a set of equivalent simulations in which each source is independently switched off.

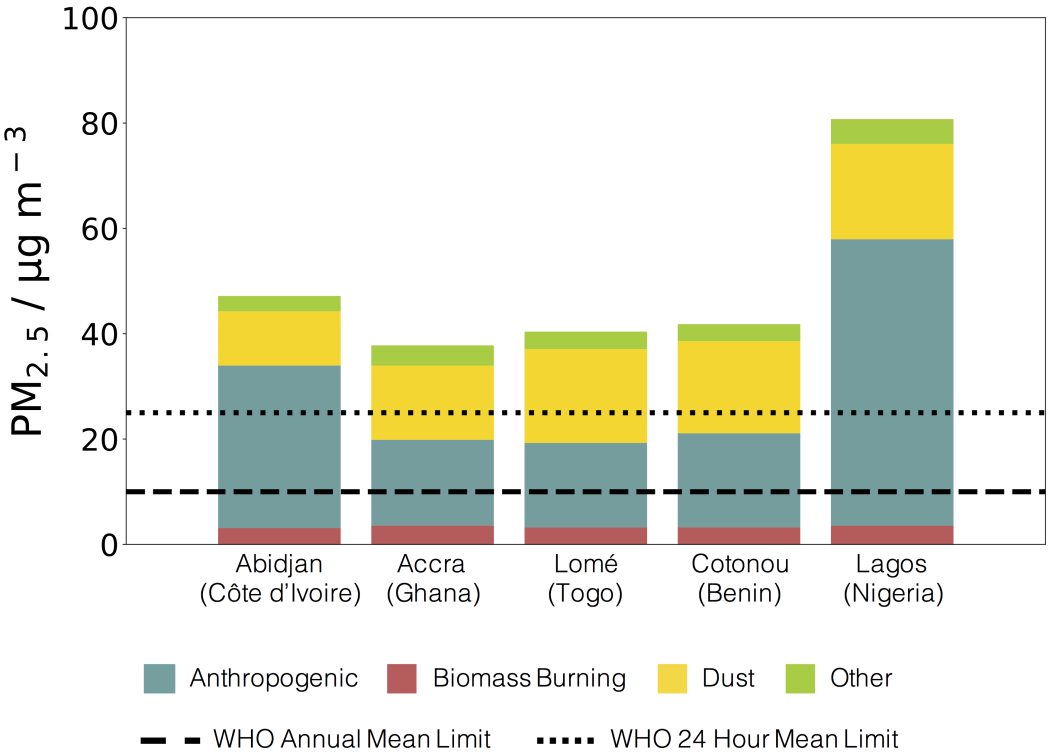

Figure 4.10: Annual mean modelled surface level $PM_{2.5}$ concentrations for the cities of Abidjan (Côte d'Ivoire), Accra (Ghana), Lomé (Togo), Cotonou (Benin) and Lagos (Nigeria). Annual mean concentrations broken down into the contributions from biomass burning, anthropogenic, dust and other sources (such as sea salt). Dashed line indicates WHO annual mean limit and dotted line indicates WHO 24 hour mean limit.

For all five of these key cities in the region, anthropogenic and dust sources are the major contributors to $PM_{2.5}$ concentrations, with the contribution from biomass burning making up only around 3 - 4 μg m^{-3} of the total concentration (Figure 4.10). Whilst all of the cities exceed the World Health Organisation (WHO) recommended guidelines, removing the contribution from biomass burning would not bring the concentrations to within the limits. Although biomass burning is an important consideration for the region, the anthropogenic and dust sources of $PM_{2.5}$ are significantly higher.

Figures 4.8 and 4.9 show that the impact of biomass burning on concentrations in these cities varies greatly throughout the year. The annual cycle of biomass burning contributions to $PM_{2.5}$ concentrations for these five cities is considered in Figure 4.11.

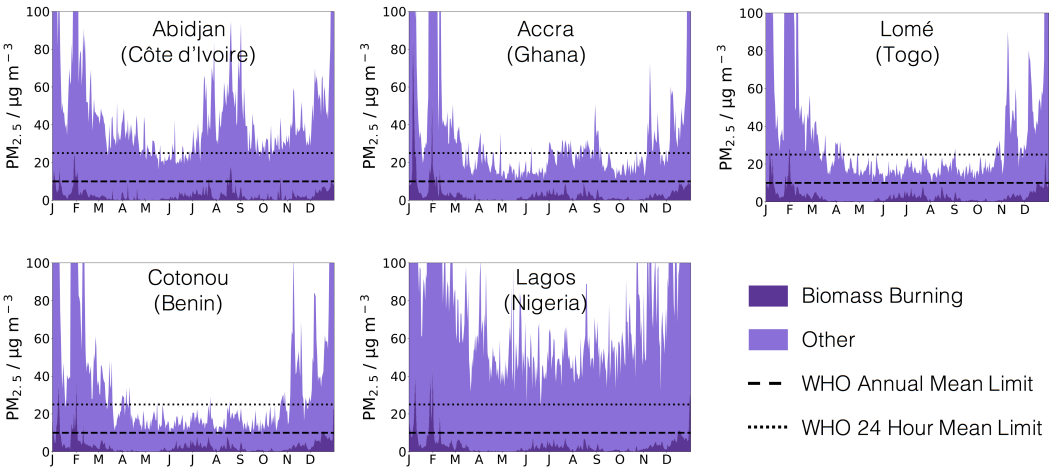

Figure 4.11: Seasonal variations in the contribution of biomass burning activities to surface level concentrations of $PM_{2.5}$ in Abidjan (Côte d'Ivoire), Accra (Ghana), Lomé (Togo), Cotonou (Benin) and Lagos (Nigeria). Data averaged daily for 2016.

Although the annual mean concentrations of $PM_{2.5}$ from biomass burning in the cities are low (Figure 4.10), when the full annual cycle is considered, the concentrations from biomass burning alone can be seen to exceed the WHO annual mean limit of 10 μg m^{-3} on a number of occasions and occasionally breach the 25 μg m^{-3} 24 hour limit. For all five of the cities, the concentrations from biomass burning are highest during the dry season months (November to March) as a result of local (West African) biomass burning events. The concentrations from biomass burning are also increased during June, July and August as a result of transported biomass burning emissions from central Africa. Whilst the impact of biomass burning on the concentrations is much smaller than from anthropogenic or dust sources, Figure 4.11 highlights that emissions from biomass burning can have large impacts on $PM_{2.5}$ concentrations at certain times of the year and should therefore still be taken into consideration when assessing the different pollutant sources impacting on human health in the region. The work of Haslett et al. [102], based on observational data collected during the DACCIWA campaign, suggests that the contribution of biomass burning pollution to aerosol mass loading in the region could be greater than suggested by the GEOS-Chem model and further observations of biomass burning in the region are required in order to better quantify the contribution. The long range transport of biomass burning components outside the West Africa domain over the year are now investigated.

4.3 Transport of pollutants from biomass burning activities

One of the key factors that controls how the concentrations of pollutants are influenced by biomass burning is the transport of the emissions from the burning region to other areas. The concentrations of a given species attributed to biomass burning emissions

is diagnosed as the difference between two equivalent global simulations - one in which the biomass burning emissions are switched on and another in which they are switched off. These simulations have been run at a horizontal resolution of 2° × 2.5° in order to investigate concentrations across the whole continent. By considering the concentrations of CO from biomass burning, the transport patterns of the pollutants emitted from the burning activities can be investigated on a continental scale.

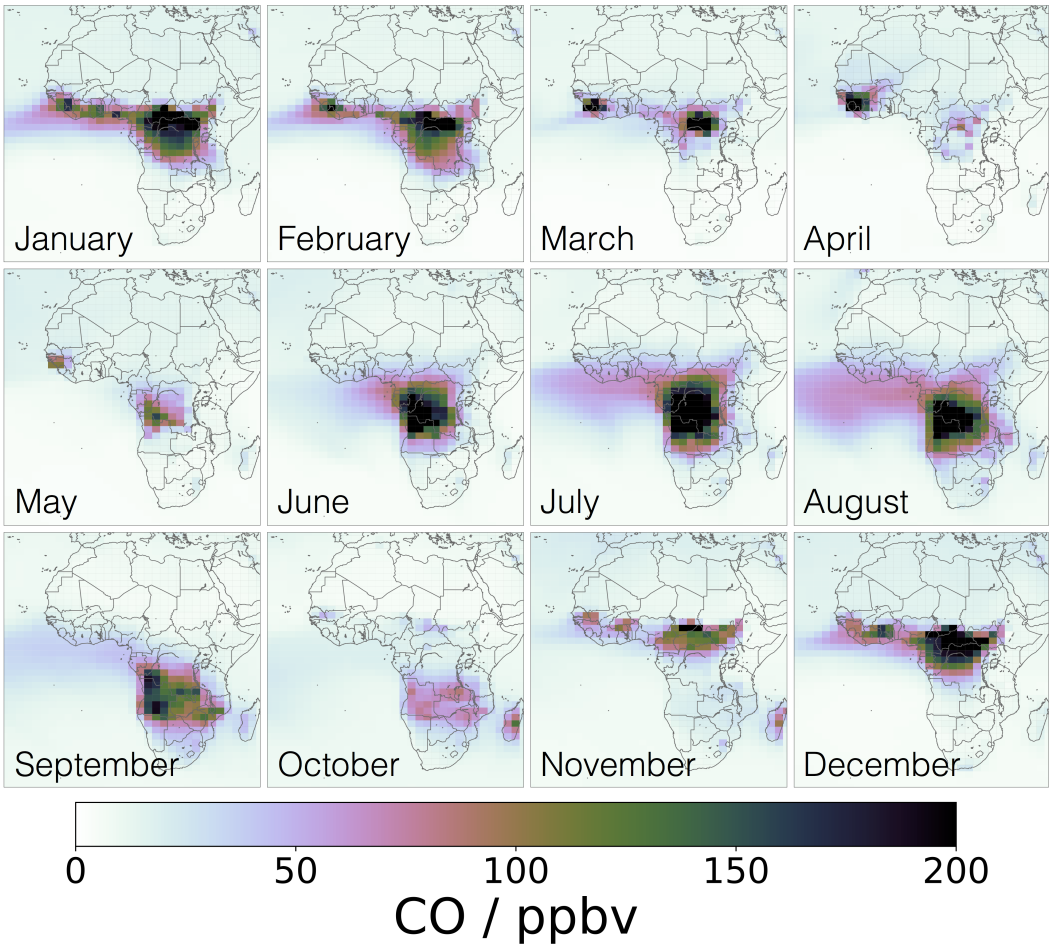

Figure 4.12: Monthly mean surface carbon monoxide concentrations from biomass burning for the African continent at 2° × 2.5° horizontal resolution for 2016.

During the West African dry season (December to February), pollutants emitted from the burning activities in the Guinea region are concentrated along the West African coastline and in the Central African Republic and northern Democratic Republic of the Congo due to the weak flow resulting from the convergence of winds along the coastline (Figure 4.8). There is some dispersion of the pollutant concentrations to the west resulting in a relatively narrow plume extending out over the ocean to the west of Guinea and Sierra Leone, south of Cape Verde.

During the wet season (June to August), large biomass burning events occur in central Africa, predominantly in the Democratic Republic of the Congo and northern Angola. These burning activities cause elevated concentrations in the vicinity of the fires and, due

to the flow of air to the north west from central Africa across the ocean, the concentrations from biomass burning can also be seen to spread out across the Atlantic Ocean and up to the West African coastline covering a latitudinal range of approximately 10 °N to 10 °S [102].

The transport of CO can be analysed in more detail by considering the vertical profile of concentrations throughout the year as a function of latitude and longitude (Figure 4.13). The domain considered is from 5 °S to 15 °N and 15 °W to 25 °E which encompasses the Guinea region and an additional area to the south and east of this region in order to capture the biomass burning in central Africa.

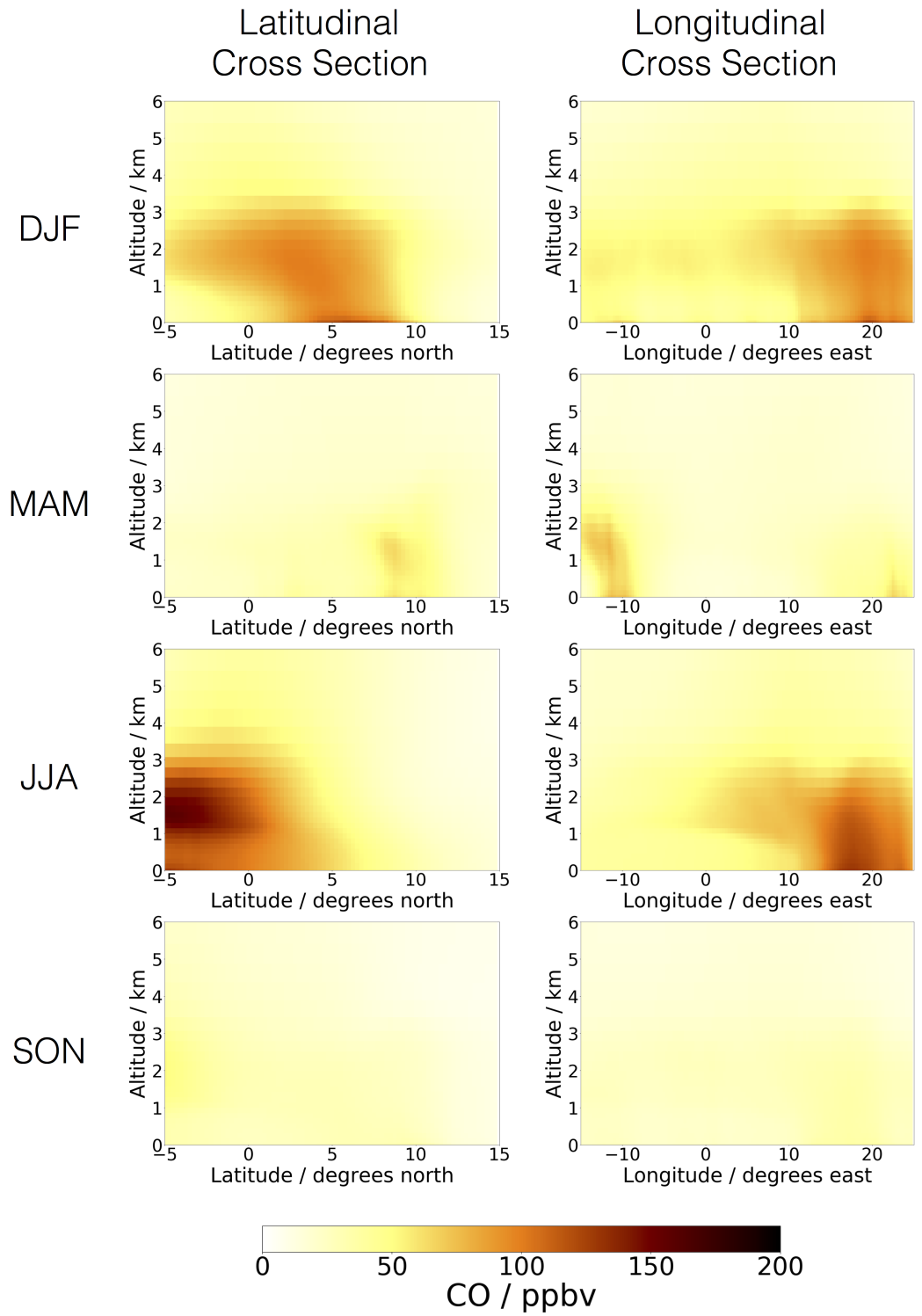

Figure 4.13: Monthly mean altitude-latitude cross section charts (left hand panel) and altitude-longitude cross section charts (right hand panel) showing the concentration of CO from biomass burning. Latitude data averaged over a longitude range of 15 °W to 25 °E. Longitude data averaged over a latitude range of 5 °S to 15 °N.

The prominent features of the biomass burning events in Africa are the large fires in central Africa during June, July and August (approximately 5 °S to 0 °N; 15 °E to 25 °E) and the fires along the West African coastline in December, January and February

(approximately 4 °N to 8 °N; 10 °E to 20 °E).

Considering firstly the fires along the West African coastline. From December to February, high concentrations of CO from biomass burning can be seen at the surface in both the latitudinal (Figure 4.13a) and longitudinal (Figure 4.13b) cross sections. These high concentrations are located at latitudes between approximately 4 °N and 8 °N and longitudes of around 10°E to 20 °E. This corresponds with the position of the West African coastline and the location of the largest fires from the maps in Figure 4.12. The latitudinal profile (Figure 4.13a) shows vertical transport of CO to an altitude of approximately 3 km followed by a southwards transport. This corresponds with the transport pattern seen in Figure 4.8 where CO concentrations from biomass burning are transported to the south west, off the western coast of Africa. The longitudinal profile (Figure 4.13b) also shows this vertical transport and some dispersion of concentrations to the west.

From Figure 4.12 it can be seen that the largest burning events during the wet season lie outside of West Africa. During June, July and August, the latitudinal profile (Figure 4.13e) shows high concentrations of CO attributed to biomass burning moving northwards into the region at an altitude of around 1 to 3 km. This follows a similar regime to the fires along the west African coastline where pollutant emissions from the burning are lifted to higher altitudes and then transported in the direction of the prevailing wind. During this season, the prevailing winds at the surface are from the central African region northwards towards the West African coastline, whereas at 2 km altitude there is a strong flow from central Africa over the ocean to the west (see stream functions in Figure 4.9). Transport to the west as a result of these easterly winds at around 2 km can be clearly seen in the longitudinal profile (Figure 4.13f). These transport patterns during the wet season result in large contributions from biomass burning to concentrations of CO across the ocean and along the Guinea coast, despite the burning events taking place thousands of kilometres away. Biomass burning events therefore not only influence pollutant concentrations in the vicinity of the fires but also thousands of kilometres from the emission sources [102, 218].

The transport of CO has been considered in Figures 4.12 and 4.13 as it is one of the key species emitted from biomass burning and its long lifetime in the atmosphere allows the transport patterns to be easily traced. There are, however, many other species emitted from the burning activities and the lifetimes and transport patterns of these different species vary. The Hovmöller diagrams in Figure 4.14 show the latitudinal trends in transport of CO, NO_x, SO_2, O_3 and $PM_{2.5}$ at the surface throughout the year.

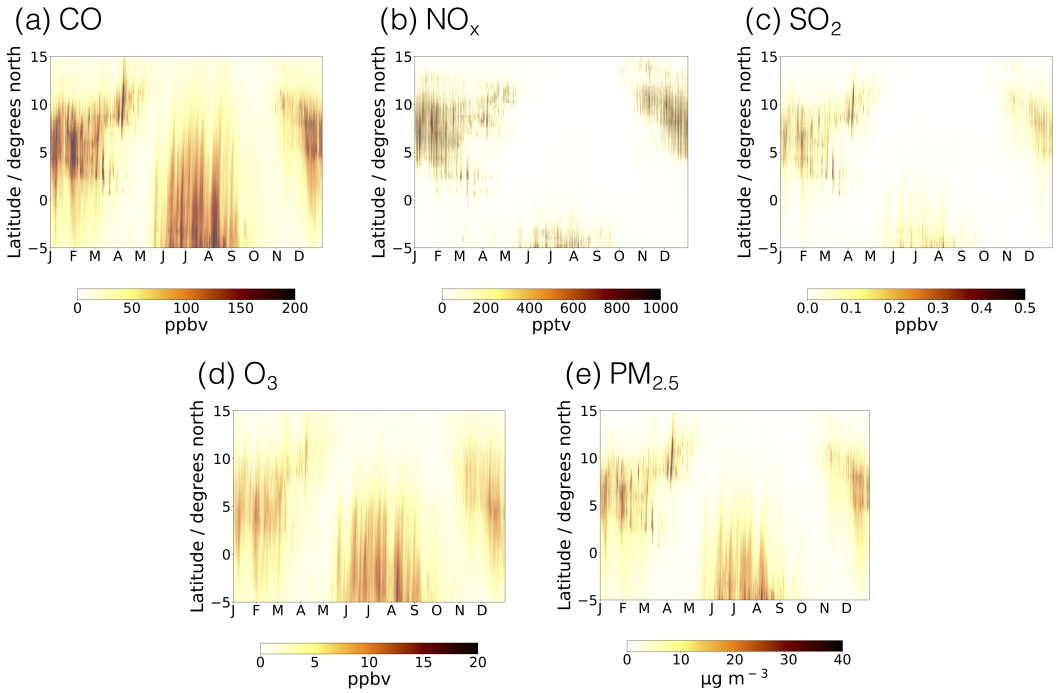

Figure 4.14: Hovmöller diagrams showing latitudinal patterns in surface level concentrations of CO, NO_x, SO_2, O_3 and $PM_{2.5}$ from biomass burning for the year 2016. Concentrations averaged for longitudes between 15 °W and 25 °E.

The transport patterns discussed above for CO are clearly visible in Figure 4.14(a). During December, January and February the biomass burning is concentrated between approximately 3 °N and 10 °N with some transport towards the south. During June, July and August strong northwards transport of CO can be seen from the central African burning events with high concentrations of CO (around 100 ppbv) extending into the coastal countries along the Guinea coast ($\sim$ 5 °N).

For NO_x and SO_2, little transport of the pollution is seen, with concentrations remaining in the vicinity of the burning events. Concentrations are highest between 5 °N and 10 °N from December to February, whilst the high concentrations from biomass burning in central Africa are not transported above approximately 2 °S during June, July and August.

O_3 and $PM_{2.5}$ both follow a pattern more similar to that of CO with pollutants emitted from the biomass burning in central Africa being transported up to the West African coastline.

As the main focus from a human health perspective is on $PM_{2.5}$, the latitudinal transport of $PM_{2.5}$ is considered further in Figure 4.15. The monthly mean concentrations, averaged between longitudes of 15 °W and 25 °E, are shown for the four major sources of $PM_{2.5}$: anthropogenic, biomass burning, dust and other.

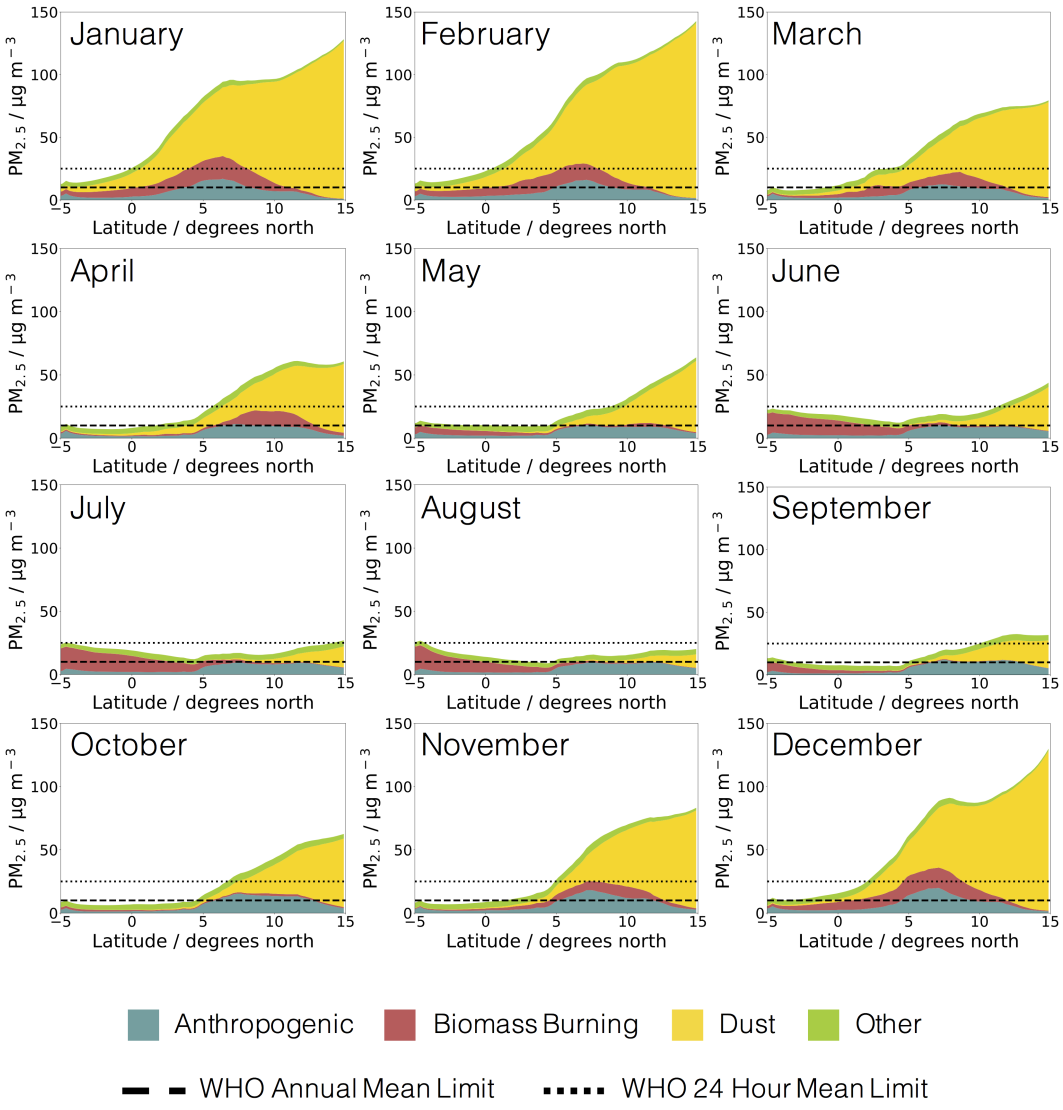

Figure 4.15: Monthly latitudinal cross sections of surface level $PM_{2.5}$ concentrations. Data averaged between longitudes of 15 °W and 25 °E for the year 2016. $PM_{2.5}$ concentrations divided into the contributions from anthropogenic, biomass burning, dust and other sources. Dashed line indicates WHO annual mean limit and dotted line indicates WHO 24 hour mean limit.

The anthropogenic component of the $PM_{2.5}$ concentrations throughout the year (Figure 4.15) is highest between 5 °N and 15 °N which corresponds with the countries along the Guinea coast, in particular with the locations of the largest cities in the region. The anthropogenic concentrations are highest during the dry season months (November to February) due to reduced dispersion caused by the meteorological convergence and low deposition due to low precipitation.

The seasonal changes in concentrations from dust are extreme. During the dry season months, the $PM_{2.5}$ concentrations north of the equator are dominated by dust sources. During the wet season, the dust concentrations are significantly reduced with a relatively small contribution remaining between 10 °N and 15 °N.

During the dry season, when biomass burning activities take place along the Guinea coastline, enhanced concentrations from the burning can be seen from 0 °N to 10 °N, whereas during the wet season, when biomass burning activities take place in central Africa, the high concentrations from biomass burning are seen between 5 °S and 5 °N.

The WHO recommended limits of 10 μg m^{-3} annual mean and 25 μg m^{-3} 24 hour mean are also illustrated on the cross section charts [274]. The annual mean limit is exceeded throughout the year in almost all locations whilst the 24 hour mean limit is exceeded over the land in West Africa (approximately 5 °N to 15 °N) during the dry season when large concentrations of dust from the Sahara move southwards into the region. The biomass burning contribution alone is seen to be in exceedance of the 10 μg m^{-3} along the West African coastline during the dry season and in central African during the wet season. This emphasises that whilst dust and anthropogenic sources might be dominant, biomass burning still remains a significant source of pollution in the region. The contribution from biomass burning is larger when considering the regional average, rather than the major cities (Figure 4.11), as many of the large scale biomass burning events take place outside urban areas.

This analysis has focused on the year 2016 (the year of the DACCIWA campaign). The interannual variability in biomass burning emissions in West Africa is now evaluated.

4.4 Interannual variability in West African biomass burning

The biomass burning emissions and transport patterns have been investigated for 2016 (the DACCIWA campaign year). Whilst the impact of the burning during this year has been assessed in detail, it is unclear whether 2016 is representative of typical burning activities. Figure 4.16 shows the annual mean emissions of CO from biomass burning for the Guinea region from 2003 to 2018, using data from the GFAS inventory.

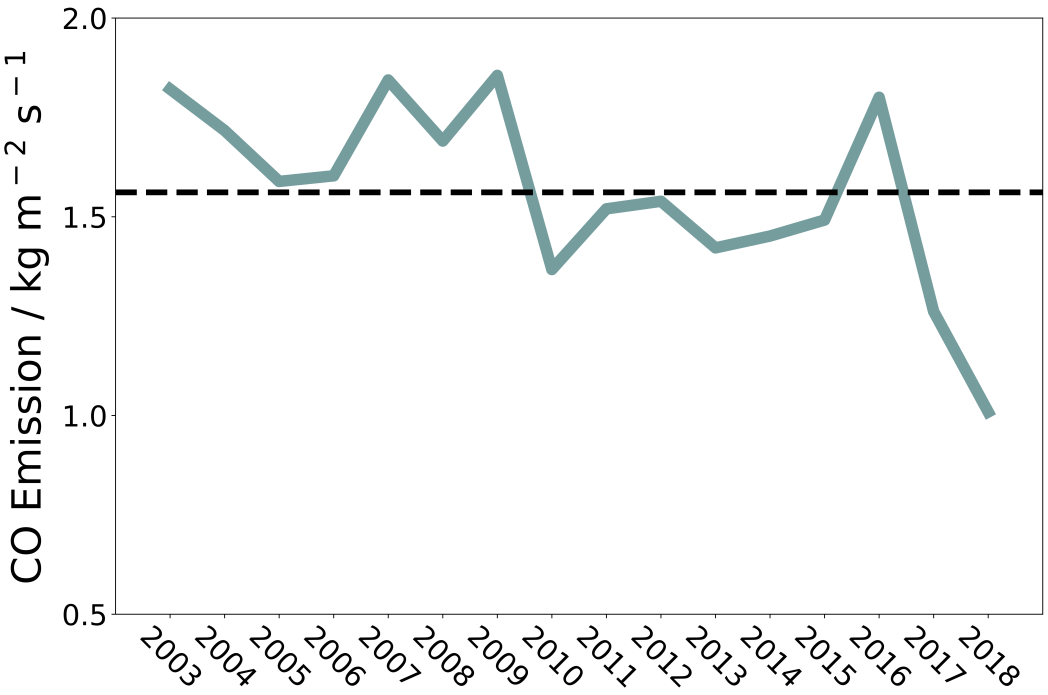

Figure 4.16: Annual mean emissions of CO from biomass burning in the Guinea region (3 °N - 15 °N; 15 °W - 15 °E). Emission data from the GFAS biomass burning inventory for the years 2003 to 2018. Dashed line represents the overall mean emission in the region from 2003 to 2018.

There is no distinct interannual trend in the emissions, although in general the biomass burning emissions may appear to show a decrease from the start of the century to present day [15,69,286]. Between 2003 and 2009, emissions were above the 16-year average, whilst from 2010 to 2018 the emissions were below this average value, with the exception of 2016.

2016 is amongst the highest years for biomass burning emissions in this 16 year period, with the mean annual emission approximately 80% higher than in 2018. Considering the lower emissions in 2017 and 2018, it is likely that conclusions drawn from the 2016 data regarding the impacts of biomass burning may over estimate the importance for these subsequent years.

Interannual differences in the seasonal variability of the biomass burning have also been investigated (Figure 4.17).

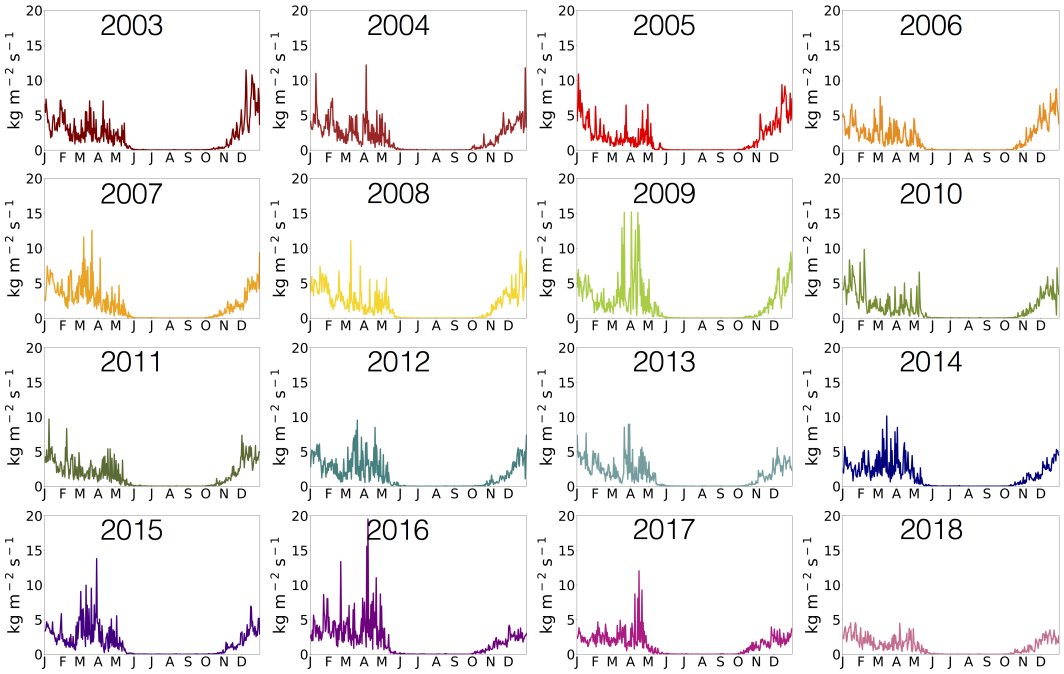

Figure 4.17: Seasonal variability in CO biomass burning emissions for the years 2003 to 2018 over the Guinea region. Daily emission data from the GFAS biomass burning inventory.

For all years, emissions from June to October are negligible in West Africa. This is the period of the West African wet season, when rainfall in the region inhibits burning and hence minimises emissions. During the dry season, the emission patterns vary between different years. In general, at the beginning of the dry season, the biomass burning emissions increase steadily over a couple of months (October to January) and the emissions then show more variability in February through to May, with emissions then decreasing between May and June.

For 2018, which is the lowest year for biomass burning emissions, the mean CO emissions do not exceed 5 kg m^{-2} s^{-1} throughout the dry season. Whereas for 2009, which is the year of highest emissions, the daily emissions of CO frequently exceed 10 kg m^{-2} s^{-1}. As well as the magnitude of the emissions, there is also variability in the timing of the peak emissions. For some years the highest emissions are seen in December (2003 and 2006), for some years the emissions peak in March (2007 and 2015), for some years the emissions peak in April (2009, 2016 and 2017), whereas for other years the emissions are more evenly distributed throughout the dry season (2011 and 2018).

The interannual variability in the biomass burning activities may be largely governed by variations in meteorology [12,68,96,164,212]. The burning is predominantly regulated by precipitation and therefore rainfall and the monsoonal transitions in the region play a key role in influencing the timing, location and magnitude of the burning events. As wildfires are influences by a wide range of factors including precipitation, temperature and deforestation the interannual variability is high and it is difficult to predict future

trends [87, 272]. However, current climate change, increased carbon dioxide levels, warmer temperatures and changing precipitation patterns are suggested to be contributing to increases in frequency and intensity of biomass burning events [87, 130].

Considering the time period from 2010 to present day, 2016 shows the highest biomass burning emissions in West Africa. The impact that the 2016 burning has on pollutant concentrations has been calculated for the entire West Africa region. For any years where the biomass burning emissions are lower than in 2016, the impacts of the biomass burning are also likely to be lower. Whilst this means that 2016 is not representative of a typical year in this decade, the conclusions drawn from the 2016 data do act as an assessment for an anomalously high year of biomass burning emissions.

4.5 Concluding remarks on the biomass burning in West Africa

Two different biomass burning emission inventories have been evaluated for the region. The GFAS inventory has been implemented in the GEOS-Chem model and is favoured due to the higher temporal resolution of the emissions, ability to incorporate injection altitudes, and its improved agreement with DACCIWA aircraft observations. Whilst incorporating injection altitudes into the emissions resulted in little change in the surface pollutant concentrations, it likely provides a better representation of the system.

Using the GFAS inventory, pollutant concentrations in West Africa have been shown to have strong seasonal influences from biomass burning. The location of the biomass burning is largely dependent on meteorology, with burning taking place in central Africa during the West African wet season and in West Africa during the dry season reflecting the rainfall distribution across the region throughout the year. This results in higher biomass burning pollutant concentrations along the Guinea coastline in the dry season when local burning is taking place. During the wet season, the concentrations from biomass burning are lower due to a lack of local sources; however, prevailing winds from the south east bring pollutants emitted from the central African burning across the Gulf of Guinea to the West African coastline. This transported pollution contributes to concentrations of long lived species such as CO, carbonaceous aerosols and fine particulate matter in the coastal area.

As well as seasonal variability in emissions, biomass burning also varies between years. West African biomass burning emissions in 2016 have been shown to be the highest in this decade. Biomass burning emissions and subsequent impacts on pollutant concentrations across the region and ultimately impacts on human health are therefore likely to be reduced in years when the biomass burning emissions fall below those of 2016.

Chapter 5

Summary and future research questions for West African air quality

West African air quality has historically been understudied and a lack of observational data for the continent significantly limits our knowledge and understanding of the atmospheric composition [184, 219]. This thesis aims to make a contribution towards addressing this information deficit. Based on the large EU funded DACCIWA programme [135], the main findings from this research are summarised below in Sections 5.1 to 5.3. Many research questions remain and these are discussed in Sections 5.4 and 5.5.

5.1 Assessment of the emission inventories for West Africa

Historically, improvements in air quality have come from understanding which emission sources are contributing the most to the air pollution problem and then targeting controls on the most significant sources. This relies upon having confidence in the veracity of emission inventories. For West Africa, confidence in the emission inventories is low [128, 151, 163] and so efforts to assess the quality of these emission inventories are important.

In this thesis, the emission inventories for West Africa have been evaluated against field observations collected from the DACCIWA aircraft campaign [86] and these observations have then been used to perform a simple optimisation of the emissions. The evaluation and optimisation process is summarised in Figure 5.1.

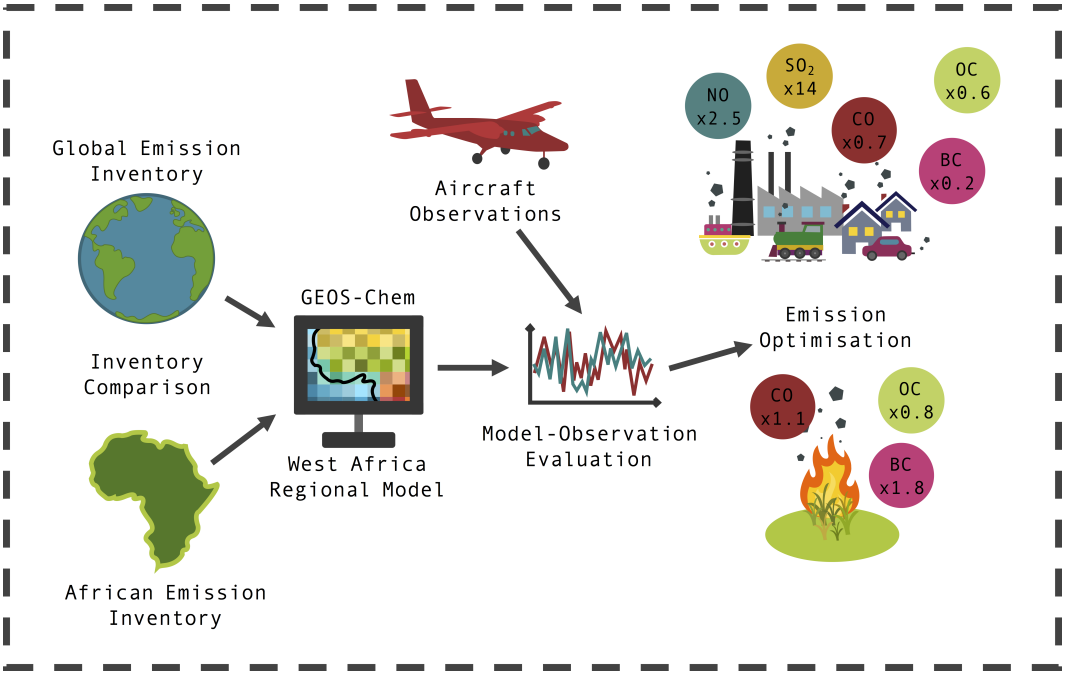

Figure 5.1: Overview of the key findings from the evaluation and optimisation of the anthropogenic and biomass burning emission inventories for West Africa.

This evaluation found serious failings in the ability of the model to simulate concentrations of key pollutants such as NO_x and inorganic aerosols (SO_4^{2-}, NO_3^-, NH_4^+) (Figure 2.11), which is attributed to failures in the emission inventories.

In general, within the GEOS-Chem chemical transport model, the Africa specific DACCIWA emissions performed better than the global EDGAR / BOND / RETRO anthropogenic inventories when compared to observations. A simple optimisation of the DACCIWA anthropogenic and GFAS biomass burning emission inventories attempted to bring together the model and the observations. Anthropogenic emissions (DACCIWA inventory) of NO and SO_2 were found to be under estimated by factors of 2.5 and 14.0 respectively. The model performance for CO was shown to be more consistent with the observations, with optimisation suggesting an anthropogenic scale factor of 0.7 and a biomass burning scale factor of 1.1. Carbonaceous aerosols show some model over estimation when compared to the aircraft observations, requiring a scaling of the anthropogenic emissions by 0.2 and 0.6 for black carbon and organic carbon respectively, and biomass burning factors of 1.8 and 0.8, again for black carbon and organic carbon respectively. It should be noted that no secondary organic carbon aerosol was included in these model simulations and so it would be likely that the reductions in organic carbon emissions would need to be larger in reality. In addition to this, large differences existed between the two black carbon instruments on board the DACCIWA aircraft (SAFIRE ATR and BAS Twin Otter) during the campaign which affects the scale factors calculated for black carbon. Although there are insufficient observations to quantify the disagreement, the evaluation also suggests that emissions of VOCs may be significantly (factors of greater than 10) under represented by

the current inventories. Due to a lack of observations, emissions of ammonia could not be evaluated. However, analysis of inorganic aerosol concentrations suggests that these emissions may too be under predicted by the current inventories.

These findings indicate that care should be taken when using the current generation of global inventories for modelling air quality in West Africa; and that whilst regional emission estimates are more representative of the pollution sources, they still show discrepancies when compared to observations of key primary pollutants such as NO_x and SO_2. These uncertainties manifest in a profound impact on the modelled surface concentrations of many species, notably particulate matter. The standard global emissions (EDGAR / BOND / RETRO) predict approximately half the $PM_{2.5}$ mass loading compared with that observed, and also simulated by the DACCIWA emissions. Similarly, O_3 concentrations increased with the optimised primary emissions. However, this made the model less consistent with the observations, with the simulations now over estimating O_3 concentrations. The reasons for these over estimations are unclear.

5.2 Seasonal influences on atmospheric composition over West Africa

The evaluation of the GEOS-Chem model performance took place for the period of available DACCIWA observations, which was essentially just one month of one year. Chapter 3 evaluated the model performance on an annual scale. The three most significant sources of emissions in West Africa are anthropogenic, dust and biomass burning and these vary depending on geographical location and season. The monsoonal climate in West Africa means that precipitation rates and wind directions vary greatly between seasons and also play a key role in influencing the pollutant concentrations in the region [12,22,68,164,194,220,245,271,281]. The key factors influencing the seasonal changes in concentrations of pollutants in the West Africa region are summarised in Figure 5.2.

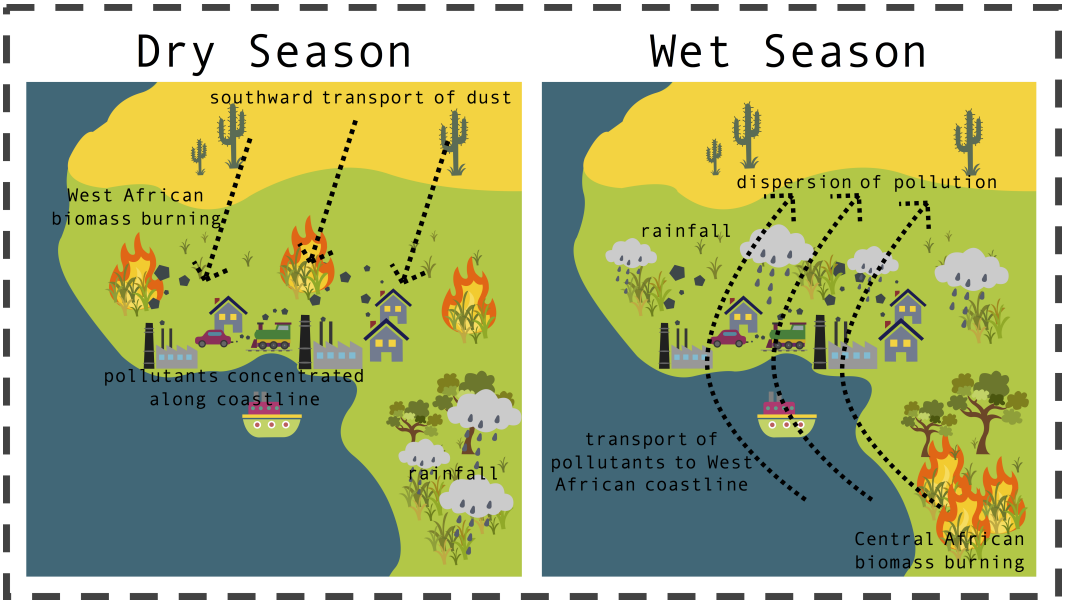

Figure 5.2: Overview of the seasonal variations in factors controlling air quality in West Africa.

Using the available observational data (AERONET [177], INDAAF [117] and DACCIWA [62] ground sites), the model (run with the uncorrected DACCIWA and GFAS emissions) is evaluated. Comparisons to the AERONET and DACCIWA ground sites showed reasonable agreement between the model and observations for particulate matter; however, the comparisons to INDAAF measurement sites suggest that there are some under predictions in NO, SO_2 and NH_3 emissions which is in agreement with the evaluation in Chapter 2.

In general, the air quality over a year can be separated into the dry season (October to March) and the wet season (April to September), driven by the monsoon flow [12, 68, 164, 167, 194, 206].

During the West African dry season, the scarcity of rainfall along the coastline reduces wet deposition of pollution which in turn contributes to higher atmospheric concentrations. The lack of rainfall also promotes biomass burning events throughout the region, leading to increased emissions of pollutants. Strong winds from the north / north east bring dust from the Sahara down to the coastline, resulting in a massive increase in particulate matter concentrations. Low wind speeds along the coastal region reduces dispersion of pollutants from anthropogenic sources and further concentrates the pollutants along the densely populated coastal region.

During the wet season, rainfall across the region increases the loss rates of atmospheric pollutants through wet deposition. It also inhibits biomass burning activities in the West African countries. The prevailing winds from central Africa flow across the Gulf of Guinea to the north east bringing pollutants from the large scale biomass burning events in central Africa to the West African coastline. These winds then move northwards, dispersing pollutants from the major cities inland and prevent the southward transport of dust from

the Sahara to the coastline. Overall, these processes lead to reduced concentrations of pollutants during the wet season.

From a human health perspective, this modelling study indicates that the concentrations of gas phase pollutants (CO, NO_2, SO_2 and O_3) are rarely found to be in exceedance of the World Health Organisation guideline values [274]. $PM_{2.5}$, however, is a significant health risk [23, 63, 149, 174, 280] and its modelled concentrations exceed the annual mean guideline (10 μg m^{-3}) throughout the year for many locations in West Africa, with exceedances of the 24 hour mean limit (25 μg m^{-3}) common in many places.

The horizontal resolution of the new West African regional model is a large improvement over the global model resolution. It is, however, important to note that the model resolution remains too coarse for studying health impacts in detail or considering exposure of the population at street level scale. It is also unable to provide any assessment of the impacts of indoor air pollution on health in the region. The conclusions drawn from this study may therefore not be representative of the true health impacts of air pollution felt by the West African population.

$PM_{2.5}$ is a complex combination of different components, sources and production pathways and the concentrations are influenced to varying extents by these different factors throughout the year [2, 16, 82, 176, 268]. Although dust and biomass burning sources are major influences on concentrations in the region, they cannot be managed on a local scale and instead require regional and continental scale strategies. Analysing the model results for the region by both area and population provided different insights into the dominant drivers of the $PM_{2.5}$ exceedances. From an area perspective, desert dust is the dominant concern for the region. However, when weighted by the population in each location, this perspective changes, with anthropogenic emissions becoming more significant. Care should therefore be taken when evaluating the dominant source of human exposure to pollutants to ensure that the correct metrics are being used.

The most prominent anthropogenic sources of $PM_{2.5}$ are residential activities such as wood fired cook stoves as well as road traffic emissions from a varied vehicle fleet [62, 140, 176]. These sources may provide suitable targets for policymakers to begin considering when assessing the best areas to focus pollution reduction strategies on. The wide range of sources and secondary production pathways means that $PM_{2.5}$ will remain a complex challenge for governments to manage.

From the perspective of agriculture and crop production, the main pollutant of concern is ozone. Arable farming in the region is predominantly fed by rainfall and therefore planting, growing and harvesting schedules follow a well defined seasonal pattern [89, 260]. As the highest ozone concentrations correspond with the dry season when few crops are grown, ozone does not currently appear to exhibit high enough concentrations to significantly impact on productivity. As with the health impact assessments, this conclusion is drawn based upon relatively coarse model data. Alternate conclusions regarding the

impacts on crop production may therefore be found if considering data at a finer resolution.

5.3 The role of biomass burning in air quality over West Africa

Unlike most of Europe and North America, the pollutant concentrations in West Africa experience a strong seasonal influence from biomass burning [96,152,212]. The evaluation of biomass burning (Chapter 4) focused mainly on the comparison between two commonly used biomass burning inventories: GFED and GFAS.

The GFAS biomass burning inventory [126] was implemented in the GEOS-Chem model. This inventory shows improved agreement between the model and the DACCIWA airborne observations compared to the default GFED inventory [9,18,97,204,253]. Unlike the GFED system, the GFAS inventory also provides information regarding the biomass burning plume injection altitudes. Incorporating this information into the model had little impact on the concentrations of pollutants at the surface, consistent with previous studies [169]. The active vertical mixing inherent in the region means that the injection of biomass burning emissions at altitude has little impact compared to injection at the surface.

Biomass burning shows strong seasonal trends in emissions, driven by the monsoonal meteorology and rainfall patterns in the region [96, 152, 212]. During the West African dry season, burning events along the West African coastline release pollutants directly into the local atmosphere. During the wet season, the burning activities take place in central Africa with some transport of pollutants across the Gulf of Guinea into the West African region. As a result, pollutant concentrations from biomass burning are highest in West Africa during the dry season, although transport from central Africa across the Gulf of Guinea results in concentrations of longer lived species such as carbon monoxide and particulate matter being elevated by biomass burning during the wet season.

The key seasonal patterns of biomass burning emissions and transport in West Africa are summarised in 5.3.

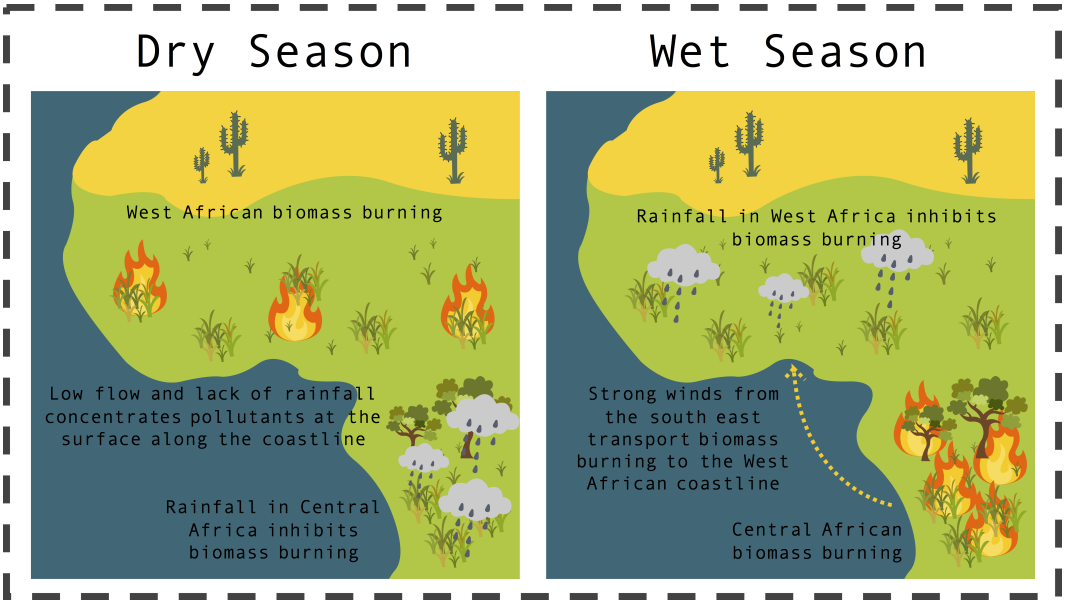

Figure 5.3: Overview of the impact of biomass burning on the West Africa region.

The modelled concentrations of $PM_{2.5}$ from biomass burning alone in West Africa are rarely in exceedance of the WHO annual mean guideline value (10 μg m^{-3}) [274], particularly in urban locations. Consequently, whilst biomass burning is a key source of pollution in the region, anthropogenic and dust emissions have a greater impact on the concentrations experienced by the general population.

In Chapter 4, the emissions and transport patterns of biomass burning were investigated for the DACCIWA campaign year of 2016. A comparison with all of the years of GFAS data (2003 to 2018) showed that 2016 was the second highest year of burning in the past decade for the West Africa region. Despite this, the biomass burning in 2016 has not been found to have a large impact on the concentrations of $PM_{2.5}$ experienced by the population. It is therefore likely that biomass burning is not a large health concern for a typical member of the population in the region compared to anthropogenic sources and dust.

5.4 Current limitations of modelling studies for assessing air quality in West Africa

Whilst this research has addressed some key questions regarding air quality in West Africa and its representation in a chemical transport model there are still many limitations to the modelling studies.

Firstly, the evaluation and optimisation of the African anthropogenic emission inventory (DACCIWA) and biomass burning inventory (GFAS) relied solely on aircraft observations from the DACCIWA campaign. Whilst the aircraft campaign collected an extensive data set of airborne measurements during the wet season, at the onset of the monsoon

period, it provides no information on how pollutant concentrations vary across the wider West Africa region, or how they change throughout the year. The conclusions drawn from the emission evaluation and optimisation are therefore only valid for the time period of the campaign, for the geographical range covered by the aircraft and for the species measured on board [86]. In order to perform a more rigorous assessment of the emissions, more data are required.

Whilst aircraft observations provide useful information about the vertical profiles of concentrations, it is often hard to relate these concentrations back to point sources of emissions at the surface. Observations from ground based sites are therefore most suited to evaluating emissions, as these sites are closest to the emission sources. The current network of available air quality observations is considerably limited with only a few sites in West Africa. One issue may be a poor knowledge of activities occurring in the region. City, regional and national agencies may be collecting observations but not making them readily available to the research community. However, it seems more likely that in many places no observations are being made.

A network of ground based measurement sites covering the West African region would therefore be highly desirable. This network should cover a wide range of environments to allow the different sources of emissions to be evaluated and to create a representative assessment of the inventories. These environments should include city centres, urban areas, industrial regions, road side locations, residential areas, agricultural land, vegetated regions and deserts. However, this list is not exhaustive.

From the modelling undertaken here, Nigeria is seen to be the largest source of anthropogenic emissions in the region, yet no observational data could be obtained from Nigeria during the DACCIWA project. Nigeria is also forecast to experience massive population growth and urbanisation, with the United Nations projecting a doubling of Nigeria's population by 2050 [199]. It is therefore important that any future network of measurement sites is able to obtain observational data from Nigeria in order to fully evaluate the emission sources in the region.

Future networks should focus on ensuring that the most useful measurements are made, rather than assuming that copying Western networks is appropriate. For example, VOCs are monitored in only a few locations in the UK, as the primary concerns are NO_2, PM and O_3. However, it would appear that there are significant concentrations of VOCs in West African cities. Similarly, SO_2 concentrations are so low in Western Europe and the United States that it is only sparsely monitored. It would appear that the high sulfur content of fuel currently used in West Africa results in a need to monitor SO_2 concentrations.

However good a surface network is, it cannot monitor all compounds in all locations. As a complement to a future surface network, satellite data could be used to evaluate the emissions and concentrations in cases where ground based observational data is lacking. The new Tropospheric Monitoring Instrument (TROPOMI) shows a capability to mea-

sure many compounds at relatively high spatial resolution globally [258]. Geostationary satellites also hold promise although it should be noted that the Sentinel 4 mission, whilst situated over Africa, will only provide geostationary observations for Europe [24].

Finally, the chemical species and reactions incorporated into the GEOS-Chem model are not exhaustive. Two notable shortcomings in the model version used here are the lack of secondary organic aerosol (SOA) and a lack of halogen chemistry. Primary organic aerosol has been shown to be one of the major components of $PM_{2.5}$ in West Africa; however, SOA (which is also a component of particulate matter) is not included in the simulations. Incorporating SOA into the model simulations would produce a more accurate representation of the chemistry and would in turn alter the concentrations and optimised scale factors for primary organic aerosol [161, 201]. Halogens can impact the oxidative capacity of the atmosphere and in particular can destroy ozone through a series of catalytic reactions [26, 192, 222, 223]. Oceans provide a large source of halogens to the atmosphere, meaning that the impacts of halogen chemistry are greater in coastal regions than inland [222, 223]. The work of Sherwen et al. [222, 223] suggests that surface ozone concentrations along the West African coastline could be reduced by around 10% to 15% as a result of this chemistry. Incorporating this chemistry into the model would provide a better representation of the system and may help alleviate some of the remaining discrepancies seen in the model when compared to observational data.

5.5 Future projections of air quality in West Africa

The modelling studies discussed in this work have a strong focus on present day air quality in West Africa. Whilst it is important to understand the present day emissions, concentrations and impacts of pollutants in the region it is imperative to have an understanding of how the emissions and concentrations may change in the future and the resulting effects on the health of the population and the environment in order to design and implement policies for regulating the emissions and mitigating the consequences.

Emissions of pollutants have been shown to change dramatically throughout the year depending upon meteorological conditions and seasonal changes in emission activities (Chapter 3). Emissions are also subject to ongoing change as a result of population growth as well as economic development [199]. West Africa is currently experiencing rapid population growth which is accompanied by increased urbanisation and industrial development [151, 199]. Air pollution in the region is largely unregulated therefore these changes are leading to large increases in emissions from anthropogenic sources [141, 151]. Estimates of these changes can be made, but it is hard to determine the resulting impacts on air quality without the use of modelling studies.

There are many different approaches that can be taken when simulating future air quality in West Africa. Three different approaches that may be easily incorporated into

GEOS-Chem modelling studies are:

1. Scale the emissions from anthropogenic inventories according to the projected rate of population change for the region

2. Scale the emissions based upon the Representative Concentration Pathways (RCPs) developed by the Intergovernmental Panel on Climate Change (IPCC)

3. Use West Africa specific future scenarios based upon realistic changes expected in the region

One of the most simple approaches is to scale the present day anthropogenic emissions by the rate of population growth. This simple approximation makes the assumption that each member of the population is responsible for an equal share of the anthropogenic emissions. The population change between present day and the desired future date can then be used to scale the anthropogenic emissions. Gridded projections of population change also enable the emission scaling to vary spatially, allowing better representation of the region [47]. For example, if population growth rates are projected to be higher in urban locations and lower in rural locations then the anthropogenic emissions in these urban areas will be scaled by higher factors than in the rural areas. Whilst this option provides a simple way of estimating the future changes in air quality, it does not reflect any future implementations of policies or new technologies.

A more complex approach is followed by the Intergovernmental Panel on Climate Change (IPCC). This has developed a set of four different Representative Concentration Pathways (RCPs) which consider different climate futures [65, 124, 173, 210, 217, 239, 257]. These scenarios provide projected emissions from 2000 to 2100 globally. This approach was used by the ETH Zurich group as part of their contribution to the DACCIWA programme. They found that these predictions suggested reduced concentrations of pollutants by 2050 due to uptake of new, lower emitting technologies in the region producing a greater impact than the increase in population and industrialisation. One of the problems with the RCP approach is that it often has to use the same factors globally. It may be that in developed western countries air pollution mitigation is an important policy resulting in reduced emissions, but it may not be the case for West Africa.

The third option is to use emission scenarios specifically designed for the West Africa region. These emission scenarios are being developed as part of work package 2 (Air Pollution and Health) of the DACCIWA project but are not currently completed. These scenarios will provide predicted future emissions for both 2030 and 2050. One scenario will provide "business as usual" emissions. This assumes that the emissions will vary as a function of the population growth but that technologies in the region will remain the same. For example, no regulation of industrial emissions will be applied, the vehicle fleet will remain the same and wood fired cooking in homes will continue. The second scenario

will provide "improved" emissions for the region. This scenario will take into account the population change but will also incorporate improvements in domestic cook stoves, improvements in charcoal production, the movement of waste burning sites out of the densely populated urban areas and an upgrade of the vehicle fleet. These scenarios reflect more realistic factors for West Africa than the IPCC approach, that influence air quality and are specific to the region.

Ideally, simulations of future air quality in the region should be based upon realistic scenarios reflecting changes in population, land use and industrial development whilst also incorporating changes in technologies and regulations for reducing pollutant emissions. It is therefore recommended that future air quality is investigated in the regional GEOS-Chem model using these regional specific future scenarios when the data becomes available. The outcomes of these studies should be disseminated to local governments and policymakers in West Africa in order that this data may help influence the development of policies for reducing concentrations of pollutants and mitigating the impacts on human and ecosystem health.

5.6 Concluding remarks

Pollutant emissions and air quality in West Africa is a complex and constantly evolving issue. Emissions in the region vary greatly depending on the sources, location and season, whilst rapid development results in emission inventories and modelling studies quickly becoming outdated.

Whilst this research has provided an insight into the key shortcomings of current inventories, long term observational data is required to fully evaluate emission inventories for the region and to enable continued assessment of the changes in emissions over time. This observational data is currently severely lacking for the West Africa region and a key focus of future research should be on establishing a more extensive observational network in the region. The combination of increased observational data and improved modelling studies as a result of this will enable air quality in the region to be better understood and will allow the impacts on health in the region to be quantified.

It is important to appreciate that the conclusions drawn from this research are based upon a single model study. It would be of great benefit to this field of research for an ensemble of models to be used to simulate the atmospheric composition in West Africa, evaluate the emission inventories and investigate health impacts. This would enable greater confidence to be placed in any conclusions drawn and would provide a wider range of scientific evidence which could be incorporated into the development of new policies in the region.

One of the key air quality challenges facing West Africa is the influence of a wide range of emission sources on the atmospheric composition. Anthropogenic sources have been shown to contribute to the pollutant concentrations experienced by the population

throughout the year, whilst biomass burning and dust show significant seasonal contributions. These different sources must be considered by policymakers when developing strategies for improving air quality in the region.

The future pollutant concentrations in West Africa are of key interest. Estimates of future air quality in the region are dependent upon realistic emission scenarios which reflect the projected increases as well as the possible regulation and technological advances. Investigating the contributions made by different sources can also assist in determining the key sectors to target with pollution reduction policies. Assessment of present day impacts of air pollution on the health of the population and the environment is required, along with the future estimates of these impacts, in order for governments and policymakers to design and implement effective policies for reducing emissions, reducing concentrations and hence reducing the adverse effects on the health of the region.

Despite the dramatic changes forecast for West Africa over the next century with regards to population, economic and industrial development, air quality in the region remains a substantially understudied area. This region should be the focus of considerably more research in the future, drawing upon existing knowledge and understanding from other parts of the world, combined with expansion of observational networks and advancement of modelling systems.

Abbreviations

AEIC	Aviation Emissions Inventory Code
AEROCOM	Aerosol Comparisons between Observations and Models
AERONET	Aerosol Robotic Network
AMMA	African Monsoon Multidisciplinary Analysis
AOD	Aerosol Optical Depth
AOT40	Accumulated exposure over a threshold of 40 ppb
BAS	British Antarctic Survey
BC	Black Carbon
BRAVO	Big Bend Regional Aerosol and Visibility Observational
CAC	Criteria Air Contaminants
CAMS	Copernicus Atmospheric Monitoring Service
CO	Carbon Monoxide
DACCIWA	Dynamics-Aerosol-Chemistry-Cloud Interactions in West Africa
DLR	Deutsches Zentrum für Luft- und Raumfahrt
DMS	Dimethyl Sulfide
ECMWF	European Centre for Medium-Range Weather Forecasts
EDGAR	Emission Database for Global Atmospheric Research
EMEP	European Monitoring and Evaluation Programme
EU	European Union
FAO	Food and Agriculture Organisation
FRP	Fire Radiative Power
GEIA	Global Emissions InitiAtive
GEOS	Goddard Earth Observing System
GEOS-FP	Goddard Earth Observing System - Forward Processing
GFAS	Global Fire Assimilation System
GFED	Global Fire Emissions Database
GMAO	Global Modeling and Assimilation Office
HEMCO	Harvard-NASA Emissions Component
HO2	Hydroperoxyl Radical

INDAAF	International Network to study Deposition and Atmospheric composition in AFrica
IPCC	Intergovernmental Panel on Climate Change
ITCZ	Inter Tropical Convergence Zone
KPP	Kinetic PreProcessor
MEGAN	Model of Emissions of Gases and Aerosols from Nature
MERRA-2	Modern-Era Retrospective analysis for Research and Applications - Version 2
mg m^{-3}	milligrams per cubic metre
MODIS	Moderate Resolution Imaging Spectroradiometer
NASA	National Aeronautics and Space Administration
NEI	National Emissions Inventory
NH_3	Ammonia
NH_4^+	Ammonium
NMVOC	Non Methane Volatile Organic Compound
NO	Nitric Oxide
NO_2	Nitrogen Dioxide
NO_x	Nitrogen Oxides
NO_3^-	Nitrate
O_2	Molecular Oxygen
O_3	Ozone
OC	Organic Carbon
OH	Hydroxyl Radical
PM	Particulate Matter
$PM_{2.5}$	Fine Particulate Matter (diameter up to 2.5 microns)
PM_{10}	Coarse Particulate Matter (diameter up to 10 microns)
ppbv	parts per billion (by volume)
ppmv	parts per million (by volume)
pptv	parts per trillion (by volume)
RCP	Representative Concentration Pathway
SAFIRE	Service des Avions Français Instrumentés pour la Recherche en Environnement
SEDAC	SocioEconomic Data and Applications Center
SO_2	Sulfur Dioxide
SO_4^{2-}	Sulfate
SOA	Secondary Organic Aerosol
SP2	Single Particle Soot Photometer

SWA	Southern West Africa
TROPOMI	TROPOspheric Monitoring Instrument
μg m^{-3}	micrograms per cubic metre
UK	United Kingdom
UN	United Nations
UV	Ultraviolet
VOC	Volatile Organic Compound
WAM	West African Monsoon
WHO	World Health Organisation

Bibliography

[1] 2B Technologies. 205 Instrument. *https://www.twobtech.com/index.html*.

[2] Adams, K., Greenbaum, D. S., Shaikh, R., van Erp, A. M., and Russell, A. G. Particulate matter components, sources, and health: Systematic approaches to testing effects. *Journal of the Air and Waste Management Association 65*, 5 (2015), 544–558.

[3] Adler, B., Kalthoff, N., and Gantner, L. Nocturnal low-level clouds over southern West Africa analysed using high-resolution simulations. *Atmospheric Chemistry and Physics 17*, 2 (2017), 899–910.

[4] Adon, M., Galy-Lacaux, C., Yoboué, V., Delon, C., Lacaux, J. P., Castera, P., Gardrat, E., Pienaar, J., Al Ourabi, H., Laouali, D., Diop, B., Sigha-Nkamdjou, L., Akpo, A., Tathy, J. P., Lavenu, F., and Mougin, E. Long term measurements of sulfur dioxide, nitrogen dioxide, ammonia, nitric acid and ozone in Africa using passive samplers. *Atmospheric Chemistry and Physics 10*, 15 (2010), 7467–7487.

[5] Adon, M., Yoboué, V., Galy-Lacaux, C., Liousse, C., Diop, B., Doumbia, E. H. T., Gardrat, E., Ndiaye, S. A., and Jarnot, C. Measurements of NO2, SO2, NH3, HNO3 and O3 in West African urban environments. *Atmospheric Environment 135*, 2 (2016), 31–40.

[6] Aerolaser. AL4021. *https://www.aero-laser.de/gas_analyzers/hcho_al4021.html*.

[7] Ainsworth, E. A., Yendrek, C. R., Sitch, S., Collins, W. J., and Emberson, L. D. The Effects of Tropospheric Ozone on Net Primary Productivity and Implications for Climate Change. *Annual Review of Plant Biology 63*, 1 (2012), 637–661.

[8] Air Quality Design. Fast NOx Instrument. *http://noxwerx.com/*.

[9] Akagi, S. K., Yokelson, R. J., Wiedinmyer, C., Alvarado, M. J., Reid, J. S., Karl, T., Crounse, J. D., and Wennberg, P. O. Emission factors for open and domestic biomass burning for use in atmospheric models. *Atmospheric Chemistry and Physics 11*, 9 (2011), 4039–4072.

[10] Alexander, B., Park, R. J., Jacob, D. J., Li, Q. B., Yantosca, R. M., Savarino, J., Lee, C. C. W., and Thiemens, M. H. Sulfate formation in sea-salt aerosols: Constraints from oxygen isotopes. *Journal of Geophysical Research 110*, D10 (may 2005), D10307.

[11] Alvarez, R., Weilenmann, M., and Favez, J. Y. Evidence of increased mass fraction of NO2 within real-world NOx emissions of modern light vehicles - derived from a reliable online measuring method. *Atmospheric Environment 42*, 19 (2008), 4699–4707.

[12] Amekudzi, L., Yamba, E., Preko, K., Asare, E., Aryee, J., Baidu, M., and Codjoe, S. Variabilities in Rainfall Onset, Cessation and Length of Rainy Season for the Various Agro-Ecological Zones of Ghana. *Climate 3*, 2 (2015), 416–434.

[13] Amos, H. M., Jacob, D. J., Holmes, C. D., Fisher, J. A., Wang, Q., Yantosca, R. M., Corbitt, E. S., Galarneau, E., Rutter, A. P., Gustin, M. S., Steffen, A., Schauer, J. J., Graydon, J. A., St Louis, V. L., Talbot, R. W., Edgerton, E. S., Zhang, Y., and Sunderland, E. M. Gas-particle partitioning of atmospheric Hg(II) and its effect on global mercury deposition. *Atmospheric Chemistry and Physics 12*, 1 (2012), 591–603.

[14] Andela, N., Kaiser, J. W., Heil, A., van Leeuwen, T. T., Wooster, M. J., van der Werf, G. R., Remy, S., and Schultz, M. G. Assessment of the Global Fire Assimilation System (GFASv1). *ECMWF Technical Memoranum 602*, June (2013).

[15] Andela, N., Morton, D. C., Giglio, L., Chen, Y., Werf, G. R. V. D., Kasibhatla, P. S., Collatz, G. J., Hantson, S., Kloster, S., Bachelet, D., Forrest, M., Lasslop, G., Mangeon, S., Melton, J. R., Yue, C., Randerson, J. T., Amsterdam, V. U., Biology, E., Biodiversity, S., and Canada, E. A human driven decline in global burned area. 1356–1362.

[16] Anderson, J. O., Thundiyil, J. G., and Stolbach, A. Clearing the Air: A Review of the Effects of Particulate Matter Air Pollution on Human Health. *Journal of Medical Toxicology 8*, 2 (2012), 166–175.

[17] Andreae, M. O. Biomass burning: Its history, use and distribution and its impact on environmental quality and global climate. *Global Biomass Burning: Atmospheric, Climatic, and Biospheric Implications*, January 1991 (1991), 3–21.

[18] Andreae, M. O., and Merlet, P. Emission of trace gases and aersols from biomass burning. *Biogeochemistry 15*, 4 (2001), 955–966.

[19] Assamoi, E. M., and Liousse, C. A new inventory for two-wheel vehicle emissions in West Africa for 2002. *Atmospheric Environment 44*, 32 (2010), 3985–3996.

[20] Balakrishnan, K., Dey, S., Gupta, T., Dhaliwal, R. S., Brauer, M., Cohen, A. J., Stanaway, J. D., Beig, G., Joshi, T. K., Aggarwal, A. N., Sabde, Y., Sadhu, H., Frostad, J., Causey, K., Godwin, W., Shukla, D. K., Kumar, G. A., Varghese, C. M., Muraleedharan, P., Agrawal, A., Anjana, R. M., Bhansali, A., Bhardwaj, D., Burkart, K., Cercy, K., Chakma, J. K., Chowdhury, S., Christopher, D. J., Dutta, E., Furtado, M., Ghosh, S., Ghoshal, A. G., Glenn, S. D., Guleria, R., Gupta, R., Jeemon, P., Kant, R., Kant, S., Kaur, T., Koul, P. A., Krish, V., Krishna, B., Larson, S. L., Madhipatla, K., Mahesh, P. A., Mohan, V., Mukhopadhyay, S., Mutreja, P., Naik, N., Nair, S., Nguyen, G., Odell, C. M., Pandian, J. D., Prabhakaran, D., Prabhakaran, P., Roy, A., Salvi, S., Sambandam, S., Saraf, D., Sharma, M., Shrivastava, A., Singh, V., Tandon, N., Thomas, N. J., Torre, A., Xavier, D., Yadav, G., Singh, S., Shekhar, C., Vos, T., Dandona, R., Reddy, K. S., Lim, S. S., Murray, C. J., Venkatesh, S., and Dandona, L. The impact of air pollution on deaths, disease burden, and life expectancy across the states of India: the Global Burden of Disease Study 2017. *The Lancet Planetary Health 3*, 1 (2019), e26–e39.

[21] Barbosa, P. M. An assessment of vegetation fire in Africa (1981-1991): Burned. *Africa 13*, 4 (1999), 933–950.

[22] Barmpadimos, I., Keller, J., Oderbolz, D., Hueglin, C., and Prévôt, A. S. One decade of parallel fine (PM 2.5) and coarse (PM 10-PM 2.5) particulate matter measurements in Europe: Trends and variability. *Atmospheric Chemistry and Physics 12*, 7 (2012), 3189–3203.

[23] Bauer, S. E. Desert Dust , Industrialization , and Agricultural Fires : Health Impacts of Outdoor Air Pollution in Africa Journal of Geophysical Research : Atmospheres. *Journal of Geophysical Research Atmospheres* (2019), 1–17.

[24] Bazalgette Courrèges-Lacoste, G., Sallusti, M., Gulde, S., Bulsa, G., Bagnasco, G., Kolm, M. G., Smith, D. J., and Maurer, R. Knowing what we breathe: Sentinel 4: a geostationary imaging UVN spectrometer for air quality monitoring. 87.

[25] Bell, M. L., Davis, D. L., and Fletcher, T. A retrospective assessment of mortality from the london smog episode of 1952: The role of influenza and pollution. *Urban Ecology: An International Perspective on the Interaction Between Humans and Nature 6*, 1 (2004), 263–268.

[26] Bell, N., Hsu, L., Jacob, D. J., Schultz, M. G., Blake, D. R., Butler, J. H., King, D. B., Lobert, J. M., and Maier-Reimer, E. Methyl iodide: Atmospheric budget and use as a tracer of marine convection in global models. *Journal of Geophysical Research Atmospheres 107*, 17 (2002).

[27] Beusen, A. H. W., Bouwman, A. F., Heuberger, P. S. C., Drecht, G. V., and Hoek, K. W. V. D. Bottom-up uncertainty estimates of global ammonia emissions from global agricultural production systems. *Atmospheric Environment 42* (2008), 6067–6077.

[28] Bey, I., Jacob, D. J., Yantosca, R. M., Logan, J. A., Field, B. D., Fiore, A. M., Li, Q., Liu, H. Y., Mickley, L. J., and Schultz, M. G. Global modeling of tropospheric chemistry with assimilated meteorology: Model description and evaluation. *Journal of Geophysical Research Atmospheres 106*, D19 (oct 2001), 23073–23095.

[29] Bond, T. C., Bhardwaj, E., Dong, R., Jogani, R., Jung, S., Roden, C., Streets, D. G., and Trautmann, N. M. Historical emissions of black and organic carbon aerosol from energy-related combustion, 1850-2000. *Global Biogeochemical Cycles 21*, 2 (jun 2007).

[30] Bond, T. C., Doherty, S. J., Fahey, D. W., Forster, P. M., Berntsen, T., Deangelo, B. J., Flanner, M. G., Ghan, S., Kärcher, B., Koch, D., Kinne, S., Kondo, Y., Quinn, P. K., Sarofim, M. C., Schultz, M. G., Schulz, M., Venkataraman, C., Zhang, H., Zhang, S., Bellouin, N., Guttikunda, S. K., Hopke, P. K., Jacobson, M. Z., Kaiser, J. W., Klimont, Z., Lohmann, U., Schwarz, J. P., Shindell, D., Storelvmo, T., Warren, S. G., and Zender, C. S. Bounding the role of black carbon in the climate system: A scientific assessment. *Journal of Geophysical Research Atmospheres 118*, 11 (2013), 5380–5552.

[31] Boucher, O., and Lohmann, U. The sulfate-CCN-cloud albedo effect. *Tellus B: Chemical and Physical Meteorology 47*, 3 (1995), 281–300.

[32] Bozonnet, C. Trade in smuggled fuel from Nigeria oils economies of west Africa. *The Guardian* (2012).

[33] Brauer, M., Amann, M., Burnett, R. T., Cohen, A., Dentener, F., Ezzati, M., Henderson, S. B., Krzyzanowski, M., Martin, R. V., Van Dingenen, R., van Donkelaar, A., and Thurston, G. D. Disease Attributable To Outdoor Air Pollution. *Environ Sci Technol 46*, 2 (2012), 652–60.

[34] Brazel, A. J., and Idso, S. B. Thermal Effects of Dust on Climate. *Annals of the Asociation of American Geographers 69*, 3 (1979), 432–437.

[35] Breider, T. J., Mickley, L. J., Jacob, D. J., Ge, C., Wang, J., Sulprizio, M. P., Croft, B., Ridley, D. A., McConnell, J. R., Sharma, S., Husain, L., Dutkiewicz, V. A., Eleftheriadis, K., Skov, H., and Hopke, P. K. Multidecadal trends in aerosol radiative forcing over the Arctic: Contribution of changes in anthropogenic aerosol to Arctic warming since 1980. *Journal of Geophysical Research 122*, 6 (2017), 3573–3594.

[36] Brosse, F., Leriche, M., Mari, C., and Couvreux, F. LES study of the impact of moist thermals on the oxidative capacity of the atmosphere in southern West Africa. *Atmospheric Chemistry and Physics 18*, 9 (may 2018), 6601–6624.

[37] Butt, E. W., Turnock, S. T., Rigby, R., Reddington, C. L., Yoshioka, M., Johnson, J. S., Regayre, L. A., Pringle, K. J., Mann, G. W., and Spracklen, D. V. Global and regional trends in particulate air pollution and attributable health burden over the past 50 years. *Environmental Research Letters 12*, 10 (2017).

[38] Cabos, W., Sein, D. V., Pinto, J. G., Fink, A. H., Koldunov, N. V., Alvarez, F., Izquierdo, A., Keenlyside, N., and Jacob, D. The South Atlantic Anticyclone as a key player for the representation of the tropical Atlantic climate in coupled climate models. *Climate Dynamics 48*, 11-12 (2017), 4051–4069.

[39] Cao, J. The Importance of Aerosols in the Earth System: Science and Engineering Perspectives. *Aerosol Science and Engineering 1*, 1 (2017), 1–6.

[40] CarbonBrief. Mapped: The world's coal power plants.

[41] Carmichael, G. R., Ferm, M., Thongboonchoo, N., Woo, J. H., Chan, L. Y., Murano, K., Viet, P. H., Mossberg, C., Bala, R., Boonjawat, J., Upatum, P., Mohan, M., Adhikary, S. P., Shrestha, A. B., Pienaar, J. J., Brunke, E. B., Chen, T., Jie, T., Guoan, D., Peng, L. C., Dhiharto, S., Harjanto, H., Jose, A. M., Kimani, W., Kirouane, A., Lacaux, J. P., Richard, S., Barturen, O., Cerda, J. C., Athayde, A., Tavares, T., Cotrina, J. S., and Bilici, E. Measurements of sulfur dioxide, ozone and ammonia concentrations in Asia, Africa, and South America using passive samplers. *Atmospheric Environment 37*, 9-10 (2003), 1293–1308.

[42] Carn, S. A., Fioletov, V. E., Mclinden, C. A., Li, C., and Krotkov, N. A. A decade of global volcanic SO2 emissions measured from space. *Scientific Reports 7* (2017), 1–12.

[43] Carslaw, D. C. Evidence of an increasing NO2/NOX emissions ratio from road traffic emissions. *Atmospheric Environment 39*, 26 (2005), 4793–4802.

[44] Carslaw, D. C., and Carslaw, N. Detecting and characterising small changes in urban nitrogen dioxide concentrations. *Atmospheric Environment 41*, 22 (2007), 4723–4733.

[45] Carslaw, D. C., Murrells, T. P., Andersson, J., and Keenan, M. Have vehicle emissions of primary NO2 peaked? *Faraday Discussions 189*, 0 (2016), 439–454.

[46] Catoire, V., Robert, C., Chartier, M., Jacquet, P., Guimbaud, C., and Krysztofiak, G. The SPIRIT airborne instrument: a three-channel infrared absorption spectrometer with quantum cascade lasers for in situ atmospheric trace-gas measurements. *Applied Physics B: Lasers and Optics 123*, 9 (2017), 1–12.

[47] Center for International Earth Science Information Network - CIESIN - Columbia University. Gridded Population of the World, Version 4 (GPWv4): Population Count, Revision 10, 2017.

[48] Chameides, W. L., and Davis, D. D. Iodine: Its possible role in tropospheric photochemistry. *Journal of Geophysical Research: Oceans 85*, C12 (1980), 7383–7398.

[49] Chin, J.-Y., and Batterman, S. A. VOC composition of current motor vehicle fuels and vapors, and collinearity analyses for receptor modeling. *Chemosphere 86*, 9 (2012), 951–958.

[50] Cuffe, S. T., Gerstle, R. W., Orning, A. A., and Schwartz, C. H. Air pollutant emissions from coal-fired power plants, report no. 2. *Journal of the Air Pollution Control Association 15*, 2 (1965), 59–64.

[51] Damian, V., Sandu, A., Damian, M., Potra, F., and Carmichael, G. R. The Kinetic PreProcessor KPP-A software environment for solving chemical kinetics. *Computers & Chemical Engineering 26*, 11 (2002), 1567–1579.

[52] D'Andrea, M. A., and Reddy, G. K. Health Risks Associated With Benzene Exposure in Children: A Systematic Review. *Global Pediatric Health 5* (2018), 2333794X1878927.

[53] David, L. M., and Nair, P. R. Diurnal and seasonal variability of surface ozone and NOx at a tropical coastal site: Association with mesoscale and synoptic meteorological conditions. *Journal of Geophysical Research 116*, D10 (2011), D10303.

[54] Debaje, S. B. Estimated crop yield losses due to surface ozone exposure and economic damage in India. *Environmental Science and Pollution Research 21*, 12 (2014), 7329–7338.

[55] Deetz, K., and Vogel, B. Development of a new gas-flaring emission dataset for southern West Africa. *Geoscientific Model Development 10*, 4 (2017), 1607–1620.

[56] Deetz, K., Vogel, H., Knippertz, P., Adler, B., Taylor, J., Coe, H., Bower, K., Haslett, S., Flynn, M., Dorsey, J., Crawford, I., Kottmeier, C., and Vogel, B. Numerical simulations of aerosol radiative effects and their impact on clouds and atmospheric dynamics over southern West Africa. *Atmospheric Chemistry and Physics 18*, 13 (2018), 9767–9788.

[57] Department for Environment Food and Rural Affairs, ., and Environment Agency, . UK Air Monitoring Networks.

[58] Department: Statistics South Africa. Coal Resources.

[59] Department: Statistics South Africa. The Importance Of Coal, 2015.

[60] Deroubaix, A., Flamant, C., Menut, L., Siour, G., Mailler, S., Turquety, S., Briant, R., Khvorostyanov, D., and Crumeyrolle, S. Interactions of atmospheric gases and aerosols with the monsoon dynamics over the Sudano-Guinean region during AMMA. *Atmospheric Chemistry and Physics 18*, 1 (2018), 445–465.

[61] Diehl, T. A Global Inventory of Volcanic SO2 Emissions for Hindcast Scenarios, 2009.

[62] Djossou, J., Léon, J.-F., Akpo, A. B., Liousse, C., Yoboué, V., Bedou, M., Bodjrenou, M., Chiron, C., Galy-Lacaux, C., Gardrat, E., Abbey, M., Keita, S., Bahino, J., Touré, N., Datchoh, E., Ossohou, M., and Awanou, C. N. Mass concentration, optical depth and carbon composition of particulate matter in the major southern West African cities of Cotonou (Benin) and Abidjan (Côte d'Ivoire). *Atmospheric Chemistry and Physics 18*, 9 (may 2018), 6275–6291.

[63] Dockery, D. W. Health Effects of Particulate Air Pollution. *Annals of Epidemiology 19*, 4 (2009), 257–263.

[64] Dominici, F., Peng, R. D., Bell, M. L., Pham, L., McDermott, A., Zeger, S. L., and Samet, J. M. Fine particulate air pollution and hospital admission for cardiovascular and respiratory diseases. *Journal of the American Medical Association 295*, 10 (2006), 1127–1134.

[65] Dooley, J. J., and Calvin, K. V. Temporal and spatial deployment of carbon dioxide capture and storage technologies across the representative concentration pathways. *Energy Procedia 4*, 2010 (2011), 5845–5852.

[66] Doumbia, E. H. T., Liousse, C., Keita, S., Granier, L., Granier, C., Elvidge, C. D., Elguindi, N., and Law, K. Flaring emissions in Africa: Distribution, evolution and comparison with current inventories. *Atmospheric Environment 199*, September 2018 (2019), 423–434.

[67] Drewnick, F., Hings, S. S., DeCarlo, P., Jayne, J. T., Gonin, M., Fuhrer, K., Weimer, S., Jimenez, J. L., Demerjian, K. L., Borrmann, S., and Worsnop, D. R. A new time-of-flight aerosol mass spectrometer (TOF-AMS) - Instrument description and first field deployment. *Aerosol Science and Technology 39*, 7 (2005), 637–658.

[68] Dunning, C. M., Black, E. C., and Allan, R. P. The onset and cessation of seasonal rainfall over Africa. *Journal of Geophysical Research 121*, 19 (2016), 11405–11424.

[69] Earl, N., and Simmonds, I. Spatial and Temporal Variability and Trends in 2001–2016 Global Fire Activity. *Journal of Geophysical Research: Atmospheres 123*, 5 (2018), 2524–2536.

[70] EC-JRC/PBL. Emission Database for Global Atmospheric Research (EDGAR). *http://edgar.jrc.ec.europa.eu* (2011).

[71] Economic Commission For Europe. Hemispheric Transport of Air Pollution 2010 Part A: Ozone And Particulate Matter. Tech. Rep. 17, 2010.

[72] Ehhalt, D. H. Photooxidation of trace gases in the troposphere Plenary Lecture. *Physical Chemistry Chemical Physics 1*, 24 (1999), 5401–5408.

[73] Emberson, L. D., Pleijel, H., Ainsworth, E. A., van den Berg, M., Ren, W., Osborne, S., Mills, G., Pandey, D., Dentener, F., Büker, P., Ewert, F., Koeble, R., and Van Dingenen, R. Ozone effects on crops and consideration in crop models. *European Journal of Agronomy 100*, December 2016 (2018), 19–34.

[74] Engelstaedter, S., Tegen, I., and Washington, R. North African dust emissions and transport. *Earth-Science Reviews 79*, 1-2 (2006), 73–100.

[75] European Commission. Air Quality Standards.

[76] Evans, M. J., Knippertz, P., Akpo, A., Allan, R. P., Amekudzi, L., Brooks, B., Chiu, J. C., Coe, H., Fink, A. H., Flamant, C., Jegede, O. O., Liousse, C., Lohou, F., Kalthoff, N., Mari, C., Marsham, J., Yoboue, V., and Zumsprekel, C. Policy relevant findings of the DACCIWA project.

[77] Eyring, V., Köhler, H. W., Van Aardenne, J., and Lauer, A. Emissions from international shipping: 1. The last 50 years. *Journal of Geophysical Research D: Atmospheres 110*, 17 (sep 2005), 171–182.

[78] Fairlie, T. D., Jacob, D. J., and Park, R. J. The impact of transpacific transport of mineral dust in the United States. *Atmospheric Environment 41*, 6 (2007), 1251–1266.

[79] Falola, I. O. Fuel smuggling. *Development and Cooperation: Economy* (2017).

[80] Felzer, B. S., Cronin, T., Reilly, J. M., Melillo, J. M., and Wang, X. Impacts of ozone on trees and crops. *Comptes Rendus - Geoscience 339*, 11-12 (2007), 784–798.

[81] Ferm, M., and Rodhe, H. Measurements of air concentrations of SO2, NO2 and NH3 at rural and remote sites in Asia. *Journal of Atmospheric Chemistry 27*, 1 (1997), 17–29.

[82] Fine, P. M., Sioutas, C., and Solomon, P. A. Secondary particulate matter in the United states: Insights from the particulate matter supersites program and related studies. *Journal of the Air and Waste Management Association 58*, 2 (2008), 234–253.

[83] Fink, A. H., Agustí-Panareda, A., Parker, D. J., Lafore, J. P., Ngamini, J. B., Afiesimama, E., Beljaars, A., Bock, O., Christoph, M., Didé, F., Faccani, C., Fourrié, N., Karbou, F., Polcher, J., Mumba, Z., Nuret, M., Pohle, S., Rabier, F., Tompkins, A. M., and Wilson, G. Operational meteorology in West Africa: Observational networks, weather analysis and forecasting. *Atmospheric Science Letters 12*, 1 (2011), 135–141.

[84] Fischer, E. V., Jacob, D. J., Yantosca, R. M., Sulprizio, M. P., Millet, D. B., Mao, J., Paulot, F., Singh, H. B., Roiger, A., Ries, L., Talbot, R. W., Dzepina, K., and Pandey Deolal, S. Atmospheric peroxyacetyl nitrate (PAN): A global budget and source attribution. *Atmospheric Chemistry and Physics 14*, 5 (2014), 2679–2698.

[85] Fisher, J. A., Jacob, D. J., Wang, Q., Bahreini, R., Carouge, C. C., Cubison, M. J., Dibb, J. E., Diehl, T., Jimenez, J. L., Leibensperger, E. M., Lu, Z., Meinders, M. B., Pye, H. O., Quinn, P. K., Sharma, S., Streets, D. G., van Donkelaar, A., and Yantosca, R. M. Sources, distribution, and acidity of sulfate-ammonium aerosol in the Arctic in winter-spring. *Atmospheric Environment 45*, 39 (dec 2011), 7301–7318.

[86] Flamant, C., Knippertz, P., Fink, A. H., Akpo, A., Brooks, B., Chiu, C. J., Coe, H., Danuor, S., Evans, M., Jegede, O., Kalthoff, N., Konaré, A., Liousse, C., Lohou, F., Mari, C., Schlager, H., Schwarzenboeck, A., Adler, B., Amekudzi, L., Aryee, J., Ayoola, M., Batenburg, A. M., Bessardon, G., Borrmann, S., Brito, J., Bower, K., Burnet, F., Catoire, V., Colomb, A., Denjean, C., Fosu-Amankwah, K., Hill, P. G., Lee, J., Lothon, M., Maranan, M., Marsham, J., Meynadier, R., Ngamini, J.-B., Rosenberg, P., Sauer, D., Smith, V., Stratmann, G., Taylor, J. W., Voigt, C., and Yoboué, V. The Dynamics–Aerosol–Chemistry–Cloud Interactions in West Africa Field Campaign: Overview and Research Highlights. *Bulletin of the American Meteorological Society 99*, 1 (jul 2017), 83–104.

[87] Flannigan, M. D., Krawchuk, M. A., De Groot, W. J., Wotton, B. M., and Gowman, L. M. Implications of changing climate for global wildland fire. *International Journal of Wildland Fire 18*, 5 (2009), 483–507.

[88] Foltz, G. R., and McPhaden, M. J. Impact of Saharan dust on tropical North Atlantic SST. *Journal of Climate 21*, 19 (2008), 5048–5060.

[89] Food and Agriculture Organization of the United Nations (FAO). Crop Calendar.

[90] Food and Agriculture Organization of the United Nations (FAO). FAOSTAT Crop Statistics.

[91] Frey, H. C., and Zheng, J. Quantification of variability and uncertainty in air pollutant emission inventories: Method and case study for utility NOx emissions. *Journal of the Air and Waste Management Association 52*, 9 (2002), 1083–1095.

[92] Froidurot, S., and Diedhiou, A. Characteristics of wet and dry spells in the West African monsoon system. *Atmospheric Science Letters 18*, 3 (2017), 125–131.

[93] Galbally, I. E., and Roy, C. R. Destruction of ozone at the earth's surface. *Quarterly Journal of the Royal Meteorological Society 106*, 449 (1980), 599–620.

[94] GEOS-Chem Community. The GEOS-Chem Model.

[95] Gerbig, C., Schmitgen, S., Kley, D., Volz-thomas, A., and Dewey, K. An improved fast-response vacuum-UV resonance fluorescence CO instrument. *Journal of Geophysical Research 104* (1999), 1699–1704.

[96] Giglio, L., Csiszar, I., and Justice, C. O. Global distribution and seasonality of active fires as observed with the Terra and Aqua Moderate Resolution Imaging Spectroradiometer (MODIS) sensors. *Journal of Geophysical Research: Biogeosciences 111*, 2 (2006), 1–12.

[97] Giglio, L., Randerson, J. T., and Van Der Werf, G. R. Analysis of daily, monthly, and annual burned area using the fourth-generation global fire emissions database (GFED4). *Journal of Geophysical Research: Biogeosciences 118*, 1 (2013), 317–328.

[98] Guenther, A. B., Jiang, X., Heald, C. L., Sakulyanontvittaya, T., Duhl, T., Emmons, L. K., and Wang, X. The model of emissions of gases and aerosols from nature version 2.1 (MEGAN2.1): An extended and updated framework for modeling biogenic emissions. *Geoscientific Model Development 5*, 6 (2012), 1471–1492.

[99] Guerreiro, C. B., Foltescu, V., and de Leeuw, F. Air quality status and trends in Europe. *Atmospheric Environment 98* (2014), 376–384.

[100] Gwilliam, K. Urban transport in developing countries. *Transport Reviews 23*, 2 (2003), 197–216.

[101] Hannak, L., Knippertz, P., Fink, A. H., Kniffka, A., and Pante, G. Why Do Global Climate Models Struggle to Represent Low-Level Clouds in the West African Summer Monsoon? *Journal of Climate 30*, 5 (mar 2017), 1665–1687.

[102] Haslett, S. L., Taylor, J. W., Evans, M., Morris, E., Vogel, B., Dajuma, A., Brito, J., Batenburg, A. M., Borrmann, S., Schneider, J., Schulz, C., Denjean, C., Bourrianne, T., Knippertz, P., Dupuy, R., Schwarzenböck, A., Sauer, D., Flamant, C., Dorsey, J., Crawford, I., and Coe, H. Remote biomass burning dominates southern West African air pollution during the monsoon. *Atmospheric Chemistry and Physics Discussions 3*, April (2019), 1–23.

[103] Heald Colette L., C. L., Jacob, D. J., Jones, D. B., Palmer, P. I., Logan, J. A., Streets, D. G., Sachse, G. W., Gille, J. C., Hoffman, R. N., and Nehrkorn, T. Comparative inverse analysis of satellite (MOPITT) and aircraft (TRACE-P) observations to estimate Asian sources of carbon monoxide. *Journal of Geophysical Research D: Atmospheres 109*, 23 (2004), 1–17.

[104] Hersey, S. P., Garland, R. M., Crosbie, E., Shingler, T., Sorooshian, A., Piketh, S., and Burger, R. An overview of regional and local characteristics of aerosols in South Africa using satellite, ground, and modeling data. *Atmospheric Chemistry and Physics 15* (2015), 4259–4278.

[105] Hess, P. G., and Zbinden, R. Stratospheric impact on tropospheric ozone variability and trends: 1990-2009. *Atmospheric Chemistry and Physics 13*, 2 (2013), 649–674.

[106] Hilboll, A., Richter, A., and Burrows, J. P. Long-term changes of tropospheric NO2 over megacities derived from multiple satellite instruments. *Atmospheric Chemistry and Physics 13*, 8 (2013), 4145–4169.

[107] Ho, D. X., Kim, K. H., Sohn, J. R., Oh, Y. H., and Ahn, J. W. Emission rates of volatile organic compounds released from newly produced household furniture products using a large-scale chamber testing method. *TheScientificWorldJournal 11* (2011), 1597–1622.

[108] Holland, M., Mills, G., Hayes, F., Buse, A., Emberson, L., Cambridge, H., Cinderby, S., Terry, A., and Ashmore, M. R. Economic assessment of crop yield losses from ozone exposure. UK Defra Report for Contract EPG 1/3/170. https://uk-air.defra.gov.uk/assets/documents/reports/cat10/final_ozone_econ_report_ver2.pdf. 76.

[109] Holloway, T., and Ii, H. L. Global distribution The sum of all CO sources in the model Pg CO / yr Tg), including fossil fuel. *Journal of Geophysical Research 105* (2000).

[110] Hopkins, J. R., Jones, C. E., and Lewis, A. C. A dual channel gas chromatograph for atmospheric analysis of volatile organic compounds including oxygenated and monoterpene compounds. *Journal of Environmental Monitoring 13*, 8 (2011), 2268–2276.

[111] Horowitz, H. M., Garland, R. M., Thatcher, M., Landman, W. A., Dedekind, Z., Van Der Merwe, J., and Engelbrecht, F. A. Evaluation of climate model aerosol seasonal and spatial variability over Africa using AERONET. *Atmospheric Chemistry and Physics 17*, 22 (2017), 13999–14023.

[112] Hu, L., Millet, D. B., Baasandorj, M., Griffis, T. J., Travis, K. R., Tessum, C. W., Marshall, J. D., Reinhart, W. F., Mikoviny, T., Müller, M., Wisthaler, A., Graus, M., Warneke, C., and de Gouw, J. Emissions of C6-C8 aromatic compounds in the United States: Constraints from tall tower and aircraft measurements. *Journal of Geophysical Research 120*, 2 (jan 2015), 826–842.

[113] Hu, L., Millet, D. B., Baasandorj, M., Griffis, T. J., Turner, P., Helmig, D., Curtis, A. J., and Hueber, J. Isoprene emissions and impacts over an ecological transition region in the U.S. Upper Midwest inferred from tall tower measurements. *Journal of Geophysical Research 120*, 8 (2015), 3553–3571.

[114] Huang, G., Brook, R., Crippa, M., Janssens-Maenhout, G., Schieberle, C., Dore, C., Guizzardi, D., Muntean, M., Schaaf, E., and Friedrich, R. Speciation of anthropogenic emissions of non-methane volatile organic compounds: A global gridded data set for 1970-2012. *Atmospheric Chemistry and Physics 17*, 12 (jun 2017), 7683–7701.

[115] Huang, J., Pan, X., Guo, X., and Li, G. Articles Health impact of China ' s Air Pollution Prevention and Control Action Plan : an analysis of national air quality monitoring and mortality data. *The Lancet Planetary Health 2*, 7 (2018), e313–e323.

[116] Hudman, R. C., Moore, N. E., Mebust, A. K., Martin, R. V., Russell, A. R., Valin, L. C., and Cohen, R. C. Steps towards a mechanistic model of global soil nitric oxide emissions: Implementation and space based-constraints. *Atmospheric Chemistry and Physics 12*, 16 (2012), 7779–7795.

[117] INDAAF. International Network to study Deposition and Atmospheric chemistry in AFrica.

[118] International Energy Agency. Statistics.

[119] Jacob, D. J. Heterogeneous chemistry and tropospheric ozone. *Atmospheric Environment 34*, 12-14 (2000), 2131–2159.

[120] Jaeglé, L., Quinn, P. K., Bates, T. S., Alexander, B., and Lin, J.-T. Global distribution of sea salt aerosols: new constraints from in situ and remote sensing observations. *Atmospheric Chemistry and Physics 11*, 7 (apr 2011), 3137–3157.

[121] Jerrett, M., Burnett, R. T., Pope III, C. A., Ito, K., Thurston, G., Krewski, D., Shi, Y., Calle, E., and Thun, M. Long-Term Ozone Exposure and Mortality. *The New England Journal Of Medicine 360*, 11 (2009), 1085–1095.

[122] Jones, D. B. A., Bowman, K. W., Logan, J. A., Heald, C. L., Liu, J., Luo, M., Worden, J., and Drummond, J. The zonal structure of tropical O3 and CO as observed by the Tropospheric Emission Spectrometer in November 2004 – Part 1: Inverse modeling of CO emissions. *Atmospheric Chemistry and Physics 9*, 11 (2009), 3547–3562.

[123] Junge, C. E. Global ozone budget and exchange between stratosphere and troposphere. *Tellus 14*, 4 (2012), 363–377.

[124] Junichi Fujino Rajesh Nair, M. K. T. M., and Matsuoka, Y. Multi-gas Mitigation Analysis on Stabilization Scenarios Using Aim Global Model. *The Energy Journal Multi-Gree*, Special Issue #3 (2006), 343–354.

[125] Junker, C., and Liousse, C. A global emission inventory of carbonaceous aerosol from historic records of fossil fuel and biofuel consumption for the period 1860–1997. *Atmospheric Chemistry and Physics 8*, 5 (mar 2008), 1195–1207.

[126] Kaiser, J. W., Heil, A., Andreae, M. O., Benedetti, A., Chubarova, N., Jones, L., Morcrette, J.-J., Razinger, M., Schultz, M. G., Suttie, M., and van der Werf, G. R. Biomass burning emissions estimated with a global fire assimilation system based on observed fire radiative power. *Biogeosciences 9*, 1 (jan 2012), 527–554.

[127] Kasemy, Z. A., Kamel, G. M., Abdel-Rasoul, G. M., and Ismail, A. A. Environmental and Health Effects of Benzene Exposure among Egyptian Taxi Drivers. *Journal of Environmental and Public Health 2019* (2019), 1–6.

[128] Keita, S., Liousse, C., Yoboué, V., Dominutti, P., Guinot, B., Assamoi, E. M., Borbon, A., Haslett, S. L., Bouvier, L., Colomb, A., Coe, H., Akpo, A., Adon, J., Bahino, J., Doumbia, M., Djossou, J., Galy-Lacaux, C., Gardrat, E., Gnamien, S., Léon, J. F., Ossohou, M., Touré N'Datchoh, E., and Roblou, L. Particle and VOC emission factor measurements for anthropogenic sources in West Africa. *Atmospheric Chemistry and Physics 18*, 10 (2018), 7691–7708.

[129] Keller, C. A., Long, M. S., Yantosca, R. M., Da Silva, A. M., Pawson, S., and Jacob, D. J. HEMCO v1.0: A versatile, ESMF-compliant component for calculating emissions in atmospheric models. *Geoscientific Model Development 7*, 4 (2014), 1409–1417.

[130] Keywood, M., Kanakidou, M., Stohl, A., Dentener, F., Grassi, G., Meyer, C. P., Torseth, K., Edwards, D., Thompson, A. M., Lohmann, U., and Burrows, J. Fire in the air: Biomass burning impacts in a changing climate. *Critical Reviews in Environmental Science and Technology 43*, 1 (2013), 40–83.

[131] Kiesewetter, G., Borken-Kleefeld, J., Schöpp, W., Heyes, C., Thunis, P., Bessagnet, B., Terrenoire, E., Gsella, A., and Amann, M. Modelling NO 2 concentrations at the street level in the GAINS integrated assessment model: Projections under current legislation. *Atmospheric Chemistry and Physics 14*, 2 (2014), 813–829.

[132] Kiesewetter, G., Schoepp, W., Heyes, C., and Amann, M. Modelling PM2.5 impact indicators in Europe: Health effects and legal compliance. *Environmental Modelling and Software 74* (2015), 201–211.

[133] Kimbrough, S., Owen, R. C., Snyder, M., and Richmond-Bryant, J. NO to NO2 Conversion Rate Analysis and Implications for Dispersion Model Chemistry Methods using Las Vegas, Nevada Near-Road Field Measurements. *Atmospheric Environment 165* (2017).

[134] Klimont, Z., Smith, S. J., and Cofala, J. The last decade of global anthropogenic sulfur dioxide: 2000-2011 emissions. *Environmental Research Letters 8*, 1 (2013).

[135] Knippertz, P., Coe, H., Chiu, J. C., Evans, M. J., Fink, A. H., Kalthoff, N., Liousse, C., Mari, C., Allan, R. P., Brooks, B., Danour, S., Flamant, C., Jegede, O. O., Lohou, F., and Marsham, J. H. The DACCIWA Project: Dynamics–Aerosol–Chemistry–Cloud Interactions in West Africa. *Bulletin of the American Meteorological Society 96*, 9 (sep 2015), 1451–1460.

[136] Knippertz, P., Evans, M. J., Field, P. R., Fink, A. H., Liousse, C., and Marsham, J. H. The possible role of local air pollution in climate change in West Africa. *Nature Climate Change 5*, 9 (2015), 815–822.

[137] Knippertz, P., Fink, A. H., Deroubaix, A., Morris, E., Tocquer, F., Evans, M. J., Flamant, C., Gaetani, M., Lavaysse, C., Mari, C., Marsham, J. H., Meynadier, R., Affo-Dogo, A., Bahaga, T., Brosse, F., Deetz, K., Guebsi, R., Latifou, I., Maranan, M., Rosenberg, P. D., and Schlueter, A. A meteorological and chemical overview of the DACCIWA field campaign in West Africa in June–July 2016. *Atmospheric Chemistry and Physics 17*, 17 (sep 2017), 10893–10918.

[138] Kopacz, M., Jacob, D. J., Henze, D. K., Heald, C. L., Streets, D. G., and Zhang, Q. Comparison of adjoint and analytical Bayesian inversion methods for constraining Asian sources of carbon monoxide using satellite (MOPITT) measurements of CO columns. *Journal of Geophysical Research Atmospheres 114*, 4 (2009), 1–10.

[139] Kuhns, H., Knipping, E. M., and Vukovich, J. M. Development of a united states–mexico emissions inventory for the big bend regional aerosol and visibility observational (bravo) study. *Journal of the Air and Waste Management Association 55*, 5 (2005), 677–692.

[140] Kundu, S., and Stone, E. A. Composition and sources of fine particulate matter across urban and rural sites in the Midwestern United States. *Environmental Science: Processes & Impacts 16*, 6 (2014), 1360–1370.

[141] Lamarque, J.-F., Bond, T. C., Eyring, V., Granier, C., Heil, A., Klimont, Z., Lee, D., Liousse, C., Mieville, A., Owen, B., Schultz, M. G., Shindell, D., Smith, S. J., Stehfest, E., Van Aardenne, J., Cooper, O. R., Kainuma, M., Mahowald, N., McConnell, J. R., Naik, V., Riahi, K., and van Vuuren, D. P. Historical (1850–2000) gridded anthropogenic and biomass burning emissions of reactive gases and aerosols: methodology and application. *Atmospheric Chemistry and Physics 10*, 15 (aug 2010), 7017–7039.

[142] Lana, A., Bell, T. G., Simó, R., Vallina, S. M., Ballabrera-Poy, J., Kettle, A. J., Dachs, J., Bopp, L., Saltzman, E. S., Stefels, J., Johnson, J. E., and Liss, P. S. An updated climatology of surface dimethlysulfide concentrations and emission fluxes in the global ocean. *Global Biogeochemical Cycles 25*, 1 (2011).

[143] Lefohn, A. S., Malley, C. S., Smith, L., Wells, B., Hazucha, M., Simon, H., Naik, V., Mills, G., Schultz, M. G., Paoletti, E., De Marco, A., Xu, X., Zhang, L., Wang, T., Neufeld, H. S., Musselman, R. C., Tarasick, D., Brauer, M., Feng, Z., Tang, H., Kobayashi, K., Sicard, P., Solberg, S., and Gerosa, G. Tropospheric ozone assessment report: Global ozone metrics for climate change, human health, and crop/ecosystem research. *Elementa 6* (2018).

[144] Leibensperger, E. M., Mickley, L. J., Jacob, D. J., Chen, W. T., Seinfeld, J. H., Nenes, A., Adams, P. J., Streets, D. G., Kumar, N., and Rind, D. Climatic effects of 1950-2050 changes in US anthropogenic aerosols-Part 1: Aerosol trends and radiative forcing. *Atmospheric Chemistry and Physics 12*, 7 (2012), 3333–3348.

[145] Lelieveld, J., and Dentener, F. J. What controls tropospheric ozone? *Journal of Geophysical Research Atmospheres 105*, D3 (2000), 3531–3551.

[146] Lenner, M. Nitrogen dioxide in exhaust emissions from motor vehicles. *Atmospheric Environment (1967) 21*, 1 (1987), 37–43.

[147] Li, M., Zhang, Q., Streets, D. G., He, K. B., Cheng, Y. F., Emmons, L. K., Huo, H., Kang, S. C., Lu, Z., Shao, M., Su, H., Yu, X., and Zhang, Y. Mapping Asian anthropogenic emissions of non-methane volatile organic compounds to multiple chemical mechanisms. *Atmospheric Chemistry and Physics 14*, 11 (jun 2014), 5617–5638.

[148] Likens, G. E., and Bormann, F. H. Acid Rain: A Serious Regional Environmental Problem. *Science 184* (1974), 1176–1180.

[149] Lim, S. S., Vos, T., Flaxman, A. D., Danaei, G., Shibuya, K., Adair-Rohani, H., Amann, M., Anderson, H. R., Andrews, K. G., Aryee, M., Atkinson, C., Bacchus, L. J., Bahalim, A. N., Balakrishnan, K., Balmes, J., Barker-Collo, S., Baxter, A., Bell, M. L., Blore, J. D., Blyth, F., and ... A comparative risk assessment of burden of disease and injury attributable to 67 risk factors and risk factor clusters in 21 regions, 1990-2010: A systematic analysis for the Global Burden of Disease Study 2010. *The Lancet 380*, 9859 (2012), 2224–2260.

[150] Lin, S.-J., and Rood, R. B. Multidimensional Flux-Form Semi-Lagrangian Transport Schemes. *Monthly Weather Review 124* (1996), 2046–2070.

[151] Liousse, C., Assamoi, E., Criqui, P., Granier, C., and Rosset, R. Explosive growth in African combustion emissions from 2005 to 2030. *Environmental Research Letters 9*, 3 (2014).

[152] Liousse, C., Guillaume, B., Grégoire, J. M., Mallet, M., Galy, C., Pont, V., Akpo, A., Bedou, M., Castéra, P., Dungall, L., Gardrat, E., Granier, C., Konaré, A., Malavelle, F., Mariscal, A., Mieville, A., Rosset, R., Serça, D., Solmon, F., Tummon, F., Assamoi, E., Yoboué, V., and Van Velthoven, P. Updated African biomass burning emission inventories in the framework of the AMMA-IDAF program, with an evaluation of combustion aerosols. *Atmospheric Chemistry and Physics 10*, 19 (2010), 9631–9646.

[153] Liu, C., Yin, P., Chen, R., Meng, X., Wang, L., Niu, Y., Lin, Z., Liu, Y., Liu, J., Qi, J., You, J., Kan, H., and Zhou, M. Ambient carbon monoxide and cardiovascular mortality: a nationwide time-series analysis in 272 cities in China. *The Lancet Planetary Health 2*, 1 (2018), e2–e3.

[154] Liu, H., Jacob, D. J., Bey, I., and Yantosca, R. M. Constraints from 210Pb and 7Be on wet deposition and transport in a global three-dimensional chemical tracer model driven by assimilated meteorological fields. *Journal of Geophysical Research Atmospheres 106*, D11 (jun 2001), 12109–12128.

[155] Liu, H., Man, H., Tschantz, M., Wu, Y., He, K., and Hao, J. VOC from Vehicular Evaporation Emissions: Status and Control Strategy. *Environmental Science and Technology 49*, 24 (2015), 14424–14431.

[156] Liu, W., Xu, Z., and Yang, T. Health Effects of Air Pollution in China. *International Journal of Environmental Research and Public Health 15*, 7 (2018), 1471.

[157] London, J., and Park, J. H. The interaction of Ozone Photochemistry and Dynamics in the Stratosphere. A Three-dimensionsal Atmospheric Model. *Canadian Journal of Chemistry 52* (1973), 1599–1609.

[158] Lumbreras, J., de Andrés, J. M., Pérez, J., Borge, R., de la Paz, D., and Rodríguez, M. E. A methodology to estimate uncertainty for emission projections through sensitivity analysis. *Journal of the Air and Waste Management Association 65*, 4 (2015), 384–394.

[159] Makra, L., and Brimblecombe, P. Selections from the history of environmental pollution, with special attention to air pollution. Part 1. *International Journal of Environment and Pollution 22*, 6 (2005), 641.

[160] Mannucci, P. M., and Franchini, M. Health effects of ambient air pollution in developing countries. *International Journal of Environmental Research and Public Health 14*, 9 (2017), 1–8.

[161] Marais, E. A., Jacob, D. J., Jimenez, J. L., Campuzano-Jost, P., Day, D. A., Hu, W., Krechmer, J., Zhu, L., Kim, P. S., Miller, C. C., Fisher, J. A., Travis, K., Yu, K., Hanisco, T. F., Wolfe, G. M., Arkinson, H. L., Pye, H. O., Froyd, K. D., Liao, J., and McNeill, V. F. Aqueous-phase mechanism for secondary organic aerosol formation from isoprene: Application to the Southeast United States and co-benefit of SO 2 emission controls. *Atmospheric Chemistry and Physics Discussions 15*, 21 (2015), 32005–32047.

[162] Marais, E. A., Jacob, D. J., Wecht, K., Lerot, C., Zhang, L., Yu, K., Kurosu, T. P., Chance, K., and Sauvage, B. Anthropogenic emissions in Nigeria and implications for atmospheric ozone pollution: A view from space. *Atmospheric Environment 99* (2014), 32–40.

[163] Marais, E. A., and Wiedinmyer, C. Air Quality Impact of Diffuse and Inefficient Combustion Emissions in Africa (DICE-Africa). *Environmental Science and Technology 50*, 19 (2016), 10739–10745.

[164] Maranan, M., Fink, A. H., and Knippertz, P. Rainfall types over southern West Africa: Objective identification, climatology and synoptic environment. *Quarterly Journal of the Royal Meteorological Society 144*, 714 (2018), 1628–1648.

[165] Martin, R., Henze, D., van Donkelaar, A., Pierce, J., Fairlie, D., and Heald, C. Particulate matter in GEOS-Chem.

[166] Martin, R. V., Jacob, D. J., Yantosca, R. M., Chin, M., and Ginoux, P. Global and regional decreases in tropospheric oxidants from photochemical effects of aerosols. *Journal of Geophysical Research: Atmospheres 108*, D3 (feb 2003).

[167] Martínez, I. R., and Chaboureau, J.-P. Precipitation and Mesoscale Convective Systems: Radiative Impact of Dust over Northern Africa. *Monthly Weather Review 146*, 9 (2018), 3011–3029.

[168] McLinden, C. A., Olsen, S. C., Hannegan, B., Wild, O., and Prather, M. J. Stratospheric ozone in 3-D models: A simple chemistry and the cross-tropopause flux. *Journal of Geophysical Research 105*, D11 (2000), 14653–14665.

[169] Menut, L., Flamant, C., Turquety, S., Deroubaix, A., Chazette, P., and Meynadier, R. Impact of biomass burning on pollutant surface concentrations in megacities of the Gulf of Guinea. *Atmospheric Chemistry and Physics 18*, 4 (feb 2018), 2687–2707.

[170] Mills, G., Sharps, K., Simpson, D., Pleijel, H., Frei, M., Burkey, K., Emberson, L., Uddling, J., Broberg, M., Feng, Z., Kobayashi, K., and Agrawal, M. Closing the global ozone yield gap: Quantification and cobenefits for multistress tolerance. *Global Change Biology 24*, 10 (2018), 4869–4893.

[171] Monks, P. S. Gas-phase radical chemistry in the troposphere. *Chemical Society Reviews 34*, 5 (2005), 376–395.

[172] Monks, P. S., Archibald, A. T., Colette, A., Cooper, O., Coyle, M., Derwent, R., Fowler, D., Granier, C., Law, K. S., Mills, G. E., Stevenson, D. S., Tarasova, O., Thouret, V., Von Schneidemesser, E., Sommariva, R., Wild, O., and Williams, M. L. Tropospheric ozone and its precursors from the urban to the global scale from air quality to short-lived climate forcer. *Atmospheric Chemistry and Physics 15*, 15 (2015), 8889–8973.

[173] Moss, R. H., Edmonds, J. A., Hibbard, K. A., Manning, M. R., Rose, S. K., van Vuuren, D. P., Carter, T. R., Emori, S., Kainuma, M., Kram, T., Meehl, G. A., Mitchell, J. F. B., Nakicenovic, N., Riahi, K., Smith, S. J., Stouffer, R. J., Thomson, A. M., Weyant, J. P., and Wilbanks, T. J. The next generation of scenarios for climate change research and assessment. *Nature 463* (feb 2010), 747.

[174] Murray, C. J., Stanaway, J. D., Afshin, A., Gakidou, E., Lim, S. S., Abate, D., Abate, K. H., Abbafati, C., Abbasi, N., Abbastabar, H., Abd-Allah, F., Abdela, J., Abdelalim, A., Abdollahpour, I., Abdulkader, R. S., Abebe, M., Abebe, Z., Abera, S. F., Abil, O. Z., Abraha, H. N., and ... Global, regional, and national comparative risk assessment of 84 behavioural, environmental and occupational, and metabolic risks or clusters of risks for 195 countries and territories, 1990-2017: A systematic analysis for the Global Burden of Disease Stu. *The Lancet* (2018), 1923–1994.

[175] Murray, L. T., Jacob, D. J., Logan, J. A., Hudman, R. C., and Koshak, W. J. Optimized regional and interannual variability of lightning in a global chemi-

cal transport model constrained by LIS/OTD satellite data. *Journal of Geophysical Research Atmospheres 117*, 20 (2012).

[176] Naidja, L., Ali-Khodja, H., and Khardi, S. Sources and levels of particulate matter in North African and Sub-Saharan cities: a literature review. *Environmental Science and Pollution Research 25*, 13 (2018), 12303–12328.

[177] NASA. AERONET: Aerosol Robotic Network.

[178] NASA. Aqua: Project Science.

[179] NASA. MODIS: Moderate Resolution Imaging Spectroradiometer.

[180] NASA. Terra: The EOS Flagship.

[181] NEPAD. Agriculture in Africa - Transformation and outlook. Tech. Rep. July, 2017.

[182] Olivier, J. G. J., Bouwman, A. F., Van Der Maas, C. W. M., and Berdowski, J. J. M. Emission Database For Global Atmospheric Research (EDGAR). *Environmental Monitoring and Assessments 31* (1994), 93–106.

[183] Olivier, J. G. J., Van Aardenne, J. A., Dentener, F. J., Pagliari, V., Ganzeveld, L. N., and Peters, J. A. H. W. Recent trends in global greenhouse gas emissions:regional trends 1970–2000 and spatial distributionof key sources in 2000. *Environmental Sciences 2*, 2-3 (2005), 81–99.

[184] OpenAQ. Map showing the most recent values for PM2.5, 2019.

[185] Otter, L., Guenther, A., Wiedinmyer, C., Fleming, G., Harley, P., and Greenberg, J. Spatial and temporal variations in biogenic volatile organic compound emissions for Africa south of the equator. *Journal of Geophysical Research 108*, June 2002 (2003), 1–12.

[186] Pacifico, F., Delon, C., Jambert, C., Durand, P., Morris, E., Evans, M. J., Lohou, F., Derrien, S., Donnou, V. H. E., Houeto, A. V., Reinares Martinez, I., and Brilouet, P.-E. Measurements of nitric oxide and ammonia soil fluxes from a wet savanna ecosystem site in West Africa during the DACCIWA field campaign. *Atmospheric Chemistry and Physics Discussions* (mar 2018), 1–37.

[187] Palmer, P. I., Jacob, D. J., Jones, D. B. A., Heald, C. L., Yantosca, R. M., Logan, J. A., Sachse, G. W., and Streets, D. G. Inverting for emissions of carbon monoxide from Asia using aircraft observations over the western Pacific. *Journal of Geophysical Research: Atmospheres 108*, D21 (2003).

[188] Pannullo, F., Lee, D., Waclawski, E., and Leyland, A. H. How robust are the estimated effects of air pollution on health? Accounting for model uncertainty using Bayesian model averaging. *Spatial and Spatio-temporal Epidemiology 18*, 2016 (2016), 53–62.

[189] Park, R. J., Jacob, D. J., Field, B. D., Yantosca, R. M., and Chin, M. Natural and transboundary pollution influences on sulfate-nitrate-ammonium aerosols in the United States: Implications for policy. *Journal of Geophysical Research D: Atmospheres 109*, 15 (aug 2004).

[190] Parliament of the United Kingdon of Great Britain and Northern Ireland. Clean Air Act 1956, 1956.

[191] Parliament of the United Kingdon of Great Britain and Northern Ireland. Clean Air Act 1993, 1993.

[192] Parrella, J. P., Jacob, D. J., Liang, Q., Zhang, Y., Mickley, L. J., Miller, B., Evans, M. J., Yang, X., Pyle, J. A., Theys, N., and Van Roozendael, M. Tropospheric bromine chemistry: Implications for present and pre-industrial ozone and mercury. *Atmospheric Chemistry and Physics 12*, 15 (2012), 6723–6740.

[193] Passant, N. R. Estimation of Uncertainties in the National Atmospheric Emissions Inventory. Tech. Rep. 1, 2003.

[194] Pfeifroth, U., Trentmann, J., Fink, A. H., and Ahrens, B. Evaluating satellite-based diurnal cycles of precipitation in the African tropics. *Journal of Applied Meteorology and Climatology 55*, 1 (2016), 23–39.

[195] Picarro. G2401m. *https://www.picarro.com/products/flight-co-co2-ch4-h2o-analyzer*.

[196] Pinder, R. W., Klopp, J. M., Kleiman, G., Hagler, G. S., Awe, Y., and Terry, S. Opportunities and challenges for filling the air quality data gap in low- and middle-income countries. *Atmospheric Environment 215*, June (2019), 116794.

[197] Pope, A., Burnett, R., Thun, M., EE, C., D, K., I, K., and GD, T. Long-term Exposure to Fine Particulate Air Pollution. *Jama 287*, 9 (2002), 1192.

[198] Pope, C. A., Rodermund, D. L., and Gee, M. M. Mortality effects of a copper smelter strike and reduced ambient sulfate particulate matter air pollution. *Environmental Health Perspectives 115*, 5 (2007), 679–683.

[199] Population Division, D. o. E., and Affairs, S. Key findings and advanced tables. *World Population Prospects 2017 Revis* (2017).

[200] Pusede, S. E., and Cohen, R. C. On the observed response of ozone to NOx and VOC reactivity reductions in San Joaquin Valley California 1995-present. *Atmospheric Chemistry and Physics 12*, 18 (2012), 8323–8339.

[201] Pye, H. O., Chan, A. W., Barkley, M. P., and Seinfeld, J. H. Global modeling of organic aerosol: The importance of reactive nitrogen (NOx and NO3). *Atmospheric Chemistry and Physics 10*, 22 (2010), 11261–11276.

[202] Rall, D. P. Review of the health effects of sulfur oxides. *Environmental Health Perspectives Vol 8*, August (1974), 97–121.

[203] Ramanathan, V., and Dickinson, R. E. The Role of Stratospheric Ozone in the Zonal and Seasonal Radiative Energy Balance of the Earth-Troposphere System. *Journal of the Atmospheric Sciences 36*, 6 (1979), 1084–1104.

[204] Randerson, J. T., Chen, Y., Van Der Werf, G. R., Rogers, B. M., and Morton, D. C. Global burned area and biomass burning emissions from small fires. *Journal of Geophysical Research G: Biogeosciences 117*, 4 (2012).

[205] Redelsperger, J.-L., Thorncroft, C. D., Diedhiou, A., Lebel, T., Parker, D. J., and Polcher, J. African Monsoon Multidisciplinary Analysis: An International Research Project and Field Campaign. *Bulletin of the American Meteorological Society 87*, 12 (dec 2006), 1739–1746.

[206] Reinares Martínez, I., and Chaboureau, J.-P. Precipitation and Mesoscale Convective Systems: Explicit versus Parameterized Convection over Northern Africa. *Monthly Weather Review 146*, 3 (2018), 797–812.

[207] Rémy, S., Veira, A., Paugam, R., Sofiev, M., Kaiser, J. W., Marenco, F., Burton, S. P., Benedetti, A., Engelen, R. J., Ferrare, R., and Hair, J. W. Two global data sets of daily fire emission injection heights since 2003. *Atmospheric Chemistry and Physics 17*, 4 (2017), 2921–2942.

[208] Ren-Jian, Z., Kin-Fai, H., and Zhen-Xing, S. The Role of Aerosol in Climate Change, the Environment, and Human Health. *Atmospheric and Oceanic Science Letters 5*, 2 (2012), 156–161.

[209] Reynolds, S. D., Blanchard, C. L., and Ziman, S. D. Understanding the effectiveness of precursor reductions in lowering 8-Hr ozone concentrations. *Journal of the Air and Waste Management Association 53*, 2 (2003), 195–205.

[210] Riahi, K., Grübler, A., and Nakicenovic, N. Scenarios of long-term socio-economic and environmental development under climate stabilization. *Technological Forecasting and Social Change 74*, 7 (sep 2007), 887–935.

[211] Ridley, D. A., Heald, C. L., and Ford, B. North African dust export and deposition: A satellite and model perspective. *Journal of Geophysical Research Atmospheres 117*, 2 (2012), 1–21.

[212] Roberts, G., Wooster, M. J., and Lagoudakis, E. Annual and diurnal African biomass burning temporal dynamics. *Biogeosciences Discussions 5*, 4 (2008), 3623–3663.

[213] Rodhe, H., Crutzen, P., and Vanderpol, A. Formation of sulfuric and nitric acid in the atmosphere during long-range transport. *Tellus 33*, 2 (1981), 132–141.

[214] Roehrig, R., Bouniol, D., Guichard, F., déric Hourdin, F., and Redelsperger, J. L. The present and future of the west african monsoon: A process-oriented assessment of CMIP5 simulations along the AMMA transect. *Journal of Climate 26*, 17 (2013), 6471–6505.

[215] Roth, G. A., Abate, D., Abate, K. H., Abay, S. M., Abbafati, C., Abbasi, N., Abbastabar, H., Abd-Allah, F., Abdela, J., Abdelalim, A., Abdollahpour, I., Abdulkader, R. S., Abebe, H. T., Abebe, M., Abebe, Z., Abejie, A. N., Abera, S. F., Abil, O. Z., Abraha, H. N., Abrham, A. R., Abu-Raddad, L. J., Accrombessi, M. M. K., Acharya, D., Adamu, A. A., Adebayo, O. M., Adedoyin, R. A., Adekanmbi, V., Adetokunboh, O. O., and ... Global, regional, and national age-sex-specific mortality for 282 causes of death in 195 countries and territories, 1980–2017: a systematic analysis for the Global Burden of Disease Study 2017. *The Lancet 392*, 10159 (2018), 1736–1788.

[216] Sacks, J. D., Stanek, L. W., Luben, T. J., Johns, D. O., Buckley, B. J., Brown, J. S., and Ross, M. Particulate matter-induced health effects: Who is susceptible? *Environmental Health Perspectives 119*, 4 (2011), 446–454.

[217] Sands, R. D., Janetos, a. C., Edmonds, J. a., Wise, M. a., Calvin, K. V., Bond-Lamberty, B., Clarke, L. E., Smith, S. J., and Thomson, a. M. The Implications of Limiting CO2 Concentrations for Agriculture, Land Use, Land Use Change Emissions and Bioenergy.

[218] Schultz, M. G., Akimoto, H., Bottenheim, J., Buchmann, B., Galbally, I. E., Gilge, S., Helmig, D., Koide, H., Lewis, A. C., Novelli, P. C., Plass-Dülmer, C., Ryerson, T. B., Steinbacher, M., Steinbrecher, R., Tarasova, O., Tørseth, K., Thouret, V., and Zellweger, C. The Global Atmosphere Watch reactive gases measurement network. *Elem Sci Anth 3* (2015), 1–23.

[219] Schultz, M. G., Schröder, S., Lyapina, O., Cooper, O. R., Galbally, I., Petropavlovskikh, I., Schneidemesser, E. V., Tanimoto, H., Elshorbany, Y., Naja, M., Seguel, R. J., Dauert, U., Eckhardt, P., Lee, M., Molloy, S., Moolla, R., Wang, T., Sharps, K., Barlasina, M. E., Bogucka, M., Bonasoni, P., Chang, L., Lam, K.-s., Laurila, T., Lee, H., Levy, I., Mazzoleni, C., Murovec, M., Navarro-comas, M., Nicodim, F., Parrish, D., Scorgie, Y., Senik, I., Simmonds, P., and Sinha, V. Tropospheric Ozone Assessment Report : Database and metrics data of global surface ozone observations. *Elementa Science of the Anthropocene* (2017).

[220] Seo, J., Park, D. R., Kim, J. Y., Youn, D., Lim, Y. B., and Kim, Y. Effects of meteorology and emissions on urban air quality: a quantitative statistical approach to long-term records (1999–2016) in Seoul, South Korea. *Atmospheric Chemistry and Physics 18* (2018), 16121–16137.

[221] Shah, A. S., Lee, K. K., McAllister, D. A., Hunter, A., Nair, H., Whiteley, W., Langrish, J. P., Newby, D. E., and Mills, N. L. Short term exposure to air pollution and stroke: Systematic review and meta-analysis. *BMJ (Online) 350*, January (2015).

[222] Sherwen, T., Evans, M. J., Carpenter, L. J., Andrews, S. J., Lidster, R. T., Dix, B., Koenig, T. K., Sinreich, R., Ortega, I., Volkamer, R., Saiz-Lopez, A., Prados-Roman, C., Mahajan, A. S., and Ordóñez, C. Iodine's impact on tropospheric oxidants: A global model study in GEOS-Chem. *Atmospheric Chemistry and Physics 16*, 2 (2016), 1161–1186.

[223] Sherwen, T., Schmidt, J. A., Evans, M. J., Carpenter, L. J., Grossmann, K., Eastham, S. D., Jacob, D. J., Dix, B., Koenig, T. K., Sinreich, R., Ortega, I., Volkamer, R., Saiz-Lopez, A., Prados-Roman, C., Mahajan, A. S., and Ordóñez, C. Global impacts of tropospheric halogens (Cl, Br, I) on oxidants and composition in GEOS-Chem. *Atmospheric Chemistry and Physics 16*, 18 (2016), 12239–12271.

[224] Shuai, J., Kim, S., Ryu, H., Park, J., Lee, C. K., Kim, G. B., Ultra, V. U., and Yang, W. Health risk assessment of volatile organic compounds exposure near Daegu dyeing industrial complex in South Korea. *BMC Public Health 18*, 1 (2018), 1–13.

[225] Sillman, S. 9.11 - Tropospheric Ozone and Photochemical Smog. In *Treatise on Geochemistry*, H. D. Holland and K. K. Turekian, Eds. Pergamon, Oxford, 2003, pp. 407–431.

[226] Silva, S. J., and Heald, C. L. Investigating Dry Deposition of Ozone to Vegetation. *Journal of Geophysical Research: Atmospheres 123*, 1 (2018), 559–573.

[227] Skonieczny, C., Mcgee, D., Winckler, G., Bory, A., Bradtmiller, L. I., and Kinsley, C. W. Monsoon-driven Saharan dust variability over the past 240 , 000 years. *Science Advances*, January (2019), 1–9.

[228] Slovic, A. D., de Oliveira, M. A., Biehl, J., and Ribeiro, H. How Can Urban Policies Improve Air Quality and Help Mitigate Global Climate Change: a Systematic Mapping Review. *Journal of Urban Health 93*, 1 (2016), 73–95.

[229] Smith, S. J., Van Aardenne, J., Klimont, Z., Andres, R. J., Volke, A., and Delgado Arias, S. Anthropogenic sulfur dioxide emissions: 1850-2005. *Atmospheric Chemistry and Physics 11*, 3 (2011), 1101–1116.

[230] Stephens, M., Turner, N., and Sandberg, J. Particle identification by laser-induced incandescence in a solid-state laser cavity. *Appl. Opt. 42*, 19 (jul 2003), 3726–3736.

[231] Stettler, M. E., Eastham, S., and Barrett, S. R. Air quality and public health impacts of UK airports. Part I: Emissions. *Atmospheric Environment 45*, 31 (oct 2011), 5415–5424.

[232] Stohl, A. Stratosphere-troposphere exchange: A review, and what we have learned from STACCATO. *Journal of Geophysical Research 108*, D12 (2003).

[233] Sukhodolov, T., Rozanov, E., Ball, W. T., Bais, A., Tourpali, K., Shapiro, A. I., Telford, P., Smyshlyaev, S., Fomin, B., Sander, R., Bossay, S., Bekki, S., Marchand, M., Chipperfield, M. P., Dhomse, S., Haigh, J. D., Peter, T., and Schmutz, W. Evaluation of simulated photolysis rates and their response to solar irradiance variability. *Journal of Geophysical Research Atmospheres 121*, January 2008 (2016), 6066–6084.

[234] Tai, A. P., and Val Martin, M. Impacts of ozone air pollution and temperature extremes on crop yields: Spatial variability, adaptation and implications for future food security. *Atmospheric Environment 169* (2017), 11–21.

[235] Tang, Q., Prather, M. J., and Hsu, J. Stratosphere-troposphere exchange ozone flux related to deep convection. *Geophysical Research Letters 38*, 3 (2011), 1–5.

[236] The Department for Environment Food and Rural Affairs. Clean Air Strategy 2019. *https://assets.publishing.service.gov.uk/government/uploads/system/uploads/attachment_da air-strategy-2019.pdf* (2019).

[237] The European Parliament. Directive 2008/50/EC OF on ambient air quality and cleaner air for Europe. *Official Journal of the European Union* (2008).

[238] Thermo Fisher Scientific. TE 49i. *https://www.thermofisher.com/uk/en/home.html*.

[239] Thomson, A. M., Calvin, K. V., Smith, S. J., Kyle, G. P., Volke, A., Patel, P., Delgado-Arias, S., Bond-Lamberty, B., Wise, M. A., Clarke, L. E., and Edmonds, J. A. RCP4.5: A pathway for stabilization of radiative forcing by 2100. *Climatic Change 109*, 1 (2011), 77–94.

[240] Tiao, G. C., Box, G. E., and Box, G. E. Analysis of los angeles photochemical smog data: A statistical overview. *Journal of the Air Pollution Control Association 25*, 3 (1975), 260–268.

[241] Townsend, C. L., and Maynard, R. Effects on health of prolonged exposure to low concentrations of carbon monoxide – Townsend and Maynard 59 (10): 708 – Occupational and Environmental Medicine. *Occupational and environmental medicine 59* (2002), 708–711.

[242] Travis, K. R., and Jacob, D. J. Systematic bias in evaluating chemical transport models with maximum daily 8-hour average (MDA8) surface ozone for air quality applications. *Geoscientific Model Development Discussions*, x (2019), 1–13.

[243] Travis, K. R., Jacob, D. J., Fisher, J. A., Kim, P. S., Marais, E. A., Zhu, L., Yu, K., Miller, C. C., Yantosca, R. M., Sulprizio, M. P., Thompson, A. M., Wennberg, P. O., Crounse, J. D., St Clair, J. M., Cohen, R. C., Laughner, J. L., Dibb, J. E., Hall, S. R., Ullmann, K., Wolfe, G. M., Pollack, I. B., Peischl, J., Neuman, J. A., and Zhou, X. Why do models overestimate surface ozone in the Southeast United States? *Atmospheric Chemistry and Physics 16*, 21 (nov 2016), 13561–13577.

[244] Tuovinen, J. P. Assessing vegetation exposure to ozone: Properties of the AOT40 index and modifications by deposition modelling. *Environmental Pollution 109*, 3 (2000), 361–372.

[245] Turner, D. B. Relationships between 24-hour mean air quality measurements and meteorological factors in nashville, tennessee. *Journal of the Air Pollution Control Association 11*, 10 (1961), 483–489.

[246] UNEP TRANSPORT. Diesel Fuel Sulphur Level: Global Status, 2017.

[247] United Nations Environment Programme. Four more countries in Africa switch to low sulfur fuels, 2017.

[248] United Nations Statistics Division. Energy Statistics Database.

[249] United States Environment Protection Agency. National Ambient Air Quality Standards.

[250] U.S. Department of Health and Human Services: Agency for Toxic Substances and Disease Registry. Toxicological Profile for Carbon Monoxide. *Agency for Toxic Substances and Disease Registry (ATSDR)*, June (2012), 1–347.

[251] Van Damme, M., Clarisse, L., Dammers, E., Liu, X., Nowak, J. B., Clerbaux, C., Flechard, C. R., Galy-Lacaux, C., Xu, W., Neuman, J. A., Tang, Y. S., Sutton, M. A., Erisman, J. W., and Coheur, P. F. Towards validation of ammonia (NH3) measurements from the IASI satellite. *Atmospheric Measurement Techniques 8*, 3 (2015), 1575–1591.

[252] Van der Werf, G. R., Randerson, J. T., Collatz, G. J., and Giglio, L. Carbon emissions from fires in tropical and subtropical ecosystems. *Global Change Biology 9*, 4 (2003), 547–562.

[253] Van Der Werf, G. R., Randerson, J. T., Giglio, L., Van Leeuwen, T. T., Chen, Y., Rogers, B. M., Mu, M., Van Marle, M. J., Morton, D. C., Collatz, G. J., Yokelson, R. J., and Kasibhatla, P. S. Global fire emissions estimates during 1997-2016. *Earth System Science Data 9*, 2 (2017), 697–720.

[254] Van Dingenen, R., Dentener, F. J., Raes, F., Krol, M. C., Emberson, L., and Cofala, J. The global impact of ozone on agricultural crop yields under current and future air quality legislation. *Atmospheric Environment 43*, 3 (2009), 604–618.

[255] Van Donkelaar, A., Martin, R. V., Leaitch, W. R., Macdonald, A. M., Walker, T. W., Streets, D. G., Zhang, Q., Dunlea, E. J., Jimenez, J. L., Dibb, J. E., Huey, L. G., Weber, R., and Andreae, M. O. Analysis of aircraft and satellite measurements from the Intercontinental Chemical Transport Experiment (INTEX-B) to quantify long-range transport of East Asian sulfur to Canada. *Atmospheric Chemistry and Physics 8* (2008), 2999–3014.

[256] Van Tienhoven, A. M., Otter, L., Lenkopane, M., Venjonoka, K., and Zunckel, M. Assessment of ozone impacts on vegetation in southern Africa and directions for future research. *South African Journal of Science 101*, 3-4 (2005), 143–148.

[257] van Vuuren, D. P., den Elzen, M. G. J., Lucas, P. L., Eickhout, B., Strengers, B. J., van Ruijven, B., Wonink, S., and van Houdt, R. Stabilizing greenhouse gas concentrations at low levels: an assessment of reduction strategies and costs. *Climatic Change 81*, 2 (mar 2007), 119–159.

[258] Veefkind, J. P., Aben, I., McMullan, K., Förster, H., de Vries, J., Otter, G., Claas, J., Eskes, H. J., de Haan, J. F., Kleipool, Q., van Weele, M., Hasekamp, O., Hoogeveen, R., Landgraf, J., Snel, R., Tol, P., Ingmann, P., Voors, R., Kruizinga, B., Vink, R., Visser, H., and Levelt, P. F. TROPOMI on the ESA Sentinel-5 Precursor: A GMES mission for global observations of the atmospheric composition for climate, air quality and ozone layer applications. *Remote Sensing of Environment 120*, 2012 (2012), 70–83.

[259] von Glasow, R., von Kuhlmann, R., Lawrence, M. G., Platt, U., and Crutzen, P. J. Impact of reactive bromine chemistry in the troposphere. *Atmospheric Chemistry and Physics Discussions 4*, 4 (2004), 4877–4913.

[260] Vrieling, A., De Leeuw, J., and Said, M. Y. Length of growing period over africa: Variability and trends from 30 years of NDVI time series. *Remote Sensing 5*, 2 (2013), 982–1000.

[261] Walton, H., Dajnak, D., Beevers, S., Williams, M., Watkiss, P., and Hunt, A. Understanding the Health Impacts of Air Pollution in London. *https://www.london.gov.uk/sites/default/files/hiainlondon_kingsreport_14072015_final.pdf*, July (2015), 1–129.

[262] Wang, C., Corbett, J. J., and Firestone, J. Improving spatial representation of global ship emissions inventories. *Environmental Science and Technology 42*, 1 (jan 2008), 193–199.

[263] Wang, P., Chen, Y., Hu, J., Zhang, H., and Ying, Q. Attribution of Tropospheric Ozone to NO x and VOC Emissions: Considering Ozone Formation in the Transition Regime. *Environmental Science and Technology 53*, 3 (2019), 1404–1412.

[264] Wang, Q., Jacob, D. J., Fisher, J. A., Mao, J., Leibensperger, E. M., Carouge, C. C., Le Sager, P., Kondo, Y., Jimenez, J. L., Cubison, M. J., and Doherty, S. J. Sources of carbonaceous aerosols and deposited black carbon in the Arctic in winter-spring: Implications for radiative forcing. *Atmospheric Chemistry and Physics 11*, 23 (2011), 12453–12473.

[265] Wang, Q., Jacob, D. J., Spackman, J. R., Perring, A. E., Schwarz, J. P., Moteki, N., Marais, E. A., Ge, C., Wang, J., and Barrett, S. R. Global budget and radiative forcing of black carbon aerosol: Constraints from pole-to-pole (HIPPO) observations across the Pacific. *Journal of Geophysical Research 119*, 1 (2014), 195–206.

[266] Wang, Y., Logan, J. A., and Jacob, D. J. Global simulation of tropospheric O 3 -NO x -hydrocarbon chemistry: 2. Model evaluation and global ozone budget. *Journal of Geophysical Research: Atmospheres 103*, D9 (feb 1998), 10727–10755.

[267] Wang, Y. X., McElroy, M. B., Jacob, D. J., and Yantosca, R. M. A nested grid formulation for chemical transport over Asia: Applications to CO. *Journal of Geophysical Research D: Atmospheres 109*, 22 (nov 2004), 1–20.

[268] Wang-Li, L. Insights to the formation of secondary inorganic PM2.5: Current knowledge and future needs. *International Journal of Agricultural and Biological Engineering 8*, 2 (2015), 1–13.

[269] Warner, J. X., Wei, Z., Strow, L. L., Dickerson, R. R., and Nowak, J. B. The global tropospheric ammonia distribution as seen in the 13 year AIRS measurement record. *Atmospheric Chemistry and Physics Discussions 15*, 24 (2015), 35823–35856.

[270] Wees, D. V., and Werf, G. R. V. D. Modelling African biomass burning emissions and the effect of spatial resolution. *Geoscientific Model Development Di*, May (2019).

[271] Wehner, B., and Wiedensohler, A. Long term measurements of submicrometer urban aerosols: Statistical analysis for correlations with meteorological conditions and trace gases. *Atmospheric Chemistry and Physics 3*, 3 (2003), 867–879.

[272] Werf, G. R. V. D., Randerson, J. T., Giglio, L., Collatz, G. J., Kasibhatla, P. S., and Arellano, A. F. Interannual variability in global biomass burning emissions from 1997 to 2004. *Atmospheric Chemistry and Physics 6*, 11 (2006), 3423–3441.

[273] Wesely, M. L. Parameterization of surface resistances to gaseous dry deposition in regional-scale numerical models. *Atmospheric Environment (1967) 23*, 6 (1989), 1293–1304.

[274] WHO. Ambient (outdoor) air quality and health, 2005.

[275] Wiedinmyer, C., Akagi, S. K., Yokelson, R. J., Emmons, L. K., Al-Saadi, J. A., Orlando, J. J., and Soja, A. J. The Fire INventory from NCAR (FINN): A high resolution global model to estimate the emissions from open burning. *Geoscientific Model Development 4*, 3 (2011), 625–641.

[276] Wilkinson, S., Mills, G., Illidge, R., and Davies, W. J. How is ozone pollution reducing our food supply? *Journal of Experimental Botany 63*, 2 (2012), 527–536.

[277] Williams, J. Organic trace gases in the atmosphere: An overview. *Environmental Chemistry 1*, 3 (2004), 125–136.

[278] World Health Organisation. WHO Global Ambient Air Quality Database, 2018.

[279] Wu, S., Mickley, L. J., Jacob, D. J., Logan, J. A., Yantosca, R. M., and Rind, D. Why are there large differences between models in global budgets of tropospheric ozone? *Journal of Geophysical Research Atmospheres 112*, 5 (mar 2007).

[280] Xing, Y. F., Xu, Y. H., Shi, M. H., and Lian, Y. X. The impact of PM2.5 on the human respiratory system. *Journal of Thoracic Disease 8*, 1 (2016), E69–E74.

[281] Xu, Y., Xue, W., Lei, Y., Zhao, Y., Cheng, S., Ren, Z., and Huang, Q. Impact of meteorological conditions on PM 2.5 pollution in China during winter. *Atmosphere 9*, 11 (2018).

[282] Young, P. J., Naik, V., Fiore, A. M., Gaudel, A., Guo, J., Lin, M. Y., Neu, J. L., Parrish, D. D., Rieder, H. E., Schnell, J. L., Tilmes, S., Wild, O., Zhang, L., Ziemke, J. R., Brandt, J., Delcloo, A., Doherty, R. M., Geels, C., Hegglin, M. I., Hu, L., Im, U., Kumar, R., Luhar, A., Murray, L., Plummer, D., Rodriguez, J., Saiz-Lopez, A., Schultz, M. G., Woodhouse, M. T., and Zeng, G. Tropospheric Ozone Assessment Report: Assessment of global-scale model performance for global and regional ozone distributions, variability, and trends. *Elem Sci Anth 6*, 1 (2018), 10.

[283] Zender, C. S., Bian, H., and Newman, D. Mineral Dust Entrainment and Deposition (DEAD) model: Description and 1990s dust climatology. *Journal of Geophysical Research 108*, D14 (jul 2003), 4416.

[284] Zender, C. S., Newman, D., and Torres, O. Spatial heterogeneity in aeolian erodibility: Uniform, topographic, geomorphic, and hydrologic hypotheses. *Journal of Geophysical Research 108*, D17 (sep 2003), 4543.

[285] Zhang, L., Gong, S., Padro, J., and Barrie, L. A size-segregated particle dry deposition scheme for an atmospheric aerosol module. *Atmospheric Environment 35*, 3 (2001), 549–560.

[286] Zubkova, M., Boschetti, L., Abatzoglou, J. T., and Giglio, L. Changes in Fire Activity in Africa from 2002 to 2016 and Their Potential Drivers. *Geophysical Research Letters* (2019), 1–11.